

Evaluation of whole-body vibrations and improvement of the driver's seat performance on a compact wheel loader

Vom Fachbereich Maschinenbau und Verfahrenstechnik
der Technischen Universität Kaiserslautern
zur Verleihung des akademischen Grades

Doktor-Ingenieur (Dr.-Ing.)

genehmigte Dissertation

von

M.Sc. Xiaojing Zhao

aus Qingzhou, Shandong, People's Republic of China

Vorsitzender:	Prof. Dr.-Ing. Jörg Seewig
Berichterstatter:	Prof. Dr.-Ing. Christian Schindler Prof. Dr.-Ing. Steffen Müller Prof. Dr. Imtiaz Haque
Dekan:	Prof. Dr.-Ing. Christian Schindler

Tag der Einreichung: 17. Dezember 2014

Tag der mündlichen Prüfung: 21. Mai 2015

Kaiserslautern, Oktober 2015

D 386

Acknowledgements

This dissertation was finished as a report of a research work at the Chair of Design in Mechanical Engineering (acronym 'KIMA' from its German name), University of Kaiserslautern, Germany. I would like to express my sincere appreciation to the following people, who gave me a great deal of support and help to complete this work. Foremost, I would like to express my sincere appreciation to my supervisor Prof. Dr.-Ing. Christian Schindler. He provided me many insightful discussions and a lot of invaluable suggestions. All of these are the primary fount of inspiration for my work. Without the excellent supervision and the continues encouragement from Prof. Schindler this dissertation would not have been finished.

I would like to give my special thanks to the members of my defense committee, Prof. Dr. Imtiaz Haque from Clemson University in USA, Prof. Dr.-Ing. Steffen Müller from TU Berlin and Prof. Dr.-Ing. Jörg Seewig from TU Kaiserslautern in Germany. I am grateful to Prof. Haque and Prof. Müller for their patience and willingness to review my dissertation, and for their precious advice for my work. My gratitude is specially given to Prof. Seewig as the chairman for his administration of the defence committee.

I would like to thank all of my colleagues in the chair of KIMA, especially Michael Kremb for the enormous help during the field tests and Stephan Rauber for the great support during the laboratory tests. My sincere thankfulness is extended to Dr. Peter Bach, Heinz-Peter Klopp and Robert Heinrich from Volvo CE, Konz, for their support and effort in the field tests. I am appreciative of the help from Prof. Dr.-Ing. Eberhard Kerscher and Werner Hauth from the Working Group Materials Testing at TU Kaiserslautern. They offered instruments and spent a lot of time for the tests of the seat components.

Finally, I would like to thank my husband Hao Li. In the past few years he always encouraged me and gave me a lot of ideas to solve difficulties in my life and work. Without his persistent support and help I could not have finished my study successfully. I wish to give my father, mother and brother the deepest gratitude and love for their understanding and support in my life.

Contents

Nomenclature	IV
Abbreviations	XIV
Abstract	XV
Kurzzusammenfassung	XVI
Zusammenfassung	XVII
1 Introduction	1
2 State of the Art	4
2.1 Effect of whole-body vibrations on the human being	5
2.1.1 Effect of whole-body vibrations on human health.....	5
2.1.2 Effect of whole-body vibrations on comfort	6
2.1.3 Human biodynamic response to whole-body vibrations	17
2.1.4 Lumped-parameter models of human body	22
2.2 Evaluation of effect of whole-body vibrations on human being.....	26
2.2.1 Evaluation of effect on human health.....	27
2.2.2 Evaluation of effect on comfort.....	37
2.3 Vibration attenuation performance of suspension seats	43
2.3.1 Metrics for seat vibration attenuation performance	43
2.3.2 Dynamics of suspension seats.....	45
2.3.3 Model and optimization of suspension seats.....	48
3 Motivation	57
4 Measurement and Analysis of Vibrations	61
4.1 Vibration measurement	61
4.1.1 Test vehicle.....	61
4.1.2 Test operations	62

4.1.3	Data acquisition equipment.....	65
4.2	Analysis of vibration characteristics.....	67
4.2.1	Purpose and method of analysis.....	67
4.2.2	Analysis results.....	68
4.3	Conclusion.....	76
5	Evaluation of Whole-Body Vibrations.....	77
5.1	Evaluation of effect on human health.....	77
5.1.1	Evaluation result according to ISO 2631-1:1997.....	77
5.1.2	Evaluation result according to ISO 2631-5:2004.....	84
5.1.3	Comparison of results of both ISO standards.....	85
5.1.4	Other detailed specifications in two ISO standards.....	90
5.2	Evaluation of effect on ride comfort.....	94
5.2.1	Evaluation result according to ISO 2631-1:1985.....	94
5.2.2	Evaluation result according to ISO 2631-1:1997.....	97
5.3	Conclusion.....	98
6	Effect of Safety Belt on Seat Transmissibility.....	101
6.1	Lap belt (case B) vs. no belt (case A).....	101
6.1.1	Comparison of seat effective amplitude transmissibility (SEAT).....	101
6.1.2	Comparison of seat transmissibility in the frequency domain.....	103
6.2	Four-point seat harness (case C) vs. no belt (case A).....	105
6.2.1	Comparison of seat effective amplitude transmissibility (SEAT).....	105
6.2.2	Comparison of seat transmissibility in the frequency domain.....	107
6.3	Four-point seat harness (case C) vs. lap belt (case B).....	109
6.3.1	Comparison of seat effective amplitude transmissibility (SEAT).....	109
6.3.2	Comparison of seat transmissibility in the frequency domain.....	112
6.4	Subjective comments on ride comfort.....	115
6.5	Conclusion.....	116

7	Optimization of Seat Suspension System	117
7.1	Investigation of dynamics of vertical seat suspension system	117
7.1.1	Laboratory seat tests	118
7.1.2	Analysis of dynamics of the vertical seat suspension system	122
7.2	Optimization of vertical seat suspension system	125
7.2.1	Seat-dummy model.....	125
7.2.2	Parameter identification	129
7.2.3	Model validation	133
7.2.4	Suspension system optimization.....	139
7.3	Optimization of longitudinal seat suspension system	151
7.3.1	Seat-driver model.....	151
7.3.2	Parameter identification	154
7.3.3	Model validation	155
7.3.4	Suspension system optimization.....	159
7.4	Combined seat-driver model in the x- and z-directions.....	168
7.5	Conclusion.....	176
8	Summary and Outlook	178
	Literature	183

Nomenclature

A_{as}	[m ²]	Surface of air spring
A_{ef}	[m ²]	Effective area of air spring
D	[m/s ²]	Acceleration dose
$Diff$	[-]	Difference between estimated vibration dose value and vibration dose value
F_{BW}	[N]	Bouc-Wen force
F_{as}	[N]	Restoring force from the air spring
F_{bz}	[N]	Force coming from the bottom end-stop buffer
F_d	[N]	Damping force
F_{dx}	[N]	Damping force of the passive hydraulic damper in the longitudinal seat suspension system
F_{dz}	[N]	Vertical component of damping force
F_{fx}	[N]	Force coming from the front end-stop buffer
F_g	[N]	Gravity force
F_{rx}	[N]	Force coming from the rear end-stop buffer
F_{tz}	[N]	Force coming from the top end-stop buffer
$FFT[i(t)]$	[-]	Complex fast Fourier transform (FFT) of input signal
$FFT[i(t)]^*$	[-]	Complex conjugation of the FFT[i(t)]
$FFT[o(t)]$	[-]	Complex FFT of output signal
$G_{Fv}(f)$	[(N·m/s)/Hz]	Cross spectral density (CSD) of force and velocity as a function of frequency
$G_{bb}(f)$	[(m/s ²) ² /Hz]	Power spectral density (PSD) of accelerations at the seat base as a function of frequency
$G_{cc}(f)$	[(m/s ²) ² /Hz]	PSD of accelerations on the seat cushion as a function of frequency
$G_{ii}(f)$	[-]	PSD of input signal as a function of frequency
$G_{io}(f)$	[-]	CSD of input and output signals as a function of frequency
$G_{oo}(f)$	[-]	PSD of the output signal as a function of frequency

J	[kg·m ²]	Moment of inertia of m_{h1z} about the connection point
$MTVV$	[m/s ²]	Maximum transient vibration value
$P_{abs}(f)$	[(N·m/s)/Hz]	Absorbed power as a function of frequency
$PSD_m(i)$	[dB/Hz]	The i^{th} value on the PSD curve of the accelerations obtained from the measurement
$PSD_s(i)$	[dB/Hz]	The i^{th} value on the PSD curve of the accelerations obtained from the simulation
R	[J/(kg·K)]	Gas constant
S_e	[MPa]	Equivalent static compressive stress
S_{ed}	[MPa]	Daily equivalent static compression dose
$SEAT_A$	[-]	Seat effective amplitude transmissibility (SEAT) in the case where the driver does not wear any safety belt
$SEAT_{AB}\%$	[-]	Difference between the SEAT values in the case where the driver wears a lap belt and in the case where the driver does not wear any safety belt
$SEAT_{AC}\%$	[-]	Difference between the SEAT values in the case where the driver wears a four-point seat harness and in the case where the driver does not wear any safety belt
$SEAT_B$	[-]	SEAT value in the case where the driver wears a lap belt
$SEAT_{BC}\%$	[-]	Difference between the SEAT values in the case where the driver wears a four-point seat harness and in the case where the driver wears a lap belt
$SEAT_C$	[-]	SEAT value in the case where the driver wears a four-point seat harness
T	[s]	Duration of vibration measurement
T_{as}	[K]	Temperature in air spring
T_d	[s]	Reference daily exposure duration, 8 h (28800 s)
T_l	[s]	Lower limit of permitted daily exposure duration
T_u	[s]	Upper limit of permitted daily exposure duration
T_w	[K]	Wall temperature of air spring
$TF(f)$	[-]	Transfer function in the frequency domain

$TVDV$	$[m/s^{1.75}]$	Total vibration dose value
$U(\chi)$	$[-]$	Objective function of optimization
V_{as}	$[m^3]$	Volume of air spring
VDV	$[m/s^{1.75}]$	Vibration dose value
VDV_b	$[m/s^{1.75}]$	VDV of frequency weighted accelerations at the seat base
VDV_c	$[m/s^{1.75}]$	VDV of frequency weighted accelerations on the seat cushion
VDV_d	$[m/s^{1.75}]$	Daily vibration dose value
VDV_i	$[m/s^{1.75}]$	VDV of frequency weighted accelerations in the i-direction on the seat cushion
VDV_m	$[m/s^{1.75}]$	VDV of accelerations obtained from the measurement
VDV_s	$[m/s^{1.75}]$	VDV of accelerations obtained from the simulation
VDV_{ss}	$[m/s^{1.75}]$	VDV of frequency weighted accelerations on the top of the suspension system
$VDVR$	$[-]$	Vibration dose value ratio
$VDVR_m$	$[-]$	VDVR obtained from the measurement
$VDVR_s$	$[-]$	VDVR obtained from the simulation
VSV	$[m/s^2]$	Vector sum value
$W_i(f)$	$[-]$	Frequency weighting in the i-direction as a function of frequency
X	$[m]$	Absolute displacement of seat base in the x-direction
\dot{X}	$[m/s]$	Absolute velocity of seat base in the x-direction
\ddot{X}	$[m/s^2]$	Absolute acceleration of seat base in the x-direction
X_s	$[m]$	Absolute displacement of m_s in the x-direction
\dot{X}_s	$[m/s]$	Absolute velocity of m_s in the x-direction
\ddot{X}_s	$[m/s^2]$	Absolute acceleration of m_s in the x-direction
X_1	$[m]$	Absolute displacement of m_{h0z} in the x-direction
\dot{X}_1	$[m/s]$	Absolute velocity of m_{h0z} in the x-direction
\ddot{X}_1	$[m/s^2]$	Absolute acceleration of m_{h0z} in the x-direction
Z	$[m]$	Absolute displacement of seat base in the z-direction

\dot{Z}	[m/s]	Absolute velocity of seat base in the z-direction
\ddot{Z}	[m/s ²]	Absolute acceleration of seat base in the z-direction
Z_s	[m]	Absolute displacement of m_s in the z-direction
\dot{Z}_s	[m/s]	Absolute velocity of m_s in the z-direction
\ddot{Z}_s	[m/s ²]	Absolute acceleration of m_s in the z-direction
Z_1	[m]	Absolute displacement of m_{d1z} (or m_{h0z}) in the z-direction
\dot{Z}_1	[m/s]	Absolute velocity of m_{d1z} (or m_{h0z}) in the z-direction
\ddot{Z}_1	[m/s ²]	Absolute acceleration of m_{d1z} (or m_{h0z}) in the z-direction
Z_2	[m]	Absolute displacement of m_{d2z} (or m_{h2z}) in the z-direction
\dot{Z}_2	[m/s]	Absolute velocity of m_{d2z} (or m_{h2z}) in the z-direction
\ddot{Z}_2	[m/s ²]	Absolute acceleration of m_{d2z} (or m_{h2z}) in the z-direction
Ω	[-]	Dimensionless angular frequency ratio
$a(f)$	[m/s ²]	Accelerations as a function of frequency
$a_m(i)$	[m/s ²]	The i^{th} acceleration value obtained from the measurement
$a_s(i)$	[m/s ²]	The i^{th} acceleration value obtained from the simulation
a_{pi}	[m/s ²]	The i^{th} peak of spine accelerations
$a_{pm}(i)$	[m/s ²]	Acceleration peak caused by the i^{th} end-stop impact in the measurement
$a_{ps}(i)$	[m/s ²]	Acceleration peak caused by the i^{th} end-stop impact in the simulation
$a_w(t)$	[m/s ²]	Frequency weighted accelerations as a function of time
$a_w(t_0)$	[m/s ²]	Running RMS values of frequency weighted accelerations as a function of time
\tilde{a}_w	[m/s ²]	Root mean square (RMS) of frequency weighted accelerations
\tilde{a}_{wb}	[m/s ²]	RMS of frequency weighted accelerations at the seat base
\tilde{a}_{wbi}	[m/s ²]	RMS value of frequency weighted accelerations in the x-, y- or z-direction at the seat backrest; 'i' represents x, y or z

\tilde{a}_{wc}	[m/s ²]	RMS of frequency weighted accelerations on the seat cushion
\tilde{a}_{wfi}	[m/s ²]	RMS value of frequency weighted accelerations in the x-, y- or z-direction on the feet floor; 'i' represents x, y or z
\tilde{a}_{wi}	[m/s ²]	RMS value of frequency weighted accelerations in the x-, y- or z-direction on the seat cushion; 'i' represents x, y or z
\tilde{a}_{wri}	[rad/s ²]	RMS value of frequency weighted accelerations in the r _x -, r _y - or r _z -direction on the seat cushion; 'i' represents x, y or z
$a_{1/3ob}(t)$	[m/s ²]	Accelerations in 1/3 octave band as a function of time
$\tilde{a}_{1/3ob}$	[m/s ²]	RMS value of accelerations in 1/3 octave band
c_c	[N·s/m]	Critical damping of a single-DOF system without the auxiliary spring k _d
c_{cx}	[N·s/m]	Linearized damping coefficient of seat cushion in the x-direction
c_{cz}	[N·s/m]	Linearized damping coefficient of the seat cushion in the z-direction
c_d	[N·s/m]	Damping coefficient of the damper
c_{dz}	[N·s/m]	Damping coefficient of the damper in the dummy between its lower and upper parts
c_{hard}	[N·s/m]	Damping coefficient of semi-active damper in hard-state
c_{hardx}	[N·s/m]	Damping coefficient of the longitudinal semi-active damper in the hard-state
c_{hz}	[N·s/m]	Equivalent damping coefficient of the driver model in the z-direction
c_r	[N·s m]	Rotational damping coefficient between m _{h1z} and m _{h0z}
c_{soft}	[N·s/m]	Damping coefficient of semi-active damper in soft-state
c_{softx}	[N·s/m]	Damping coefficient of the longitudinal semi-active damper in the soft-state

c_{x1}	[N·s/m]	Damping coefficient of the longitudinal passive hydraulic damper at low speeds in the compression stage
c_{x2}	[N·s/m]	Damping coefficient of the longitudinal passive hydraulic damper at high speeds in the compression stage
c_{x3}	[N·s/m]	Damping coefficient of the longitudinal passive hydraulic damper at low speeds in the extension stage
c_{x4}	[N·s/m]	Damping coefficient of the longitudinal passive hydraulic damper at high speeds in the extension stage
c_1	[N·s/m]	Damping coefficient of the passive hydraulic damper at low speeds in the compression stage
c_2	[N·s/m]	Damping coefficient of the passive hydraulic damper at high speeds in the compression stage
c_3	[N·s/m]	Damping coefficient of the passive hydraulic damper at low speeds in the extension stage
c_4	[N·s/m]	Damping coefficient of the passive hydraulic damper at high speeds in the extension stage
d_{mx}	[m]	Maximum stroke of longitudinal seat suspension system
d_{mz}	[m]	Maximum stroke of vertical seat suspension system
d_{soft}	[m]	Maximum suspension travel when the semi-active damper in the soft-state
d_{softx}	[m]	Maximum suspension travel of the longitudinal seat suspension when the semi-active damper in the soft-state
d_x	[m]	Distance between the middle position of the longitudinal seat suspension and the front or the rear end-stop buffer
d_z	[m]	Distance between the middle position of the vertical seat suspension and the bottom or the top end-stop buffer
d_0	[m]	Amplitude of sinusoidal displacement excitation
d_1	[N·s/m]	Linear damping coefficient
d_2	[N·(s/m) ²]	Quadratic damping coefficient
d_3	[N·(s/m) ³]	Cubic damping coefficient

e	[m]	Distance between the center of gravity of m_{h1z} and the connection point
$eVDV$	[m/s ^{1.75}]	Estimated vibration dose value
f	[Hz]	Frequency of sinusoidal displacement excitation
f_{nx}	[Hz]	Natural frequency of the seat-driver system with the longitudinal seat suspension system
h_0	[m]	Initial height of air spring
j	[-]	Imaginary unit, $(-1)^{1/2}$
k_{BW}	[N/m]	Positive stiffness of Bouc-Wen model of hysteresis
k_{as}	[N/m]	Stiffness coefficient of air spring
k_{b1}	[N/m]	Linear stiffness coefficient of bottom end-stop buffer
k_{b2}	[N/m ²]	Quadratic stiffness coefficient of bottom end-stop buffer
k_{b3}	[N/m ³]	Cubic stiffness coefficient of bottom end-stop buffer
k_{b4}	[N/m ⁴]	Quartic stiffness coefficient of bottom end-stop buffer
k_{cx}	[N/m]	Linearized stiffness of seat cushion in the x-direction
k_{cz}	[N/m]	Linearized stiffness of seat cushion in the z-direction
k_d	[N/m]	Stiffness of the auxiliary spring in the seat model
k_{dz}	[N/m]	Stiffness of springs in the dummy between its lower and upper parts
k_{f1}	[N/m]	Linear stiffness coefficient of front end-stop buffer
k_{f3}	[N/m ³]	Cubic stiffness coefficient of front end-stop buffer
k_{hz}	[N/m]	Equivalent stiffness of the driver model in the z-direction
k_r	[N·m]	Rotational stiffness coefficient between m_{h1z} and m_{h0z}
k_{r1}	[N/m]	Linear stiffness coefficient of rear end-stop buffer
k_{r3}	[N/m ³]	Cubic stiffness coefficient of rear end-stop buffer
k_{t1}	[N/m]	Linear stiffness coefficient of top end-stop buffer
k_{t2}	[N/m ²]	Quadratic stiffness coefficient of top end-stop buffer
k_{t3}	[N/m ³]	Cubic stiffness coefficient of top end-stop buffer
k_{t4}	[N/m ⁴]	Quartic stiffness coefficient of top end-stop buffer
k_x	[N/m]	Stiffness of spring in the longitudinal seat suspension

l_x	[m]	Longitudinal component of the length of the damper
m_{as0}	[kg]	Initial air mass inside air spring
m_d	[kg]	Equivalent mass of a seated driver
m_{d1z}	[kg]	Mass of the dummy lower part
m_{d2z}	[kg]	Mass of the dummy upper part
m_{h0z}	[kg]	Mass of component converting the excitations in the vertical direction to the response in the longitudinal direction
m_{h1z}	[kg]	Equivalent mass of the lower part of a seated person
m_{h2z}	[kg]	Equivalent mass of the upper part of a seated person
m_s	[kg]	Mass of the seat sprung part
p	[-]	Asymmetry factor, ratio of c_3 to c_1
p_{as}	[Pa]	Air pressure inside air spring
p_x	[-]	Asymmetry factor of the longitudinal passive hydraulic damper, ratio of c_{x3} to c_{x1}
p_0	[Pa]	Atmospheric pressure
$t_m(i)$	[s]	Duration of the i^{th} end-stop impact in the measurement
$t_s(i)$	[s]	Duration of the i^{th} end-stop impact in the simulation
t_0	[s]	Time of observation (instantaneous time)
v	[m/s]	Maximum velocity of the damper
$v(f)$	[m/s]	Velocity as a function of frequency
v_c	[m/s]	Transition velocity of the passive hydraulic damper in the compression stage
v_{cx}	[m/s]	Transition velocity of the longitudinal passive hydraulic damper in the compression stage
v_e	[m/s]	Transition velocity of the passive hydraulic damper in the extension stage
v_{ex}	[m/s]	Transition velocity of the longitudinal passive hydraulic damper in the extension stage
α	[rad]	Angle that e has with the horizontal when the model is in equilibrium

α_{as}	[W/(m ² ·K)]	Overall heat transfer coefficient of an air spring
β	[m ⁻¹]	Parameter of Bouc-Wen model of hysteresis
γ	[m ⁻¹]	Parameter of Bouc-Wen model of hysteresis
γ_c	[-]	Damping reduction factor in the compression stage
γ_{cx}	[-]	Damping reduction factor of the longitudinal passive hydraulic damper in the compression stage
γ_e	[-]	Damping reduction factor in the extension stage
γ_{ex}	[-]	Damping reduction factor of the longitudinal passive hydraulic damper in the extension stage
$\gamma_{io}(f)$	[-]	Coherence between the input and the output signals
$\bar{\delta}_{PSD}$	[-]	Mean value of the relative errors between the PSD curves of the simulated and the measured accelerations
δ_{VDV}	[-]	Difference between simulated VDV and measured VDV
δ_{VDVR}	[-]	Difference between simulated and measured VDVRs
$\bar{\delta}_a$	[-]	Mean value of the relative errors between the simulated and the measured accelerations
$\bar{\delta}_{ap}$	[-]	Mean value of the relative errors between the simulated and the measured acceleration peaks caused by the end-stop impacts
δ_{as}	[-]	Reduction ratio of air spring
δ_d	[-]	Reduction ratio of damper
$\bar{\delta}_t$	[-]	Mean value of the relative errors between the durations of the simulated and the measured end-stop impacts
θ	[rad]	Angle of rotation of m_{h1z}
$\dot{\theta}$	[rad/s]	Rotational velocity of m_{h1z}
$\ddot{\theta}$	[rad/s ²]	Rotational acceleration of m_{h1z}
κ	[-]	Adiabatic coefficient
ξ_v	[-]	Dimensionless damping ratio
σ	[rad]	Phase of $G_{FV}(f)$
τ	[s]	Integration time for running averaging

χ	[-]	Vector of parameters to be optimized
φ	[rad]	Angle between the damper and the horizontal direction
φ_0	[rad]	Angle between the damper and the horizontal direction when the seat is in the middle position
ω	[rad/s]	Angular frequency of the excitations
ω_0	[rad/s]	Undamped natural frequency of the suspension seat

Abbreviations

CF	Crest Factor
CSD	Cross Spectral Density
CWL	Compact Wheel Loader
DOF	Degree of Freedom
DPMI	Driving-Point Mechanical Impedance
FFT	Fast Fourier Transform
GKS	Ganzkörperschwingungen
HGCZ	Health Guidance Caution Zone
ISO	International Organization for Standardization
LBP	Low Back Pain
LPM	Lumped-Parameter Model
MTVV	Maximum Transient Vibration Value
OVTV	Overall Vibration Total Value
PSD	Power Spectral Density
RCB	Reduced Comfort Boundary
RMS	Root Mean Square
RPC	Remote Parameter Control
SEAT	Seat Effective Amplitude Transmissibility
STHT	Seat-to-Head Transmissibility
TVDV	Total Vibration Dose Value
VDV	Vibration Dose Value
VDVR	Vibration Dose Value Ratio
VSV	Vector Sum Value
WBV	Whole-Body Vibrations

Abstract

Whole-body vibrations (WBV) have adverse effects on ride comfort and human health. Suspension seats have an important influence on the WBV severity. In this study, WBV were measured on a medium-sized compact wheel loader (CWL) in its typical operations. The effect of short-term exposure to the WBV on the ride comfort was evaluated according to ISO 2631-1:1985 and ISO 2631-1:1997. ISO 2631-1:1997 and ISO 2631-5:2004 were adopted to evaluate the effect of long-term exposure to the WBV on the human health. Reasons for the different evaluation results obtained according to ISO 2631-1:1997 and ISO 2631-5:2004 were explained in this study. The WBV measurements were carried out in cases where the driver wore a lap belt or a four-point seat harness and in the case where the driver did not wear any safety belt. The seat effective amplitude transmissibility (SEAT) and the seat transmissibility in the frequency domain in these three cases were analyzed to investigate the effect of a safety belt on the seat transmissibility. Seat tests were performed on a multi-axis shaking table in laboratory to study the dynamic behavior of a suspension seat under the vibration excitations measured on the CWL. The WBV intensity was reduced by optimizing the vertical and the longitudinal seat suspension systems with the help of computational simulations. For the optimization multi-body models of the seat-dummy system in the laboratory seat tests and the seat-driver system in the field vibration measurements were built and validated.

Kurzzusammenfassung

Ganzkörperschwingungen (GKS) haben negative Auswirkungen auf den Fahrkomfort und die menschliche Gesundheit. Die Sitzfederungen haben einen hohen Einfluss auf die Stärke der GKS. In dieser Forschungsarbeit wurden die GKS auf einem mittelgroßen Kompaktrader gemessen. Die Wirkungen der Kurzzeitbelastungen von GKS des Radladers auf den Menschen hinsichtlich des Fahrkomforts wurden entsprechend ISO 2631-1:1985 und ISO 2631-1:1997 bewertet. Zur Bewertung der Auswirkungen der Langzeitbelastungen von GKS des Radladers auf die Gesundheit des Menschen wurden ISO 2631-1:1997 und ISO 2631-5:2004 herangezogen. Dabei ergaben sich unterschiedliche Ergebnisse für beide jeweiligen Normen, die im Rahmen dieser Arbeit erläutert wurden. Die GKS wurden für drei unterschiedliche Szenarien gemessen: ohne Sicherheitsgurt, mit Beckengurt und mit Vierpunktgurt. Der Sitzübertragungsfaktor SEAT, sowie die entsprechende Sitzübertragungsfunktion in diesen drei Szenarien wurden analysiert, um den Einfluss des Sicherheitsgurts auf das Übertragungsverhalten des Sitzes zu untersuchen. Weiterhin wurden auf einem Schwingungsprüfstand die Sitzversuche durchgeführt, in denen der Sitz mit den am Radlader gemessenen Vibrationen angeregt wurde, um das Übertragungsverhalten des Sitzes zu analysieren. Um die Intensität der GKS zu reduzieren wurden die Vertikal- und Längssitzfederungen mit Computersimulationen optimiert. Hierfür wurden Mehrkörpermodelle des in den Prüfstandsversuchen verwendeten Sitz-Fahrerdummy-Systems, sowie des in den Feldmessungen benutzten Sitz-Fahrer-Systems aufgebaut und validiert.

Zusammenfassung

Heutzutage ist eine Vielzahl von Personen einem hohen Niveau von Ganzkörperschwingungen (GKS) bei der täglichen Arbeit ausgesetzt, wie z.B. die Fahrer von Traktoren, Baumaschinen und Transportfahrzeugen. GKS können akute körperliche Reaktionen zur Folge haben, wie z.B. Muskelermüdung, Unbehagen und verringerte Leistungsfähigkeit. Darüber hinaus kann es insbesondere langfristig zur Beeinträchtigung der Gesundheit kommen, beispielsweise zur Erkrankung der Lendenwirbelsäule. Da der Sitz, je nach Auslegung der Sitzfederung mehr oder weniger stark die Schwingungen auf den Fahrer überträgt, bietet er das größte Reduzierungspotential bezüglich GKS.

Im Rahmen mehrerer aktueller Forschungsarbeiten wird die Wirkung von Langzeitbelastungen auf die menschliche Gesundheit untersucht und bewertet. In den meisten Arbeiten wurden diese Bewertungen entsprechend ISO 2631-1:1997 vorgenommen. Nach der Veröffentlichung der Norm ISO 2631-5:2004 beschäftigten sich einige Arbeiten mit der Abschätzung der Gesundheitsrisiken nach ISO 2631-1:1997 und ISO 2631-5:2004. Beide Normen geben Grenzen für das Gesundheitsrisiko an und führen zu unterschiedlichen Ergebnissen, was zu Diskussionen über die Höhe der Grenzwerte geführt hat. Bis heute beschäftigen sich wenige Forschungsarbeiten mit der Bewertung der kurzfristigen Auswirkung von GKS. Für die Bewertung der Kurzzeitbelastungen, sind Verfahren in zwei ISO-Normen beschrieben: ISO 2631-1:1985 und ISO 2631-1:1997. Obwohl der Kompaktraktor einen großen Marktanteil besitzt, wurde die Intensität der auftretenden GKS nur im Rahmen weniger Forschungsaktivitäten untersucht.

Die Intensität der GKS kann durch die Verbesserung des Übertragungsverhaltens der Sitzfederungen, d.h. die Reduktion bzw. Isolation von Schwingungsanregungen, reduziert werden. Hier wurde viel Aufwand betrieben, das Übertragungsverhalten des gefederten Sitzes zu studieren und die Sitzfederungen zu optimieren. In vorangegangenen Forschungsarbeiten wurde der Einfluss des Sitzkissens, der Sitzfederung und der Anschläge sowie der dynamischen Eigenschaften des Fahrers hinsichtlich des Übertragungsverhaltens des Sitzes untersucht. Der Einfluss des Sicherheitsgurts auf das Übertragungsverhalten des Sitzes wurde bisher noch nicht erforscht. Viele Arbeiten verwenden Mehrkörpermodelle, um das dynamische Verhalten des Sitz-Fahrer-Systems für die vertikale Richtung zu simulieren. Durch

die Verwendung entsprechender Optimierungsverfahren innerhalb der Computersimulation, lässt sich das Übertragungsverhalten der vertikalen Sitzfederung verbessern. Dabei stellte sich heraus, dass die Verwendung eines zusätzlichen Luftspeichers oder eine Anpassung der Dämpfungskoeffizienten des Dämpfers zu einer Erhöhung der Schwingungsisolierungseigenschaft der vertikalen Sitzfederung führen. Darüber hinaus kann die Stärke der durch die Anschläge verursachten Schwingungstöße durch eine Optimierung von deren Kraft-Weg-Eigenschaften reduziert werden.

Bei Baumaschinen treten hohe GKS nicht nur für die vertikale-, sondern auch für die Längsrichtung auf. Entsprechende Sitze mit Längsfederungen sind bereits auf dem Markt verfügbar. Bezüglich der Untersuchung und Verbesserung des Übertragungsverhaltens der Längsfederung wurden wenige Forschungsarbeiten durchgeführt. Im Rahmen dieser Forschungsarbeiten wurden einfach Fahrermodelle vorgestellt und verwendet.

Die drei wichtigsten Aufgaben der vorliegenden Arbeit sind: die Bewertung des Einflusses der in einem Kompaktrader auftretenden GKS, die Untersuchung des Einflusses des Sicherheitsgurts auf das Übertragungsverhalten des Sitzes, und die Verbesserung der Schwingungsisolierungseigenschaft der Vertikal- und Längsfederung des Sitzes.

Der Einfluss der Kurzzeitbelastungen, die sich bei der Benutzung eines Kompaktraders ergeben, wurde entsprechend ISO 2631-1:1985 und ISO 2631-1:1997 bewertet. Der Einfluss der Langzeitbelastungen auf die menschliche Gesundheit wurde entsprechend ISO 2631-1:1997 und ISO 2631-5:2004 bewertet. Zusätzlich wurden die Ergebnisse der beiden Normen verglichen. Die Ursachen der unterschiedlichen Ergebnisse für beide Normen wurden erläutert.

Es wurden Schwingungsmessungen bei Feldversuchen für drei unterschiedliche Szenarien durchgeführt: ohne Sicherheitsgurt, mit Beckengurt und mit Vierpunktgurt. Der Sitzübertragungsfaktor SEAT, sowie die entsprechende Sitzübertragungsfunktion wurden in diesen drei Szenarien analysiert, um den Einfluss des Sicherheitsgurts auf das Übertragungsverhalten des Sitzes zu untersuchen.

Der Sitz des Kompaktraders hat eine passive, vertikale Sitzfederung. Die Sitzversuche wurden auf einem Schwingungsprüfstand durchgeführt, um die

dynamischen Eigenschaften der vertikalen Sitzfederung zu erproben. Hierbei wurden zur Anregung die Beschleunigungssignale aus dem Kompaktrader verwendet. Das Übertragungsverhalten der vertikalen Sitzfederung wurde durch eine Optimierung des passiven hydraulischen Dämpfers und der Anschläge verbessert. Weiterhin wurde das Übertragungsverhalten einer semi-aktiven vertikalen Sitzfederung verbessert, durch die Optimierung des semi-aktiven Dämpfers, welche eine ‚Weich-Hart‘ Regelung verwendet. Eine Längssitzfederung wurde entworfen und optimiert, um das Übertragungsverhalten des Sitzes in Längsrichtung zu verbessern. Die Optimierung einer passiven- und einer semi-aktiven Längssitzfederung wurde durchgeführt, ebenso wie die Optimierung der vertikalen Sitzfederung. Das verbesserte Übertragungsverhalten der passiven Sitzfederung wurde mit dem der semi-aktiven Variante verglichen.

Diese Arbeit trägt einige innovative Untersuchungsergebnisse zur Bewertung von Schwingungsbelastungen, sowie der Untersuchung des Sitzübertragungsverhaltens und der Optimierung der Sitzfederungen bei. Zuerst zeigt diese Arbeit detaillierte Bewertungsergebnisse der GKS auf einem Kompaktrader. Anhand des Vergleichs der unterschiedlichen Ergebnisse für ISO 2631-1:1997 und ISO 2631-5:2004, sowie durch die entsprechende Diskussion der Bewertungsmaßnahmen in beiden Normen, lassen sich einige Empfehlungen für die Verbesserung der ISO-Normen in der Zukunft ableiten. Zweitens wurde der Einfluss des Sicherheitsgurts auf das Übertragungsverhalten des Sitzes untersucht. Die Untersuchungsergebnisse helfen dem Hersteller bei der Auswahl des optimalen Sicherheitsgurts. Die Optimierung der vertikalen- und der Längssitzfederung reduziert die GKS auf dem Kompaktrader signifikant. Das Fahrermodell, welches im Rahmen dieser Arbeit verwendet wird, ist in der Lage, das vertikale und longitudinale Schwingungsverhalten des Fahrers unter vertikaler Anregung zu simulieren. Mithilfe der in dieser Arbeit beschriebenen Optimierungsverfahren und Sitz-Fahrer-Modelle, lassen sich auch die Schwingungsisolierungseigenschaften der Sitze in anderen Fahrzeugen verbessern.

1 Introduction

Vibrations became a recognizable environmental stressor in the 1920s and 1930s, at the time when mobile machines, such as agricultural tractors, motor vehicles and aircraft, were becoming prevalent [1],[2]. Whole-body vibrations (WBV) refer to the vibrations transmitted into the entire human body from the physical contact with a vibrating source, usually through standing, sitting or reclining on a vibrating surface [3]. A large number of people is exposed to WBV throughout the working world. Workplaces with high levels of WBV are numerous and mainly include the driver seats on agricultural tractors, construction machines and transportation vehicles. It has been proven that long-term exposure to WBV is associated with a series of health problems, especially in the human back area. Short-term exposure to WBV can cause drivers transitory reactions, such as muscle fatigue, loss of balance and ride discomfort. These reactions can reduce the driver's ability to control the vehicle and could lead to traffic accidents in the worst case.

Lots of studies have been carried out since the 1930s to investigate the human subjective sensations under various vibration excitations. The boundaries of excitation magnitudes for different levels of subjective sensations as well as the 'equal sensation contours' were obtained from these studies. They contributed to the development of the ISO 2631-1 standards. The current edition of the ISO 2631-1 was published in 1997, i.e. ISO 2631-1:1997 [4]. It is widely used all over the world to evaluate the effect of WBV on the human health. A procedure for the evaluation of the effect of short-term exposure to WBV on the comfort is introduced in ISO 2631-1:1997 as well. In 2004, part 5 of ISO 2631, ISO 2631-5:2004 [5], was published, in which a new evaluation procedure is introduced. This procedure can be used to evaluate the effect of WBV containing multiple shocks on the human health. After the publication of ISO 2631-5:2004, both ISO 2631-1:1997 and ISO 2631-5:2004 were used in research works to predict the health risks simultaneously. However, different prediction results were obtained according to these two ISO standards. This caused discussions about the boundaries of the health guidance caution zone (HGCZ) in the two standards.

Suspension systems are installed on vehicles to reduce the WBV. The vibration attenuation performance of a suspension seat has an important influence on the WBV severity. The seat transmissibility is used to evaluate this property. Some

studies investigated the effect of seat cushion, seat suspension components and end-stop buffers on the seat transmissibility. It is also affected by the dynamic behavior of the driver, which is significantly influenced by the kind of fixation to the seat. There is no doubt that a safety belt affects the driver dynamic behavior and accordingly the seat transmissibility by restricting the movement of the driver.

Computational simulation is an efficient and economical method to find out the optimal configurations of technical systems. This is also true for the seat suspension system. Several multi-body models of the suspension seat-driver system were developed to simulate the dynamic behavior of this system in the vertical or the horizontal directions. With the help of computational simulations, lots of studies were carried out for the improvement of the vibration attenuation performance of the vertical seat suspension system, which can for example be improved by using an additional volume for the air spring, selecting more suitable dampers or optimizing the properties of the end-stop buffers. Longitudinal vibrations on construction vehicles are also severe. There are also several studies carried out to improve the vibration attenuation performance of the longitudinal seat suspension system by optimizing the stiffness and damping coefficients.

Compact wheel loaders (CWLs) have a large market in the world due to their small size but ample lift capacity and maneuverability [6]. In order to protect the CWL drivers from the health and safety risks caused by WBV, the primary objectives of this research work are to thoroughly evaluate effects of WBV arising from a CWL on human health and ride comfort; to investigate the effect of a safety belt on the seat transmissibility in order to select a proper type of the safety belt for a more comfortable working environment for the drivers; and to optimize the longitudinal and the vertical seat suspension systems in order to improve the vibration attenuation performance of the seat and to reduce the WBV on the seat cushion. To achieve these objectives, the tasks carried out in this research work are described as follows:

In chapter 2 the previous studies on the WBV and the suspension seat dynamics are reviewed in the following four aspects: (1). the human subjective sensations under various excitations and the human biodynamic response to vibrations; (2). evaluation methods of effects of WBV on human health and ride comfort; (3). the human body models and the suspension seat models used to simulate the dynamic behavior of the suspension seat-driver system; (4). investigation results and optimization solutions of the vibration attenuation performance of suspension seats.

In chapter 3 motivations of this research work are given on the basis of the literature review in chapter 2.

In chapter 4 the field tests of vibration measurement on a medium-sized CWL are introduced. The influence of operational conditions (including driving speed, bucket load condition and unevenness of road surface) on the vibration characteristics is studied.

In chapter 5 evaluations of the effects of WBV arising from the CWL on the human health and the ride comfort are carried out according to the ISO standards. The health evaluation results obtained according to ISO 2631-1:1997 are compared to those obtained according to ISO 2631-5:2004. The reasons for the different results with the two ISO standards are explained. In addition, the details of the evaluation procedures in these two standards (such as frequency weighting filters and spine models) are discussed with respect to whether they are suitable for the WBV on this CWL.

In chapter 6 the effect of a safety belt on the seat transmissibility is studied based on the analysis of the seat effective amplitude transmissibility (SEAT) and the seat transfer function in the following three cases: the driver wearing a lap belt, the driver wearing a four-point seat harness and the driver wearing no safety belt.

Chapter 7 focuses on analyzing the dynamic characteristics of the suspension seat used on the CWL and improving the seat vibration attenuation performance. Multi-body models are built and validated to simulate the dynamic behavior of the seat-occupant system in the vertical and the longitudinal directions. The vertical and the longitudinal seat suspension systems are optimized with the help of these models to reduce the WBV on the CWL.

In chapter 8 short summaries of this research work and recommendations for future research work are presented.

2 State of the Art

Exposure to whole-body vibrations (WBV) is a dominant inducement of muscle fatigue, ride discomfort, loss of balance and some health problems like musculoskeletal disorders. Accordingly, it can result in a decrease of work efficiency and has the potential to cause traffic accidents and to lead to occupational disability for many working people. Since the 1930s, a large amount of effort has been done to investigate the relationship between the WBV exposure and the human subjective response, to develop the procedures to evaluate the effects of WBV on the human health and the ride comfort, and to reduce the WBV by optimizing suspension systems.

Drivers of vehicles generally take the seated posture in the vehicle driving direction. Due to this reason, the literature review in this chapter focuses only on the seated persons, whose coordinate system for the measurement and evaluation of WBV is illustrated in Fig. 2.1. The x-direction is the longitudinal direction from the back to the chest. The y-direction is the lateral direction from the right side to the left side. The z-direction is the vertical direction from the buttocks to the head. Rotation about the x-, y- and z-directions is designated as the roll (r_x), pitch (r_y) and yaw (r_z) directions, respectively.

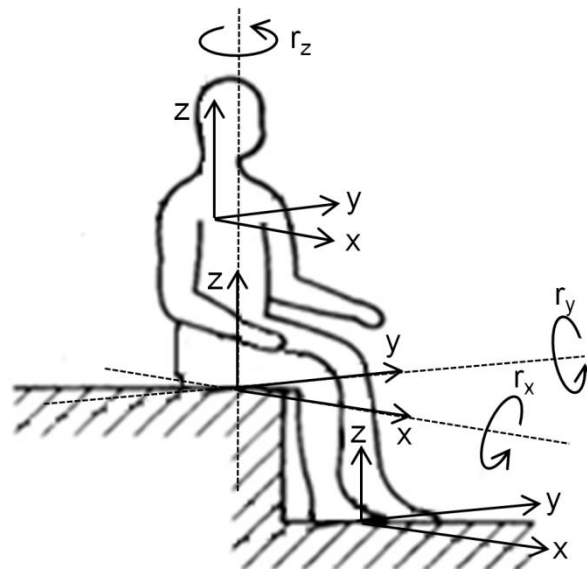


Fig. 2.1: Coordinate system of a seated person for WBV measurement and evaluation [4]

2.1 Effect of whole-body vibrations on the human being

Over the past few decades, a large number of studies have been carried out to investigate the effects of WBV on the human being. Some of them investigated the effect of long-term exposure to WBV on the human health and the effect of short-term exposure on the subjective sensation of comfort. Others investigated the human biodynamic response to the WBV.

2.1.1 Effect of whole-body vibrations on human health

Long-term exposure to WBV has adverse effects on the human musculoskeletal system, especially the lumbar spine. It is associated with a series of back problems, such as degenerative disorders of the spine, spinal disc disease and failure, and low back pain (LBP) [3],[7]. Results from previous epidemiological studies show that the LBP is more prevalent with vibration exposed workers than with non-exposed workers. For example, Boshuizen et al. investigated in 1990 that the prevalence of back pain is about 10% higher with tractor drivers than with workers not exposed to WBV [8]. Bovenzi et al. investigated that the prevalence of LBP is higher with professional drivers than with workers not exposed to WBV [9],[10].

Some authors attempted to find out the relationship between the long-term exposure to WBV and the health risks by means of reviewing high-qualified epidemiological studies. Based on the review of 19 epidemiological literature sources between 1960 and 1984 about the effect of long-term exposure to WBV on the human health, Hulshof and van Zanten concluded that the long-term exposure to WBV is harmful to the spinal system and may result in LBP, early degeneration of the lumbar spinal system and herniated disc [11]. Bovenzi and Hulshof reviewed the epidemiological studies published between 1986 and 1997 to update the information on the epidemiological evidence of adverse health effects of WBV. It was concluded from these studies that an occupational exposure to WBV is associated with an increased risk of LBP, sciatic pain, and degenerative changes in the spinal system, such as lumbar intervertebral disc disorders [12]. Lings and Leboeuf-Yde in 2000 reviewed 24 epidemiological literature sources published between 1992 and 1999 concerning the association between the WBV exposure and the LBP, and concluded that the LBP is more frequent in the group exposed to WBV [13]. Kittusamy and Buchholz in 2004 reviewed 10 studies and concluded that more musculoskeletal symptoms (specifically

in the low back area) are observed among the group exposed to WBV than the group not exposed to WBV [14].

There are enough epidemiological evidences to make a clear conclusion that the long-term exposure to WBV is associated with the work-related musculoskeletal disorders, especially the symptom of LBP. However, the WBV is not the only factor which contributes to the LBP. Prolonged sitting and awkward postures also play an important role in the prevalence of the LBP [1],[9],[10],[14],[15]. Additionally, the prevalence of musculoskeletal disorders or LBP with professional drivers is affected by some ergonomic, psychosocial and physical factors. Unsuitable ergonomic work conditions, such as uncomfortable back support, uncomfortable seat and narrow space for drivers, result in the increase of risks of LBP [16],[17]. The physical work load such as manual handling shows an association with the increase of risks of LBP as well [1],[10],[15]. Regular physical activities are helpful to decrease the risks of LBP [17],[18]. Moreover, individual factors, such as age and body mass index, are proven to have an influence on the risks of LBP also [9],[10],[15]. In the study by Alperovitch-Najenson et al., the following psychosocial factors showed significant association with the prevalence of LBP with bus drivers: limited rest periods during a work day, traffic jams on the bus route, lack of accessibility to the bus stop and passengers' hostility [17].

All of the aforementioned factors are combined together with the WBV to affect the human health. It is impossible to separate the WBV from other factors to investigate the adverse effects of WBV on the human health. This makes it tough to outline a clear dose relationship between the WBV exposure and the health risks [3],[11]-[13].

2.1.2 Effect of whole-body vibrations on comfort

Short-term exposure to WBV can cause transitory reactions of the human, such as increase of heart rate, headache, muscle fatigue, loss of balance and discomfort [3]. As a reaction to the environment, comfort is a pleasant sense associated with physiological, psychological and physical states [19]-[21]. Unequivocal definitions of comfort and discomfort are still not given, as well as the borderline between comfort and discomfort [19]. In some research works comfort and discomfort were defined as two discrete states, where comfort was simply defined as absence of discomfort and vice versa [19],[22],[23]. Many other researchers defined comfort and discomfort as two opposites on a continuous rating scale, ranging from extreme discomfort through

a neutral state to extreme comfort [19],[21],[24]. Feeling of discomfort is mainly associated with pain, tiredness, soreness, and numbness. And feeling of comfort is mainly associated with relaxation and well-being [19],[25].

Studies on the relationship between the subjective sensations and the short-term exposure to WBV started in the early 1930s. These studies were carried out based on laboratory experiments, where two investigation methods were adopted. In all these experiments, the acceleration, either its amplitude or the root mean square (RMS) value, was selected as the parameter to evaluate the vibration severity.

In the first method, tested persons adjusted the amplitudes of vibration excitations until their subjective sensations reached the predefined levels [26]-[31]. Or the tested persons were exposed to vibration excitations with different amplitudes and judged their sensation levels after the exposure [32],[33]. Curves of subjective sensation levels obtained in different studies based on this method are shown from Fig. 2.2 to Fig. 2.7.

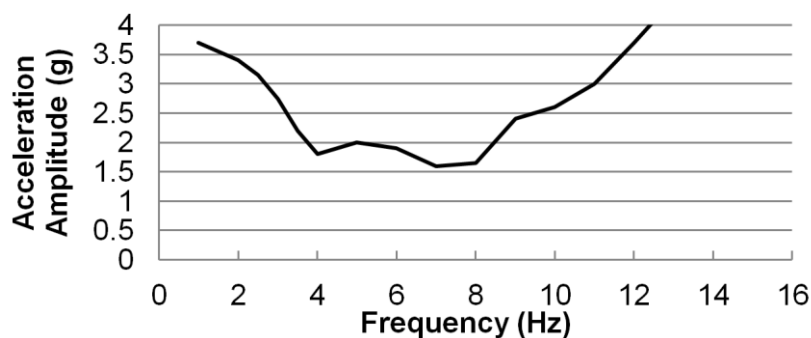


Fig. 2.2: Boundary of 'Human Vibration Tolerance' under vertical sinusoidal vibration excitations obtained by Ziegenruecker and Magid in 1959 (Tested persons sat on a seat with seat back and no cushions on seat and back) [26]

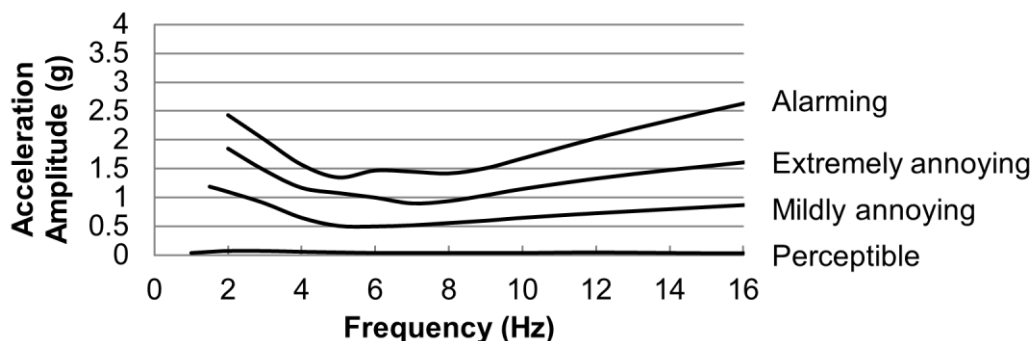


Fig. 2.3: Subjective sensation levels under vertical sinusoidal vibration excitations obtained by Chaney in 1964 (Tested persons sat on a cushioned seat with seat back)

[27]

It is obvious from figures 2.2 and 2.3 that the tested persons were most sensitive to vertical vibrations at frequencies between 4 Hz and 8 Hz. The boundary of the 'Human Vibration Tolerance' in Fig. 2.2 is higher than that of 'Alarming' in Fig. 2.3, especially at frequencies above 8 Hz. The boundary of 'Perceptible' in Fig. 2.3 shows that the human sensitivity keeps almost constant from 1 Hz to 16 Hz, when the excitation amplitude is very small.

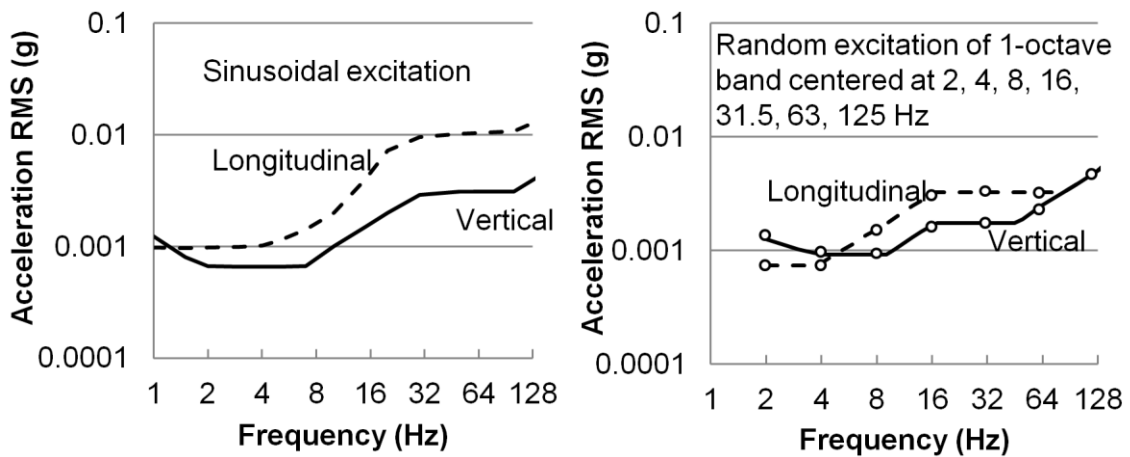


Fig. 2.4: Perceptible threshold obtained by Miwa (Tested persons sat on an aluminum vibration table without cushions, RMS: root mean square) [28],[29]

It can be observed in Fig. 2.4 that there is a little difference between the perceptible thresholds under sinusoidal excitations and random excitations. In the longitudinal direction, the tested persons were more sensitive to the random excitations. In the vertical direction, they were more sensitive to the sinusoidal excitations at frequencies below 8 Hz, but less sensitive at frequencies between 16 Hz and 64 Hz. Fig. 2.4 also shows that in the vertical direction the tested persons were most sensitive to vibrations in the range of 2-8 Hz under sinusoidal excitations, but only in the range of 4-8 Hz under random excitations. In both excitation modes, they were most sensitive to vibrations below 4 Hz in the longitudinal direction. The vertical perceptible thresholds in Fig. 2.4 are lower than that in Figure 2.3.

The human sensitivity in the roll and the pitch directions shown in Fig. 2.5 is the same with that in Fig. 2.6 between 2 Hz and 16 Hz, because the same investigation method was adopted in the studies [30] and [31]. Fig. 2.6 shows that the human sensitivity decreases largely with the increase of the excitation frequency in four directions: longitudinal, lateral, roll and pitch directions. The human sensitivity to longitudinal vibrations is similar to that to lateral vibrations. The boundary of 'Uncomfortable' in the vertical direction lies between the boundaries of 'Perceptible' and 'Mildly annoying'

in Fig. 2.3. It varies slightly depending on the excitation frequency, same as the boundary of 'Perceptible' in Fig. 2.3.

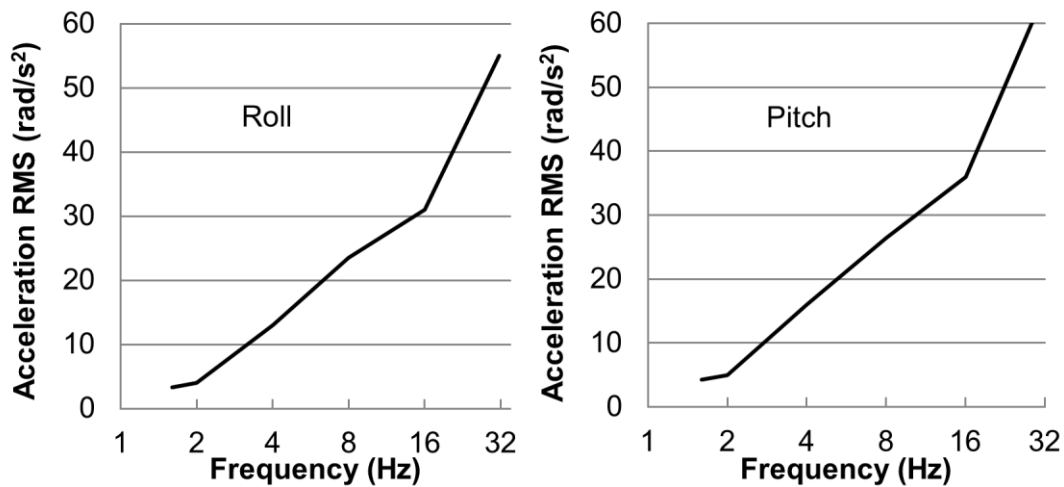


Fig. 2.5: 'Uncomfortable' boundaries under sinusoidal vibration excitations in the roll and the pitch directions obtained by Parsons and Griffin in 1978 (Tested persons sat on a wooden plate without cushions.) [30]

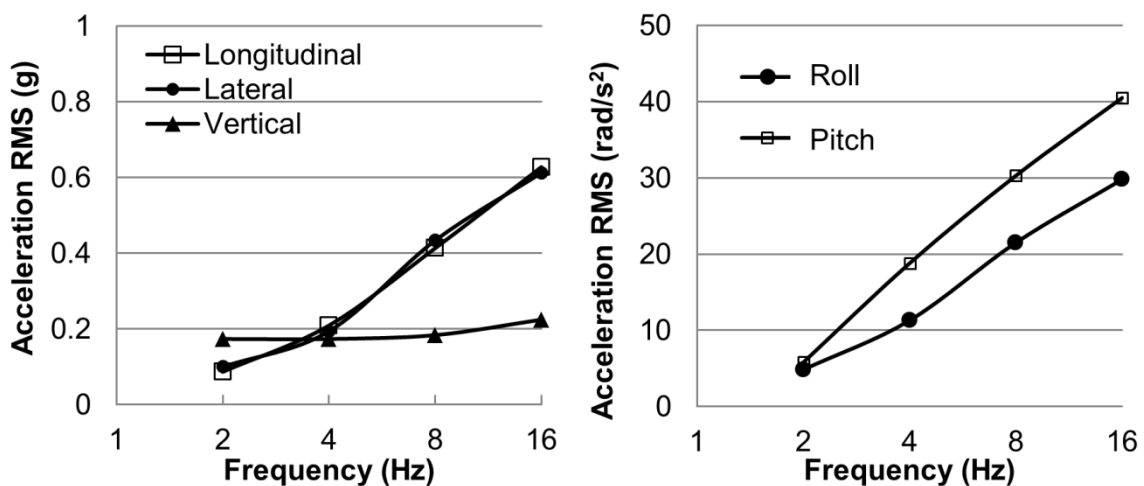


Fig. 2.6: 'Uncomfortable' boundaries under sinusoidal vibration excitations in five directions obtained by Parsons and Griffin in 1978 (Tested persons sat on a wooden plate without cushions.) [31]

The boundary of 'Tolerance' in the vertical direction in Fig. 2.7 shows that the tested persons were most sensitive to vibrations in the range of 4-6 Hz. It is at the same level with the boundary of 'Uncomfortable' in Fig. 2.6 below 8 Hz. In this direction, the boundary of 'Unpleasantness' is at the same level with the boundary of 'Perceptible' in Fig. 2.3. In horizontal directions, the tested persons were most sensitive to vibrations at frequencies below 3 Hz. The boundary of 'Uncomfortable' in Fig. 2.6 is between the boundaries of 'Tolerance' and 'Unpleasantness' in this figure.

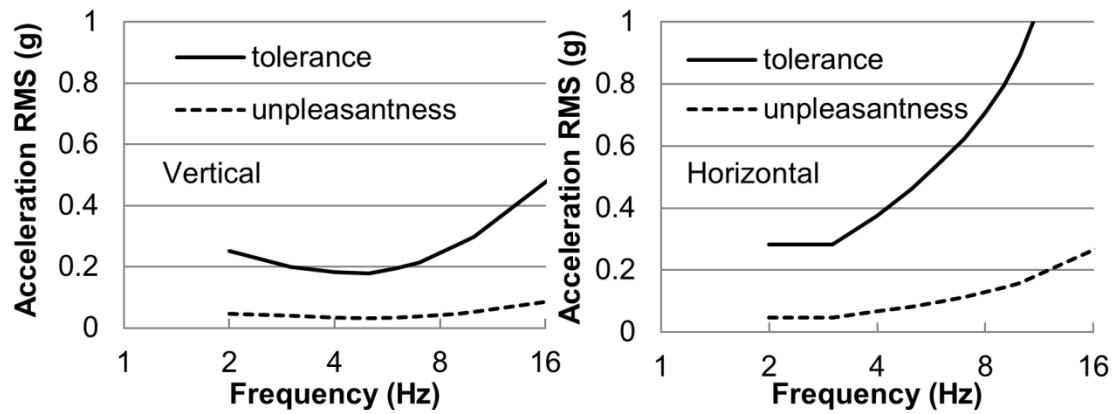


Fig. 2.7: Tolerance limits and levels of unpleasantness under sinusoidal vibration excitations in the vertical and the horizontal directions with 3 min exposure obtained by Miwa in 1968 (sat on an aluminum vibration table without cushions) [32]

In the second method, tested persons were exposed to a 'reference' excitation and a 'test' excitation alternately. They adjusted the amplitude of the 'test' excitation until it produced the same sensation level as the 'reference' excitation [28],[29],[34]-[39]. Or the tested persons estimated the intensity level of the 'test' excitation relative to the 'reference' excitation [40],[41]. With this method 'equal sensation contours' were obtained to express the relationship between subjective sensations and amplitudes of vibration excitations at different frequencies. These 'equal sensation contours' are shown in Fig. 2.8 to Fig. 2.12. The values marked on the curves in these figures represent the amplitudes of the reference excitations.

Fig. 2.8 shows that in the vertical direction the tested persons were most sensitive to sinusoidal vibrations at around 5 Hz, and below 3 Hz in the longitudinal direction. Fig. 2.9 shows that the tested persons were most sensitive to sinusoidal vibrations in the range of 4-16 Hz in the vertical direction, and below 5 Hz in the longitudinal direction. The comparison of Fig. 2.8 and Fig. 2.9 shows that the tested persons were more sensitive to sinusoidal vibrations than to random vibrations at frequencies below 12 Hz in the vertical direction and below 5 Hz in the longitudinal direction.

Fig. 2.10 shows that the tested persons were most sensitive to vertical vibrations at around 5 Hz, no matter the gender of them. 'Equal sensation contours' of women are a little lower than those of men. This means that females are more sensitive to vertical vibrations than males.

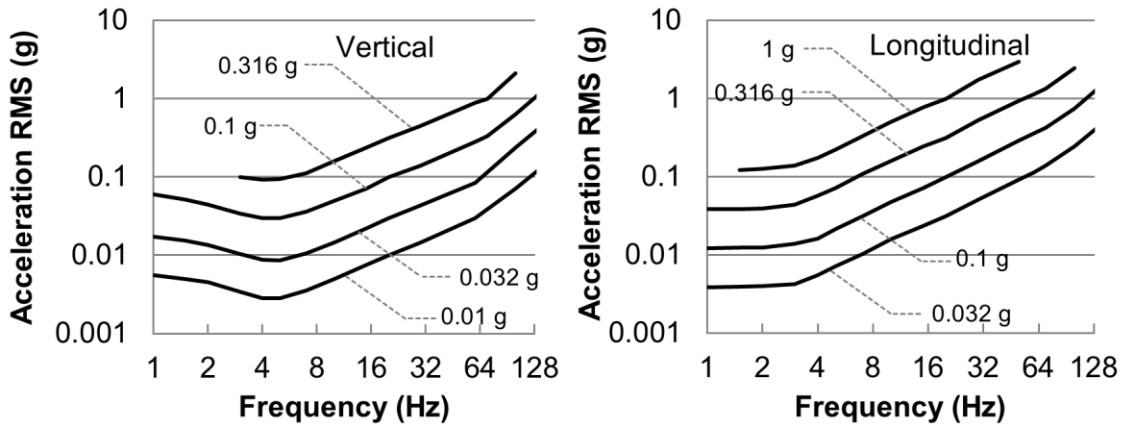


Fig. 2.8: 'Equal sensation contours' in the vertical and the longitudinal directions obtained by Miwa in 1967 (Reference excitation: sinusoidal vibrations at 20 Hz. Test excitation: sinusoidal vibrations.) [28]

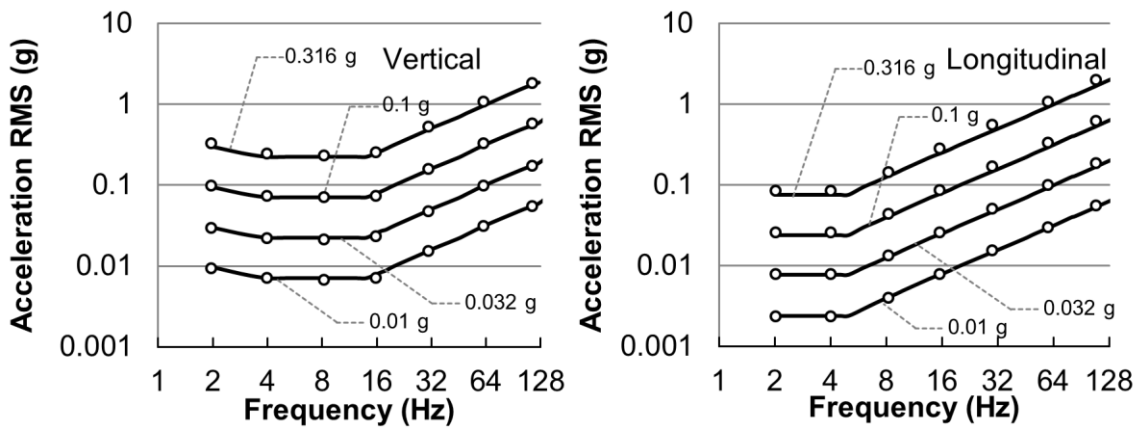


Fig. 2.9: 'Equal sensation contours' in the vertical and the longitudinal directions obtained by Miwa in 1969 (Reference excitation: sinusoidal vibrations at 20 Hz. Test excitation: 1-octave random vibrations centered at 2, 4, 8, 16, 31.5, 63, 125 Hz.) [29]

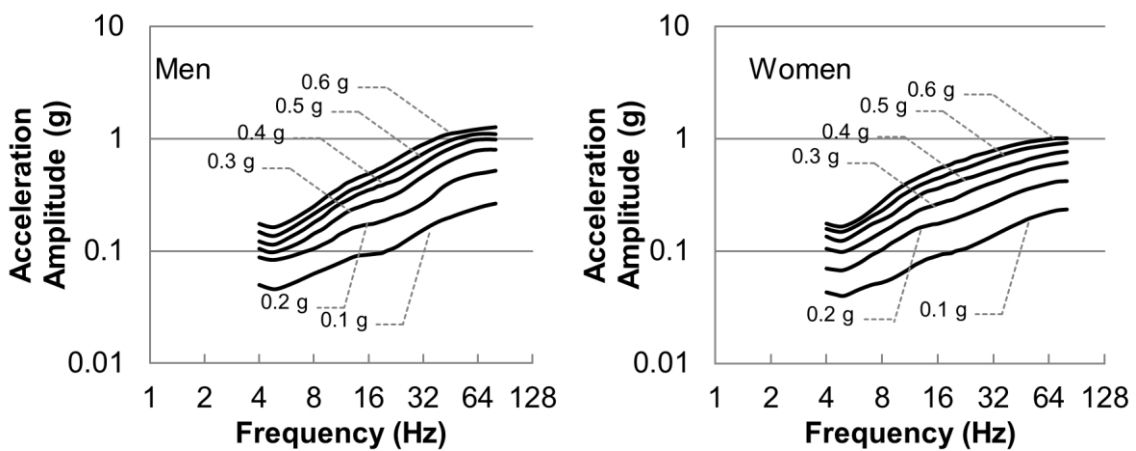


Fig. 2.10: 'Equal sensation contours' in the vertical direction obtained by Jones and Saunders in 1972 (Reference excitation: sinusoidal vibrations at 20 Hz. Test excitation: sinusoidal vibrations.) [34]

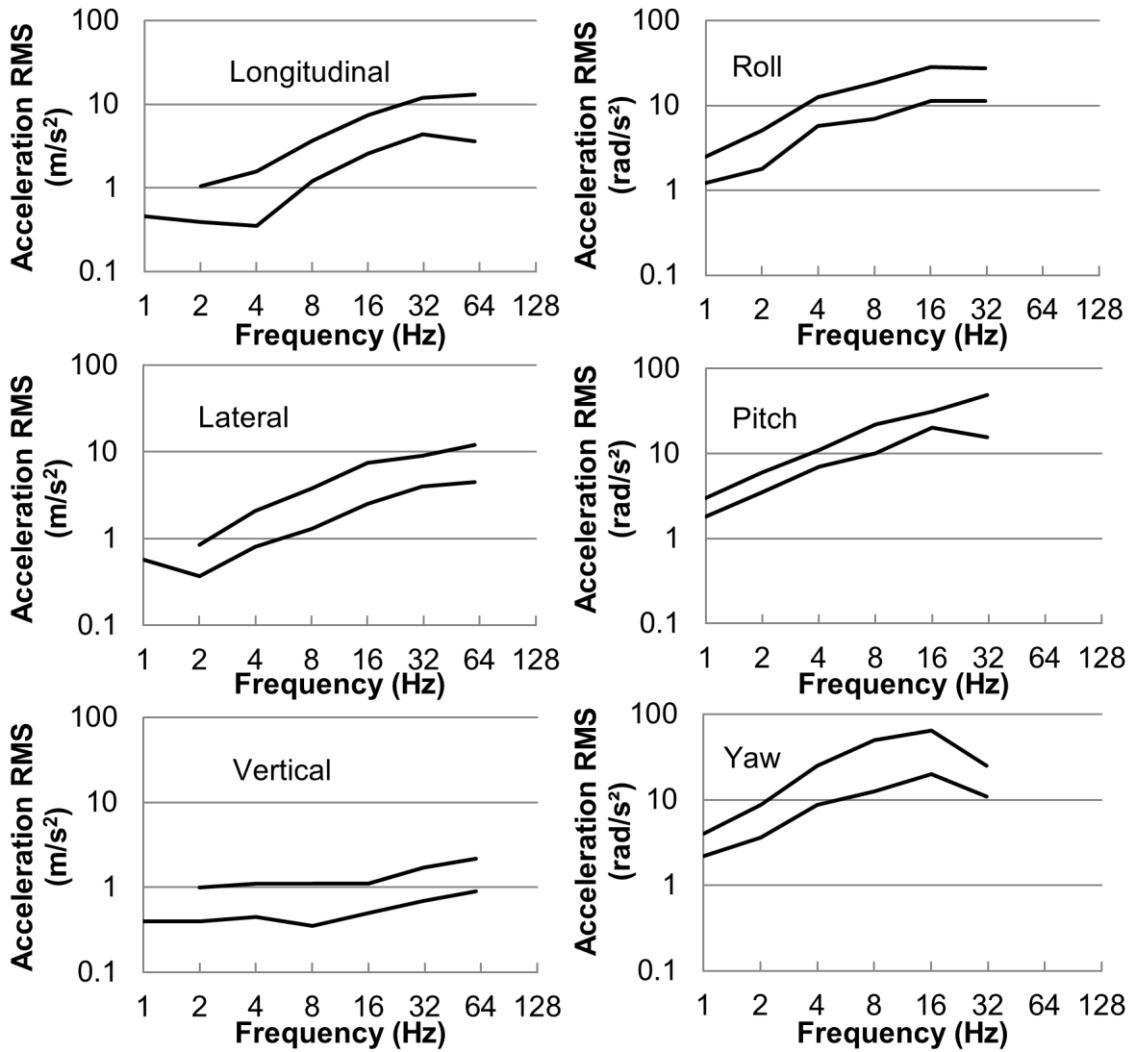


Fig. 2.11: Sensation contours equivalent to 10 Hz vertical sinusoidal vibrations with RMS of 0.5 and 1.25 m/s² obtained by Griffin and Parsons et al. in 1982 [35],[36]

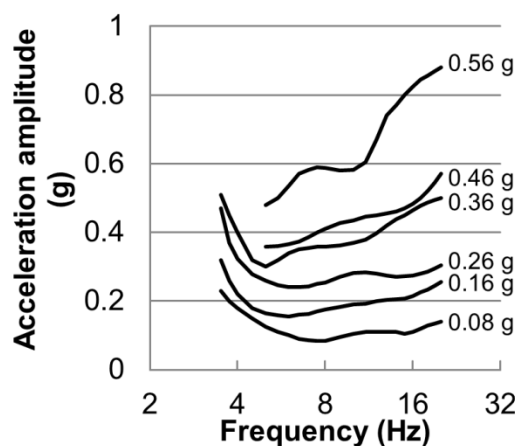


Fig. 2.12: 'Equal sensation contours' in the vertical direction obtained by Shoenberger and Harris in 1971 (Reference excitation: sinusoidal vibrations at 9 Hz) [40]

Fig. 2.11 shows that the human sensitivity decreases with the increase of the excitation frequency up to about 16 Hz in the longitudinal, lateral, roll, pitch and yaw

directions. The contours of the human sensation in the vertical direction are relatively flat in the frequency domain. The characteristics of the sensation contours in this figure are similar to those in Fig. 2.6.

It can be observed in Fig. 2.12 that the tested persons were most sensitive to vibrations at frequencies between 4 Hz and 8 Hz in the vertical direction. Under excitations with low magnitudes, the sensation contours are relatively flat between 4 Hz and 16 Hz like the curves in Fig. 2.3, Fig. 2.6, Fig. 2.7 and Fig. 2.11. Under excitations with high magnitudes, the contours have a peak at around 5 Hz.

2.1.2.1 Subjective sensations under sinusoidal and random excitations

In most of the above mentioned studies, sinusoidal excitations were adopted to investigate the relationship between the subjective sensations and the vibration excitations. In a few studies investigations were carried out with random excitations. It was observed that subjective sensations under sinusoidal excitations are different from those under random excitations with equivalent vibration intensity.

Miwa studied that human beings were more sensitive to sinusoidal vibrations than to one octave random vibrations at frequencies below 12 Hz in the vertical direction and below 5 Hz in the longitudinal direction [29]. This can be observed by comparing Fig. 2.8 and Fig. 2.9.

In contrast, Donati et al. investigated that tested persons appeared to be slightly more sensitive to random excitations than to sinusoidal excitations in the range of 1-10 Hz. This difference was observed in all three translational directions and it decreased with the increase of the excitation frequency [37]. Additionally, investigations by Corbridge and Griffin show that random vibrations produce slightly larger discomfort than sinusoidal vibrations in the frequency range of 0.5-5 Hz [41].

Mistrot et al. did not observe a difference between the averaged sensitivity to sinusoidal excitations and one-third octave random vibrations centered at 3.15 Hz [39].

2.1.2.2 Subjective sensations under excitations in different directions

Most studies investigated the subjective sensations when the tested persons were exposed to excitations in translational directions. Only a small number of studies focused on rotational excitations. Some studies attempted to find out the relationship between the subjective sensations under excitations in different directions.

Miwa investigated in 1967 that the subjective sensations under longitudinal sinusoidal vibrations are stronger by 10 dB¹ than those under vertical sinusoidal vibrations below 5 Hz, as shown in Fig. 2.8 [28],[42]. In 1969 he investigated that in terms of random excitations subjective sensations under longitudinal vibrations are stronger than those under vertical vibrations below 16 Hz, as shown in Fig. 2.9 [29].

The analysis in the study by Kirby et al. shows that the discomfort of tested persons exposed to multi-axial vibrations cannot be evaluated using vibrations in only one direction [43]. Humans are more sensitive to multi-axial random vibrations than to single-axial random vibrations. Equivalent comfort curves under multi-axial random vibrations are 15-20% lower than those under single-axial vibrations [44]. Studies [45] and [46] show that the vector sum value (VSV) of the root mean square (RMS) of the vibration accelerations in both axes give an adequate prediction of the subjective sensations, when tested persons are exposed to dual-axial vibrations.

2.1.2.3 Subjective sensations with different exposure durations

A few studies investigated the effect of exposure durations on the subjective sensations. Jones and Saunders obtained the 'reduced comfort boundary (RCB)' when the tested persons were exposed to vertical sinusoidal excitations with different durations, as shown in Fig. 2.13 [34].

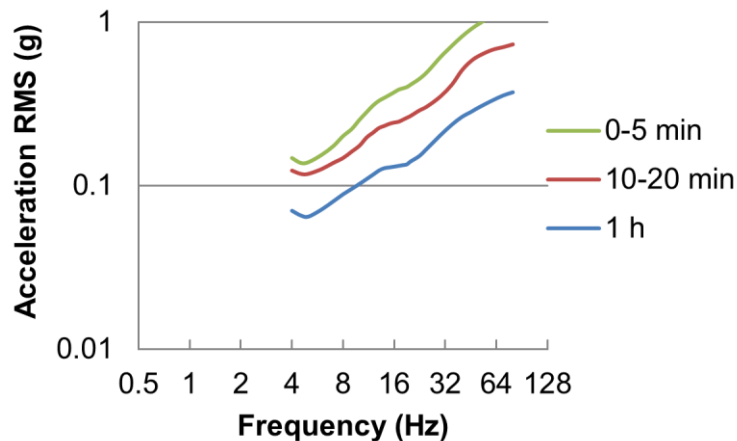


Fig. 2.13: Reduced comfort boundary (RCB) under the vertical sinusoidal excitations obtained by Jones and Saunders [34]

Miwa obtained in 1968 the tolerance limits and the levels of unpleasantness for a 3 min exposure, Fig. 2.7. He studied that if the exposure is shorter than 10 min, the exposure duration has no effect on the sensations of tolerance and unpleasantness;

¹ 1 dB=20log₁₀(a/a_{ref}); a_{ref}=10⁻³g; a is the acceleration RMS values, as the values of curves in Fig. 2.8.

if the exposure exceeds 10 min, the sensation-duration relationship is similar to that in ISO/TC 108/WG 7/Secr. 6:1966² [32]. Fig. 2.14 shows the diagrams with the tolerance limits and the levels of unpleasantness for different durations derived from the sensation-duration relationship of Miwa. Demic and Lukic as well obtained a series of boundaries of 'comfortable ride' for persons exposed to longitudinal or vertical random excitations with different durations [44]. These boundaries are shown in Fig. 2.15.

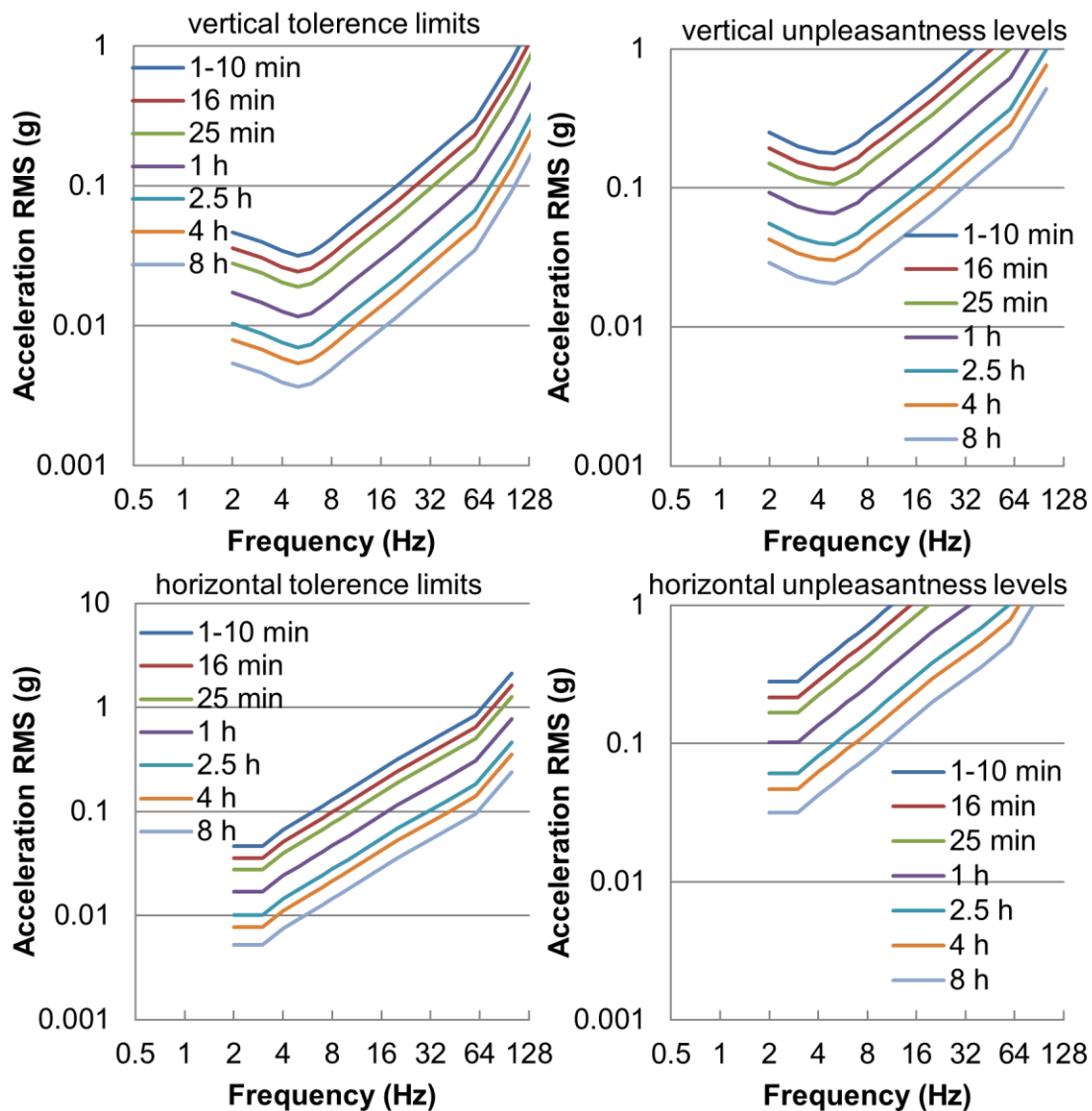


Fig. 2.14: Tolerance limits and levels of unpleasantness for different durations derived from the sensation-duration relationship of Miwa

² The sensation-duration relationship in ISO/TC 108/WG 7/Secr. 6:1966 is same with that in ISO 2631-1:1985 [47].

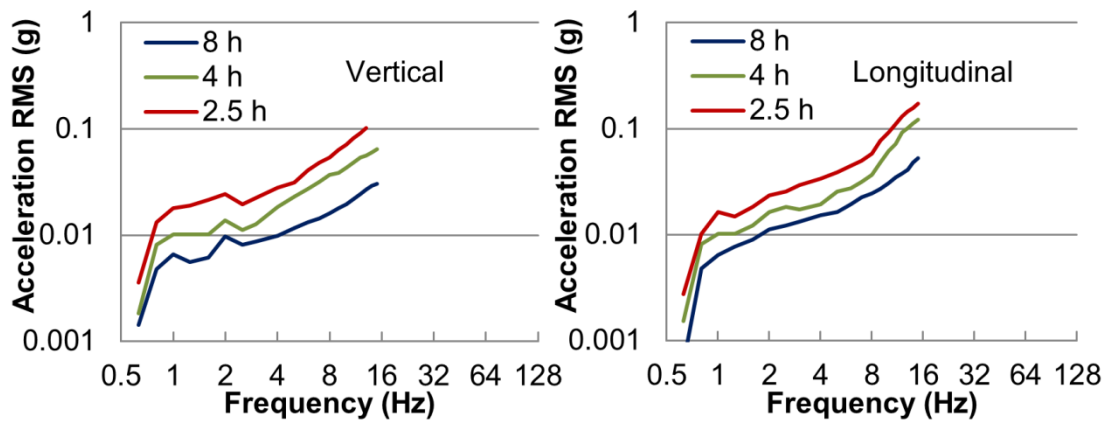


Fig. 2.15: Boundaries of 'comfortable ride' under vertical or longitudinal random excitations obtained by Demic and Lukic in 2002 [44]

Fig. 2.13 to Fig. 2.15 show that the comfort decreases with the increase of the exposure duration. The RCB curves in Fig. 2.13 are at the same level with the levels of unpleasantness in Fig. 2.14. The curves in Fig. 2.15 are a little different from those in Fig. 2.13 and Fig. 2.14 at frequencies above 2 Hz, where in the vertical direction the peaks occur at around 2.5-3 Hz in Fig. 2.15, but at around 5 Hz in Fig. 2.13 and Fig. 2.14. At frequencies from 2 Hz to 3 Hz, the curves in the longitudinal direction in Fig. 2.14 are flat, but they rise with the frequency in Fig. 2.15. These differences are mainly caused by the different investigation methods in three studies, especially the excitation signals. Random vibrations in 1/3 octave bands were used in the study by Demic and Lukic, but the sinusoidal vibrations were used in two other studies. The study by Demic and Lukic also gives the boundaries of 'comfortable ride' below 2 Hz [44]. It can be observed that the tested persons were most sensitive to vertical and longitudinal vibrations below 1 Hz. The authors attributed this to the psychological aspects based upon the walking process [44].

It is obvious that there are discrepancies existing in the relationship between the subjective sensations and the vibration excitations obtained in the studies involved in section 2.1.2. They are possibly caused by the following reasons: 1). difference in magnitude, frequency and direction of the excitation signals; 2). influence of some factors on the subjective sensations, such as noise, posture of tested persons and environment of experiment; 3). limited number of tested persons in the experiment. However, it is valid to make a conclusion from these studies that the discomfort caused by WBV is affected by several factors, such as the frequency and acceleration magnitude of the vibration excitations, the excitation directions and the exposure durations. Generally, human beings are most sensitive to vibrations in the

range of 4-6 Hz in the vertical direction, and at frequencies below 5 Hz in the longitudinal direction. It was investigated in some studies that the human sensitivity to lateral vibrations has similar characteristics as that to longitudinal vibrations. In the three rotational directions, the human sensitivity decreases with the increase of the excitation frequency. There is no doubt that discomfort increases with the excitation magnitudes and durations.

2.1.3 Human biodynamic response to whole-body vibrations

Four parameters can be used to study the human biodynamic response to WBV: the driving-point mechanical impedance (DPMI), the apparent mass, the absorbed power and the seat-to-head transmissibility (STHT). To gain the first three parameters, accelerations and forces measured at the driving point are needed. The driving point is the contact point at the interface between the tested person and the vibrating surface. For the seated person, the driving point is on the top surface of the seat cushion. For the fourth parameter, accelerations measured at the driving point and at the head are needed. The DPMI, the apparent mass and the STHT are defined as ratios and are calculated as transfer functions. The transfer function is usually calculated based on the cross spectral density (CSD) method as formulated in Eq. (2.1). [48]-[50]

$$TF(f) = \frac{G_{io}(f)}{G_{ii}(f)} = \frac{FFT[i(t)]^* \cdot FFT[o(t)]}{FFT[i(t)]^* \cdot FFT[i(t)]} \quad (2.1)$$

with

$FFT[i(t)]$	Complex fast Fourier transform (FFT) of input signal
$FFT[i(t)]^*$	Complex conjugation of the $FFT[i(t)]$
$FFT[o(t)]$	Complex FFT of output signal
$G_{ii}(f)$	Power spectral density (PSD) of input signal as a function of frequency
$G_{io}(f)$	CSD of input and output signals as a function of frequency
$TF(f)$	Transfer function in the frequency domain

The input and output signals for the calculation of the DPMI, the apparent mass and the STHT are listed in Tab. 2.1.

Tab. 2.1: Input and output signals to calculate the DPMI, the apparent mass and the STHT

Calculated parameters	Input signal	Output signal
DPMI	Velocity at the driving point	Force at the driving point
Apparent mass	Acceleration at the driving point	Force at the driving point
STHT	Acceleration at the driving point	Acceleration at the head

The velocity at the driving point can be converted from the acceleration at the same position using Eq. (2.2) [48].

$$v(f) = \frac{a(f)}{2\pi f} \quad (2.2)$$

with

$a(f)$ Acceleration as a function of frequency in m/s^2
 $v(f)$ Velocity as a function of frequency in m/s

The absorbed power is defined as the product of force and velocity at the driving point. The instantaneous vibration power transmitted to the human body is calculated as the CSD of force and velocity at the driving point. The real part of the instantaneous power represents the power absorbed by the human body. The absorbed power can be calculated using Eq. (2.3). [50]

$$P_{abs}(f) = \text{Re}\{G_{Fv}(f)\} = |G_{Fv}(f)| \cos \sigma(f) \quad (2.3)$$

with

$G_{Fv}(f)$ CSD of force and velocity as a function of frequency in $(\text{N}\cdot\text{m/s})/\text{Hz}$
 $P_{abs}(f)$ Absorbed power as a function of frequency in $(\text{N}\cdot\text{m/s})/\text{Hz}$
 σ Phase of $G_{Fv}(f)$ in rad

Frequencies where peaks occur can be observed from curves of these four parameters in the frequency domain. These frequencies are the resonance frequencies of the human as a mass-spring-damper system. By analyzing these four parameters, the human in-line and cross-axial biodynamic response to WBV was studied by many researchers.

2.1.3.1 Human in-line biodynamic response

The human in-line biodynamic response in the three translational directions is nonlinear and affected by a series of factors, such as the employment of a backrest, the excitation magnitude, the posture or the muscle tension of the person, the gender, and more. Due to the nonlinearity of the human biodynamic response, the primary resonance frequencies of humans were observed in a wide frequency range. In the longitudinal direction, the primary resonance frequencies of seated persons were observed in the range from 1 Hz to 6 Hz [51]-[54]. In the lateral direction, they lie below 2.5 Hz [51]-[54]. In the vertical direction, they were observed in the range from 4 Hz to 6 Hz [52],[53],[55]-[60]. These frequency ranges are in general consistent with the most sensitive frequency ranges reviewed in section 2.1.2.

In some studies, the secondary resonance frequencies in the lateral direction were observed in the range from 5 Hz to 7 Hz [52],[54]. In the vertical direction they were observed in the range from 8 Hz to 12 Hz [52],[53],[55]-[60].

The backrest has a pronounced influence on the human biodynamic response in the longitudinal direction, where the employment of a backrest results in a obvious increase of the primary resonance frequency of the seated person. In Tab. 2.2, a comparison of the primary resonance frequencies in the longitudinal direction with and without a backrest is presented.

Tab. 2.2. Primary resonance frequencies of seated persons in the longitudinal direction with and without a backrest

Authors	Primary resonance frequency	
	Without backrest	With a rigid backrest
Nawayseh and Griffin [50]	Around 1 Hz	In the range of 3-5 Hz
Fairley and Griffin [51]	Around 0.7 Hz	Around 3.5 Hz
Nawayseh and Griffin	Below 3 Hz [61]	In the range of 2-6 Hz [62]
Mansfield and Maeda [63]	Below 1 Hz	In the range of 2-4 Hz
Qiu and Griffin	Below 2 Hz [64]	In the range of 3-6 Hz [65]

The influence of the backrest on the primary resonance frequency of the seated person in the lateral and the vertical directions is not that significant. Fairley and Griffin investigated that the primary resonance frequency of the seated person in the

lateral direction shifts from about 0.7 Hz without backrest to about 1.5 Hz with a backrest [51]. Mansfield and Maeda investigated that the primary resonance frequency of the seated person in the lateral direction is almost constant and less than 2 Hz, no matter with or without a backrest [63]. With a backrest, the primary resonance frequency of the seated person in the vertical direction increases only a little bit [55].

The excitation magnitude has a significant influence on the human biodynamic response as well. The primary resonance frequency of the seated person decreases with the increase of the excitation magnitude. This phenomenon is significant in the longitudinal and the vertical directions, of which the variation of the primary resonance frequency depending on the excitation magnitude is presented in Tab. 2.3. It is negligible in the lateral direction [51],[53],[54].

Tab. 2.3. Variation of primary resonance frequency of the seated person depending on the excitation magnitudes

Authors	Magnitude of excitations (m/s² RMS)	Primary resonance frequency (Hz)	Direction
Hinz et al. [53]	From 0.25 to 2.0	From 2.94 to 2.18	longitudinal
Hinz et al. [53]	From 0.25 to 2.0	From 5.14 to 4.41	vertical
Fairley and Griffin [55]	From 0.25 to 2.0	From 6 to 4	vertical
Qiu and Griffin [65]	From 0.25 to 1.0	From 4.9 to 3.5	longitudinal
Qiu and Griffin [65]	From 0.25 to 1.0	From 5.9 to 4.7	vertical
Matsumoto and Griffin [66]	From 0.35 to 1.4	From 5.25 to 4.25 ³	vertical
Matsumoto and Griffin [66]	From 0.35 to 1.4	From 5.0 to 4.38 ⁴	vertical
Matsumoto and Griffin [66]	From 0.35 to 1.4	From 5.13 to 4.5 ⁵	vertical

In addition to the above mentioned aspects, gender results in different characteristics of the human biodynamic response as well. It has been proven that females and males have different biodynamic responses to WBV in all three translational directions. The difference mainly occurs in the lateral and the vertical directions,

³ with the normal muscle tension

⁴ with the buttocks muscles tensed

⁵ with the abdominal muscles tensed

where the secondary resonance frequency is more distinct for the female than for the male. [52],[54],[57],[60]

Additionally, the human biodynamic response is affected by the posture and the muscle tension. Compared to the relaxed body posture, the erect posture or the tensed muscle results in a higher primary resonance frequency of the seated person in the vertical direction. [55],[57],[60]

In a few studies it was investigated that the location of the feet, the arm angle, and the hand position affect the human biodynamic response as well [61],[62],[67]-[69].

2.1.3.2 Human cross-axial biodynamic response

After a sufficient understanding of the human in-line biodynamic response, several studies were devoted to the investigation of the human cross-axial biodynamic response. It is defined as the human biodynamic response in one direction when the human is exposed to the vibrations in another direction. In studies by Nawayseh and Griffin it was proven that vibration excitations in the longitudinal direction cause large human biodynamic response in the vertical direction and relative small response in the lateral direction [61],[62]. Qiu and Griffin investigated that vibration excitations in the vertical direction cause large human biodynamic response in the longitudinal direction [64],[65].

The human cross-axial biodynamic response is also nonlinear and affected by many factors, such as the excitation magnitude and the existence of a backrest. It was investigated that the primary resonance frequency of the seated person in one direction decreases with the increase of the excitation magnitude in the other direction under dual-axial (the longitudinal and the vertical directions) excitations. The primary resonance frequency of the seated person in the longitudinal direction was observed in the range from 3 Hz to 8 Hz under vertical excitations, no matter with or without a backrest. Two resonance frequencies of the seated person were observed in the vertical direction under longitudinal vibrations without a backrest: one is at around 1 Hz; the other is in the range from 3 Hz to 8 Hz. With the backrest the resonance frequency at around 1 Hz disappears. [64],[65]

2.1.4 Lumped-parameter models of human body

Lumped-parameter models (LPMs) with different degrees of freedom (DOF) of the human body were developed to simulate the human biodynamic response in the three translational directions. In the vertical direction, LPMs with single-DOF up to four-DOF of the human body were generally utilized in the suspension seat-occupant models to simulate the dynamic behavior of the human body. Sometimes, a rigid mass was employed to represent the human body. Only a few studies focus on the development of a LPM to simulate the human biodynamic response in the longitudinal or the lateral direction. Several models consider the human rotational movement as well (refer to Fig. 2.19 in 2.1.4.2 and Fig. 2.22 in 2.1.4.4).

2.1.4.1 Lumped-parameter models in the vertical direction

In the study by Rakheja et al., two LPMs of the human body (a single-DOF model and a two-DOF model) were integrated with a suspension seat model to study the dynamic response of the suspension seat-occupant system [70]. The single-DOF model was proposed by Coermann and Whittwer [71], and the two-DOF model was proposed by Suggs et al. [72]. These two LPMs are illustrated in Fig. 2.16.

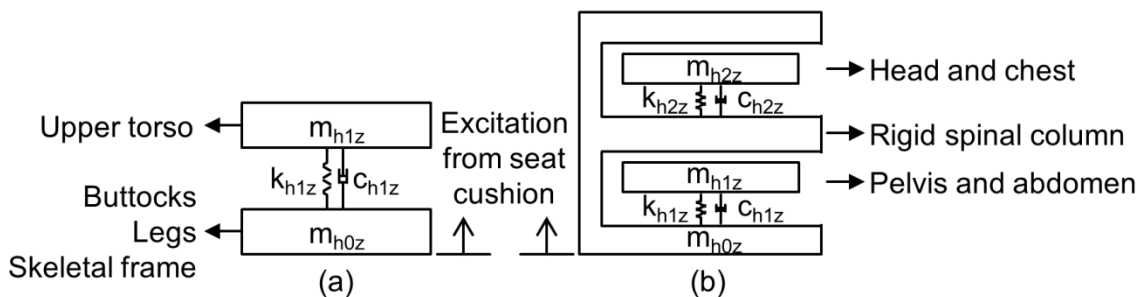


Fig. 2.16. Single-DOF (a) and two-DOF (b) LPMs of the human body used in the suspension seat-occupant models by Rakheja et al. [70]-[72]

In the study by Tchernychouk et al., in addition to the two LPMs in Fig. 2.16, a four-DOF LPM of the human body was integrated with a nonlinear cushion model to simulate the dynamic characteristics of the cushion-occupant system [73]. This four-DOF LPM, which was proposed by Boileau [74], is illustrated in Fig. 2.17.

In the study by Stein et al., suspension seat-occupant models were developed to predict the vibration attenuation performance of a suspension seat. Two three-DOF LPMs and a rigid mass were adopted to simulate the dynamic behavior of the driver [75]. These two LPMs, which are illustrated in Fig. 2.18, were introduced in ISO 5982 [76] and DIN 45676 [77] respectively.

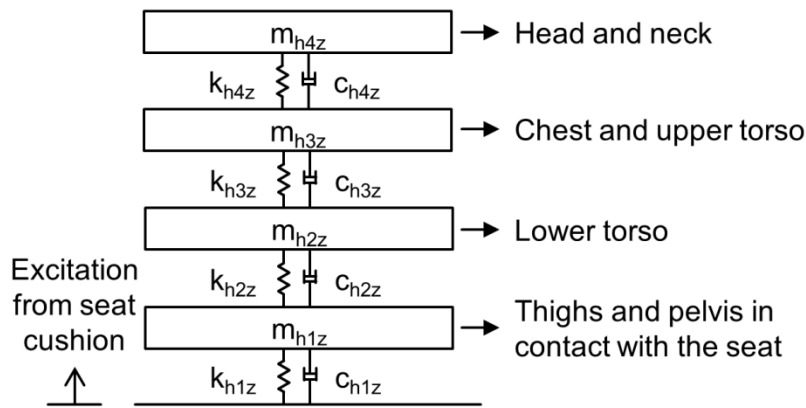
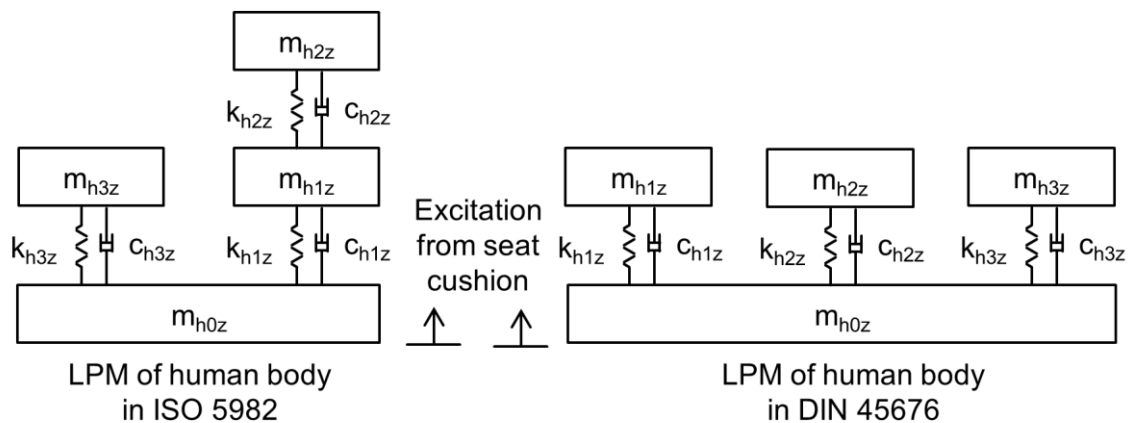


Fig. 2.17. Four-DOF LPM of the human body proposed by Boileau [74]



These two models do not correspond to physiological structure of the human body.

Fig. 2.18. Three-DOF LPMs of human body introduced in ISO 5982 and DIN 45676 [75]-[77]

2.1.4.2 Lumped-parameter models in the longitudinal direction

In the study by Fleury et al. two three-DOF lumped-parameter models (LPMs) were proposed to simulate the dynamic behavior of the cushion-occupant system in the longitudinal direction [78]. These two models are illustrated in Fig. 2.19. The 'Model A' was proposed for the case that there is no connection between driver and seat back. The 'Model B' was proposed for the case that there is connection between driver and seat back.

In the study by Stein et al. a two-DOF LPM of the cushion-occupant system was developed to simulate the dynamic behavior of this system in the longitudinal direction [79]. Interaction with the steering wheel was taken into consideration in this model, as shown in Fig. 2.20.

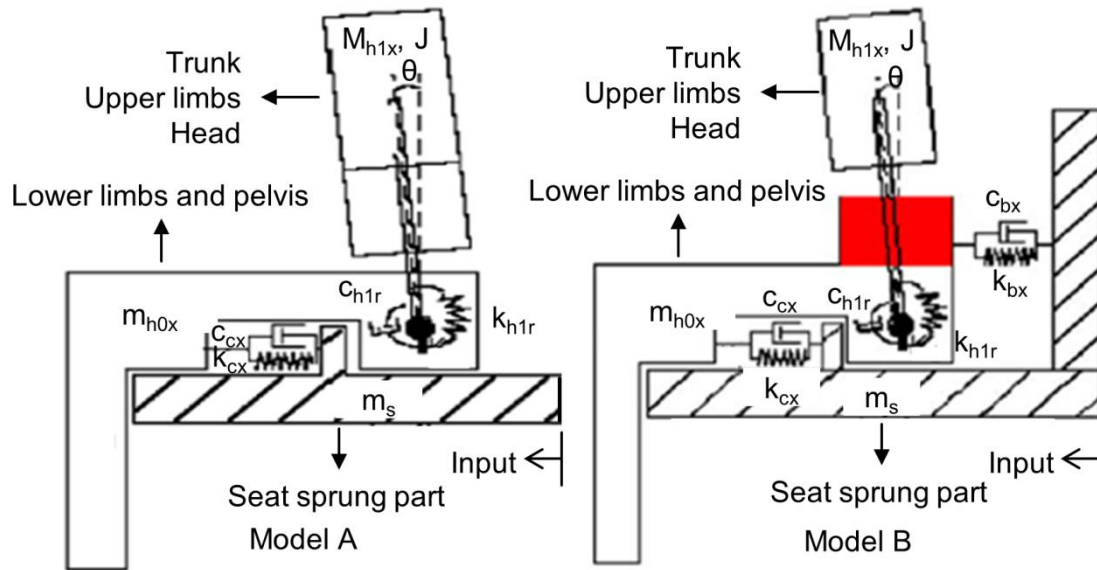


Fig. 2.19. LPMs of cushion-occupant system in the longitudinal direction developed by Fleury et al. [78]

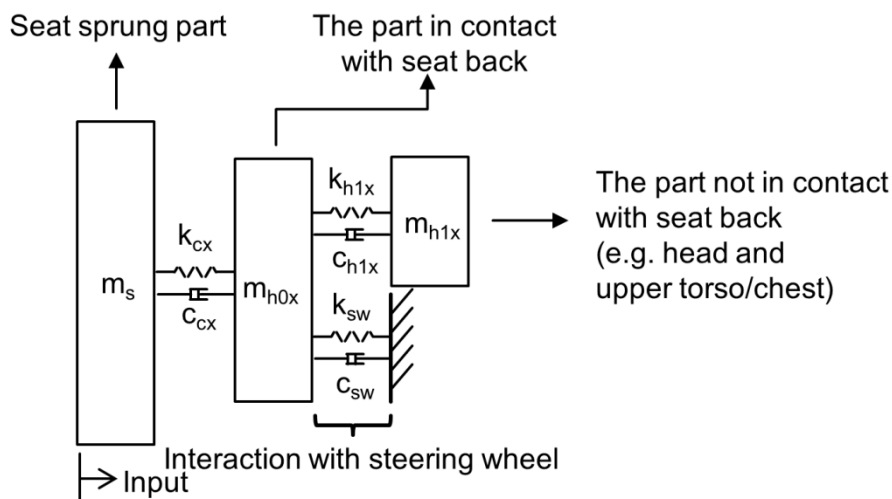


Fig. 2.20. Two-DOF LPM of cushion-occupant system in the longitudinal direction developed by Stein et al. [79]

2.1.4.3 Lumped-parameter models in the lateral direction

Stein et al. also proposed three three-DOF lumped-parameter models (LPMs) of a seat back-occupant system, as illustrated in Fig. 2.21, to calculate the apparent mass of the human body in the lateral direction [80]. Compared to the 'Model D', the discrepancies between measured and simulated apparent mass with the 'Model C' or the 'Model E' are much smaller. The 'Model C' was determined as the best model because it has a similar structure as the human torso.

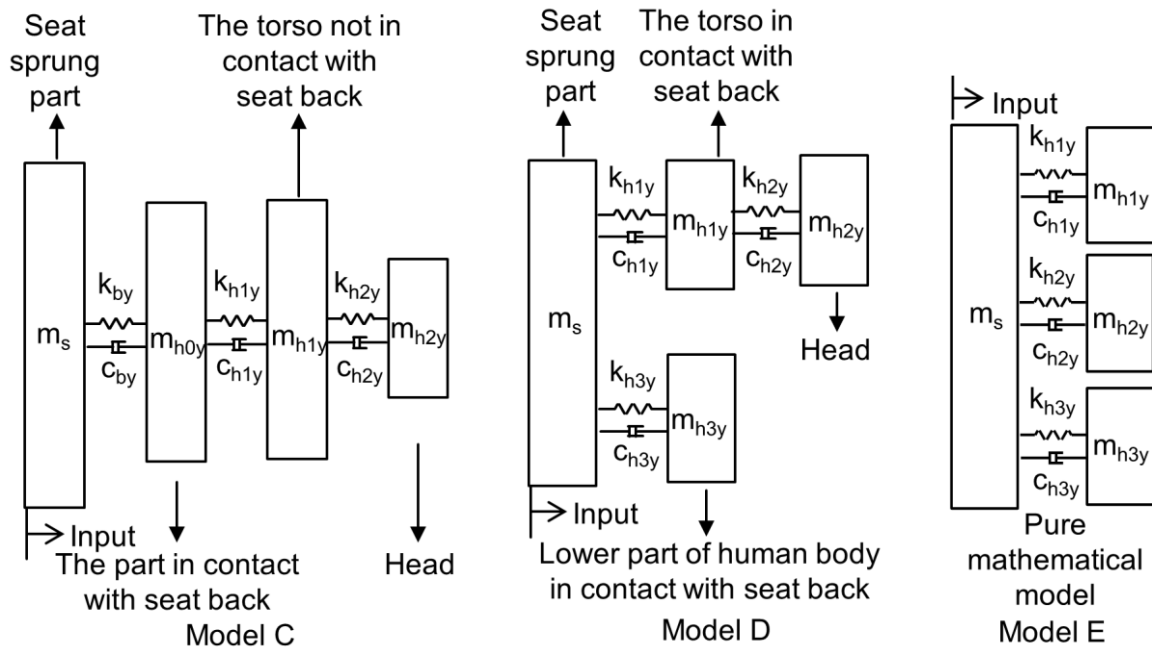


Fig. 2.21. Three-DOF LPMs of seat back-occupant system in the lateral direction proposed by Stein et al. [80]

2.1.4.4 A model to simulate the human cross-axial biodynamic response

The above mentioned lumped-parameter models (LPMs) were proposed to simulate the human in-line biodynamic response. The review mentioned in section 2.1.3.2 shows that the human cross-axial biodynamic response is also obvious. Nawayseh and Griffin proposed a LPM to simulate the human in-line (vertical response to vertical excitations) and cross-axial (longitudinal response to vertical excitations) biodynamic response simultaneously [81]. This model, as shown in Fig. 2.22, is not used in other studies for the simulation of the dynamic behavior of a suspension seat-occupant system.

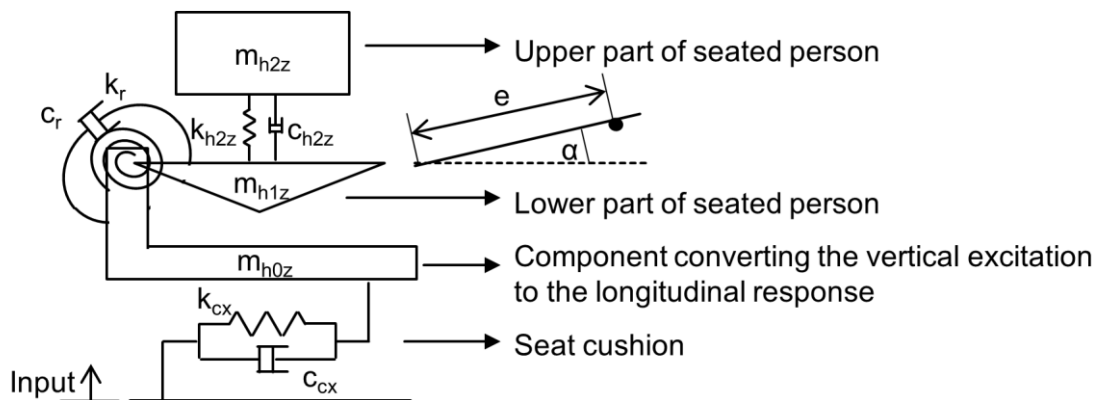


Fig. 2.22. LPM of cushion-occupant system proposed by Nawayseh and Griffin to simulate the human in-line and cross-axial biodynamic response [81]

2.2 Evaluation of effect of whole-body vibrations on human being

The International Organization for Standardization (ISO) publishes the ISO 2631 standards. In these standards procedures to evaluate the effects of whole-body vibrations (WBV) on the human health and the ride comfort are proposed. The preparations of the ISO 2631 started in 1966. The norm was first published in 1974 and then republished in 1978. In the 1978 version, editorial changes were made, including corrections of errors in tables and figures. A set of amendments was issued in the 1982 version. A combination of the content in the 1978 version and the amendments in the 1982 version was republished in 1985 (ISO 2631-1:1985 [47]). A complete revision of ISO 2631-1:1985 was published in 1997, i.e. ISO 2631-1:1997 [4]. [82],[83] Today the ISO 2631-1:1997 is the primary standard to evaluate the effects of WBV on the human health and the ride comfort.

As a general standard for the evaluation of WBV exposure levels, the ISO 2631-1:1997 makes a reference to ISO 2631 Parts 2 and 4 concerning the WBV in buildings (1-80 Hz) and in fixed-guideway transport systems respectively [84],[85]. Part 3 of ISO 2631 [86], concerning the vertical WBV in the frequency range of 0.1-0.63 Hz, was firstly published in 1985 and finally integrated into ISO 2631-1:1997.

In 2004, Part 5 of ISO 2631, ISO 2631-5:2004 [5], was published, in which a new health hazard assessment method is introduced. This method was developed in a research program conducted by the United States Army Aeromedical Research Laboratory [87]. The ISO 2631-5:2004 is used to evaluate the health effects caused by WBV containing multiple shocks.

Another three standards from Europe, BS 6841:1987 [88], 2002/44/EC [89] and VDI 2057:2002 [90], are also extensively used to evaluate the effects of WBV on the human health. The evaluation procedures in these three standards are roughly similar to that in ISO 2631-1:1997. The main difference between BS 6841:1987 and ISO 2631-1:1997 is that the frequency weighting filters for the vertical accelerations on the seat cushion are different. In addition, in BS 6841:1987 the vibration total value of the three translational accelerations on the seat cushion and the longitudinal accelerations on the seat backrest is recommended to evaluate the effects of WBV on the human health. But in ISO 2631-1:1997 the highest value or the vibration total value of the three translational accelerations on the seat cushion is recommended. The boundaries of the health guidance caution zone (HGCZ) in ISO 2631-1:1997 and

the three European standards are also different. All of these differences have been discussed exhaustively in studies by Griffin [82],[91].

2.2.1 Evaluation of effect on human health

Different procedures are given in ISO 2631-1:1997 and ISO 2631-5:2004 to evaluate the effects of WBV on the human health. Each procedure includes six steps, as described in Tab. 2.4. Detailed specifications in each step of these procedures are introduced in the following paragraphs of this section.

Tab. 2.4. General evaluation procedures in ISO 2631-1:1997 and ISO 2631-5:2004

	ISO 2631-1:1997	ISO 2631-5:2004
Step 1	Measure and store accelerations in the x-, y- and z-directions on the seat cushion.	
Step 2	Calculate the frequency weighted accelerations using the frequency weighting filters.	Calculate the spine accelerations using the spine models.
Step 3	Calculate the root mean square (RMS) value \tilde{a}_w , the vibration dose value (VDV) and the maximum transient vibration value (MTVV).	Identify the acceleration peaks.
Step 4	Analyze the values of crest factor (CF), $MTVV/\tilde{a}_w$ and $VDV/(\tilde{a}_w T^{1/4})$ to determine the suitable quantification method (T represents the duration of vibration measurement in s).	Calculate the acceleration dose D.
Step 5	Select directions for the evaluation.	Calculate the equivalent static compressive stress S_e .
Step 6	Estimate the daily WBV exposure and compare with the health guidance caution zone (HGCZ). Calculate the permitted daily exposure duration.	

The crest factor (CF) in Tab. 2.4 can be calculated with Eq. (2.4) [4].

$$CF = \left| \frac{\max(a_w(t))}{\tilde{a}_w} \right| \quad (2.4)$$

with $a_w(t)$ Frequency weighted accelerations as a function of time in m/s^2
 \tilde{a}_w Root mean square (RMS) value of frequency weighted accelerations in m/s^2

2.2.1.1 Evaluation procedure in ISO 2631-1:1997

In step 2, the frequency weighting filter W_d is used for the accelerations in the x- and y-directions. The W_k filter is used for the accelerations in the z-direction. Details of the frequency weighting filters are described in ISO 8041 [92], including the mathematical expressions and the numerical values. The curves of W_d and W_k are illustrated in Fig. 2.23.

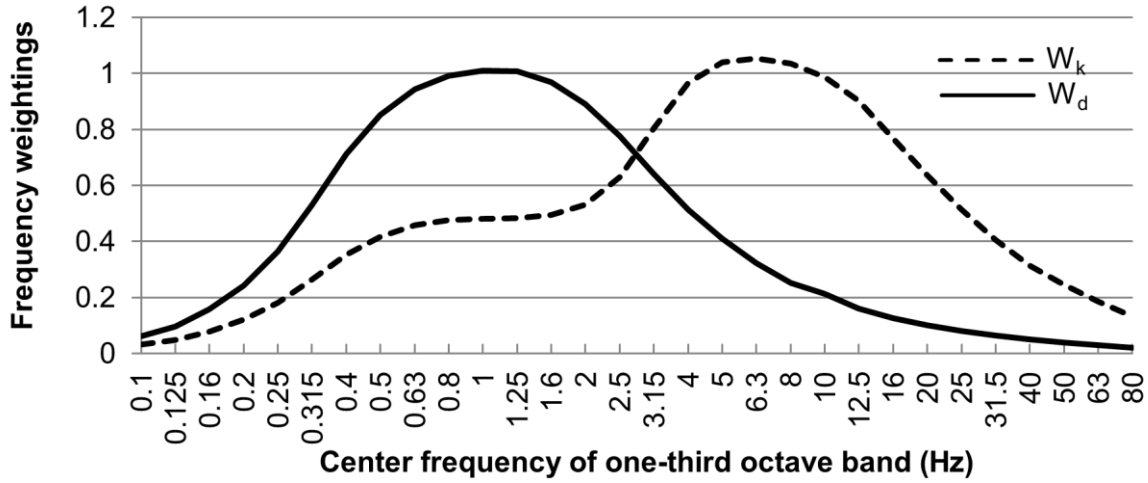


Fig. 2.23: Curves of frequency weighting filters W_d and W_k

In step 3, the RMS value \tilde{a}_w , the VDV and the MTVV of the frequency weighted accelerations are calculated with Eq. (2.5)-(2.8).

$$\tilde{a}_w = \left[\frac{1}{T} \int_0^T a_w^2(t) dt \right]^{1/2} \quad (2.5)$$

$$MTVV = \max[a_w(t_0)] \quad (2.6)$$

$$a_w(t_0) = \left[\frac{1}{\tau} \int_{t_0-\tau}^{t_0} a_w^2(t) dt \right]^{1/2} \quad (2.7)$$

$$VDV = \left[\int_0^T a_w^4(t) dt \right]^{1/4} \quad (2.8)$$

with

$a_w(t_0)$	Running RMS values of frequency weighted accelerations as a function of time in m/s^2
τ	Integration time for running averaging in s
t_0	Time of observation (instantaneous time) in s

In step 4, the suitable quantification method is determined depending on the values of CF, $MTVV/\tilde{a}_w$ and $VDV/(\tilde{a}_w T^{1/4})$. If the value of CF does not exceed 9, the RMS

method is sufficient to evaluate the effect of WBV. Otherwise, the RMS method has the potential to underestimate the effect of WBV. In this case, the MTVV method or the VDV method should be used to quantify the WBV. When the value of $MTVV/\tilde{a}_w$ exceeds 1.5, the MTVV method should be used. When the value of $VDV/(\tilde{a}_w T^{1/4})$ exceeds 1.75, the VDV method should be used. If the RMS method is sufficient to evaluate the effect of WBV, the RMS value should be converted to the estimated vibration dose value (eVDV) with Eq. (2.9).

$$eVDV = 1.4\tilde{a}_w T^{1/4} \quad (2.9)$$

However, it is not specified which method should be used in the case where the CF exceeds 9, the value of $MTVV/\tilde{a}_w$ is lower than 1.5 and the value of $VDV/(\tilde{a}_w T^{1/4})$ is smaller than 1.75; or in the case where the CF is smaller than 9, the value of $MTVV/\tilde{a}_w$ exceeds 1.5 and the value of $VDV/(\tilde{a}_w T^{1/4})$ exceeds 1.75. The former case has not been observed in the previous literatures, but the latter occurs in this research work as discussed later in chapter 5.

In step 5, two rules are introduced to select the directions for the evaluation of the effect of WBV on the human health:

- 1) Evaluation of the effect of WBV on the human health shall be made by using the highest RMS value or VDV of frequency weighted accelerations in any direction on the seat cushion.
- 2) When vibrations in two or more directions are comparable, the vibration total value on the seat cushion can be used as an additional estimate of the health risk. If the RMS method is used, the vibration total value refers to the vector sum value (VSV), which is formulated in Eq. (2.10). If the VDV method is used, it refers to the total VDV (TVDV), which is formulated in Eq. (2.11). The values of the multiplying factors m_x , m_y and m_z are 1.4, 1.4 and 1 respectively.

$$VSV = \sqrt{m_x^2 \tilde{a}_{wx}^2 + m_y^2 \tilde{a}_{wy}^2 + m_z^2 \tilde{a}_{wz}^2} \quad (2.10)$$

$$TVDV = (m_x^4 VDV_x^4 + m_y^4 VDV_y^4 + m_z^4 VDV_z^4)^{1/4} \quad (2.11)$$

with

\tilde{a}_{wi}	RMS value of frequency weighted accelerations in the x-, y- or z-direction on the seat cushion in m/s^2 ; 'i' represents x, y or z
VDV_i	VDV of the frequency weighted accelerations in the i-direction on the seat cushion in $m/s^{1.75}$

However, the method to judge whether the vibrations in two directions are comparable or not is not specified in ISO 2631-1:1997. This leads to the confusion to decide whether the highest value or the vibration total value on the seat cushion should be used for the evaluation.

In step 6, the VDV_d represents the daily WBV exposure in ISO 2631-1:1997. The VDV_d is calculated with Eq. (2.12).

$$VDV_d = VDV \left(\frac{T_d}{T} \right)^{1/4} \quad (2.12)$$

with

T_d	Reference daily exposure duration, 8 h
VDV_d	Daily vibration dose value in $m/s^{1.75}$

The upper and lower limits of the permitted daily exposure duration, T_u and T_l , are calculated with Eq. (2.13) and (2.14). In ISO 2631-1:1997 the upper boundary (UB) of the health guidance caution zone (HGCZ) is $17 m/s^{1.75}$ and the lower boundary (LB) is $8.5 m/s^{1.75}$.

$$T_u = T \left(\frac{UB}{VDV} \right)^4 \quad (2.13)$$

$$T_l = T \left(\frac{LB}{VDV} \right)^4 \quad (2.14)$$

2.2.1.2 Evaluation procedure in ISO 2631-5:2004

In step 2, the spine model in the x- and y-directions is a linear single degree of freedom (DOF) model, which is shown in Fig. 2.24 (a). In the z-direction, the spine model is a non-linear recurrent neural network model, as shown in Fig. 2.24 (b). These two spine models have not been epidemiologically validated.

In step 4, the acceleration dose D in each translational direction is calculated with Eq. (2.15).

$$D = \left[\sum a_{pi}^6 \right]^{1/6} \quad (2.15)$$

with

a_{pi}	The i^{th} peak of spine accelerations in m/s^2
----------	--

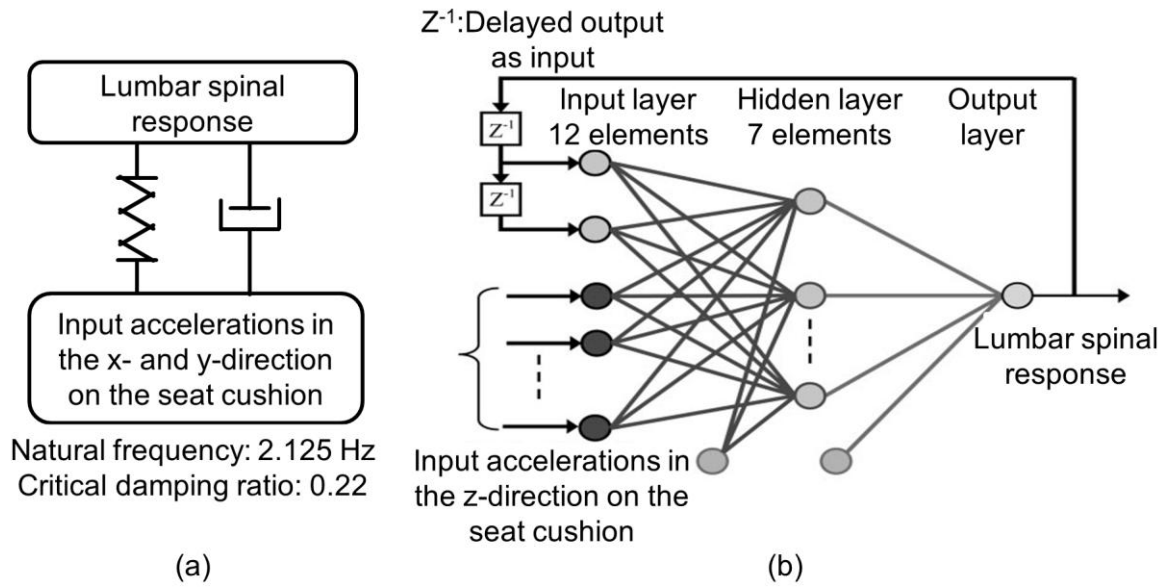


Fig. 2.24: (a). Spine model in the x- and y-directions; (b). Spine model in the z-direction [87]

In step 5, the equivalent static compressive stress S_e is calculated with Eq. (2.16). The values of m_x , m_y and m_z are 0.015, 0.035 and 0.032 MPa/(m/s²) respectively.

$$S_e = \left[(m_x D_x)^6 + (m_y D_y)^6 + (m_z D_z)^6 \right]^{1/6} \quad (2.16)$$

In step 6, the daily equivalent static compression dose S_{ed} represents the daily WBV exposure in this standard. It is calculated with Eq. (2.17).

$$S_{ed} = S_e \left[\frac{T_d}{T} \right]^{1/6} \quad (2.17)$$

The upper and lower limits of the permitted daily exposure duration, T_u and T_l , are calculated with Eq. (2.18) and Eq. (2.19). The upper boundary (UB) and the lower boundary (LB) of the HGCZ in ISO 2631-5:2004 are 0.8 MPa and 0.5 MPa respectively.

$$T_u = T \left(\frac{UB}{S_e} \right)^6 \quad (2.18)$$

$$T_l = T \left(\frac{LB}{S_e} \right)^6 \quad (2.19)$$

2.2.1.3 Application of standardized evaluation procedures

A large number of studies have been carried out to evaluate the WBV exposure levels on different types of machines using the procedure in ISO 2631-1:1997. A part of these evaluations are summarized in Tab. 2.5 to Tab. 2.8. Due to the similarity of the evaluation procedures in BS 6841:1987, 2002/44/EC, VDI 2057:2002 and ISO 2631-1:1997, the evaluations carried out according to these three standards are also included in the tables.

Tab. 2.5: Investigation of WBV exposure levels on construction vehicles and mining equipment (1)

Year	Vehicle type (Number of vehicles)	Operation tasks in measurement	Standard	Method	Direction ⁶	Range of RMS (m/s ²) / VDV (m/s ^{1.75}) / S _{ed} (MPa)
2001 [93]	Excavator (4)	Filling trench, digging and driving	ISO 2631-1	RMS	(2)	0.17-3.03
2009 [94]	Excavator (7)	Excavating and loading soil/rocks into trucks, or pushing coal into tip	ISO 2631-1	VDV	(2)	3.88-9.25
2009 [94]	Excavator (7)		ISO 2631-5	S _{ed}	(1)	0.42-2.32
2010 [95]	Excavator (55)	Drain clearing, weed clearing, pouring concrete, tracking, pile driving or rock breaking	2002/44/EC	RMS	(2)	0.04-5.81
2004 [96]	Heavy haul truck (4)	Loading, full hauling, dumping, empty hauling (on ground covered with thick snow and frozen road)	ISO 2631-1	RMS	(1)	0.55-7.10
2006 [97]	Underground haul truck (1)	Loading, full hauling, dumping load, empty hauling	ISO 2631-1	RMS	(2)	1.20
2006 [97]	Surface haul truck (2)	Up ramp(with a full load) and down ramp (empty)	ISO 2631-1	RMS	(2)	0.28, 0.37

⁶ Symbol (1) represents the vibration total value of accelerations in three directions on the seat cushion; Symbol (2) represents the highest RMS value or VDV in three directions on the seat cushion

Tab. 2.6: Investigation of WBV exposure levels on construction vehicles and mining equipment (2)

Year	Vehicle type (Number of vehicles)	Operation tasks in measurement	Standard	Method	Direction ⁷	Range of RMS (m/s ²) / VDV (m/s ^{1.75}) / S _{ed} (MPa)
2001 [93]	Mobile crane (2)	Driving	ISO 2631-1	RMS	(2)	0.50, 0.67
2005 [98]	Wheel loader (9)	Loading material into lorries/crusher machines, or distributing material between different sections of a site	ISO 2631-1	RMS	(2)	0.36-0.84
2006 [99]	Track-type loader (6)	Leveling the ground with the bucket and loading material into aggregate lorries	ISO 2631-1	RMS	(2)	0.75-1.12
2006 [97]	Bulldozer (1)	Pushing (surface operation)	ISO 2631-1	RMS	(2)	1.96
2006 [97]	Surface grader (1)	Pushing and leveling	ISO 2631-1	RMS	(2)	0.79
2006 [97]	Load Haul Dump (3)	Loading, full hauling, dumping load, empty hauling	ISO 2631-1	RMS	(2)	0.67-2.01
2009 [94]	Load Haul Dump (10)	Loading, conveying and dumping soil/rocks/coal	ISO 2631-1	VDV	(2)	3.35-14.80
2009 [94]	Load Haul Dump (10)		ISO 2631-5	S _{ed}	(1)	0.28-1.90
2006 [100]	Scraper (33)	Loading, full hauling, dumping load, empty hauling	ISO 2631-1	RMS	(1)	0.55-2.55
2010 [95]	Mini digger (13)	Digging trench on tarmac or walkway on gravel road	2002/44/EC	RMS	(2)	0.28-4.13
2010 [95]	Dumper (9)	Driving empty on gravel or paved road	2002/44/EC	RMS	(2)	0.17-0.95
2010 [95]	Mini dumper (12)	Driving with full of stone or lifting and dumping stone	2002/44/EC	RMS	(2)	0.29-1.65

⁷ Same with footnote 6

Tab. 2.7: Investigation of WBV exposure levels on agricultural vehicles

Year	Vehicle type (Number of vehicles)	Operation tasks in measurement	Standard	Method	Direction ⁸	Range of RMS (m/s ²) / VDV (m/s ^{1.75}) / S _{ed} (MPa)
1998 [101]	Tractor (2)	Real working conditions	ISO 2631-1	RMS	(1)	0.426, 0.890
2001 [93]	Tractor (7)	Driving on tarmac roads or a grass field	ISO 2631-1	RMS	(2)	0.54-1.00
2002 [102]	Tractor (5)	Driving over ISO smooth artificial test track at 10, 12, 13, 14, 15, 16, 18, 20, 24 & 30 km/h Driving over ISO rough artificial test track at 4, 5, 6 & 7 km/h	ISO 2631-1	RMS	(1)	1.44-4.54
2010 [95]	Tractor (10)	Driving with trailer on grass or stone terrains	2002/44/EC	RMS	(2)	0.04-0.42
1998 [101]	Head feed combine (3)	Real working conditions	ISO 2631-1	RMS	(1)	0.414, 0.566, 1.026
1998 [101]	Riding rice power (1)		ISO 2631-1	RMS	(1)	0.351
1998 [101]	Transplanter (1)		ISO 2631-1	RMS	(1)	0.587
1998 [101]	Farm carrier (1)		ISO 2631-1	RMS	(1)	0.999
1998 [101]	Cultivator (1)		ISO 2631-1	RMS	(1)	0.541
2010 [95]	Lawnmower (19)	Driving on a grass field and cutting grass	2002/44/EC	RMS	(2)	0.08-1.21
2010 [95]	Chipping machine (3)	Chipping wood on gravel terrains	2002/44/EC	RMS	(2)	0.76-0.98
2011 [103]	Quad bike (~)	Real working conditions	2002/44/EC	VDV	(2)	7.3-33.5
2011 [103]	Quad bike (~)		ISO 2631-5	S _{ed}	(1)	0.1-0.8

⁸ Same with footnote 6

Tab. 2.8: Investigation of WBV exposure levels on transportation vehicles

Year	Vehicle type (Number of vehicles)	Operation tasks in measurement	Standard	Method	Direction ⁹	Range of RMS (m/s ²) / VDV (m/s ^{1.75}) / S _{ed} (MPa)
2001 [93]	Car (25)	Driving on public roads	ISO 2631-1	RMS	(2)	0.26-0.75
2001 [93]	Van (9)		ISO 2631-1	RMS	(2)	0.36-0.57
2001 [93]	Bus (10)		ISO 2631-1	RMS	(2)	0.38-0.89
2001 [93]	Armoured vehicle (4)	No description	ISO 2631-1	RMS	(2)	0.29-1.52
2004 [104]	Highway transport truck (4)	Driving on highways with full of freight	ISO 2631-1	RMS	(1)	0.226-1.536
2001 [93]	Lift truck (11)	Empty/loaded driving on tarmac or uneven concrete terrain	ISO 2631-1	RMS	(2)	0.53-1.00
2010 [95]	Forklift (6)	Driving with load of stone on concrete terrain	2002/44/EC	RMS	(2)	0.41-1.00
2010 [95]	Single cab pick up (10)	Driving through town or driving in yard	2002/44/EC	RMS	(2)	0.31-1.17
2010 [95]	Double cab pick up (18)	Driving through town or the National Park, or driving in yard	2002/44/EC	RMS	(2)	0.2-0.8
2001 [93]	Lorry (16)	No description	ISO 2631-1	RMS	(2)	0.42-1.28
2010 [95]	Lorry (3)	Driving empty on paved road	2002/44/EC	RMS	(2)	0.82-0.83

A wide range of WBV exposure levels are observed in these tables. It is mainly caused by the operational variations in the measurement. These variations exist in vehicle size, driving speed, roughness of road surface, operation task or working cycle, driver, seat, tire pressure and so on. Many studies investigated the influence of these variations on the WBV exposure levels. It was examined that the WBV exposure level increases with the driving speed and the roughness of the road surface [102],[105], but decreases with the vehicle size [102],[106]. The working

⁹ Same with footnote 6

places and the operation tasks have also a significant influence on the WBV exposure levels [95],[98],[99],[103],[107],[108]. Kumar studied that the gender of the driver does not have a significant effect on the WBV exposure levels, but the weight is of importance [96]. Milosavljevic et al. investigated that the increased age, the work experience and the driving experience are significantly associated with the reduction of the daily WBV exposure [103]. Adams et al. proved that the central tire inflation system on the agricultural tractors has a large capability to reduce the WBV exposure levels [109].

2.2.1.4 Comparison of evaluation results obtained according to ISO 2631-1:1997 and ISO 2631-5:2004

It can be observed from tables in section 2.2.1.3 that the evaluations of the WBV exposure levels in most research works were carried out according to ISO 2631-1:1997 and 2002/44/EC. After the publication of ISO 2631-5:2004, both ISO 2631-1:1997 and ISO 2631-5:2004 were used to predict the health risks caused by WBV. Different prediction results were obtained according to these two ISO standards.

In the study by Alem in 2005 [87] over 1000 WBV measurements were carried out on United States army vehicles. Forty of them with high shock content were selected to predict the health risks using the root mean square (RMS) method, the vibration dose value (VDV) method and the equivalent static compressive stress S_e method. Health risks predicted with the S_e method are higher than those predicted with the RMS method and the VDV method. Aye predicted the health risks caused by WBV arising from various mining machines according to ISO 2631-1:1997 and ISO 2631-5:2004 [94]. Results showed that the S_e method results in higher predicted health risks than the VDV method. He in 2009 obtained the same conclusion that higher health risks caused by WBV on excavators are predicted with the S_e method in ISO 2631-5:2004 rather than the VDV method in ISO 2631-1:1997 [110].

A contrary conclusion was obtained in many studies that health risks predicted with the VDV method in ISO 2631-1:1997 are higher than those predicted with the S_e method in ISO 2631-5:2004. For example, compared to the S_e method, the VDV method results in higher predicted health risks caused by WBV on locomotives [111], load-haul-dumps [112], all-terrain vehicles [113] and surface haulage trucks [114].

In the study by Chen et al. health risks caused by WBV on motorcycles predicted with the VDV method are similar to those predicted with the S_e method [115], as well as by WBV arising from forklifts in the study by Deshmukh [116].

Different health risks predicted according to two ISO standards caused discussions about the health guidance caution zone (HGCZ) in these two standards. Alem [87] suggested a linear relationship between the daily vibration dose value (VDV_d) and the daily equivalent static compression dose (S_{ed}) of the WBV on the army vehicles. Based on this relationship, the HGCZ in ISO 2631-1:1997 was lowered to 3.5-4.8 $m/s^{1.75}$. However, only the WBV measurements with high shock content were used to determine the VDV_d - S_{ed} relationship. Over 90% WBV measurements were excluded from the determination of this relationship, because these measurements have small VDV_d and S_{ed} values. In other words, the linear VDV_d - S_{ed} relationship suggested by Alem is only available for the WBV with high shock content on the army vehicles. Based on the conclusions in studies [111] and [112], Eger et al. suggested that it should be considered to lower the HGCZ in ISO 2631-5:2004 [112].

2.2.2 Evaluation of effect on comfort

Procedures to evaluate the effect of WBV on the comfort are introduced in ISO 2631-1:1985 and ISO 2631-1:1997. According to ISO 2631-1:1985, the evaluation could be made independently along each of the three translational directions on the seat cushion. In these three directions, a set of reduced comfort boundary (RCB) curves from 1 Hz to 80 Hz was defined for different exposure durations. In ISO 2631-1:1997, the vector sum value (VSV) of the root mean square (RMS) values of weighted accelerations in six directions on the seat cushion as well as in three translational directions at the seat backrest and on the cabin floor is recommended for the comfort evaluation.

2.2.2.1 Evaluation procedure in ISO 2631-1:1985

The procedure in ISO 2631-1:1985 to evaluate the discomfort caused by WBV includes three steps, as described in Tab. 2.9.

Tab. 2.9. Procedure in ISO 2631-1:1985 for the evaluation of discomfort caused by WBV

Step 1	Measure and store accelerations in three translational directions on the seat cushion.
Step 2	Calculate the RMS value of the accelerations in each 1/3 octave band.
Step 3	Compare the RMS values with the RCB curves.

In step 2, the RMS value of the accelerations in each 1/3 octave band is calculated with Eq. (2.20).

$$\tilde{a}_{1/3ob} = \left[\frac{1}{T} \int_0^T a_{1/3ob}^2(t) dt \right]^{1/2} \tag{2.20}$$

with

$a_{1/3ob}(t)$ Accelerations in 1/3 octave band as a function of time in m/s^2

$\tilde{a}_{1/3ob}$ RMS value of accelerations in 1/3 octave band in m/s^2

The RCB curves in step 3 are illustrated in Fig. 2.25.

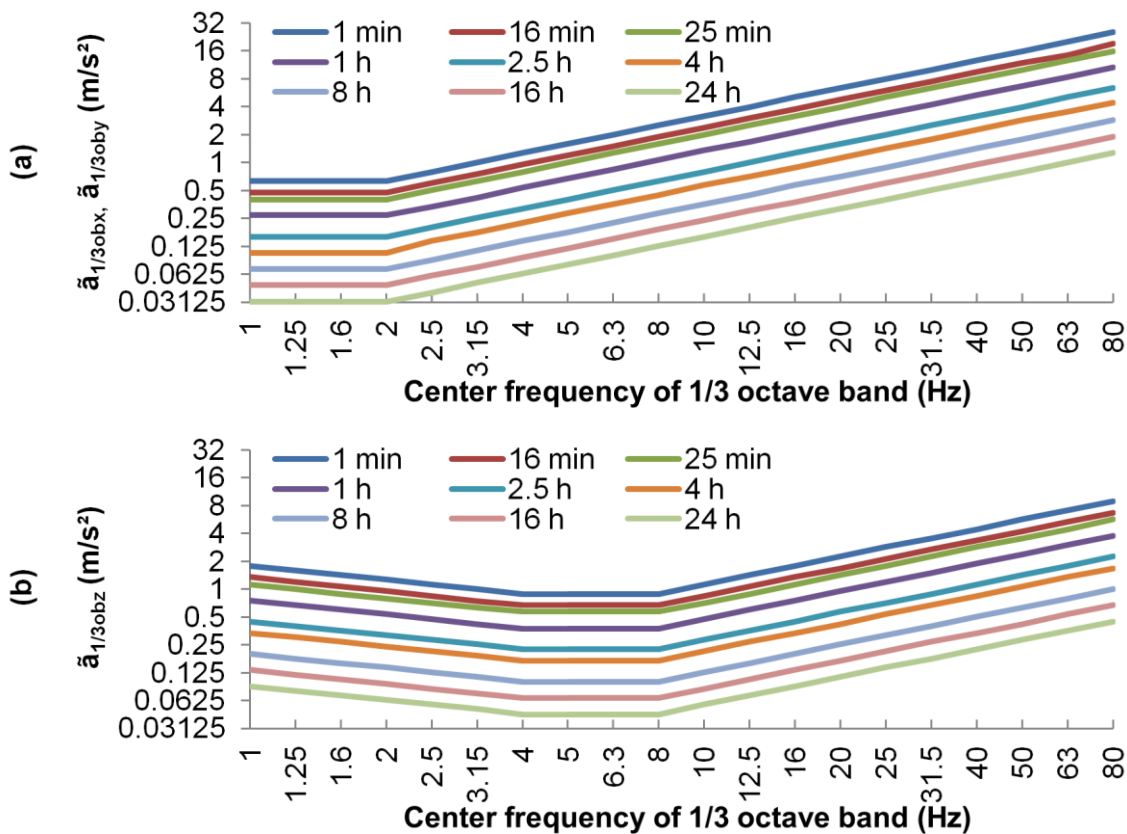


Fig. 2.25: (a). RCB curves in the x- and y-directions; (b). RCB curves in the z-direction

In Fig. 2.25 (a), the curves represent the RCB for different exposure durations from 1 Hz to 80 Hz in the x- and y-directions, where the lowest boundaries lie in the range of 1-2 Hz. In Fig. 2.25 (b), the curves represent the RCB in the z-direction, where the lowest boundaries are in the range of 4-8 Hz.

2.2.2.2 Evaluation procedure in ISO 2631-1:1997

In ISO 2631-1:1997, similar to the procedure to evaluate the effect of WBV on the health, the procedure to evaluate the effect of WBV on the comfort includes six steps as well, as described in Tab. 2.4 (p. 27).

In step 1, in order to evaluate the ride discomfort caused by WBV, accelerations should be measured in three translational directions on the seat cushion, at the seat backrest and on the feet floor, as well as in three rotational directions on the seat cushion.

In step 2, the frequency weighting filters and the multiplying factors in the above mentioned directions are listed in Tab. 2.10.

Tab. 2.10: The frequency weighting filter and the multiplying factor in each direction for the evaluation of the discomfort caused by WBV

Location	Direction	Frequency weighting filter	Multiplying factor
Seat cushion	x	W_d	$m_x=1$
	y	W_d	$m_y=1$
	z	W_k	$m_z=1$
	r_x	W_e	$m_{rx}=0.63$
	r_y	W_e	$m_{ry}=0.4$
	r_z	W_e	$m_{rz}=0.2$
Seat backrest	x	W_c	$m_{bx}=0.8$
	y	W_d	$m_{by}=0.5$
	z	W_d	$m_{bz}=0.4$
Feet floor	x	W_k	$m_{fx}=0.25$
	y	W_k	$m_{fy}=0.25$
	z	W_k	$m_{fz}=0.4$

Curves of frequency weighting filters W_d and W_k are shown in Fig. 2.23 (p. 28). Curves of frequency weighting filters W_e and W_c are illustrated in Fig. 2.26.

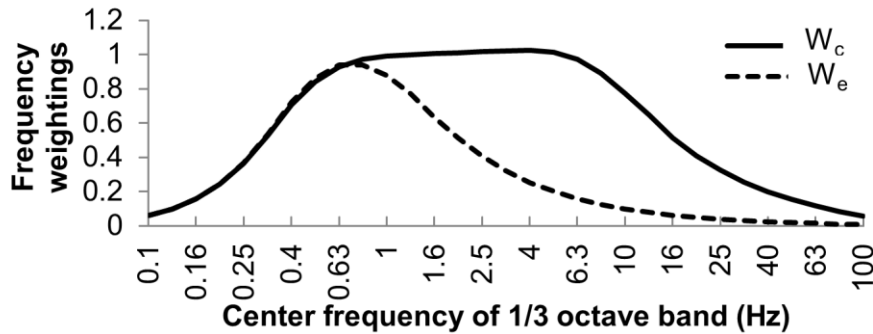


Fig. 2.26: Curves of the frequency weighting filters W_e and W_c

The step 3 and step 4 are same with those introduced in section 2.2.1.1. In step 5, two rules are introduced in ISO 2631-1:1997 to select the directions to evaluate the effect of WBV on the ride comfort:

- 1) If the weighted value determined in any direction is less than 25% of the maximum value at the same point but in another direction, it can be excluded.
- 2) If the point vibration total value at one point is less than 25% of the maximum point vibration total value, it can be excluded.

In step 6, the ‘approximate indications of likely reactions to various magnitudes of overall vibration total values’ are listed in Tab. 2.11. Here the overall vibration total value (OVTV) can be calculated with Eq. (2.21). For the directions selected for the evaluation in step 5, the multiplying factors can adopt the values given in the rightmost column of Tab. 2.10. For the directions excluded in step 5, the multiplying factors are zero. No boundary of the maximum transient vibration value (MTVV) or the vibration dose value (VDV) for the comfort evaluation is recommended in ISO 2631-1:1997.

$$OVTV = \sqrt{m_x^2 \tilde{a}_{wx}^2 + m_y^2 \tilde{a}_{wy}^2 + m_z^2 \tilde{a}_{wz}^2 + m_{rx}^2 \tilde{a}_{wrx}^2 + m_{ry}^2 \tilde{a}_{wry}^2 + m_{rz}^2 \tilde{a}_{wrx}^2 + m_{bx}^2 \tilde{a}_{wbx}^2 + m_{by}^2 \tilde{a}_{wby}^2 + m_{bz}^2 \tilde{a}_{wbz}^2 + m_{fx}^2 \tilde{a}_{wfx}^2 + m_{fy}^2 \tilde{a}_{wfy}^2 + m_{fz}^2 \tilde{a}_{wfx}^2} \quad (2.21)$$

with

\tilde{a}_{wri}	RMS value of frequency weighted accelerations in the r_x -, r_y - or r_z -direction on the seat cushion in rad/s^2 ; ‘i’ represents x, y or z
\tilde{a}_{wbi}	RMS value of frequency weighted accelerations in the x-, y- or z-direction at the seat backrest in m/s^2
\tilde{a}_{wfi}	RMS value of frequency weighted accelerations in the x-, y- or z-direction on the feet floor in m/s^2

Tab. 2.11: The magnitudes of overall vibration total values for the approximate indications of likely reactions of comfort

Overall vibration total value	Indications
Less than 0.315 m/s ²	Not uncomfortable
0.315 m/s ² to 0.63 m/s ²	A little uncomfortable
0.5 m/s ² to 1 m/s ²	Fairly uncomfortable
0.8 m/s ² to 1.6 m/s ²	Uncomfortable
1.25 m/s ² to 2.5 m/s ²	Very uncomfortable
Larger than 2 m/s ²	Extremely uncomfortable

2.2.2.3 Correlation between objective prediction and subjective judgment about ride discomfort

The correlation between the objective evaluation with different methods and the subjective judgment about the ride discomfort caused by WBV has been investigated in several studies.

In the study by Hansson and Wikström, objective and subjective evaluations of ride discomfort caused by WBV on forestry machines were carried out. Tri-axial accelerations on the seat cushion were used in the objective evaluation. A total of thirteen objective evaluation methods were adopted, including the root mean square (RMS) value of weighted accelerations in each 1/3 octave band in each direction, the vector sum value (VSV) of RMS values of weighted accelerations in three directions in each 1/3 octave band, the RMS value of weighted accelerations from 1 Hz to 80 Hz in each direction and the VSV of RMS values of weighted accelerations from 1 Hz to 80 Hz in all three directions. The results show that the last one has the highest correlation with the subjective evaluation. [117]

In the study by Mistrot et al., twenty two lorry drivers rated the discomfort of sixteen different rides. The ride discomfort was predicted using objective methods as well. The objective methods include the highest RMS value and the VSV of RMS values of weighted accelerations in three translational directions on the seat cushion. The correlation between the subjective rating and the objective predictions shows that the latter method is the best objective method to predict the discomfort. [39]

In the study by Fairley, eleven professional drivers rated the discomfort caused by WBV on four different agricultural tractors during sixteen rides. Tri-axial accelerations were measured on the cabin floor, on the seat cushion and at the seat backrest. Twenty objective methods were used to predict the ride discomfort. Results show that the best objective method to predict the discomfort caused by WBV on agricultural tractors is again the VSV of RMS values of frequency weighted accelerations in three translational directions on the seat cushion. [118]

The study by Hassan and McManus also proves that the VSV of RMS values of frequency weighted accelerations in three translational directions on the seat cushion can be used to predict the ride discomfort caused by WBV on heavy vehicles. Additionally, it was studied that the subjective reactions to WBV match 'the approximate indications of likely reactions to various magnitudes of overall vibration total values (Tab. 2.11)' in ISO 2631-1:1997 very well. [119]

In the study by Mansfield et al., twenty four persons were exposed to fifteen vertical excitations including random vibrations, repeated shocks and combination of random vibrations and shocks. The discomfort was objectively evaluated using the RMS value, the vibration dose value (VDV), the maximum transient vibration value (MTVV) and the absorbed power. The correlation between these objective evaluations and the subjective rating was investigated. It shows that the absorbed power is the best objective method to predict the discomfort caused by the above mentioned excitations. The VDV method is better than the RMS method and the MTVV method for the discomfort prediction. Due to the difficulty in measuring the force in the field tests to calculate the absorbed power, the VDV method was recommended as the most appropriate method to evaluate the discomfort caused by continuous vibrations or repeated shocks. The worst prediction result was obtained using the MTVV method. [120] However, Jönsson and Johansson studied that the MTVV method is better than the VDV method and the RMS method to predict the ride discomfort caused by WBV on forklifts [121].

In the study by Els, the RMS value of the vertical accelerations on the seat cushion was recommended to determine the ride discomfort on a landmine protected military vehicle. Investigations in this study show that the 'approximate indications of likely reactions to various magnitudes of overall vibration total values (Tab. 2.11)' in ISO 2631-1:1997 correspond very well with the subjective comments. [122]

2.3 Vibration attenuation performance of suspension seats

In general, small and medium sized construction vehicles such as compact wheel loaders (CWLs) are equipped with three suspensions: tires, rubber elements between vehicle frame and cabin, as well as the seat suspension system. Generally no axle suspension system is equipped on these vehicles.

Tires of construction vehicles provide primary isolation of the vibrations generated by the unevenness of the ground. These tires are typically large and soft, thus filter out a part of vibrations and shocks. If these tires are soft enough, more vibration energy can be absorbed. However, in this case, the rolling resistance of the tires is very large. This increases the energy consumption. On the other hand, high thermal and mechanical stress in the tire material is generated. This increases the wear of the tires. In one word, tires on construction vehicles cannot be designed too soft to sufficiently isolate vibrations. [123]

In order to keep the handling stability and the operational safety, rubber elements between vehicle frame and cabin are rather stiff. The principal function of these rubber elements is to avoid the metal to metal impact. The capability of these rubber elements to isolate the vibrations is limited.

As a main contact component between driver and vehicle, the suspension seat plays a significant role in reducing the vibrations transmitted to the driver. Since the mass of the driver and the seat is relatively small compared to the entire vehicle, modifications of the seat suspension system hardly affect the dynamic behavior of the entire vehicle. This leads to the fact that suspension seat modifications are much easier to be carried out than modifications of a cabin or an axle suspension system. In order to improve the vibration attenuation performance of suspension seats, a lot of studies have been carried out to investigate their dynamic characteristics and to optimize the seat suspension system.

2.3.1 Metrics for seat vibration attenuation performance

The seat transmissibility is used to evaluate the vibration attenuation performance of a suspension seat. Two parameters are usually used to investigate the seat transmissibility: the seat effective amplitude transmissibility (SEAT) and the seat transmissibility in the frequency domain derived from the cross spectral density (CSD) method.

The SEAT value is an objective metric for seat vibration isolation efficiency. It can be used to predict the dynamic seat comfort and to select the best seat for a specific vibration excitation [124],[125]. The SEAT value represents the ratio of the overall weighted accelerations on the seat cushion to the overall weighted accelerations at the seat base. Three methods, as formulated from Eq. (2.22) to Eq. (2.24), are widely used to calculate the SEAT value [124]-[128]. The first two methods (Eq. (2.22) and Eq. (2.23)) are used for the vibrations with a low crest factor (CF), and the third one (Eq. (2.24)) is more suitable for the vibrations with a high CF. In general, vibrations on construction vehicles have a high CF [94],[129],[130]. This means that the third method should be used to calculate the SEAT value of a seat exposed to the vibrations on construction vehicles.

$$SEAT = \left[\frac{\int G_{cc}(f)W_i^2(f)df}{\int G_{bb}(f)W_i^2(f)df} \right]^{1/2} \quad (2.22)$$

$$SEAT = \frac{\tilde{a}_{wc}}{\tilde{a}_{wb}} \quad (2.23)$$

$$SEAT = \frac{VDV_c}{VDV_b} \quad (2.24)$$

with

$G_{bb}(f)$	PSD of accelerations at the seat base as a function of frequency in $(m/s^2)^2/Hz$
$G_{cc}(f)$	PSD of accelerations on the seat cushion as a function of frequency in $(m/s^2)^2/Hz$
VDV_b	VDV of frequency weighted accelerations at the seat base in $m/s^{1.75}$
VDV_c	VDV of frequency weighted accelerations on the seat cushion in $m/s^{1.75}$
$W_i(f)$	Frequency weighting in the i-direction as a function of frequency
\tilde{a}_{wb}	RMS value of frequency weighted accelerations at the seat base in m/s^2
\tilde{a}_{wc}	RMS value of frequency weighted accelerations on the seat cushion in m/s^2

The seat transmissibility at different frequencies cannot be obtained from the SEAT value. The seat transmissibility in the frequency domain can be obtained using the CSD method as formulated in Eq. (2.1) (p. 17). Here the input signal is the accelerations at the seat base and the output signal is the accelerations on the seat cushion.

2.3.2 Dynamics of suspension seats

With the excitation magnitude increasing from zero to a quite high level, the dynamics of a suspension seat experience five different states, as shown in Fig. 2.27.

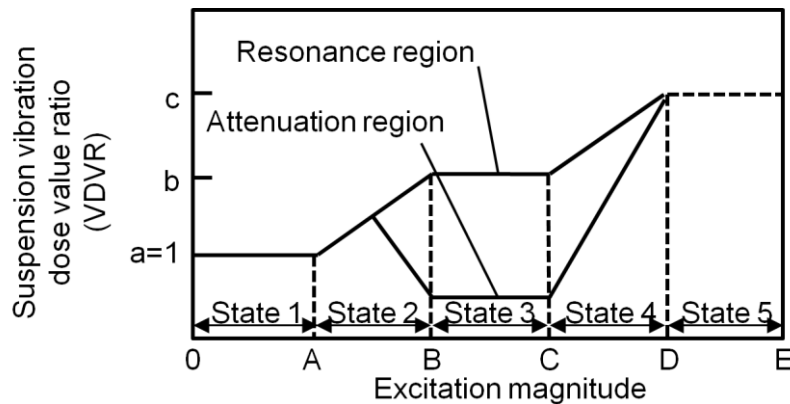


Fig. 2.27: States of dynamics of suspension seat [131]

The vibration dose value ratio (VDVR) of the suspension system can be calculated with Eq. (2.25). [131]

$$VDVR = \frac{VDV_{ss}}{VDV_b} \quad (2.25)$$

with

$$VDV_{ss} \quad \text{VDV of frequency weighted accelerations on the top of the suspension system in } \text{m/s}^{1.75}$$

In State 1, the excitation magnitude is too low to overcome the friction of the suspension mechanism. The seat suspension is locked by friction and the seat sprung part moves together with the seat base like a rigid seat.

In State 2, the seat sprung part starts to move relatively to the seat base. The VDVR possibly increases in this state, due to the non-linearity of the suspension system, such as the friction or gaps between moving parts. [131]

In these two states, friction of the suspension mechanism has a large influence on the seat vibration attenuation performance. It has been investigated that lower friction results in improved seat vibration attenuation performance under excitations with low and moderate magnitudes [132]. This is due to the fact that the lower friction reduces the maximum excitation magnitude of the State 1 (A in Fig. 2.27). For example, it was studied that 50% reduction in friction causes the seat to start isolating at an excitation magnitude of $0.6 \text{ m/s}^{1.75}$ instead of $1.2 \text{ m/s}^{1.75}$ [132]. The friction of the suspension mechanism can be lowered by good lubrication.

In State 3, the VDVR is high or low at a constant value depending on the seat natural frequency and the frequency of the excitation. If the frequency of the excitation is higher than 1.4 times of the seat natural frequency, the vibration excitation is attenuated by the seat suspension system and the VDVR is lower than one. Otherwise, it is higher than one. It has been proven that the damping coefficient of the seat suspension system plays an important role in the seat transmissibility in this state. Ma et al. investigated the damping requirement for a suspension seat exposed to different vibration excitations. Higher damping is desirable to improve the seat vibration attenuation performance, when the seat is exposed to vibrations which predominate around the seat resonant frequency, irrespective of the excitation magnitudes. When the seat is exposed to vibrations which predominate around a relatively higher frequency, a higher damping coefficient leads to a higher SEAT value under excitations with moderate magnitudes. [133] This conclusion is consistent with that in the study by Gunston, where increasing the damping by 50% leads to an increase in SEAT values up to 5%, when the seat is exposed to vibrations at 2.5 Hz with moderate magnitudes [132].

Seat suspension systems on earth-moving vehicles usually have a low stiffness and a short free stroke. On the other hand, earth-moving vehicles are exposed to vibrations and shocks, which are severe enough to cause the seat suspension systems exceeding their free stroke. This leads to the fact that impacts with the end-stop buffers occur. [131],[134] In this case the seat dynamics are in the State 4. With the increase of the excitation magnitude, more end-stop impacts occur and the suspension hits the end-stop buffers more heavily. Now the seat dynamics are in the State 5. In these two states, end-stop impacts result in the increase of the VDVR. Higher damping coefficients of the seat suspension system are desirable to reduce the number of end-stop impacts and the vibration severity generated by the end-stop impacts [132],[133],[135]. It was investigated that 50% reduction in the damping coefficient results in an increase of SEAT value up to 150% under the excitations with high magnitudes due to more and severer end-stop impacts [132].

In addition to selecting a proper suspension damping, optimizing the properties of the end-stop buffers (such as the stiffness coefficient, the damping coefficient and the length) also contributes to the reduction of the VDVR [134],[136],[137]. In the study by Wu and Griffin [136], a suspension seat was tested when it was equipped with both top and bottom buffers or when it was equipped with just bottom buffers. The

test results show that the acceleration peaks generated by end-stop impacts are greatly reduced by using top buffers. In this study, three end-stop buffers with different force-deflection characteristics were equipped on the seat in the seat tests. The force-deflection characteristics of these three end-stop buffers are shown in Fig. 2.28. Test results show that the end-stop buffer C results in the lowest VDVR under the excitations with high magnitudes. In the study by Rebelle [137], the stiffness coefficients, the damping coefficients and the thickness of an end-stop buffer were optimized. The optimization results show that a non-linear force-deflection relationship coupled with a damping is the best solution to reduce the vibration severity generated by the end-stop impacts.

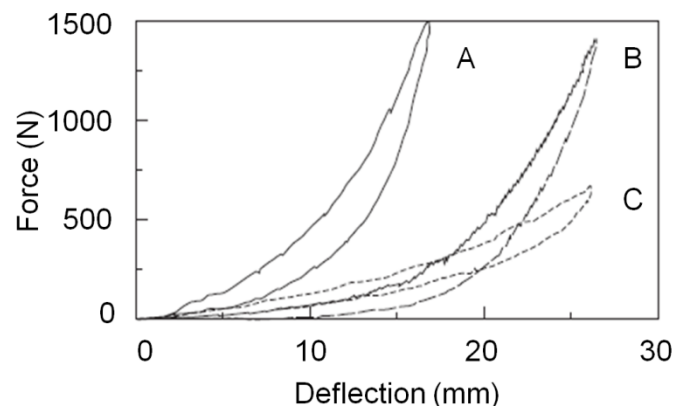


Fig. 2.28: Force-deflection characteristics of three end-stop buffers used in the seat tests in study [136]

In the paragraphs above, the influence of the suspension components on the seat dynamic characteristics is introduced. Because seat and driver interact with each other, the seat dynamic behavior is affected by the dynamic characteristics of the driver as well. It was observed that the nonlinearity of the human body has a significant influence on the seat transmissibility [138].

In order to reduce risks of being injured in case of an accident, it is recommended by local laws or regulations to use a safety belt during the daily operation of earth-moving machines. The effectiveness of a safety belt is studied especially for the case that a car crash occurs [139]-[142]. From the studies by Wyllie and Griffin, it can be noticed that the safety belt affects the driver behavior in the vibrational environment during normal vehicle operations [143],[144]. There is no doubt that the safety belt plays an important role in restricting the movement of the driver. This results in the change of the seat-driver dynamics and accordingly the seat transmissibility.

However, there is little research analyzing the effect of the safety belt on the seat transmissibility.

2.3.3 Model and optimization of suspension seats

2.3.3.1 Model for the vertical direction

In previous studies several methods to build a seat-occupant model with a vertical seat suspension system were introduced. The basic method is building a lumped parameter model (LPM), as introduced in studies [70], [133] and [145]. The LPMs in these three studies have the similar structure as illustrated in Fig. 2.29.

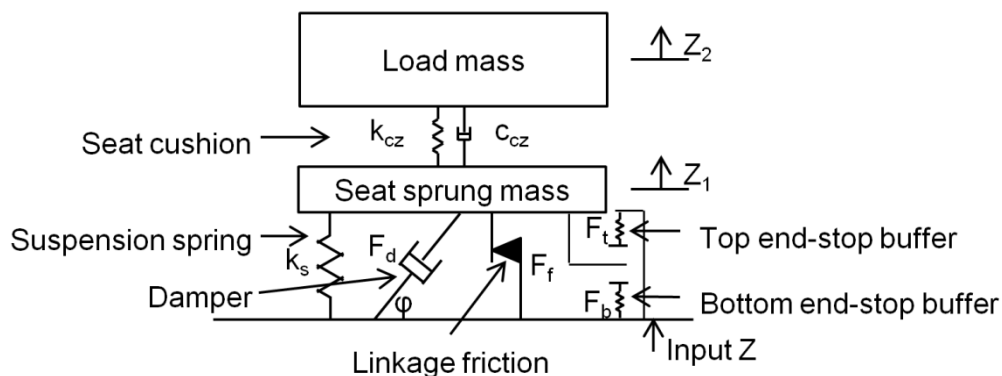


Fig. 2.29: General structure of the LPM of the seat-occupant system with a vertical seat suspension system

To build a LPM, the static and dynamic properties of all seat components need to be measured, such as the force-deflection relationship of cushion, spring and end-stop buffers, and the force-velocity relationship of cushion, damper and end-stop buffers, as well as the friction force of the suspension mechanism. These properties are simplified and parameterized in the LPM. The seat cushion can be represented using a linear spring with a linear damper. The air spring can be simplified as a linear spring for a given load mass. The force-velocity relationship of a passive hydraulic damper is usually expressed using a piecewise linear function. End-stop buffers are modeled as pure springs with both linear and nonlinear stiffness coefficients.

In the studies [75] and [145], the nonlinear curve-fitting method was used to identify the parameters of a suspension seat model. In these two studies, the parameters of the suspension seat model were determined not by static or dynamic tests of the seat components, but by the nonlinear curve-fitting in least-squares sense. The seat-occupant model proposed in the study [75] is illustrated in Fig. 2.30. The seat transfer function was obtained from laboratory seat tests and field vibration measurements.

The calculated transfer function of the seat was obtained with Eq. (2.26)-(2.30) [75]. Parameters of this model, k_{as} , k_d and c_d , were determined by minimizing the quadratic error between the measured and the calculated seat transfer functions.

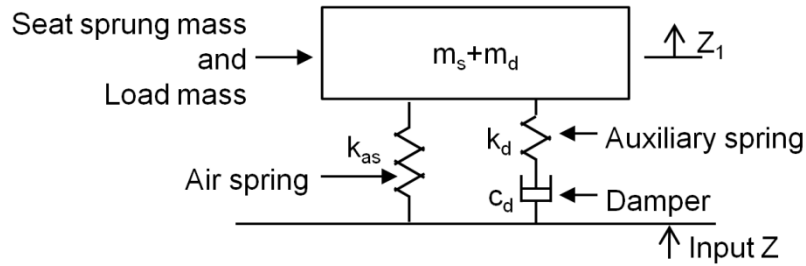


Fig. 2.30: Seat-occupant model in study [75]

$$TF(j\Omega) = \frac{2\xi_v \frac{(k_{as} + k_d)}{k_d} (j\Omega) + 1}{2\xi_v \frac{k_{as}}{k_d} (j\Omega)^3 + (j\Omega)^2 + 2\xi_v \frac{(k_{as} + k_d)}{k_d} (j\Omega) + 1} \quad (2.26)$$

$$\Omega = \omega / \omega_0 \quad (2.27)$$

$$\omega_0 = \sqrt{k_{as} / (m_s + m_d)} \quad (2.28)$$

$$\xi_v = c_d / c_c \quad (2.29)$$

$$c_c = 2\sqrt{k_{as} (m_s + m_d)} \quad (2.30)$$

with

Ω	Dimensionless angular frequency ratio
c_c	Critical damping of a single-DOF system without the auxiliary spring k_d in N·s/m
c_d	Damping coefficient of the damper in N·s/m
j	Imaginary unit, $(-1)^{1/2}$
k_{as}	Stiffness coefficient of air spring in N/m
k_d	Stiffness of the auxiliary spring in the seat model in N/m
m_d	Equivalent mass of a seated driver in kg
m_s	Mass of the seat sprung part in kg
ξ_v	Dimensionless damping ratio
ω	Angular frequency of the excitations in rad/s
ω_0	Undamped natural frequency of the suspension seat in rad/s

In the study [145], the vertical seat suspension system was modeled as a combination of a linear spring-damper element and a Bouc-Wen force element, as shown in Fig. 2.31. The Bouc-Wen force was used to represent the friction force of the suspension mechanism based on the Bouc-Wen model of hysteresis [145], which

was proposed by Bouc [146],[147] and extended by Wen [148], and is widely used to describe the nonlinear hysteretic behavior of a system [149],[150]. The Bouc-Wen model of hysteresis is essentially described with a first-order nonlinear differential equation that relates the input displacement to the output restoring force in a hysteretic way [150]. In the study [145], the simulated accelerations on the seat cushion were obtained by solving the equations of motion of the seat-occupant model. Parameters of the seat-occupant model were determined by minimizing the quadratic error between the simulated and the measured accelerations on the seat cushion.

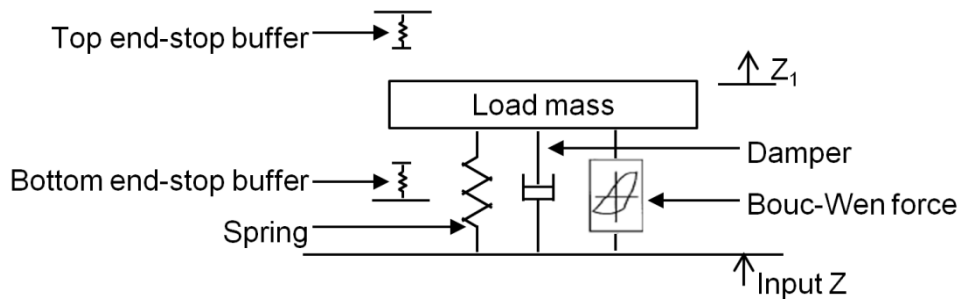


Fig. 2.31: Seat-occupant model proposed in study [145]

In addition, the method to build a model of an air suspension seat based on the aerothermodynamics and the fluid dynamics was introduced in studies by Maciejewski et al. [151],[152]. The schematic illustration of the seat-occupant model is shown in Fig. 2.32. The equations of motion of this model are formulated in Eq. (2.31)-(2.40) [151].

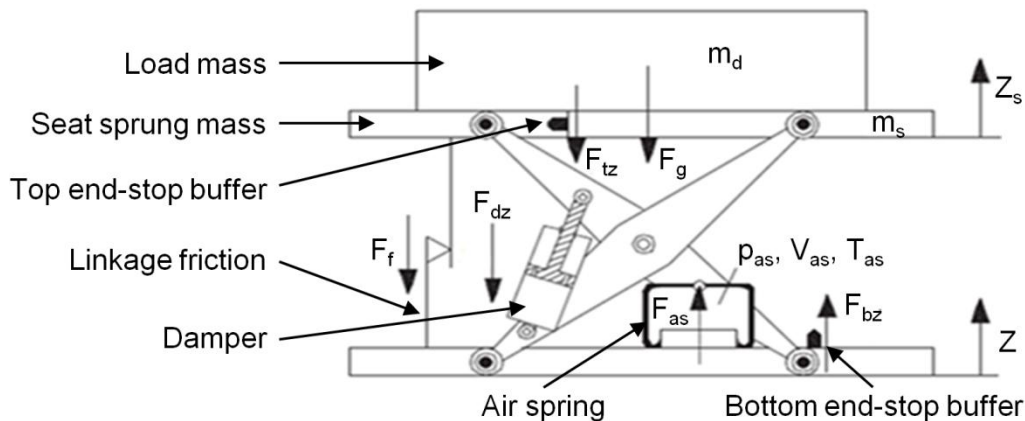


Fig. 2.32: Schematic illustration of an air suspension seat-occupant model [151]

$$(m_d + m_s)\ddot{Z}_s = F_{as} + F_{dz} + F_{BW} + F_{tz} + F_{bz} + F_g \quad (2.31)$$

$$F_{as} = \frac{1}{\delta_{as}} A_{ef} (p_{as} - p_0) \quad (2.32)$$

$$\dot{p}_{as} V_{as} + \kappa p_{as} \dot{V}_{as} + (\kappa - 1) A_{as} \alpha_{as} (T_{as} - T_w) = 0 \quad (2.33)$$

$$V_{as} = A_{ef} \left(\frac{Z_s - Z}{\delta_{as}} + h_0 \right) \quad (2.34)$$

$$T_{as} = \frac{p_{as} V_{as}}{m_{as0} R} \quad (2.35)$$

$$F_{dz} = -\frac{1}{\delta_d} \left(d_3 \left(\frac{\dot{Z}_s - \dot{Z}}{\delta_d} \right)^3 + d_2 \left(\frac{\dot{Z}_s - \dot{Z}}{\delta_d} \right)^2 + d_1 \left(\frac{\dot{Z}_s - \dot{Z}}{\delta_d} \right) \right) \quad (2.36)$$

$$\dot{F}_{BW} = -k_{BW} (\dot{Z}_s - \dot{Z}) + \gamma \left| \dot{Z}_s - \dot{Z} \right| F_{BW} + \beta (\dot{Z}_s - \dot{Z}) |F_{BW}| \quad (2.37)$$

$$F_{bz} = -k_{b3} (Z_s - Z + d_z)^3 - k_{b1} (Z_s - Z + d_z) \quad -d_z > Z_s - Z \quad (2.38)$$

$$F_{tz} = -k_{t3} (Z_s - Z - d_z)^3 - k_{t1} (Z_s - Z - d_z) \quad d_z < Z_s - Z \quad (2.39)$$

$$F_g = -(m_d + m_s)g \quad (2.40)$$

with

A_{as}	Surface of air spring in m^2
A_{ef}	Effective area of air spring in m^2
F_{BW}	Bouc-Wen force in N
F_{as}	Restoring force from the air spring in N
F_{bz}	Force coming from the bottom end-stop buffer in N
F_d	Damping force in N
F_{dz}	Vertical component of damping force in N
F_g	Gravity force in N
F_{tz}	Force coming from the top end-stop buffer in N
R	Gas constant in $J/(kg \cdot K)$
T_{as}	Temperature in air spring in K
T_w	Wall temperature of air spring in K
V_{as}	Volume of air spring in m^3
Z	Absolute displacement of seat base in the z-direction in m
Z_s	Absolute displacement of m_s in the z-direction in m
d_1	Linear damping coefficient in $N \cdot s/m$

d_2	Quadratic damping coefficient in $\text{N}\cdot(\text{s}/\text{m})^2$
d_3	Cubic damping coefficient in $\text{N}\cdot(\text{s}/\text{m})^3$
d_z	Distance between the middle position of the vertical seat suspension system and the bottom or the top end-stop buffer in m
h_0	Initial height of air spring in m
k_{BW}	Positive stiffness of Bouc-Wen model of hysteresis in N/m
k_{b1}	Linear stiffness coefficient of bottom end-stop buffer in N/m
k_{b3}	Cubic stiffness coefficient of bottom end-stop buffer in N/m^3
k_{t1}	Linear stiffness coefficient of top end-stop buffer in N/m
k_{t3}	Cubic stiffness coefficient of top end-stop buffer in N/m^3
m_{as0}	Initial air mass inside air spring in kg
p_{as}	Air pressure inside air spring in Pa
p_0	Atmospheric pressure in Pa
α_{as}	Overall heat transfer coefficient of an air spring in $\text{W}/(\text{m}^2\cdot\text{K})$
γ	Parameter of Bouc-Wen model of hysteresis in m^{-1}
β	Parameter of Bouc-Wen model of hysteresis in m^{-1}
δ_{as}	Reduction ratio of air spring
δ_d	Reduction ratio of damper
κ	Adiabatic coefficient

2.3.3.2 Optimization of the vertical seat suspension system

Air suspension seats are widely used on modern earth-moving vehicles. The air suspension system is generally comprised of an air spring, an inclined passive hydraulic damper and end-stop buffers. Improvement of the seat vibration attenuation performance can be achieved by optimizing the dynamic properties of the air spring, selecting proper damping coefficients of the damper and optimizing the stiffness and damping coefficients of the end-stop buffers. Hostens et al. proposed a method to improve the vibration attenuation performance of a passive air suspension seat. An additional air reservoir was used to lower the natural frequency of the seat. In addition, a throttle valve was inserted between the air spring and the additional air reservoir to provide variable damping coefficients. The laboratory tests show that the new proposed air suspension system provides a better vibration attenuation performance for seats on agricultural machinery or other vehicles with similar vibration excitations. [153] Maciejewski et al. optimized the volume of the additional air reservoir and the throttling critical conductance. Experiment results confirm that with the optimized air suspension system the vibration attenuation performance of the seat is improved up to 4 Hz, especially with heavier drivers. In addition, seat transmissibility at the seat resonance frequency is reduced efficiently under the low frequency excitations (such as the vibration input spectral class EM3 in ISO 7096

[154]). But reduction of the seat transmissibility is negligible under the high frequency excitations (such as the vibration input spectral class EM6 in ISO 7096 [154]). [151] In another study by Maciejewski et al., the air flow between the air spring and the additional air reservoir was actively controlled to change the air spring force and to improve the vibration attenuation performance. The investigation shows that the active air suspension system provides a better vibration attenuation performance than the passive air suspension system in the frequency range of 0-4 Hz. [155]

High magnitudes of vibrations and shocks on earth-moving vehicles can cause large suspension travel and severe end-stop impacts for suspension seats. It is important to keep the suspension travel in a reasonable range in order to provide a stable and safe environment to the driver. Ma et al. suggested that a further reduction in the seat natural frequency would not be feasible. The vibration attenuation performance of a suspension seat could be improved by selecting appropriate suspension damping coefficients. [133] Wu et al. proposed a procedure to improve the vibration attenuation performance of a passive air suspension seat [156]. This procedure includes two stages. In the first stage, the optimal stiffness and damping coefficients of the seat suspension system were determined by minimizing the seat effective amplitude transmissibility (SEAT) under random excitations with low and moderate magnitudes, while limiting the suspension dynamic deflection below the free stroke. In the second stage, improvement of the seat performance, under high magnitude excitations involving end-stop impacts, was realized by optimizing the force-deflection characteristics of end-stop buffers through minimizing the vibration dose value ratio (VDVR) of the seat suspension system. In the first stage of the optimization, two random excitations standardized in ISO 7096 for tractor scrapers were used. To solve the optimization problem in the second stage, two types of excitations with varying magnitudes were used: (1). sinusoidal excitations with frequencies in the vicinity of the seat resonant frequency and with the root mean square (RMS) value ranging from 0.7 to 2.8 m/s²; (2). standardized excitations in ISO 7096 for tractor scrapers multiplied by factors of 1.0, 1.5 and 2.0. Wu and Griffin adopted a semi-active damper with electrorheological fluid to reduce the occurrence and severity of end-stop impacts in a suspension seat [157]. After reviewing different control policies of the semi-active damper, they proposed a new 'soft-hard' control policy which is formulated in Eq. (2.41).

$$c = \begin{cases} c_{hard} & |d| > d_{soft} \\ c_{soft} & |d| \leq d_{soft} \end{cases} \quad (2.41)$$

with

c_{soft}	Damping coefficient of the semi-active damper in the soft-state in N·s/m
c_{hard}	Damping coefficient of the semi-active damper in the hard-state in N·s/m
d_{soft}	Maximum suspension travel when the semi-active damper in the soft-state in m

Wu and Griffin investigated the effect of d_{soft} and c_{hard} on the reduction of the VDVR in laboratory seat tests. The results show that a shorter d_{soft} as well as a higher c_{hard} helps to prevent the occurrence of end-stop impacts and to reduce the vibration severity in case of an end-stop impact. In the laboratory seat tests, vibration attenuation performance of the suspension seat with this 'soft-hard' controlled semi-active damper was evaluated under random excitations with various magnitudes. The results show that the new proposed 'soft-hard' control policy enables the seat suspension to achieve a better vibration attenuation performance, irrespective of excitation magnitudes. [157]

2.3.3.3 Model for the longitudinal direction

Most studies focus on the investigation of the seat dynamics and the improvement of the seat vibration attenuation performance in the vertical direction. But during daily operation of construction vehicles, drivers are exposed to random multi-axial vibrations. The longitudinal vibrations on construction vehicles are also severe. Seats with a longitudinal suspension system have been supplied by seat manufacturers already. However, only a few studies investigated the dynamic behavior and the vibration attenuation performance of a seat with a longitudinal suspension system. Models of the longitudinal seat suspension system were quite simple in these limited studies. They were generally comprised of a spring, a damper, a friction force element and two end-stop buffers, as shown in Fig. 2.33 [78],[158],[159].

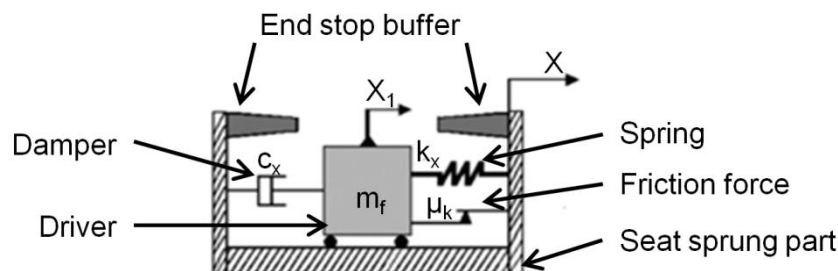


Fig. 2.33: Seat-occupant model with a longitudinal suspension system [158],[159]

2.3.3.4 Optimization of the longitudinal seat suspension system

In the study by Fleury and Mistrot, a longitudinal seat suspension system was optimized by satisfying the following four constraints [78]:

- 1) Transmissibility between the lower body of the driver and the excitation point should be lower than 1.
- 2) Transmissibility between the upper body of the driver and the excitation point should be lower than 1.
- 3) Suspension travel should be shorter than the suspension free stroke to ensure that no end-stop impact occurs.
- 4) Interaction force between the driver's back and the seat backrest should be lower than a preset value of 100 N.

The authors developed two cushion-occupant models to calculate the transmissibility and the interaction force between the driver and the excitation points. These models are illustrated in Fig. 2.19 (p. 24). The original and the optimal parameters of the longitudinal seat suspension system are presented in Tab. 2.12. With the optimized longitudinal seat suspension system, the SEAT value decreases by about 50%. [78]

Tab. 2.12: Parameters of the original and the optimized longitudinal seat suspension system [78]

	Stiffness coefficient (N/m)	Damping (N·s/m)	Free stroke (mm)
Original	1000	600	± 13
Optimal	3400	600	± 20

The seat-occupant model in the studies by Stein et al. on the optimization of the longitudinal seat suspension system is illustrated in Fig. 2.33. [158],[159]

In the study [158], the damper was supposed to work at low velocities with a constant damping coefficient. Firstly, the authors used the 'fminsearch' function in MATLAB to search the optimal stiffness and damping coefficients for the minimum seat effective amplitude transmissibility (SEAT). This function finds the minimum of a function of several variables in the neighborhood of an initially chosen point. However, the optimal stiffness and damping coefficients determined by this method are extremely low. Taking into consideration the ergonomic and psychological reasons, the results

were not accepted by the authors. Secondly, the authors investigated the variation of the SEAT value depending on the damping coefficient and determined the optimal damping coefficient, while the stiffness coefficient was kept unchanged. With the optimal damping coefficient, the SEAT value in the longitudinal direction could be reduced by about 10%.

In the study [159], the damping coefficients of the longitudinal seat suspension system were optimized when the seat was exposed to two types of excitations: the terrain excitation and the impulse excitation. The terrain excitation was measured when a wheel loader was driven on rough terrain, and the impulse excitation was measured during a bucket loading operation of the wheel loader [78]. Under these two excitations, the damper works not only at low speeds but also at high speeds. In this case, the force-velocity relationship of the damper is nonlinear, as shown by the solid line in Fig. 2.34. Different optimal damping coefficients were obtained under the above mentioned two excitations, as shown by two dash lines in Fig. 2.34. Compared to the damping coefficients optimized under the impulse excitation, they optimized under the terrain excitation provide a better suspension vibration attenuation performance for both excitations.

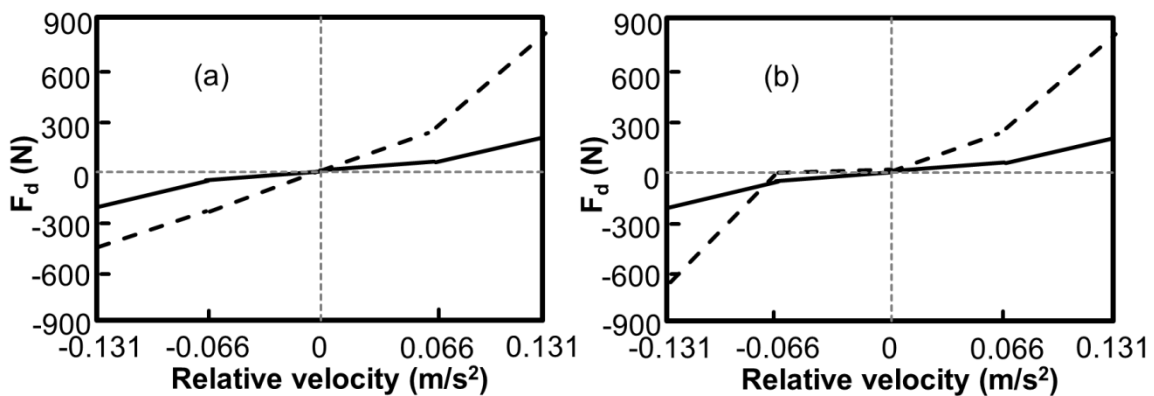


Fig. 2.34: Comparison between the original (solid line) and the optimized (dash line) force-velocity curves of damper (a). with the optimization result under the terrain excitation, (b). with the optimization result under the impulse excitation [159]

3 Motivation

People with long-term exposure to whole-body vibrations (WBV), such as the occupational drivers of earth-moving vehicles, suffer health-related consequences of WBV. Absence from work and disability pension due to WBV-related health problems lead to time consuming and economic losses for both employers and employees. The temporary reactions of drivers caused by the short-term exposure to WBV, such as muscle fatigue, ride discomfort and loss of balance, can affect the drivers' ability to control the vehicle, reduce the work efficiency and even can cause safety problems. In Europe the directive 2002/44/EC [89] lays down the minimum requirement on the daily vibration exposure for the member states. To protect drivers from health and safety risks caused by WBV, the WBV exposure levels on the vehicles need to be evaluated at first. If the minimum requirement is not satisfied, technical and organizational methods should be implemented to reduce the exposure levels. Accordingly, the first main objective of this research work is to propose improvements for the current evaluation procedures and use them to evaluate the WBV exposure levels. The second main objective is to reduce the WBV exposure levels by optimizing the vehicle suspension systems and by improving the driver's sitting situations.

To achieve the first main objective, the tasks needed to be carried out are described as follows:

A large effort has been made in previous studies to evaluate the WBV exposure levels on various vehicles in different work tasks and at different work places. Compact wheel loaders (CWLs) are widely used in construction activities, due to their small size but still ample lift capacity and maneuverability. However, only a few investigations on the WBV exposure levels arising from CWLs were carried out. Accordingly, the first task in this research work is to evaluate the WBV exposure levels on a CWL. In this part of work, the permitted daily exposure durations will be calculated, and the health risks caused by WBV will be predicted. For the health evaluation, two different procedures are introduced in two ISO standards: ISO 2631-1:1997 and ISO 2631-5:2004. It is confusing to decide which of these two standards should be chosen for the evaluation of WBV from the CWL, because no application condition is clearly defined in these standards. Therefore, both of them are used to fulfill the first task.

Several studies also adopted these two standards to predict the health risks caused by WBV from different types of vehicles. Some of these studies found out that the evaluation procedure in ISO 2631-1:1997 is more stringent and the boundaries of the health guidance caution zone (HGCZ) in this standard should be increased. Other studies obtained a contrary conclusion. Taking this research state into account, the second task in this work is to compare the evaluation results obtained according to ISO 2631-1:1997 and ISO 2631-5:2004, as well as to find out the reasons for the different evaluation results. In this part of work, it will be discussed whether the HGCZ boundaries in these two standards are equal. If not, the equal boundaries of the HGCZ need to be found out. With the equal boundaries, the permitted daily exposure durations should be calculated again to study whether there are any other reasons for the different evaluation results.

Several details of the evaluation procedure in ISO 2631-1:1997 are obscure, such as how to select the suitable quantification method and the vibration directions for the evaluation. It is clearly explained in ISO 2631-5:2004 that the given evaluation procedure has not been validated. Therefore, the third task in this work is to discuss whether the details of the procedures in both standards are suitable or not to evaluate the WBV arising from the CWL. This task aims to propose suggestions on the improvement of these details for the standard revision in the future.

There is still no study carried out to evaluate the effect of short-term exposure to WBV on the ride comfort of the CWLs. ISO 2631-1:1997 and ISO 2631-1:1985 introduce the procedures for the ride comfort evaluation. With the procedure in ISO 2631-1:1997, the levels of the ride discomfort can be obtained by calculating the vector sum values (VSV) of root mean square (RMS) values of accelerations in different directions. With the procedure in ISO 2631-1:1985, the exposure durations for reduced comfort can be obtained by comparing the RMS values of accelerations in 1/3 octave band with the reduced comfort boundary (RCB) curves. The fourth task in the thesis is to evaluate the ride discomfort caused by WBV on the CWL using both ISO 2631-1:1997 and ISO 2631-1:1985. This part of work gives the levels of the ride discomfort as well as the exposure durations for the reduced comfort on the CWL.

To achieve the second main objective, the tasks needed to be carried out are described as follows:

In general, small-sized construction vehicles are not equipped with axle and cabin suspension systems. Consequently, the influence of the suspension seat on the WBV exposure levels becomes significantly important. Lots of studies analyzed the influence of seat cushion and seat suspension components on the seat transmissibility. The driver's dynamic behavior affects the seat transmissibility as well, because the driver and the seat interact with each other. The safety belt restricts the movement of the driver and accordingly affects the seat transmissibility. In previous studies the effectiveness of a safety belt was studied only for the case that a car collision occurs. No study was carried out to investigate the effect of a safety belt on the seat transmissibility. This investigation will be carried out as the fifth task in this work based on the analysis of the seat effective amplitude transmissibility (SEAT) and the seat transmissibility in the frequency domain. The purpose of this part of work is to find out the proper configuration of the safety belt for a more comfortable sitting situation.

Due to the variety of operational conditions, suspension seats on construction vehicles are exposed to vibrations with a wide range of magnitudes. As reviewed in section 2.3.2, under excitations with different magnitudes, dynamic characteristics of a suspension seat are in different states, and different suspension configurations are required to effectively attenuate vibrations. The range of the magnitude of seat excitations and the seat dynamic characteristics under these excitations should be taken into consideration to determine the optimal suspension configuration. In previous studies the seat suspension system was optimized under the standardized excitation signals from ISO 7096 [154] multiplied by different factors. These excitations cannot reflect the range of the magnitude of seat excitations in real operations. It means that the optimal suspension configuration determined under these excitations may be not the best one under the real operational conditions. The sixth task in this thesis therefore is to find out an optimization solution for the seat suspension system based on the investigation of the excitations measured in various CWL operations and the analysis of the dynamic characteristics of the suspension seat under these excitations.

For seats exposed to vibrations with a wide range of magnitudes, their vibration attenuation performance can be efficiently improved by optimizing a passive hydraulic damper or a semi-active damper controlled depending on the suspension dynamic deflections. But no study compares the improvement of the vibration

attenuation performance achieved by the optimization of these two types of dampers. This comparison will be carried out as the seventh task in this work in order to select the optimal damper for the seat suspension system.

Most of the previous studies concentrated on investigation and improvement of the vibration attenuation performance of the vertical seat suspension system. Although longitudinal vibrations on construction vehicles are also severe, only a few studies optimized the longitudinal seat suspension system. In these studies human models are too simple to accurately simulate the human dynamic behavior. This possibly leads to incorrect optimization results. As the eighth task of this research work the optimization of the longitudinal seat suspension system will be carried out. For this, a human model with which the human dynamic behavior can be accurately simulated needs to be employed.

4 Measurement and Analysis of Vibrations

4.1 Vibration measurement

In order to analyze the characteristics of vibrations in different typical operations of compact wheel loaders (CWLs), to evaluate the effects of whole-body vibrations (WBV) arising from CWLs on the human health and the ride comfort, to study the effect of a safety belt on the seat transmissibility, as well as to obtain the excitation signals for the seat tests in laboratory, field tests of vibration measurement on a CWL were carried out. The detailed description of the field tests is presented in this chapter.

4.1.1 Test vehicle

The vibration accelerations were measured on a medium-sized CWL. The weight of the CWL is around 6400 kg when the bucket is empty and around 7900 kg when the bucket is full of gravels. The transmission has two gears. The highest speed in the first gear is around 6.9 km/h and about 19.8 km/h in the second gear. The CWL is not equipped with axle suspension system. Four rubber elements are installed between the vehicle frame and the cabin as a suspension system. The seat on the CWL does not have any suspension system in the longitudinal and the lateral directions. It is supported on a scissors linkage mechanism in the vertical direction. The vertical seat suspension system is comprised of a passive air spring and an inclined passive hydraulic damper. The free stroke of the vertical seat suspension system is 88 mm. When it is exceeded, the impact against the top or the bottom end-stop buffer occurs. The seat height is adjustable with the help of a build-in air compressor. The seat also provides adjustment of the inclination of backrest and seat cushion.

The vibration accelerations were measured in three cases. Case A is that the driver did not wear a safety belt. Case B is that the driver wore an automatic lap belt, as shown in Fig. 4.1 (a). The automatic lap belt is the original safety belt provided by the seat manufacturer. It is activated and locked up when vibrations are severe. In case B, the movement of the driver is restricted only when the lap belt is locked up. Case C is that the driver wore a four-point seat harness, as shown in Fig. 4.1 (b). In this case, the movement of the driver is highly restricted.

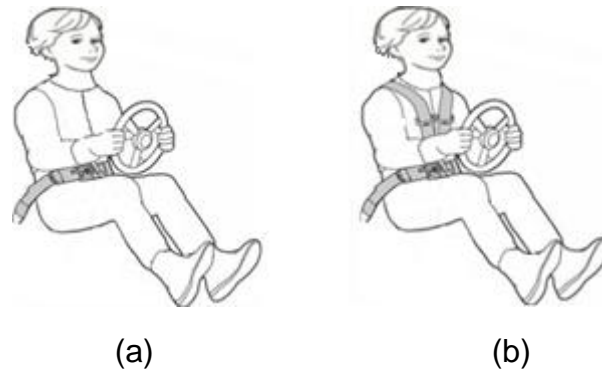


Fig. 4.1: (a). Schematic drawing of the case that the driver wears a lap belt; (b). Schematic drawing of the case that the driver wears a four-point seat harness

4.1.2 Test operations

The accelerations were measured in ten different typical CWL operations with the same experienced driver. The test operations and the measurement durations are listed in Tab. 4.1. The driver's weight is 80 kg, and his height is 1.75 m. The vibration measurements were carried out in all ten operations in cases B and C. Due to the limited testing time, the measurements in case A were carried out only in operations OP-1.3, OP-2.1, OP-2.3, OP-3.1 and OP-4.

Tab. 4.1: Operations of the CWL in the field tests and the measurement durations

		Test operations ¹⁰	Speed (km/h)	Repetition	Duration (s)	Distance (m)	
Group (Gr.) 1	OP-1.1	Driving on a loop with different types of road	(1)	6.9	3	360	681
	OP-1.2		(2)	6.9	3	360	679
	OP-1.3		(1)	19.8	3	126	684
	OP-1.4		(2)	19.8	3	126	687
Gr. 2	OP-2.1	Driving over two alternating obstacles	(1)	6.9	4	44	82
	OP-2.2		(2)	6.9	4	44	82
	OP-2.3		(1)	19.8	4	44	240
Gr. 3	OP-3.1	Driving over two inline obstacles	(1)	6.9	4	44	81
	OP-3.2		(2)	6.9	4	44	80
Gr. 4	OP-4	V-cycle	-	9	305	322	

¹⁰ Symbol (1) represents the empty bucket and symbol (2) represents the bucket with full of gravels.

The first group of operations, OP-1.1 to OP-1.4, deals with driving on a test loop with different types of road, which is shown in Fig. 4.2. It is comprised of asphalt and concrete road with smooth surface, compacted soil road and gravel road with rough surface, and short slopes.



Fig. 4.2: The loop with different types of road for driving

The second operation group, OP-2.1 to OP-2.3, refers to the driving over two alternating obstacles, while the third group, OP-3.1 and OP-3.2, involves the driving over two inline obstacles.

The layout of the operation with two alternating obstacles is shown in Fig. 4.3, and that with two inline obstacles is shown in Fig. 4.4. The obstacles were fixed on a smooth concrete road. Each operation in the second and the third groups can be divided into the following three steps. In the first step, the CWL was driven about 25 m of distance on the concrete road to stabilize the vehicle speed; in the second step, it was driven over the obstacles at a constant speed; in the third step, after the obstacles it was driven about 50 m of distance on the concrete road and then turned by about 180 degrees. This procedure in each operation was repeated four times. The vibration signal in each repetition was selected from 1 s before the first obstacle until 10 s after the first obstacle for the analysis.

The two obstacles on both sides have the same dimensions. The height of each obstacle is 0.08 m, the width is 0.5 m, and the length is 1 m, as shown in Fig. 4.5.

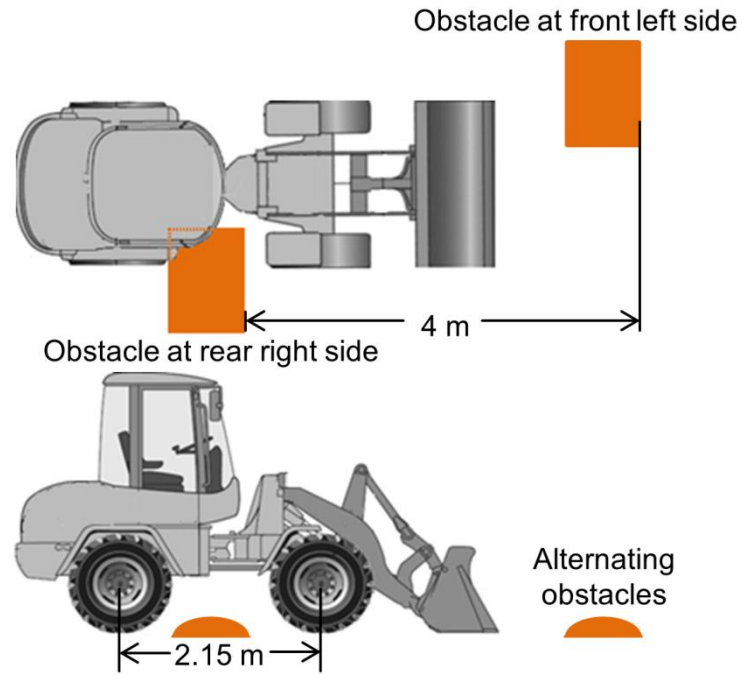


Fig. 4.3: Top and front views of the layout of the operation with two alternating obstacles

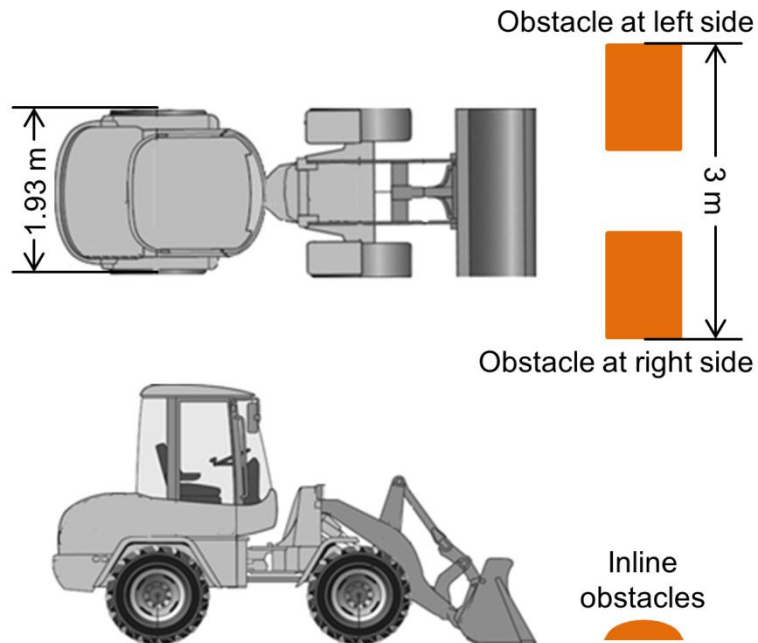


Fig. 4.4: Top and front views of the layout of the operation with two inline obstacles



Fig. 4.5: Front and side views of the obstacle

The fourth operation group OP-4 deals with the V-cycle. It is a typical operation of CWLs and includes six steps, as shown in Fig. 4.6 (a). In step (1), the CWL is driven forward from the starting location to the material stack; in step (2), the bucket is filled with the material; in step (3), the CWL is driven backward to the starting location and turned by approximately 90 degrees to the right to face the dumping place; in step (4), it is driven forward from the starting location to the dumping place; in step (5), it dumps the material at the dumping place; in step (6), it is driven backward from the dumping place to the starting location. [160] The material stack used for the measurements is shown in Fig. 4.6 (b).

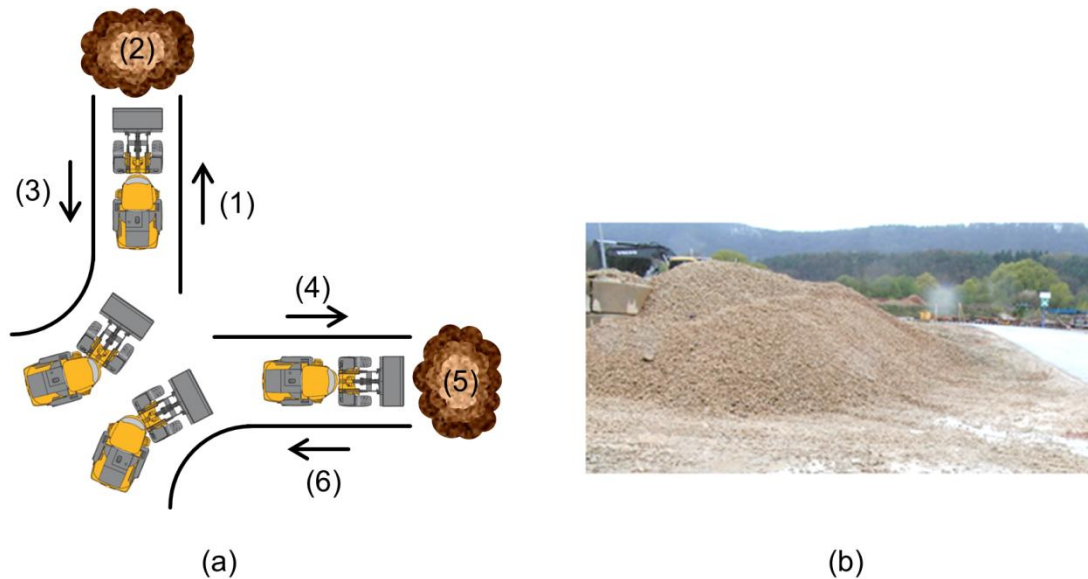


Fig. 4.6: (a). V-cycle; (b). Material stack for the V-cycle

4.1.3 Data acquisition equipment

The whole data acquisition equipment used in the field tests includes eight tri-axial accelerometers (PCB PIEZOTRONICS ICP 356A16), two tri-axial seat pad accelerometers (a PCB PIEZOTRONICS ICP 356B41 and an Endevco Model 2560), a gyroscope (3DM-GX3-25), an imc™ Cronos-PL-16 chassis and a laptop.

Four tri-axial accelerometers were fixed at the four corners on the vehicle frame just below the four rubber elements, which act as a suspension for the cabin. Another four tri-axial accelerometers were fixed at the four corners on the cabin floor just upon the four rubber elements. These eight tri-axial accelerometers can measure accelerations ranging from 0.5 Hz to 4500 Hz in three translational directions. One tri-axial seat pad accelerometer (PCB PIEZOTRONICS ICP 356B41) was fixed on the top surface of the seat cushion and the other (Endevco Model 2560) was fixed on

the seat backrest. These two seat pad accelerometers can measure three translational accelerations ranging from 0.5 Hz to 1000 Hz. The gyroscope was fixed at the seat base (approximately in the middle of the cabin floor). It can measure three translational accelerations and three angular velocities. Locations of all sensors on the CWL are illustrated in Fig. 4.7.

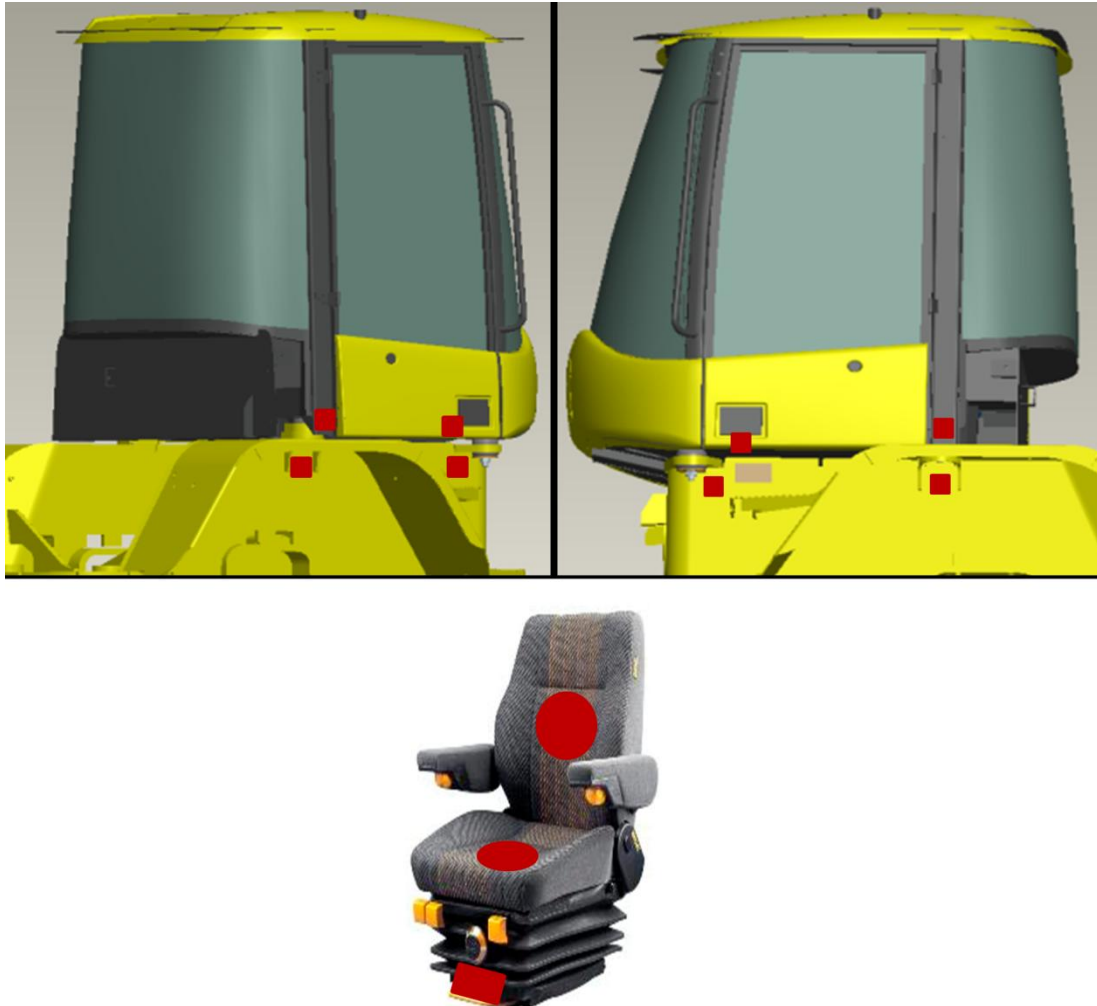


Fig. 4.7: Locations of sensors on the CWL (marked using red color)

All ten accelerometers were connected to the imcTM chassis, which converts the analog signals to the digital ones, stores and transmits the data to the laptop. The software imc DEVICES 2.6 in the laptop was used to display the signals, to control the chassis and to store the data coming from the chassis. The gyroscope was connected to the laptop through a USB port. Using a Labview program, the signals picked up by the gyroscope were converted to digital signals and stored in the laptop. The battery of the CWL provided power for the whole acquisition equipment.

The sampling frequency of the signals picked up by the accelerometers was set to 10,000 Hz. It was set to 1000 Hz for the signals picked up by the gyroscope.

4.2 Analysis of vibration characteristics

4.2.1 Purpose and method of analysis

The purpose of this analysis is to study the characteristics of vibration excitations under the seat on the CWL, as well as the influence of the operational conditions, such as the driving speed, the bucket load condition and the unevenness of road surface, on the vibrations of the CWL. To achieve this purpose, signals measured on the cabin floor or the frame should be analyzed. Because these signals have negligible differences, especially at low frequencies, only the analysis of vibrations measured at the middle of the cabin floor (at the seat base) is discussed in this section.

For the analysis the root mean square (RMS) value of the accelerations in each 1/3 octave band ($\tilde{a}_{1/3ob}$) is used, which was calculated with Eq. (2.20) (p. 38). Due to the following four reasons, only the vibrations in three translational directions were analyzed.

- 1) The characteristics of vibrations at the seat base are analyzed for the optimization of seat suspension systems later in chapter 7. Because the seat is equipped with suspension systems only in translational directions, rotational excitations are not needed to be taken into account for the optimization.
- 2) The influence of the operational conditions on the CWL vibrations is studied with the purpose to reduce the WBV at their source by selecting proper operational conditions, accordingly to reduce the health risks and the ride discomfort. Only the translational vibrations are desired to evaluate the effects of WBV on human health and ride comfort.
- 3) Because the seat base position is at about 0.9 m above the roll and the pitch axes of the CWL, the rotational movement of the CWL affects the magnitudes of the translational vibrations at the seat base. The variation of the rotational movement can be studied by analyzing the translational vibrations.
- 4) Angular velocities were picked up by the gyroscope, rather than the rotational accelerations. Analysis of the rotational accelerations derived from the angular velocities may lead to inaccurate results.

4.2.2 Analysis results

4.2.2.1 Influence of driving speed

In Fig. 4.8 to Fig. 4.10, the values of the $\tilde{a}_{1/3ob}$ in the three translational directions at the seat base when the CWL was driven at the lower speed of 6.9 km/h (slow) are compared with those at the higher speed of 19.8 km/h (fast). It can be observed that the driving speed has a large influence on the vibration intensity. The corresponding driving operations are those that were carried out at both speeds, i.e.:

- unloaded driving on the loop (OP-1.1 and OP-1.3)
- loaded driving on the loop (OP-1.2 and OP-1.4)
- unloaded driving over alternating obstacles (OP-2.1 and OP-2.3)

Fig. 4.8 shows the comparison of the longitudinal vibrations.

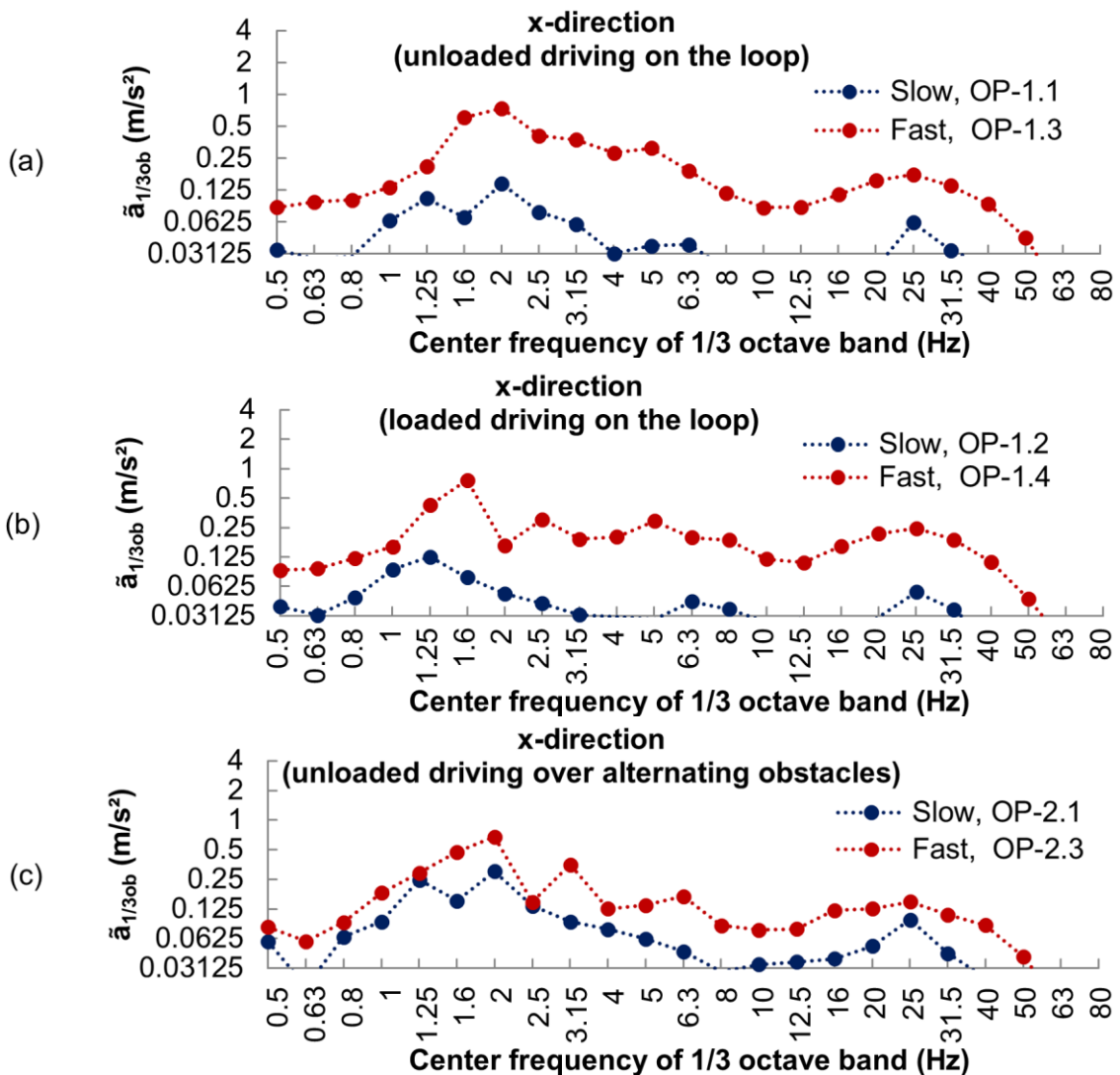


Fig. 4.8: Comparison of longitudinal vibrations at the seat base in the slow and the fast driving

In Fig. 4.8 (a) and (c) it can be observed that the maximum RMS value occurs at about 2 Hz during the unloaded driving on the loop and over the alternating obstacles. It shifts to lower frequencies in Fig. 4.8 (b) during the loaded driving on the loop. The shift of the frequency at which the maximum RMS value occurs is caused by the change of the bucket load condition and hardly affected by the driving speed. The longitudinal vibrations are strongly affected by the pitch movement of the CWL, which means it highly depends on the pitch dynamic properties of the CWL. The bucket load condition has a large influence on the pitch dynamic properties, such as the natural frequency in the pitch direction.

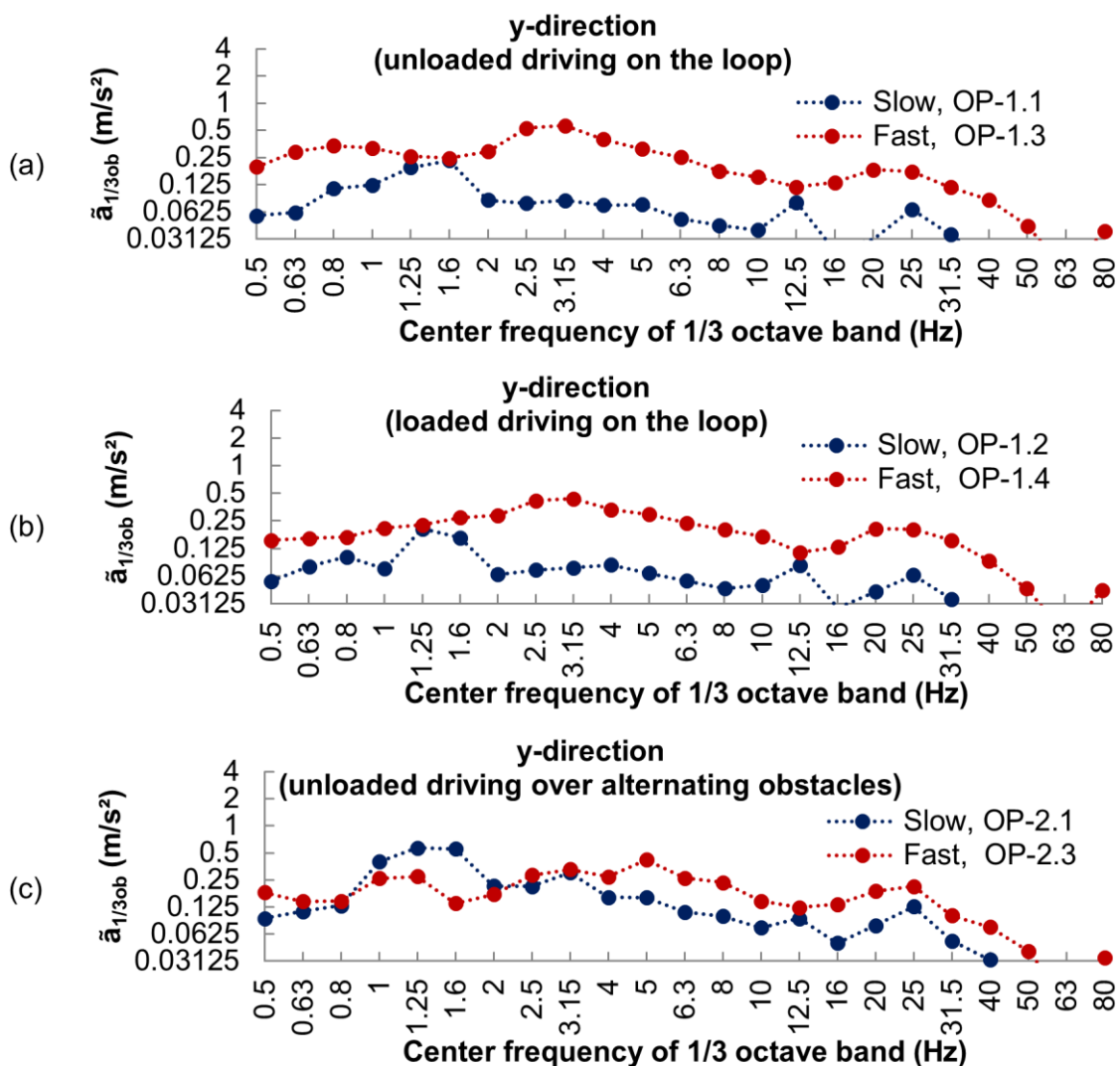


Fig. 4.9: Comparison of lateral vibrations at the seat base in the slow and the fast driving

Fig. 4.9 shows the comparison of the lateral vibrations. In Fig. 4.9 (a) and (b) it can be observed that for slow driving on the loop the maximum RMS value occurs at about 1.6 Hz and 1.25 Hz respectively, but shifts to 3.15 Hz while fast driving. In Fig.

4.9 (c), it is shown that the maximum RMS value also occurs at about 1.25 Hz with slow driving over the alternating obstacles, but shifts to 5 Hz while fast driving. It can be concluded that in the lateral direction the frequency where the maximum RMS value occurs increases with the driving speed, and that the bucket load has a minor influence. The lateral vibrations are mainly caused by the vehicle roll movement, which is generated by the relative height of the road unevenness on the left and the right wheel paths. The frequency of the excitations for the roll movement increases with the vehicle speed. It brings the result that the roll movement and accordingly the lateral vibrations shift to higher frequencies at a higher driving speed.

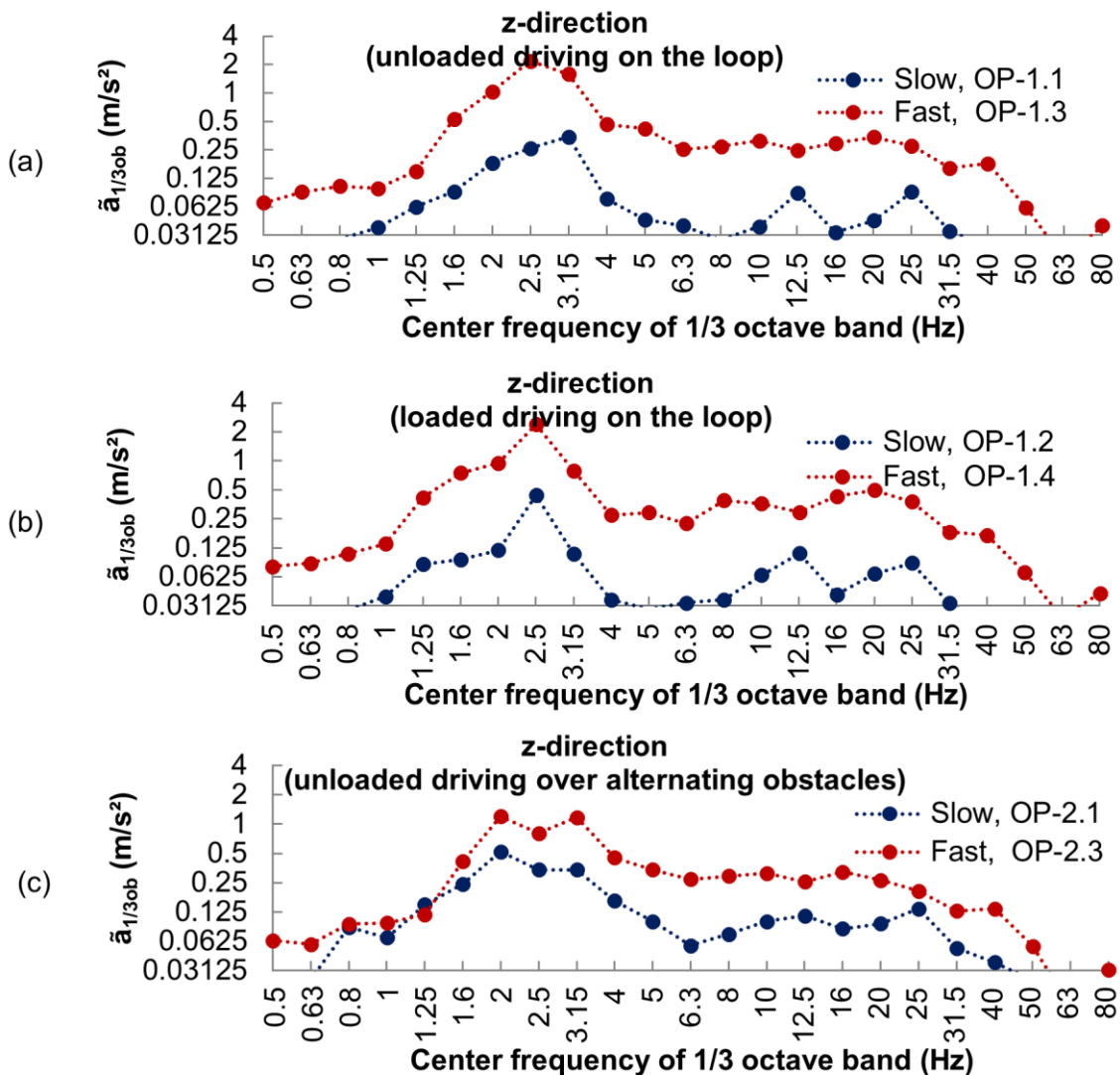


Fig. 4.10: Comparison of vertical vibrations at the seat base in the slow and the fast driving

Fig. 4.10 shows the comparison of the vertical vibration results. The maximum RMS values occur between 2 and 3.15 Hz. In this direction the driving speed has a small influence on the frequency where the maximum RMS value occurs. The vertical

vibration characteristics is mainly depended on the vertical dynamic properties of the CWL. The frequency where the maximum RMS value occurs is the natural frequency of the CWL in the vertical direction.

4.2.2.2 Influence of bucket load condition and unevenness of road surface

In this section, at first the influence of the bucket load condition on the vibrations of the CWL is discussed. The RMS values of the accelerations in 1/3 octave band ($\tilde{a}_{1/3ob}$) in the three translational directions at the seat base when the CWL was driven with the empty bucket (unloaded driving) are compared with those when the CWL was driven with the bucket full of gravels (loaded driving). The comparison results are illustrated in Fig. 4.11 to Fig. 4.13. The corresponding operations are those that were carried out with both bucket load conditions, i.e.:

- slow driving on the loop (OP-1.1 and OP-1.2)
- fast driving on the loop (OP-1.3 and OP-1.4)
- slow driving over alternating obstacles (OP-2.1 and OP-2.2)
- slow driving over inline obstacles (OP-3.1 and OP-3.2)

Fig. 4.11 shows the comparison of the longitudinal vibrations. It can be observed that the influence of the bucket load condition is only obvious at frequencies between 1 Hz and 5 Hz. The RMS values during loaded driving are smaller than those during unloaded driving in the frequency range of 1.6-5 Hz, and slightly bigger between 0.5 and 1.6 Hz. The maximum RMS value in the longitudinal direction occurs at 2 Hz during the unloaded driving, and shifts to 1.25 Hz or 1.6 Hz during the loaded driving. The difference of longitudinal vibrations between loaded and unloaded driving is due to the fact that the heavier vehicle weight leads to the decrease of the vehicle's natural frequency in the pitch direction.

Fig. 4.12 shows the comparison of the lateral vibrations. It can be observed that the influence of bucket load condition on the lateral vibrations is negligible, especially at frequencies higher than 4 Hz.

Fig. 4.13 shows the comparison of the vertical vibrations. It can be noticed that the influence of bucket load condition on the vertical vibrations is also quite small. The RMS values in the loaded driving are smaller than those in the unloaded driving in the range of 2.5-6.3 Hz, but a little larger in the range of 1-2 Hz. This is also due to

the fact that a heavier vehicle weight leads to a lower vehicle's natural frequency in the vertical direction.

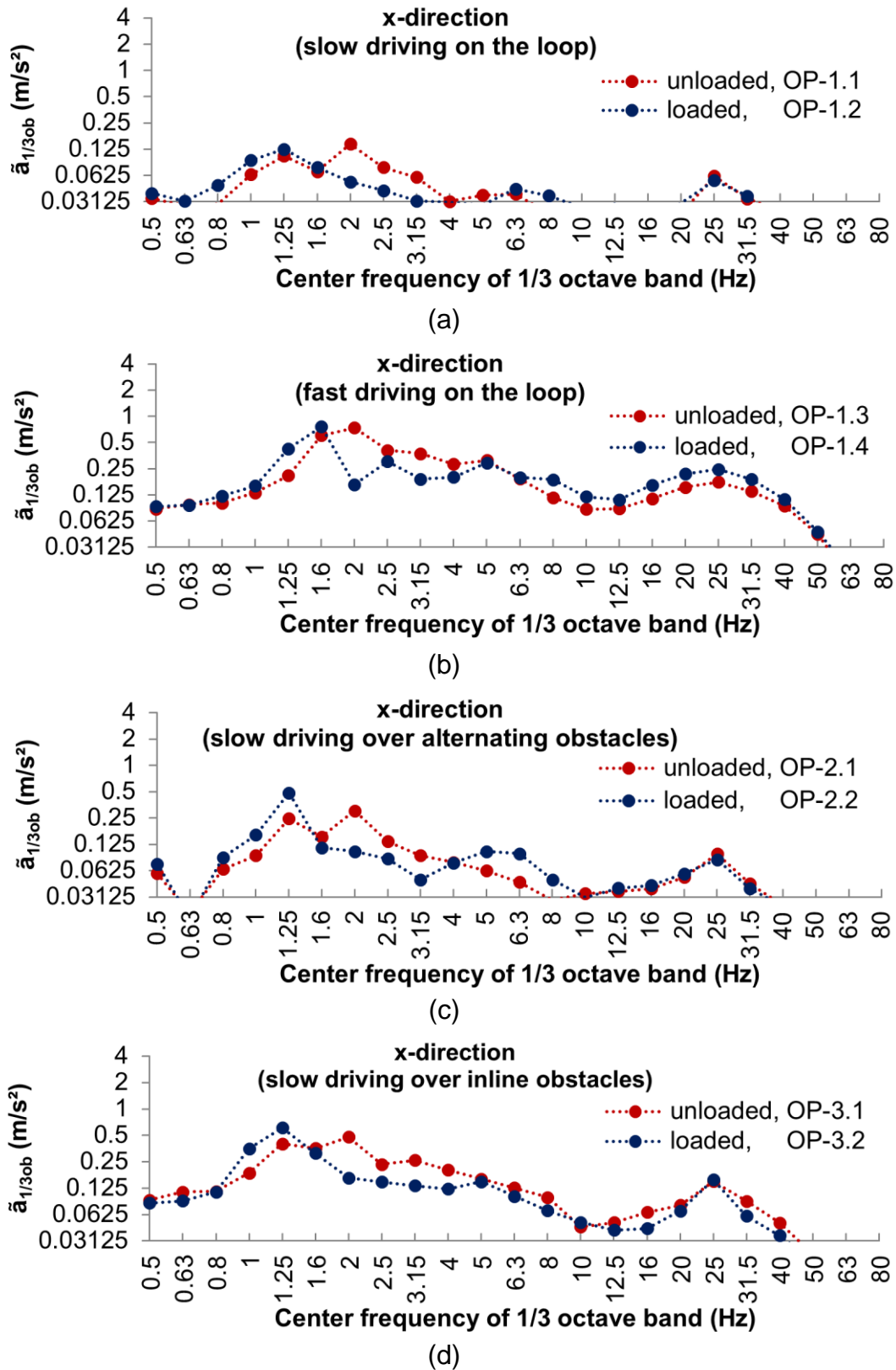


Fig. 4.11: Comparison of longitudinal vibrations at the seat base in unloaded and loaded driving

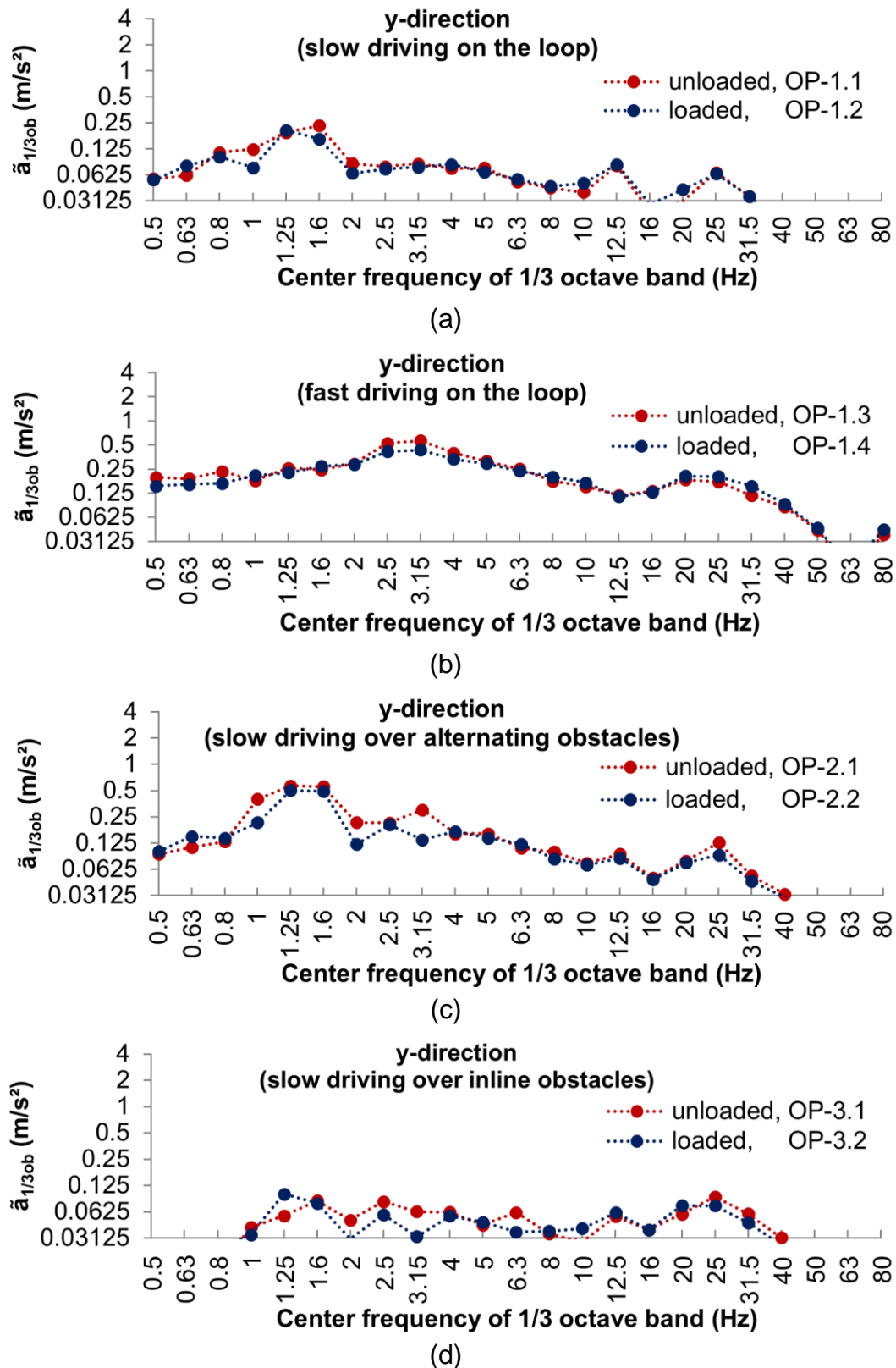


Fig. 4.12: Comparison of lateral vibrations at the seat base in unloaded and loaded driving

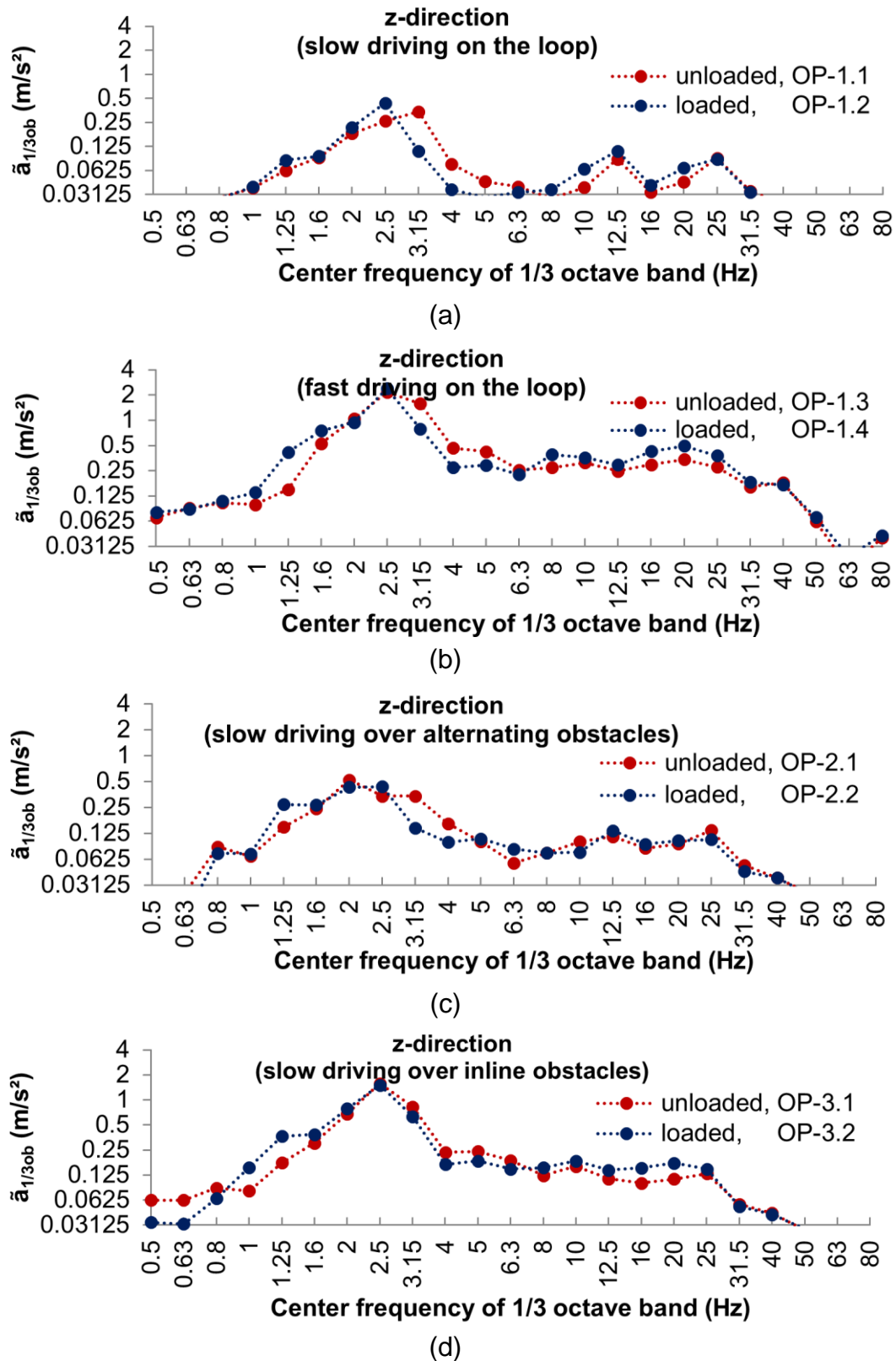


Fig. 4.13: Comparison of vertical vibrations at the seat base in unloaded and loaded driving

The influence of unevenness of road surface can be studied by comparing the values of $\tilde{a}_{1/3ob}$ in driving over alternating obstacles ((c) in Fig. 4.11-Fig. 4.13) with those in driving over inline obstacles ((d) in Fig. 4.11-Fig. 4.13).

By comparing Fig. 4.11 (c) and (d) it can be observed that the frequency where the maximum RMS value occurs during driving over the inline obstacles is the same as that while during driving over the alternating obstacles. The longitudinal vibrations during driving over the inline obstacles are larger than those during driving over the alternating obstacles in the whole frequency range. The same conclusion can be obtained for the vertical vibrations by comparing Fig. 4.13 (c) and (d).

By comparing Fig. 4.12 (c) and (d) it can be noticed that the lateral vibrations during driving over alternating obstacles are much larger than those during the driving over inline obstacles. In the driving operations with alternating obstacles, the height difference of the tracks on which the left and the right wheels are driven at the same time is larger than that in the operations with inline obstacles. It generates a large roll movement of the vehicle and accordingly causes large lateral vibrations.

4.2.2.3 Vibrations during the V-cycle

The vibration characteristics during all driving operations with a constant speed are discussed in sections 4.2.2.1 and 4.2.2.2. Here the vibration characteristics during the V-cycle are analyzed. The RMS values of accelerations in 1/3 octave band ($\tilde{a}_{1/3ob}$) in the operation of V-cycle are illustrated in Fig. 4.14.

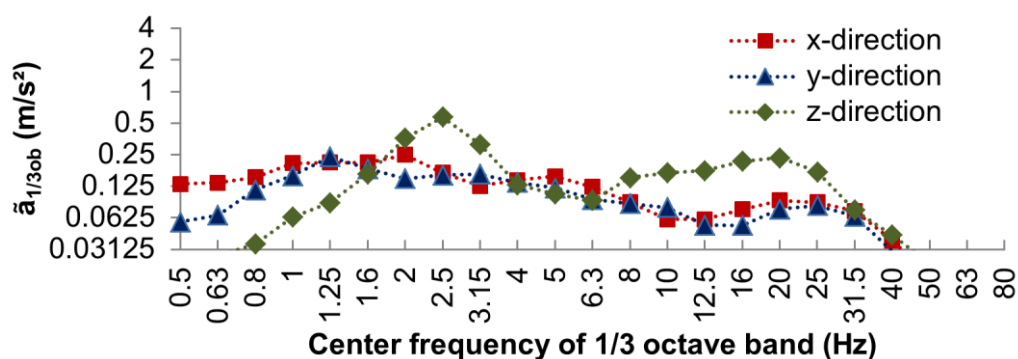


Fig. 4.14: The RMS values of accelerations in 1/3 octave band in three translational directions on the cabin floor during the V-cycle

It can be observed that during the V-cycle the RMS values in the longitudinal direction vary in a small range at frequencies below 6.3 Hz. The longitudinal vibrations are mainly generated when stopping and accelerating the vehicle, as well as when loading the materials. The RMS values in the lateral direction are almost

constant at frequencies between 1 Hz and 4 Hz. The lateral vibrations are principally generated during the turning of the vehicle. In the vertical direction, there is a clear peak of the RMS values at 2.5 Hz. In this direction, vibrations are generated by the unevenness of the road during driving and by the bucket shaking when dumping the materials.

4.3 Conclusion

In this chapter field tests of vibration measurements on a medium-sized compact wheel loader (CWL) in ten operations are introduced. The vibration characteristics on the CWL in the frequency domain are obtained from the analysis of the root mean square (RMS) values of accelerations in 1/3 octave band. In the longitudinal direction the maximum RMS values occur in the range of 1.25-2 Hz. In the lateral direction they occur in the range of 1.25-1.6 Hz in the slow driving and in the range of 3.15-5 Hz in the fast driving. In the vertical direction the maximum RMS values occur mainly in the frequency range of 2-3.15 Hz.

The influence of the driving speed, the bucket load condition and the unevenness of road surface on the vibration characteristics at the middle of the cabin floor (at the seat base) is discussed as well. The driving speed has a large influence on the vibration intensity on the CWL. On the other hand, the increase of driving speed results in a large increase of the frequency at which the maximum RMS value occurs in the lateral direction. The unevenness of the road surface has a significant influence on the vibration intensity as well. When the left and the right wheels are driven over bumps with the same dimension at the same time, the bumps cause high magnitudes for the longitudinal and the vertical vibrations. When they are driven over bumps with different heights, a large roll movement is generated. This leads to high magnitudes for lateral vibrations. The bucket load condition has a quite small influence on the vibration intensity on the CWL.

5 Evaluation of Whole-Body Vibrations

Several procedures are introduced in the ISO standards to evaluate the effects of whole-body vibrations (WBV) on the human health and the ride comfort. In order to have a complete understanding of the effects of WBV arising from the compact wheel loader (CWL), all of these procedures are utilized. The effect of WBV arising from the CWL on the human health is evaluated using procedures in ISO 2631-1:1997 and ISO 2631-5:2004. That on the ride comfort is evaluated using procedures in ISO 2631-1:1985 and ISO 2631-1:1997. The vibrational accelerations measured when the driver wore the lap belt (originally installed on the seat) are used for the evaluation in this chapter.

5.1 Evaluation of effect on human health

Different procedures are described in ISO 2631-1:1997 and ISO 2631-5:2004 to evaluate the effect of WBV on the human health. Both ISO standards are used in this section for the evaluation of WBV arising from the CWL. The evaluation results obtained according to these two standards are compared. In addition, it is discussed whether the detailed specifications in these procedures are suitable to evaluate the WBV arising from the CWL or not.

5.1.1 Evaluation result according to ISO 2631-1:1997

According to ISO 2631-1:1997, the suitable quantification method as well as the directions of WBV for the evaluation should be determined at the beginning of the evaluation.

5.1.1.1 Determination of the suitable quantification method

According to ISO 2631-1:1997, in order to determine the suitable quantification method to evaluate the effect of WBV on the human health, the values of crest factor (CF, Eq. (2.4), p. 27), $MTVV/\tilde{a}_w$ and $VDV/(\tilde{a}_w T^{1/4})$ should be calculated and compared with the critical values specified in the standard. The $MTVV$ and VDV represent maximum transient vibration value (Eq. (2.6) and (2.7), p. 28) and vibration dose value (Eq. (2.8), p. 28) respectively. The \tilde{a}_w (Eq. (2.5), p. 28) is the root mean square (RMS) value of frequency weighted accelerations and T represents the measurement

duration. The values of CF, $MTVV/\bar{a}_w$ and $VDV/(\bar{a}_w T^{1/4})$ of the three translational accelerations on the seat cushion in all test operations are presented in Fig. 5.1.

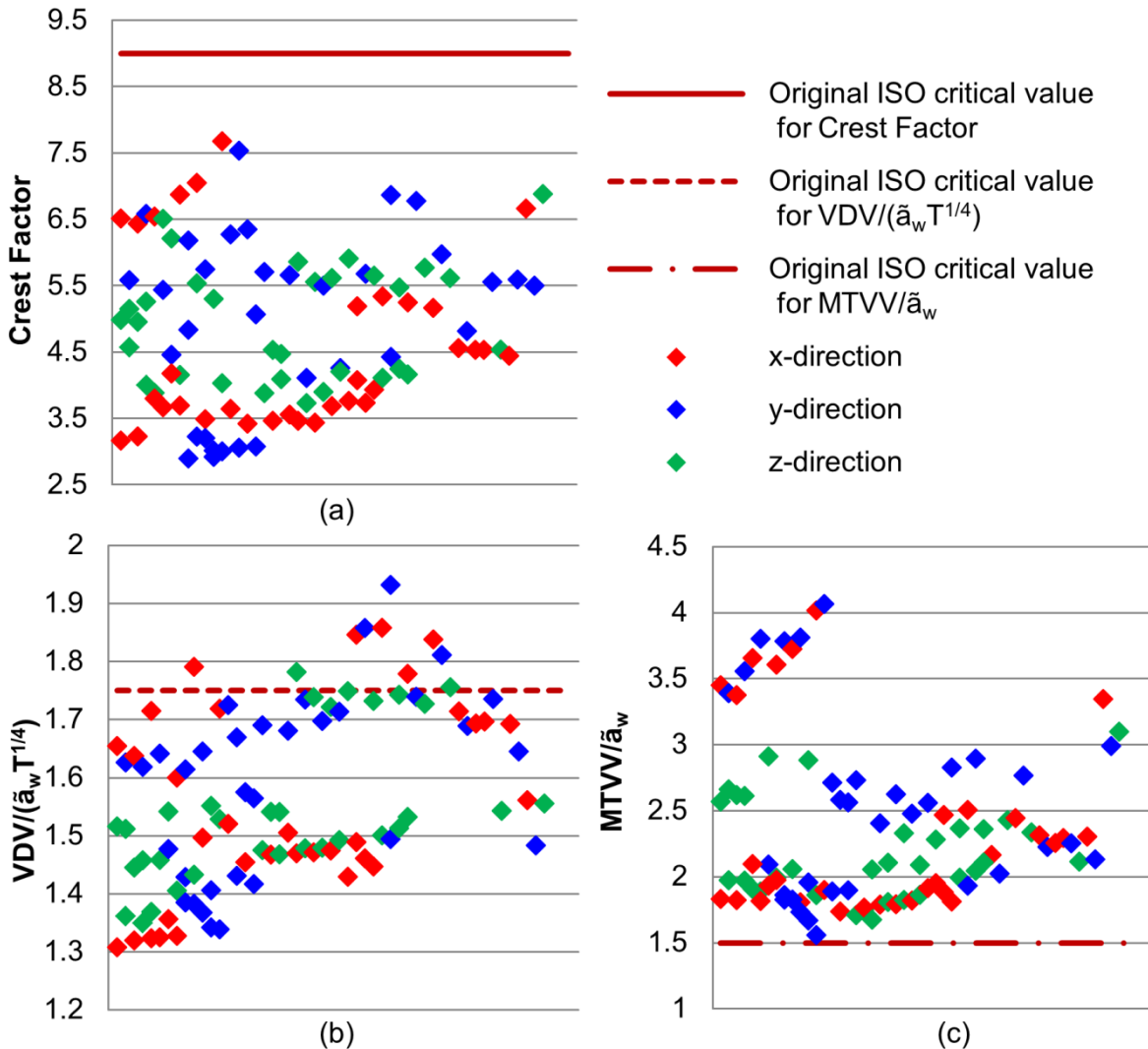


Fig. 5.1: Values of crest factor, $VDV/(\bar{a}_w T^{1/4})$ and $MTVV/\bar{a}_w$ of accelerations in three translational directions on the seat cushion in all test operations (ten operations repeated three or four times)

As shown in Fig. 5.1 (a), all values of the CF are below the critical limit value 9. Fig. 5.1 (b) displays that a part of the $VDV/(\bar{a}_w T^{1/4})$ values exceed the critical limit value 1.75. As shown in Fig. 5.1 (c), all values of $MTVV/\bar{a}_w$ exceed the critical limit value 1.5. The values of CF in Fig. 5.1 (a) show that the RMS method is in principle sufficient to evaluate the effect of WBV arising from the CWL. However, the values of $VDV/(\bar{a}_w T^{1/4})$ and $MTVV/\bar{a}_w$ in Fig. 5.1 (b) and (c) show that the RMS method has the potential to underestimate the effect of WBV, and the VDV method or the MTVV method should be used for the evaluation. In summary, the suitable quantification

method cannot be determined from the analysis of the values of CF, $MTVV/\tilde{a}_w$ and $VDV/(\tilde{a}_w T^{1/4})$ according to ISO 2631-1:1997. Three questions remain unsolved:

- 1) Does the RMS method underestimate the effect of WBV arising from the CWL on the human health?
- 2) Which method should be used to quantify the WBV on the CWL?
- 3) How should the critical values of CF, $MTVV/\tilde{a}_w$ and $VDV/(\tilde{a}_w T^{1/4})$ be modified to determine a suitable quantification method for the WBV on the CWL?

In order to answer these three questions, in this research work the difference between the estimated vibration dose value (eVDV, Eq. (2.9), p. 29) and the VDV is calculated as the value of Diff with Eq. (5.1) and analyzed.

$$Diff = \frac{VDV - eVDV}{eVDV} * 100\% \quad (5.1)$$

In Fig. 5.2, the values of CF, $MTVV/\tilde{a}_w$ and $VDV/(\tilde{a}_w T^{1/4})$ are divided into three groups according to the Diff value:

- 1) The VDV is considerably larger than the eVDV ($Diff \geq 10\%$) (marked with green square points). In this case, the RMS method underestimates the effect of WBV. The VDV method should be used for the evaluation.
- 2) The VDV is larger than the eVDV, but the difference between both values is not large ($0 \leq Diff < 10\%$) (marked with black triangle points). In this case, both the RMS method and the VDV method can be used for the evaluation.
- 3) The VDV is smaller than the eVDV ($Diff < 0$) (marked with blue round points). In this study, no Diff value is less than -10%. If $-10\% \leq Diff < 0$, both the RMS method and the VDV method can be used for the evaluation.

As shown in Fig. 5.2 the VDV is larger than the eVDV in most of the test operations (green square and black triangle points). And in more than half of these operations, the difference between VDV and eVDV exceeds 10% (green square points). For these test operations the RMS method underestimates the effect of WBV arising from the CWL on the human health. Therefore, the VDV method is adopted to evaluate the effect of WBV in this research work.

In Fig. 5.2 (a), there is a clear boundary ($CF=4.5$) between the case where the Diff exceeds 10% and the case where it stays below 10%. So, if the value of CF is larger than 4.5, the VDV is larger than eVDV and the difference between both values exceeds 10%. It means that the eVDV (or the RMS method) has the potential to

underestimate the health risks. In this situation, the VDV method should be used. From this research it is proposed to modify the critical value for the CF from 9 to 4.5, in order to harmonize the crest factor precondition of the ISO 2631-1:1997 with the Diff precondition. In Fig. 5.2 (b) and (c), clear boundaries for $VDV/(\tilde{a}_w T^{1/4})$ and $MTVV/\tilde{a}_w$ are observed between the case where the Diff exceeds 10% and the case where it stays below 10%. This boundary for $VDV/(\tilde{a}_w T^{1/4})$ is 1.54 and for $MTVV/\tilde{a}_w$ is 2. In this research work the critical values of $VDV/(\tilde{a}_w T^{1/4})$ and $MTVV/\tilde{a}_w$ are proposed to be modified from 1.75 and 1.5 to 1.54 and 2 respectively, in order to harmonize the precondition given in ISO 2631-1:1997 with the Diff precondition.

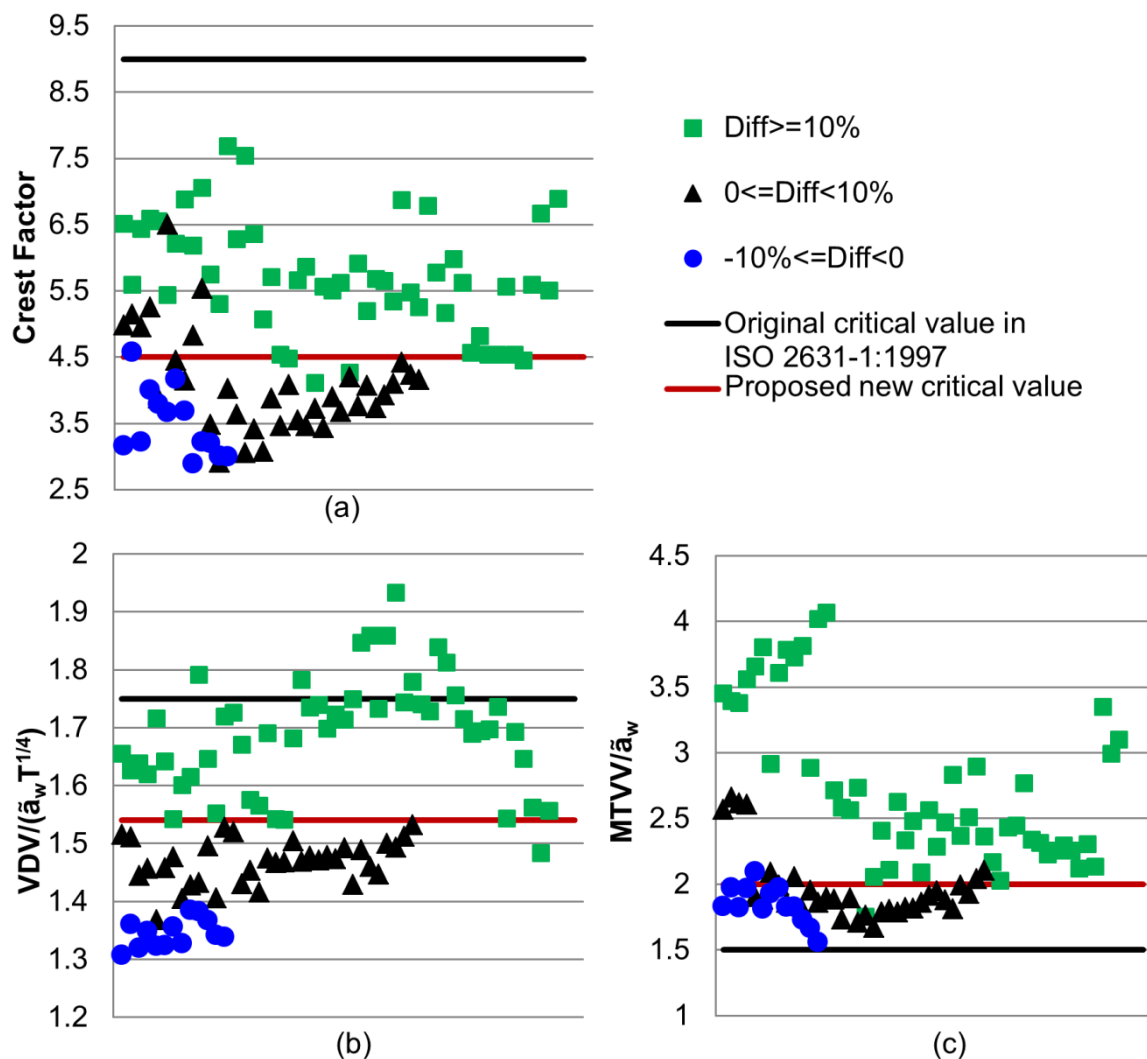


Fig. 5.2: Modification of critical values for (a) Crest Factor, (b) $VDV/(\tilde{a}_w T^{1/4})$ and (c) $MTVV/\tilde{a}_w$

With the modified critical values of CF, $VDV/(\tilde{a}_w T^{1/4})$ and $MTVV/\tilde{a}_w$ it is possible to select the suitable quantification method for vibrations which have similar characteristics to those on the CWL. The Diff value can be used to select the suitable

quantification method for all types of vibrations. If the Diff value exceeds 10%, the RMS method has the potential to underestimate the vibration effects. In this case, the VDV method should be used to evaluate the vibration effects on the human health. If the Diff value is less than -10%, the RMS method should be used to evaluate the vibration effects. In the case where $|\text{Diff}|$ does not exceed 10%, both RMS method and VDV method can be used for the evaluation.

5.1.1.2 Selection of directions for evaluation

In order to select the WBV directions for the evaluation, it is necessary to compare the V DVs in the three translational directions on the seat cushion. The three V DVs and the total vibration dose value (TV DV, Eq. (2.11), p. 29) in each test operation are listed in Tab. 5.1, where the maximum V DV in each operation is marked with red color.

Tab. 5.1: V DVs in three translational directions and the TV DVs on the seat cushion in all test operations

Operation	VDV ($\text{m/s}^{1.75}$)			TV DV ($\text{m/s}^{1.75}$)	$(\text{TV DV} - \text{Max}_{\text{VDV}}) / \text{Max}_{\text{VDV}} * 100$ (%) ¹¹
	x	y	z		
OP-1.1	10.57	14.98	10.78	16.63	10.95
OP-1.2	10.57	13.59	9.56	15.31	12.67
OP-1.3	39.99	30.96	37.55	48.35	20.91
OP-1.4	45.30	39.66	36.78	54.02	19.24
OP-2.1	21.86	34.11	13.46	35.65	4.51
OP-2.2	22.65	26.39	12.46	29.64	12.32
OP-2.3	47.52	27.37	40.35	53.69	12.99
OP-3.1	43.29	14.83	25.58	44.69	3.23
OP-3.2	45.69	10.28	29.75	47.64	4.28
OP-4	23.18	17.17	16.81	25.98	12.08

As shown in Tab. 5.1, in some operations the difference between the V DVs in two or three directions is not large. For example, in operations OP-1.1 to OP-1.4 and OP-4 the V DVs in three directions have a similar magnitude. In the operation OP-2.2 the

¹¹ Max_{VDV} is the maximum V DV in three directions.

VDVs in the x- and y-directions have a similar magnitude. In the operation OP-2.3 the VDV in the x- and z-directions have a similar magnitude. According to ISO 2631-1:1997 the TVDV should be used to evaluate the effect of WBV in the operations OP-1.1 to OP-1.4, OP-2.2, OP-2.3 and OP-4.

There is no criterion in ISO 2631-1:1997 to judge whether two VDV are at the same level or not. From the VDV in Tab. 5.1, it is hard to make a conclusion whether the VDV in two directions at the same level or not in some operations, such as the VDV in the x- and y-directions in the operation OP-2.1, as well as the VDV in the x- and z-directions in operations OP-3.1 and OP-3.2. For these operations, it cannot be decided which value should be used for the evaluation, the maximum VDV or the TVDV. In order to solve this problem, the differences between the TVDVs and the maximum VDV are analyzed, as shown in the first column from the right in Tab. 5.1. It can be observed that the differences between the TVDVs and the maximum VDV are quite small in the test operations OP-2.1, OP-3.1 and OP-3.2. In this case, both of the TVDV and the maximum VDV can be used to evaluate the effect of WBV on the human health.

Based on the analysis above, the TVDV is select in this research work to evaluate the effect of WBV arising from the CWL on the human health.

5.1.1.3 Evaluation result

In reality, the CWL does not execute any one of the operations in Tab. 5.1 exclusively during the whole day. In other words, each of the operations in Tab. 5.1 cannot be separately used to represent the daily work of the CWL. So, typical scenarios are to be defined by suitable mix of the operations. The main task of the CWL is to move materials from one location to another. The CWL mainly executes V-cycle like operation OP-4 and material transportation over short distances. In order to represent the daily work of the CWL, seven scenarios were proposed. These scenarios are comprised of operations OP-4, OP-1.1 and OP-1.2 respectively OP-4, OP-1.3 and OP-1.4. The repetition numbers of operations OP-1.1 and OP-1.2 or operations OP-1.3 and OP-1.4 are different in these scenarios. They represent the different transportation distances between two V-cycles. A detailed description of these scenarios is presented in Tab. 5.2. Because operations OP-1.1 to OP-1.4 include driving over several short slopes, the operations of driving over obstacles are not

included in the proposed scenarios. All of these scenarios were used to estimate the daily WBV exposure and the permitted daily exposure durations.

Based on the conclusions in sections 5.1.1.1 and 5.1.1.2, the total vibration dose value (TVDV) on the seat cushion is selected to evaluate the effect of WBV arising from the CWL on the human health. The TVDVs and the durations of all scenarios repeated nine times are presented in Tab. 5.3.

Tab. 5.2: Description of the proposed operational scenarios for the CWL

Scenario	Number of OP-4	Number of driving operations			
		OP-1.1	OP-1.2	OP-1.3	OP-1.4
S1	1	0	0	0	0
S2-Slow	1	3	3	0	0
S3-Slow	1	6	6	0	0
S4-Slow	1	9	9	0	0
S2-Fast	1	0	0	3	3
S3-Fast	1	0	0	6	6
S4-Fast	1	0	0	9	9

Tab. 5.3: TVDVs and the durations for all scenarios repeated nine times

Scenario	TVDV (m/s ^{1.75})	Duration (s)
S1	8.333	305
S2-Slow	9.936	2465
S3-Slow	11.006	4625
S4-Slow	11.8315	6785
S2-Fast	20.8319	1061
S3-Fast	24.694	1817
S4-Fast	27.299	2573

The permitted daily exposure durations for all scenarios were calculated using Eq. (2.13) and (2.14) at page 30. The results are presented in Fig. 5.3. The blue line indicates the 8 h duration representing a work day.

As shown in Fig. 5.3, only for the scenario S4-Slow, the permitted daily exposure duration can reach 8 h. They hardly reach 8 h for another two scenarios (S2-Slow and S3-Slow). For the scenario of pure V-cycle (S1), the permitted daily exposure duration just reaches 1.5 h. Considering the health risks caused by WBV on the CWL, the driver should not be exposed to the vibrations in scenarios comprised of V-cycle and fast driving (S2-Fast to S4-Fast) longer than 8 minutes.

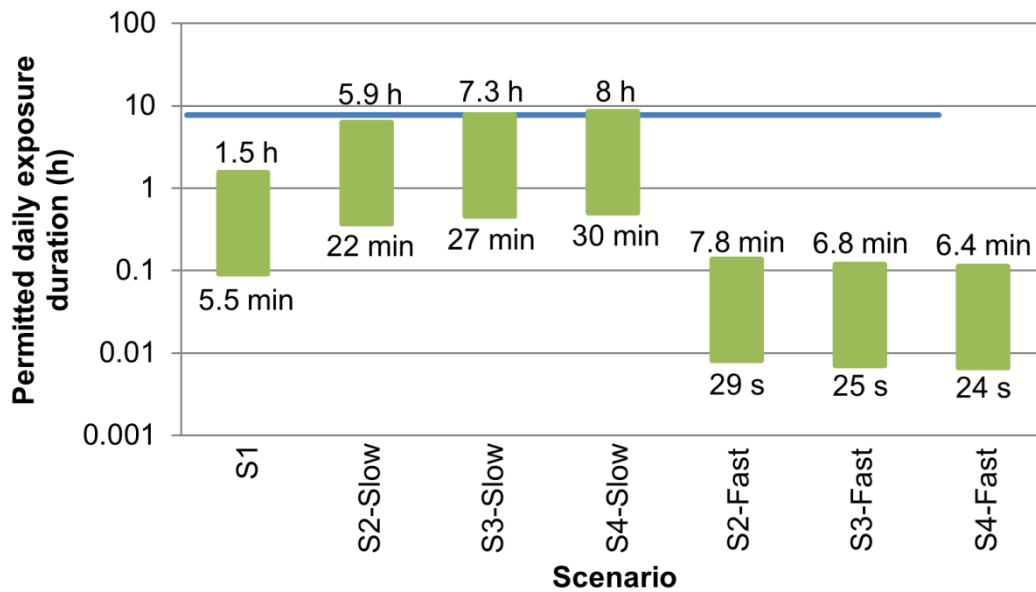


Fig. 5.3: The permitted daily exposure durations for all scenarios estimated according to ISO 2631-1:1997

5.1.2 Evaluation result according to ISO 2631-5:2004

According to the procedure in ISO 2631-5:2004, the equivalent static compressive stress S_e is to be used for the evaluation of the WBV effects on the human health. This standard has no other option of the evaluation method and requires vibrations in all three translational directions on the seat cushion for the evaluation, so that no evaluation method and vibration direction have to be selected contrary to ISO 2631-1:1997. The S_e values for all scenarios repeated nine times were calculated using Eq. (2.16) at page 31 and are presented in Tab. 5.4.

The permitted daily exposure durations of all scenarios were calculated with Eq. (2.18) and (2.19) at page 31 and are illustrated in Fig. 5.4. The blue line still indicates the 8 h duration representing a work day. The red line indicates the 24 h of a whole day. The permitted daily exposure durations for the scenario of pure V-cycle and the scenarios comprised of V-cycle and slow driving can reach 8 hours. According to ISO

2631-5:2004, exposure to the vibrations in the scenarios comprised of V-cycle and fast driving can cause health risks, even when it lasts only 1.5 minutes.

Tab. 5.4: S_e values for all operational scenarios repeated nine times

Scenario	S_e (MPa)
S1	0.342
S2-Slow	0.377
S3-Slow	0.401
S4-Slow	0.419
S2-Fast	1.204
S3-Fast	1.352
S4-Fast	1.446

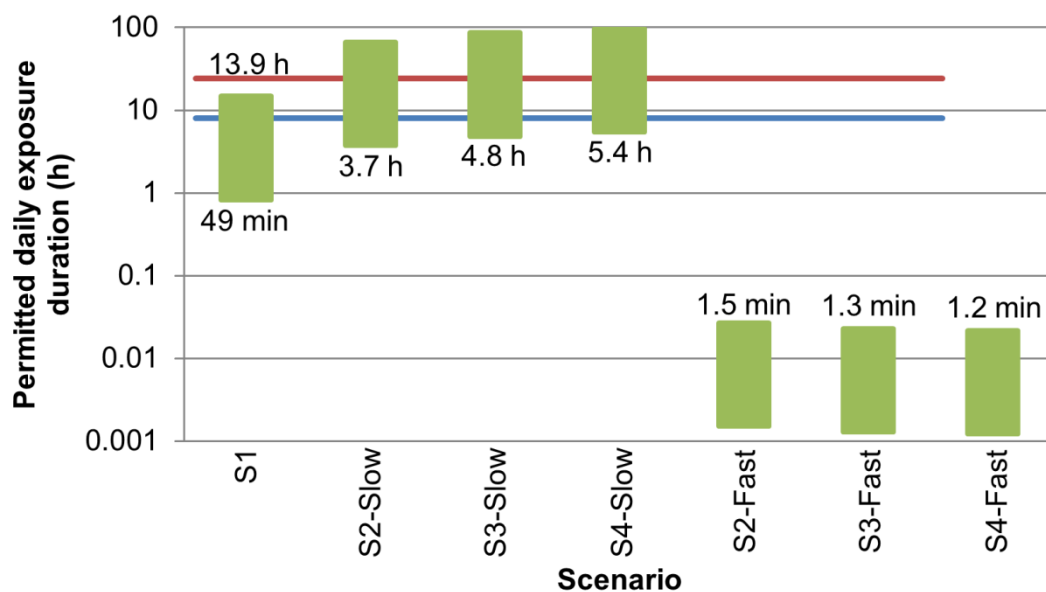


Fig. 5.4: The permitted daily exposure durations for all scenarios estimated according to ISO 2631-5:2004

5.1.3 Comparison of results of both ISO standards

In ISO 2631-1:1997 and ISO 2631-5:2004 the daily WBV exposure is represented using the daily vibration dose value (VDV_d , Eq. (2.12), p. 30) and the daily equivalent static compression dose S_{ed} (Eq. (2.17), p. 31), respectively. The VDV_d , S_{ed} and the predicted health risks according to ISO 2631-1:1997 and ISO 2631-5:2004 are listed in Tab. 5.5. As shown in this table, health risks predicted according to ISO 2631-

5:2004 are lower than those predicted according to ISO 2631-1:1997 for three scenarios (S1, S2-Slow and S3-Slow). The same health risks were predicted according to these two ISO standards for the other four scenarios.

Tab. 5.5: Daily WBV exposure and predicted health risks according to ISO 2631-1:1997 and ISO 2631-5:2004

Scenario	ISO 2631-1:1997		ISO 2631-5:2004	
	VDV _d (m/s ^{1.75})	Health risks	S _{ed} (MPa)	Health risks
S1	25.976	High	0.729	Moderate
S2-Slow	18.370	High	0.568	Moderate
S3-Slow	17.386	High	0.544	Moderate
S4-Slow	16.982	Moderate	0.533	Moderate
S2-Fast	47.550	High	2.088	High
S3-Fast	49.272	High	2.143	High
S4-Fast	49.933	High	2.163	High

From Fig. 5.3, Fig. 5.4 and Tab. 5.5 it can be noticed that the evaluation results obtained according to ISO 2631-1:1997 and ISO 2631-5:2004 are different. It can be possibly caused by one or both of the following two reasons:

- 1) The boundaries of the health guidance caution zone (HGCZ) in the two standards may be unequal;
- 2) The vibration intensities quantified using the vibration dose value (VDV) method in ISO 2631-1:1997 and the equivalent static compressive stress (S_e) method in ISO 2631-5:2004 may be at different levels.

In order to identify the reasons, the following tasks need to be carried out. At first it needs to be studied whether the boundaries of the HGCZ in the two standards are equal. If yes, then the difference of evaluation results with two ISO standards is not caused by the HGCZ but by the quantification methods in both standards. If not, the equivalent boundaries of the HGCZ need to be found out and the permitted daily exposure durations need to be calculated using these equivalent boundaries. In this case, if the permitted daily exposure durations calculated according to the VDV methods and the S_e method are the same, the reason for the different evaluation results with two ISO standards can be identified as the unequal boundaries of the

HGCZ in both standards. Otherwise, the reason can be identified as both the unequal boundaries and the quantification methods in two standards.

The VDV_d and S_{ed} values of the WBV measured in all ten test operations (OP-1.1 to OP-4 in Tab. 4.1) are illustrated in Fig. 5.5. Here the WBV in all the ten operations were used only for the purpose to include more types of WBV into the analysis. It can be observed that there are two VDV_d values within the HGCZ and eight above the HGCZ in ISO 2631-1:1997 represented by two blue lines. There is one S_{ed} value below the HGCZ, three within the HGCZ and six above the HGCZ in ISO 2631-5:2004 represented by two red lines. This means that the HGCZ in ISO 2631-5:2004 is generally higher than that in ISO 2631-1:1997. The same conclusion can also be obtained from the Tab. 5.5. This proves that the HGCZ boundaries in ISO 2631-1:1997 are not equivalent to those in ISO 2631-5:2004 for the evaluation of the effect of WBV on the human health. In the next step, the equivalent boundaries need to be found out.

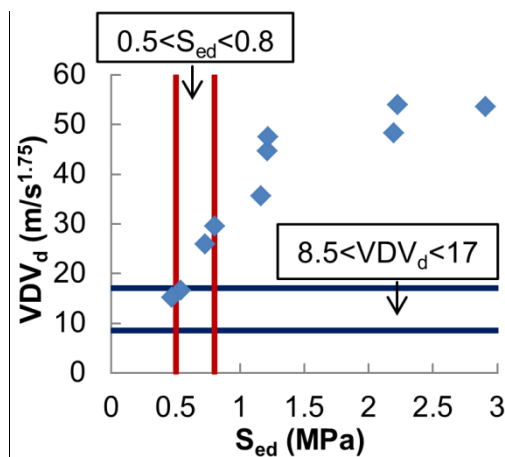


Fig. 5.5: The VDV_d and S_{ed} values of the WBV measured on the CWL in all ten test operations

The boundaries of VDV_d equivalent to those of S_{ed} can be found out by analyzing the relationship between the VDV_d and S_{ed} values. A polynomial relationship between $\lg(VDV_d)$ and $\lg(S_{ed})$ was observed and is expressed by Eq. (5.2). With this equation, the boundaries of S_{ed} equivalent to those of VDV_d in ISO 2631-1:1997 could be calculated as 0.34 and 0.52 MPa. The boundaries of VDV_d equivalent to those of S_{ed} in ISO 2631-5:2004 could be calculated as 16.1 and 29.3 m/s^{1.75}.

$$\lg(VDV_d) = -1.0756 * [\lg(S_{ed})]^2 + 0.8446 * \lg(S_{ed}) + 1.5587 \quad (5.2)$$

After the equivalent boundaries of VDV_d and S_{ed} are obtained, in the next step, the permitted daily exposure durations need to be calculated with the equivalent

boundaries, in order to determine the reasons for the different evaluation results obtained according to the two ISO standards. The permitted daily exposure durations of seven scenarios calculated using two sets of equivalent boundaries are shown in Fig. 5.6.

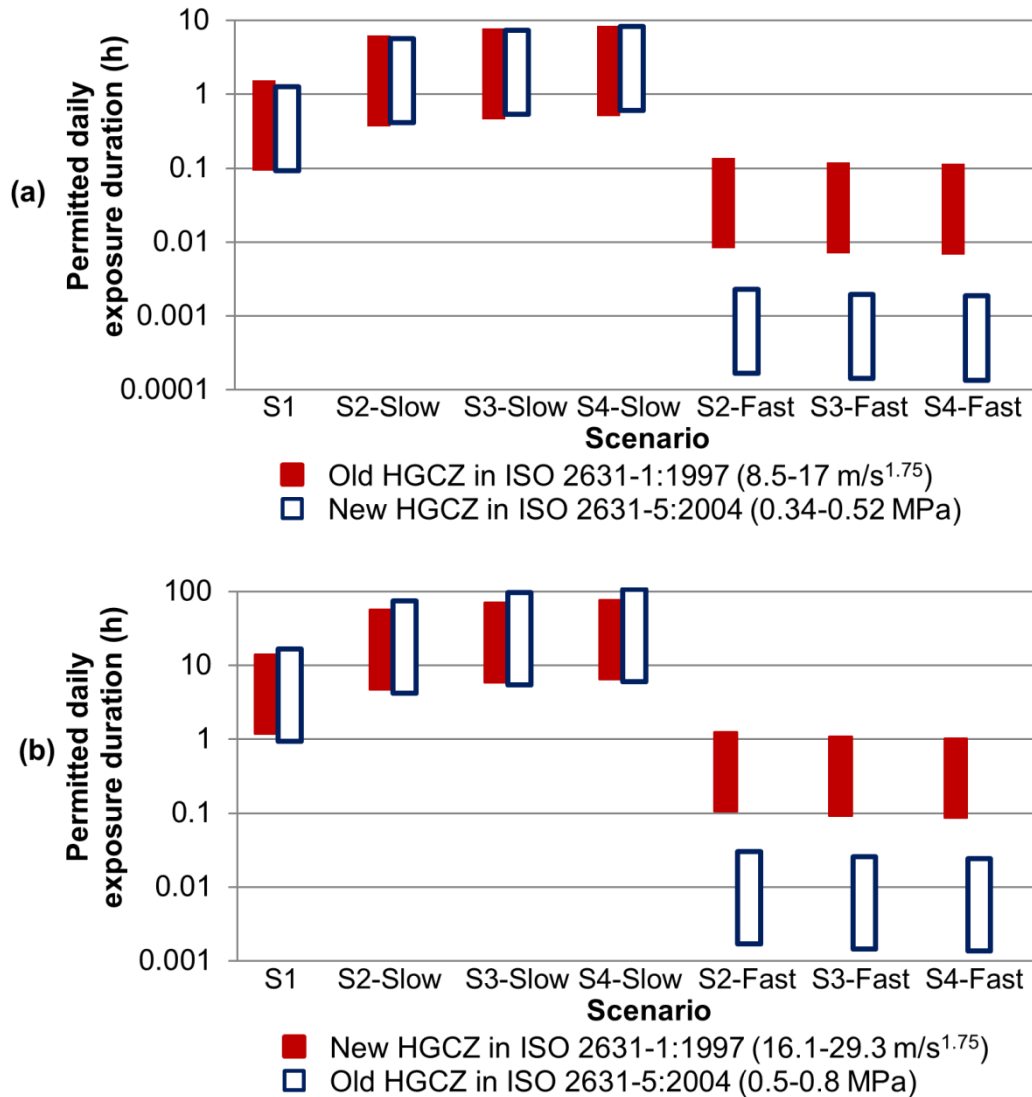


Fig. 5.6: (a). The permitted daily exposure durations estimated using the old HGCZ in ISO 2631-1:1997 and the new HGCZ in ISO 2631-5:2004; (b). The permitted daily exposure durations estimated using the new HGCZ in ISO 2631-1:1997 and the old HGCZ in ISO 2631-5:2004

It can be observed in Fig. 5.6 that for the scenario of pure V-cycle (S1) and the scenarios comprised of V-cycle and slow driving (S2-Slow to S4-Slow), similar permitted daily exposure durations were obtained using two sets of equivalent boundaries. It means that for these scenarios the different permitted daily exposure

durations in Fig. 5.3 and Fig. 5.4 are caused by the unequal boundaries of the HGCZ in ISO 2631-1:1997 and ISO 2631-5:2004.

For scenarios comprised of V-cycle and fast driving (S2-Fast to S4-Fast), shorter permitted daily exposure durations are always estimated by the S_e method in ISO 2631-5:2004. It means that for these scenarios the different permitted daily exposure durations in Fig. 5.3 and Fig. 5.4 are caused not only by the unequal boundaries of the HGCZ but also by the quantification methods in two standards and the WBV types. The VDV method in ISO 2631-1:1997 calculates the total value of the frequency weighted accelerations, however, the S_e method in ISO 2631-5:2004 only picks up the peaks of the spine accelerations. The vibrations when the CWL is driven at a high speed are severe and contain a lot of shocks with high amplitudes. Therefore, higher vibration intensity is estimated with the S_e method. On the other hand, the S_e method uses the sixth power instead of the fourth power of the VDV method. It makes the S_e method more sensitive to the peaks. All of these reasons bring the result that the S_e method in ISO 2631-5:2004 is more stringent than the VDV method in ISO 2631-1:1997 for the WBV in the scenarios comprised of V-cycle and fast driving.

The ISO 2631-1:1997 was found underestimating the health risks caused by some types of WBV. A more stringent evaluation procedure is needed. This is the motivation to develop the ISO 2631-5:2004. [87] In this study for the WBV in scenarios S1 and S2-Slow to S4-Slow, the health risks predicted by ISO 2631-5:2004 are lower than by ISO 2631-1:1997. This is contradictory to the motivation for developing the ISO 2631-5:2004. It means that ISO 2631-5:2004 is not suitable to predict the health risks caused by the WBV in scenarios S1 and S2-Slow to S4-Slow. This requires that in the revision of ISO 2631-5:2004 the preconditions of using this standard need to be included.

For scenarios S1 and S2-Slow to S4-Slow the same health risks can be predicted using ISO 2631-5:2004 and ISO 2631-1:1997, when the HGCZ in ISO 2631-5:2004 is lowered. No matter the original or the lowered HGCZ in ISO 2631-5:2004 is used, for WBV in scenarios S2-Fast to S4-Fast ISO 2631-5:2004 is always more stringent than ISO 2631-1:1997. This is in accord with the motivation to develop the ISO 2631-5:2004. In future studies it should be validated whether the original or the lowered HGCZ in ISO 2631-5:2004 should be used to predict the health risks.

5.1.4 Other detailed specifications in two ISO standards

Both procedures in ISO 2631-1:1997 and ISO 2631-5:2004 to evaluate the effect of WBV on the human health consist of several detailed specifications. These specifications include the quantification methods, the vibration locations and directions for the evaluation, the frequency weighting filters or the spine models, the multiplying factors and the health guidance caution zone (HGCZ).

In section 5.1.1 to 5.1.3 some of these specifications are discussed, including the determination of the suitable quantification method and the selection of the desired vibration directions in ISO 2631-1:1997, as well as the quantification methods and the boundaries of HGCZ in two ISO standards. There are other specifications in these two standards which need to be discussed in this research work, such as the frequency weighting filters in ISO 2631-1:1997 and the spine models in ISO 2631-5:2004, as well as the multiplying factors in both ISO standards. Several questions about these specifications are left unanswered. For example: 1). is it correct using the same frequency weighting filter or the same spine model to realize the human biodynamic response in the x- and y-directions? 2). are the frequency weighting filters and the spine models sufficient to realize the human biodynamic response? 3). is the human subjective sensitivity to vibrations in each direction equally weighted in both ISO standards? These questions are discussed in the following paragraphs. The discussion is based on the investigation results presented in the previous literatures.

5.1.4.1 Frequency weighting filters and spine models

According to ISO 2631-1:1997, frequency weighting filters (Fig. 2.23 (p. 28)) are adopted to reflect the human subjective sensitivity to WBV in the frequency domain. In ISO 2631-5:2004 two spine models (Fig. 2.24 (p. 31)) are introduced to simulate the human biodynamic response to WBV. In this research work the spine transmissibility is used to analyze the characteristics of the human biodynamic response simulated by the spine models. The spine transmissibility in the frequency domain was calculated using Eq. (2.1) (p. 17). To calculate the spine transmissibility, the input signals are the accelerations measured on the seat cushion. The output signals are the spine accelerations calculated using the spine models.

In ISO 2631-1:1997 the same frequency weighting filter W_d is used for the accelerations in the x- and y-directions on the seat cushion. The curve of W_d in the frequency domain is presented in Fig. 2.23 (p. 28). It can be observed that it has high

weighting factors in the frequency range of 0.5-2 Hz. The transmissibility of the spine model in the x- and y-directions in ISO 2631-5:2004 is shown in Fig. 5.7. Because this spine model is a linear single degree of freedom (DOF) model, the spine transmissibility in these two directions is not affected by the input signals. The figure shows the resonance frequency of the spine model in the x- and y-directions at 2.125 Hz.

Contrary to that, as stated in section 2.1.3.1, the human biodynamic response in the x- and y-directions is nonlinear and affected by many factors, such as the employment of a backrest, the excitation magnitude and the human gender. The principal resonance frequency of the seated person in the x-direction was observed by many researchers in a wide range from 1 Hz to 6 Hz. It in the y-direction was observed at frequencies lower than 2 Hz.

There is no doubt that the linear single-DOF spine model in ISO 2631-5:2004 cannot simulate the nonlinear human biodynamic response in the x- and y-directions properly. The filter W_d in ISO 2631-1:1997 weights vibrations in the range of 0.5-2 Hz with comparably high factors. Therefore it seems to be suitable to be used to reflect the characteristics of human subjective sensitivity in the y-direction. The principal resonance frequency of the seated person in the x-direction is at frequencies below 2 Hz without a backrest. In this case, the W_d seems to be suitable to reflect the characteristics of the human subjective sensitivity in the x-direction. However, when a backrest is used, the principal resonance frequency of the seated person in the x-direction occurs in the range of 2-6 Hz. In this case, the W_d is not adequate to reflect the characteristics of the human subjective sensitivity in this direction.

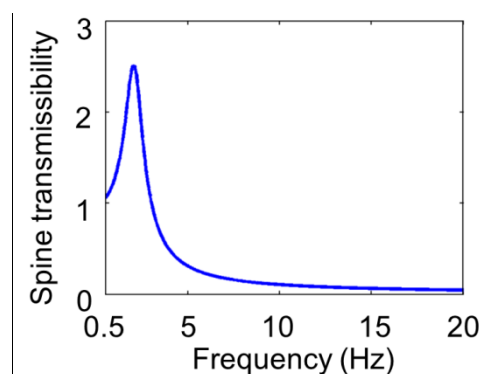


Fig. 5.7: Transmissibility of the spine model in the x- and y-directions in ISO 2631-5:2004

Curves of transmissibility of the spine model in the z-direction are presented in Fig. 5.8. Because this spine model is a nonlinear model, the spine transmissibility is

affected by the input signal. In other words, curves of the transmissibility are different when the input signals are obtained from different CWL operations. In Fig. 5.8 it can be noticed that the human biodynamic response simulated by the spine model in the z-direction has a large variation, when the driver is exposed to the WBV in different CWL operations. It can be observed that the spine transmissibility has the first peak at frequencies ranging from 4 Hz to 5 Hz in all operations. This is consistent with the investigation results in previous studies that the principal resonance frequency of the seated person in the z-direction occurs in the range of 4-6 Hz, as reviewed in section 2.1.3.1.

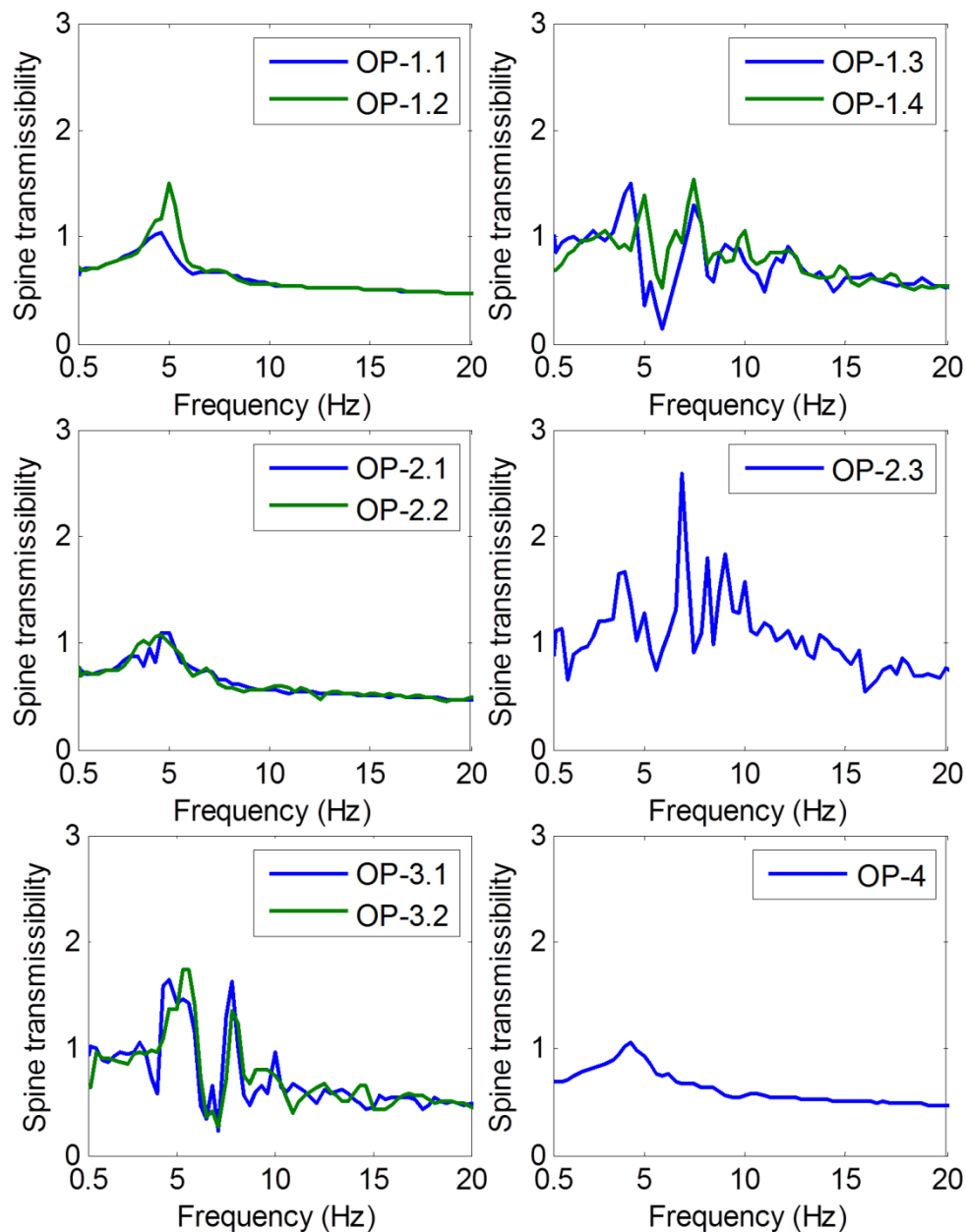


Fig. 5.8: Transmissibility of spine model in the z-direction in ISO 2631-5:2004

Under excitations with high magnitudes (OP-1.3, OP-1.4, OP-2.3, OP-3.1 and OP-3.2), the second peaks can be observed at around 8 Hz. But they do not appear in the transmissibility under excitations with low and medium magnitudes (OP-1.1, OP-1.2, OP-2.1, OP-2.2 and OP-4). This is inconsistent with the investigation results in previous studies. For example, in the study by Matsumoto and Griffin [56], the second peak was observed only on the curve of the transmissibility between the seat and the fifth lumbar vertebrae, but not on curves of the transmissibility between the seat and the first or the third lumbar vertebrae. In the study by Mansfield and Griffin [59], the second peaks of the seat to lumbar spine transmissibility were always observed at frequencies between 8 Hz to 10 Hz when the RMS values of the excitations range from 0.25 to 2.5 m/s². Due to the above mentioned discussion, the spine model in the z-direction in ISO 2631-5:2004 still needs to be validated or improved at least for the persons exposed to the CWL vibrations.

In ISO 2631-1:1997, the filter W_k is used for weighting the vertical accelerations on the seat cushion. Curve of W_k in Fig. 2.23 (p. 28) shows that seated persons are most sensitive to vertical vibrations in a wide range of 4-12.5 Hz, where the first and the second resonance frequencies of seated persons were observed in the previous studies. It means that the W_k seems to be suitable to be used to reflect the characteristics of the human subjective sensitivity to vibrations in the z-direction.

5.1.4.2 Human subjective sensitivity in different directions

Both ISO 2631-1:1997 and ISO 2631-5:2004 adopt multiplying factors to reflect the relative human subjective sensitivity to vibrations in different directions. Multiplying factors in the x-, y- and z-directions in ISO 2631-5:2004 are 0.015, 0.035 and 0.032 respectively. This means that a person has a similar sensitivity to vibrations in the y- and z-directions, but is less sensitive to vibrations in the x-direction. In the ISO 2631-1:1997 multiplying factors in the x-, y- and z-directions are 1.4, 1.4 and 1. Different from the other standard, here the person has a similar sensitivity to vibrations in the x- and y-directions but is less sensitive to vibrations in the z-direction. It can be concluded that the human subjective sensitivity to vibrations in different directions is inconsistent in these two ISO standards.

5.2 Evaluation of effect on ride comfort

Procedures to evaluate the effect of WBV on ride comfort are introduced in two ISO standards: ISO 2631-1:1985 and ISO 2631-1:1997. According to the ISO 2631-1:1997, the overall vibration total value (OVTV) (Eq. (2.21), p. 40) should be calculated and compared with the boundaries for the approximate indications of likely reactions of comfort (Tab. 2.11, p. 41). The OVTV is a numerical value, which cannot be used to analyze the vibration characteristics depending on the frequency and the exposure duration. This analysis can be carried out by calculating the root mean square (RMS) value of accelerations in each 1/3 octave band ($\tilde{a}_{1/3ob}$, Eq. (2.20), p. 38) and comparing it to the reduced comfort boundary (RCB, Fig. 2.25, p. 38) according to the ISO 2631-1:1985. Therefore, although ISO 2631-1:1985 has been replaced by its successor ISO 2631-1:1997, it is still used for the ride comfort evaluation in this research work.

5.2.1 Evaluation result according to ISO 2631-1:1985

According to the evaluation procedure in ISO 2631-1:1985, the RMS values of accelerations in the 1/3 octave band ($\tilde{a}_{1/3ob}$) in the three translational directions on the seat cushion in the seven scenarios (Tab. 5.2, p. 83) were calculated using Eq. (2.20) (p. 38) and compared with the RCB curves given in this standard. The comparison results are illustrated in Fig. 5.9 to Fig. 5.11. The differences of RMS values in scenarios S2-Fast, S3-Fast and S4-Fast are very small. The RMS values in the scenario S3-Fast are not given in these figures, because it is very hard to recognize them from the RMS values in scenarios S2-Fast and S4-Fast. In fact they are between the RMS values in scenarios S2-Fast and S4-Fast.

As shown in Fig. 5.9, in the scenario of pure V-cycle and the scenarios comprised of V-cycle and slow driving, the maximum RMS value in the x-direction occurs at 2 Hz. It occurs at 1.6 Hz in three scenarios comprised of V-cycle and fast driving. The longitudinal vibrations are mainly caused by the pitch movement of the vehicle during driving, as well as by stopping and accelerating the vehicle during V-cycle. As observed in Fig. 4.8 (p. 68), the shift of the frequency at which the maximum RMS value at the seat base occurs is hardly affected by the driving speed. Therefore, in Fig. 5.9 on the seat cushion the frequency at which the maximum RMS value occurs shifts to a lower frequency with the increase of the vehicle speed can be attributed to the nonlinearity of the longitudinal dynamics of the seat-driver system.

In Fig. 5.10 the maximum RMS value in the y-direction occurs at 1.25 Hz in the scenario of pure V-cycle and the scenarios comprised of V-cycle and slow driving. It occurs at 2.5 Hz in the scenarios comprised of V-cycle and fast driving. The lateral vibrations are mainly generated by the roll movement of the vehicle during driving, as well as by the turning of the vehicle during V-cycle. The excitation frequency for the roll movement increases as the vehicle speed. Accordingly, the roll movement as well as the lateral vibrations shifts to a higher frequency range, when the vehicle speed increases.

In Fig. 5.11 the maximum RMS value in the z-direction occurs at 2.5 Hz in all scenarios. The vertical vibrations are mainly generated by the unevenness of the road surface and largely affected by the whole vehicle dynamics.

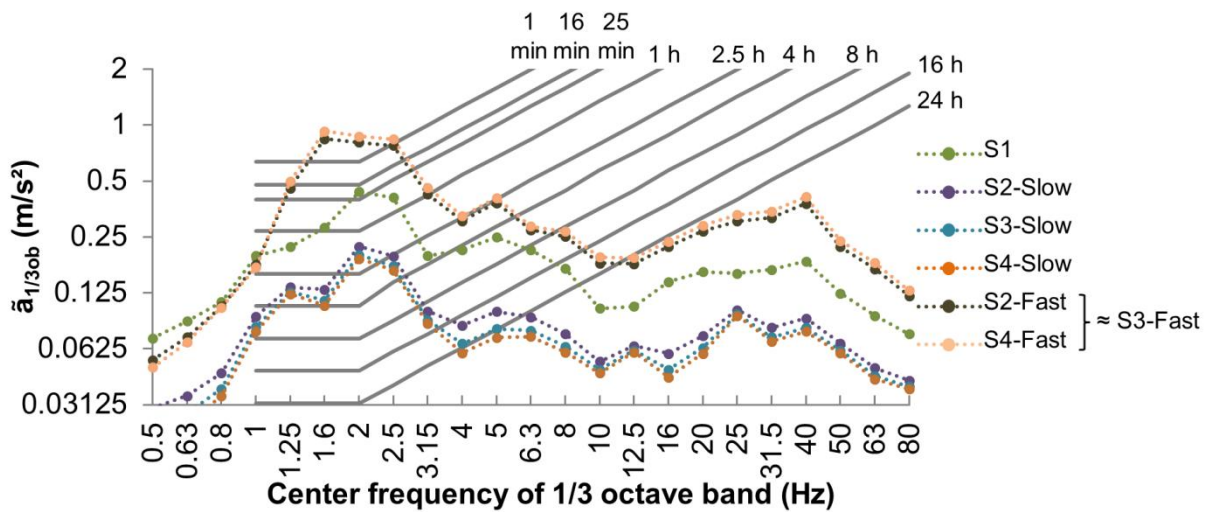


Fig. 5.9: Comparison of RMS values and RCB in the x-direction

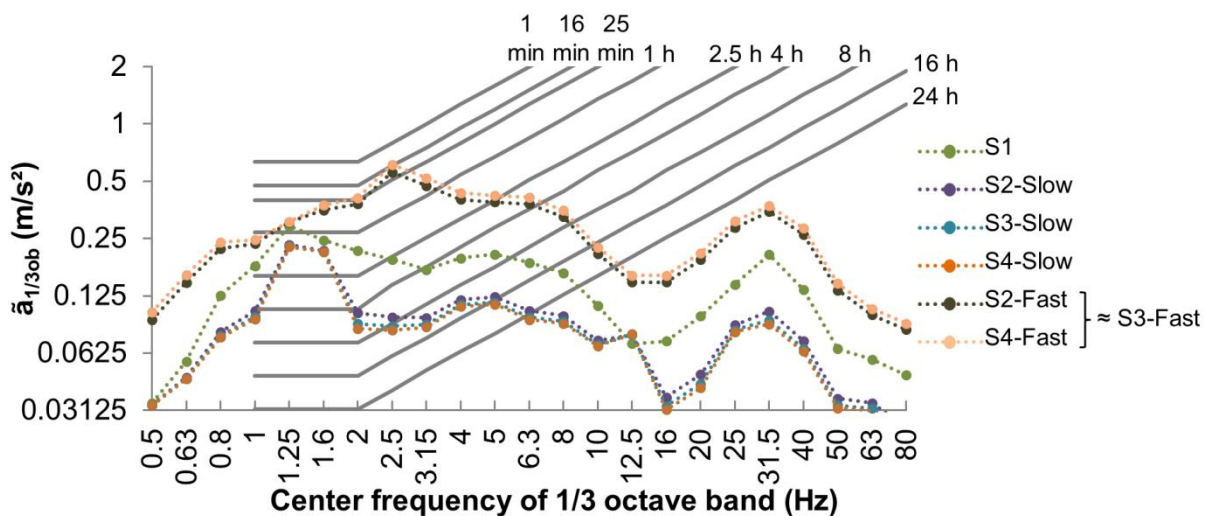


Fig. 5.10: Comparison of RMS values and RCB in the y-direction

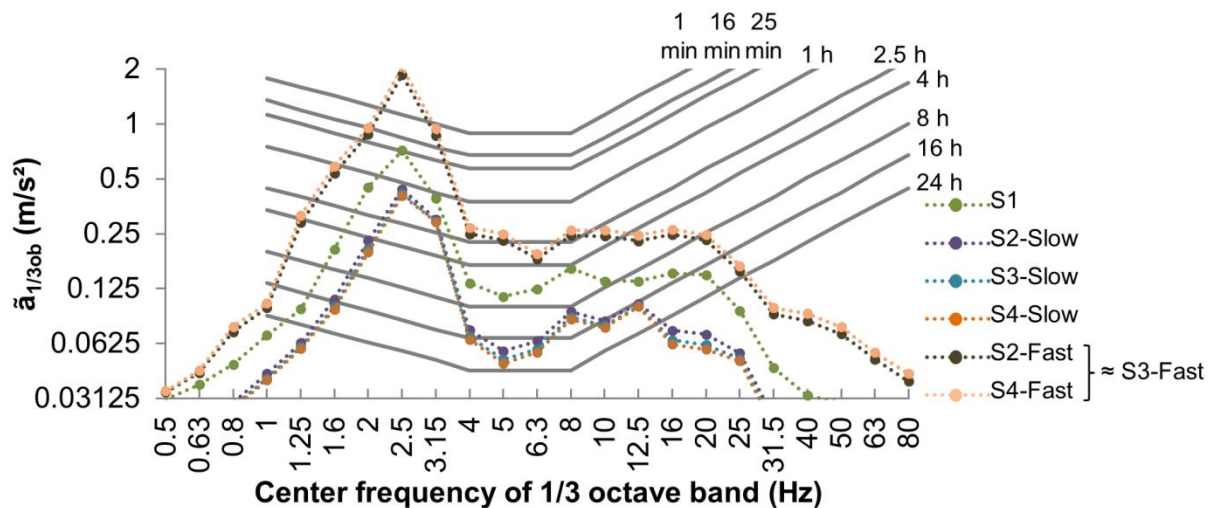


Fig. 5.11: Comparison of RMS values and RCB in the z-direction

It can be noticed that in scenarios comprised of V-cycle and slow driving (S2-Slow to S4-Slow) accelerations in the x-, y- and z-directions are at the same level. In the other scenarios (S1, S2-Fast to S4-Fast) the acceleration levels in the x- and z-directions are higher than those in the y-direction. During the V-cycle, the longitudinal vibrations caused by the decelerating and accelerating of the vehicle, and the vertical vibrations caused by the road unevenness and by the loading and dumping of materials, are larger than the lateral vibrations caused by the turning of the vehicle. During the fast driving, the pitch and the vertical movements are severer than the roll movement. Therefore the longitudinal and the vertical vibrations are larger than the lateral vibrations.

The permitted exposure durations for all scenarios are taken from Fig. 5.9 to Fig. 5.11 and summarized in Tab. 5.6. It can be concluded that the permitted exposure durations for ride comfort estimated by the WBV in the x- and z-directions are equal to or shorter than those estimated by the WBV in the y-direction. For the scenarios comprised of V-cycle and slow driving, the permitted exposure durations for ride comfort can reach 1 h. If the exposure duration in the scenario of pure V-cycle exceeds 16 min, the WBV on the CWL will lead to ride discomfort. In consideration of ride comfort, the CWL should not be driven on an uneven road surface at a speed as high as 19.8 km/h.

Tab. 5.6: Permitted exposure durations for ride comfort estimated according to ISO 2631-1:1985

Scenario	Permitted exposure durations		
	x-direction	y-direction	z-direction
S1	16 min	25 min	16 min
S2-Slow	1 h	1 h	1 h
S3-Slow	1 h	1 h	1 h
S4-Slow	1 h	1 h	1 h
S2-Fast	< 1 min	16 min	< 1 min
S3-Fast	< 1 min	16 min	< 1 min
S4-Fast	< 1 min	16 min	< 1 min

5.2.2 Evaluation result according to ISO 2631-1:1997

Similar to the evaluation of WBV effect on the human health according to ISO 2631-1:1997, the suitable quantification method and the vibration directions should be determined at the beginning of the evaluation of the WBV effect on the ride comfort according to this standard.

Three quantification methods are described in ISO 2631-1:1997. However, boundaries of vibration dose value (VDV) and maximum transient vibration value (MTVV) for different levels of ride discomfort are not given in this standard. Therefore, only the RMS method can be used to determine the levels of ride discomfort caused by WBV on the compact wheel loader (CWL).

There is still debate about the vibration directions needed for the evaluation of the WBV effect on ride comfort. It is defined in ISO 2631-1:1997 that the WBV in three translational directions on the seat cushion, on the seat backrest and at the feet as well as WBV in three rotational directions on the seat cushion should be used to evaluate the effect of WBV on the ride comfort. It means that vibrations on the seat backrest and at the feet lead to a decrease in the ride comfort compared to that evaluated only using the vibrations on the seat cushion. This is contrary to the investigation by Wyllie and Griffin that vibrations at the feet lead to an increase of ride comfort when the feet are supported [143]. On the other hand, as reviewed in section 2.2.2.3, it has been proven that there is a high coherence between the objective

prediction and the subjective judgment about the ride comfort, if the vector sum value (VSV) of the RMS values of frequency weighted accelerations in the three translational directions on the seat cushion is used as the objective method [39],[117]-[119]. In view of the above, the accelerations measured in three translational directions on the seat cushion are used to evaluate the effect of WBV on the ride comfort in this research work.

The VSVs on the seat cushion in all scenarios were calculated with Eq. (2.10) (p. 29). A comparison between the VSVs and the boundaries for different levels of ride discomfort given in ISO 2631-1:1997 (Tab. 2.11, p. 41) is presented in Fig. 5.12.

It can be observed that VSVs in all scenarios exceed the boundary for the level of 'Uncomfortable'. The VSVs in the scenarios comprised of V-cycle and fast driving even exceed the boundary for the level of 'Extremely Uncomfortable' a little.

From the evaluation results according to ISO 2631-1:1985 and ISO 2631-1:1997, it can be summarized that the WBV on the CWL can cause ride discomfort. In order to protect the driver from the ride discomfort, the CWL should not be operated at high speeds on a rough road surface.

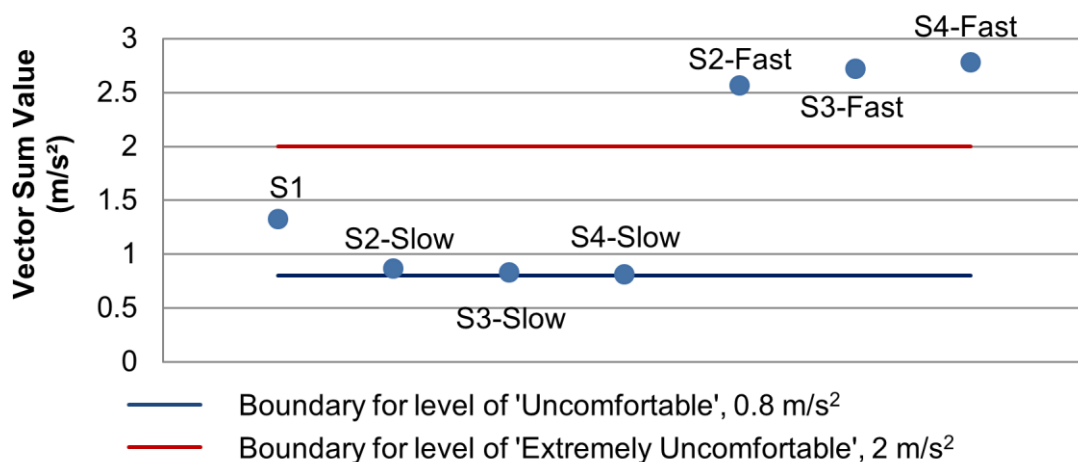


Fig. 5.12: VSVs on the seat cushion in all scenarios and the boundaries for levels of 'Uncomfortable' and 'Extremely Uncomfortable' in ISO 2631-1:1997

5.3 Conclusion

The main conclusions obtained based on the analysis in this chapter are as follows:

- 1) Several specifications in the ISO 2631-1:1997 standard are ambiguous when they are used to evaluate the effect of WBV on the human health. Amendments are proposed in this research work for these specifications. At first, the critical

values of crest factor (CF), $MTVV/\bar{a}_w$ and $VDV/(\bar{a}_w T^{1/4})$ in the standard are not sufficient to determine the suitable quantification method for the WBV on the compact wheel loader (CWL). They are proposed to be modified from 9, 1.5 and 1.75 to 4.5, 2 and 1.54. The modified critical values can be used to determine the suitable quantification method for the WBV which have the same characteristics as those on the CWL. The difference between the estimated vibration dose value (eVDV) and the vibration dose value (VDV) is represented as the Diff value in this study. It can be used to determine the suitable quantification method for all types of WBV. Secondly, it is not clearly defined in ISO 2631-1:1997 how to select the vibration directions for the evaluation. Based on the analysis, this study suggests that VDV_s in all three translational directions on the seat cushion should be used in combination to evaluate the effect of WBV arising from the CWL on the human health.

- 2) Some specifications in ISO 2631-1:1997 and ISO 2631-5:2004 are doubtful for the evaluation of WBV on a CWL, such as the frequency weighting filter W_d in ISO 2631-1:1997 for the longitudinal vibrations, both spine models in ISO 2631-5:2004 and the multiplying factors in both ISO standards. More investigations on the relationship between the human response and the WBV exposure are still needed to validate or improve these specifications.
- 3) Different health evaluation results were obtained according to ISO 2631-1:1997 and ISO 2631-5:2004. They are caused by the unequal boundaries of the health guidance caution zone (HGCZ) in both standards, as well as the quantification methods and the properties of the WBV on the CWL. For the WBV arising from the CWL, the boundaries of the HGCZ in ISO 2631-5:2004 are higher than those in ISO 2631-1:1997. The relationship between the daily vibration dose values (VDV_d) and the daily equivalent static compression dose values (S_{ed}) of the WBV on the CWL was obtained. Based on this relationship, two sets of equivalent HGCZ boundaries for S_{ed} and VDV_d were obtained. Using these two sets of equivalent boundaries, similar permitted daily exposure durations were obtained for the scenario of pure V-cycle or the scenarios comprised of V-cycle and slow driving. For the scenarios comprised of V-cycle and fast driving, the permitted daily exposure durations estimated using the equivalent static compressive stress (S_e) method are much shorter than those estimated using the VDV method. This is because the S_e method is more stringent than the VDV

method for the WBV containing a lot of shocks, such as the WBV measured on the CWL during fast driving.

- 4) The evaluation results in this study show that long-term exposure to the WBV arising from the CWL has the potential to cause health risks, and short-term exposure can lead to ride discomfort. This indicates that there is a necessity to reduce the WBV on the CWL. It can be achieved by optimizing suspension systems on the CWL and by improving the driver sitting situations. The driver sitting situation can be improved by selecting a proper type of safety belt for the driver. Optimization of the cabin and axle suspension systems is relatively complicated, because the limited space and the whole vehicle dynamics need to be taken into account. Employment of a cabin or axle suspension system can also increase the cost of the vehicle. In contrast, optimization of the seat suspension system is much easier and more economical. It can be taken as the first step for the improvement of suspension systems and for the reduction of WBV on the CWL.

6 Effect of Safety Belt on Seat Transmissibility

Because seat and driver interact with each other, the seat transmissibility is affected by the dynamic characteristics of the driver. In addition, the safety belt constrains the movement of the driver and affects his or her dynamic characteristics. Therefore, the safety belt has an effect on the seat transmissibility.

In the field tests of vibration measurement, accelerations on the seat cushion and at the seat base were measured in three cases of safety belt wearing: the driver did not wear a safety belt (case A), the driver wore an automatic lap belt (case B) and the driver wore a four-point seat harness (case C). According to previous literatures, two parameters can be used to study the seat transmissibility: the seat effective amplitude transmissibility (SEAT) (Eq. (2.24), p. 44) and the seat transmissibility in the frequency domain derived from the cross spectral density (CSD) method (Eq. (2.1), p. 17). In this chapter these two parameters are analyzed to investigate the effect of different safety belts on the seat transmissibility. Additionally, comments on the comfort made by the driver are used as an aspect to evaluate the effect of a safety belt on the ride comfort.

6.1 Lap belt (case B) vs. no belt (case A)

To study the effect of a lap belt on the seat transmissibility, SEAT values and seat transmissibility in the frequency domain in case B are compared with those in case A. This comparison involves five operations (OP-1.3, OP-2.1, OP-2.3, OP-3.1 and OP-4), those in which the vibration measurements in case A were carried out.

6.1.1 Comparison of seat effective amplitude transmissibility (SEAT)

The SEAT values in the three translational directions in cases A and B are given in Tab. 6.1, where these values are classified into the following three groups:

- 1) The SEAT value exceeds 1 (marked with red color). This means that the vibration intensity is amplified by the seat-driver system.
- 2) The SEAT value is lower than 1 (marked with black color). In this situation, vibrations from the seat base are attenuated by the seat-driver system.
- 3) The SEAT value is equal to 1 (marked with green color). The vibration intensity on the seat cushion is equal to that at the seat base.

Tab. 6.1: SEAT values in cases A and B

Test operation	Direction	SEAT value	
		case A	case B
OP-1.3	x	1.64	1.63
	y	1.22	1.10
	z	1.00	0.93
OP-2.1	x	1.62	1.46
	y	1.11	1.08
	z	0.95	0.93
OP-2.3	x	1.48	1.65
	y	1.36	1.16
	z	1.15	0.90
OP-3.1	x	1.55	1.48
	y	1.37	1.49
	z	1.28	0.93
OP-4	x	1.08	1.12
	y	1.02	1.07
	z	0.87	0.84

In Tab. 6.1, the SEAT values in the x-direction are larger than those in the y- and z-directions. All SEAT values in the x- and y-directions exceed 1. It means that the longitudinal and the lateral vibrations from the seat base are amplified by the seat-driver system. The lowest SEAT values occur in the z-direction. In case B, the SEAT values in the z-direction in all five operations are less than 1. It means that in these operations the vertical vibrations from the seat base are attenuated by the seat-driver system when the lap belt is used. The differences between the SEAT values in cases A and B were calculated with Eq. (6.1) and are illustrated in Fig. 6.1.

$$SEAT_{AB} \% = \frac{SEAT_B - SEAT_A}{SEAT_A} * 100\% \quad (6.1)$$

with

$SEAT_A$ SEAT value in the case where the driver does not wear any safety belt

$SEAT_{AB} \%$ Difference between the SEAT values in the case where the driver wears a lap belt and in the case where the driver does not wear any safety belt

$SEAT_B$ SEAT value in the case where the driver wears a lap belt

The positive $SEAT_{AB}\%$ value means that the lap belt causes an increase of the SEAT value. Fewer vibrations are attenuated by the seat-lap belt-driver configuration than the seat-no belt-driver configuration. The negative value means that the lap belt causes a decrease of the SEAT value. More vibrations are attenuated by the seat-lap belt-driver configuration.

In Fig. 6.1, in the x- and y-directions most $SEAT_{AB}\%$ values are in the range from -10% to 10%. This means that the differences between the SEAT values in cases A and B are quite small. In the x-direction, two positive $SEAT_{AB}\%$ values occur in operations OP-2.3 and OP-4. In the y-direction, two positive values occur in operations OP-3.1 and OP-4, and negative values can be observed especially in operations OP-1.3 and OP-2.3. In the z-direction, all $SEAT_{AB}\%$ values are negative. It indicates that the lap belt causes a decrease of SEAT values in the z-direction in these operations. The decrease is significant in operations with a high level of vibrations, such as operations OP-2.3 and OP-3.1.

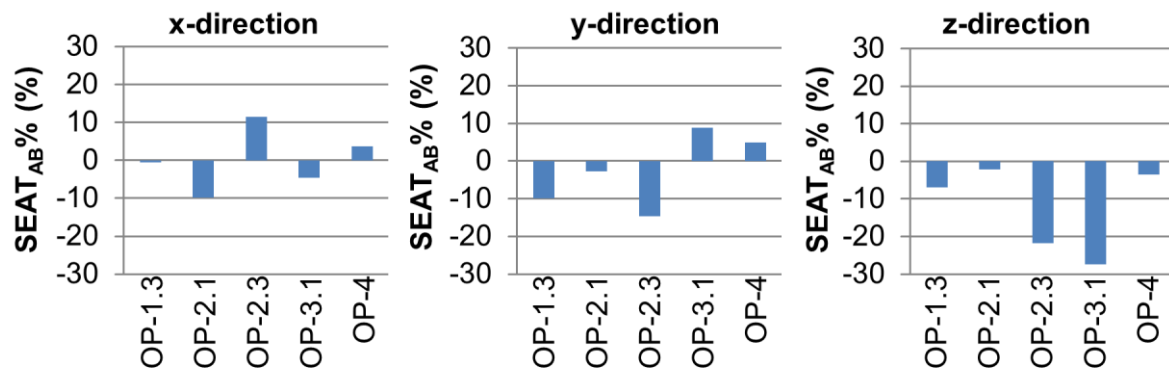


Fig. 6.1: Differences between the SEAT values in cases A and B

6.1.2 Comparison of seat transmissibility in the frequency domain

The curves of seat transmissibility in the frequency range of 0.5-16 Hz in case B are compared with those in case A in Fig. 6.2.

It can be noticed that in the x-direction the lap belt causes an increase of the seat transmissibility at frequencies lower than 3 Hz in operations OP-2.3 and OP-4. This is the reason for two positive $SEAT_{AB}\%$ values in Fig. 6.1. It also causes a decrease of the seat transmissibility at frequencies above 6 Hz, especially in operations OP-2.1 and OP-3.1. This is the reason for the negative $SEAT_{AB}\%$ values.

In the y-direction, the lap belt causes an increase of the seat transmissibility at frequencies lower than 2.5 Hz. The increase is obvious in operations OP-2.3, OP-3.1

and OP-4. This leads to the positive $SEAT_{AB}\%$ values in Fig. 6.1. It can also be observed that the lap belt causes a decrease of the seat transmissibility at frequencies ranging from 2.5 Hz to 5 Hz in the operation OP-3.1 and at frequencies above 4 Hz in another four operations, especially in the operation OP-2.3. This is the reason for the negative $SEAT_{AB}\%$ values.

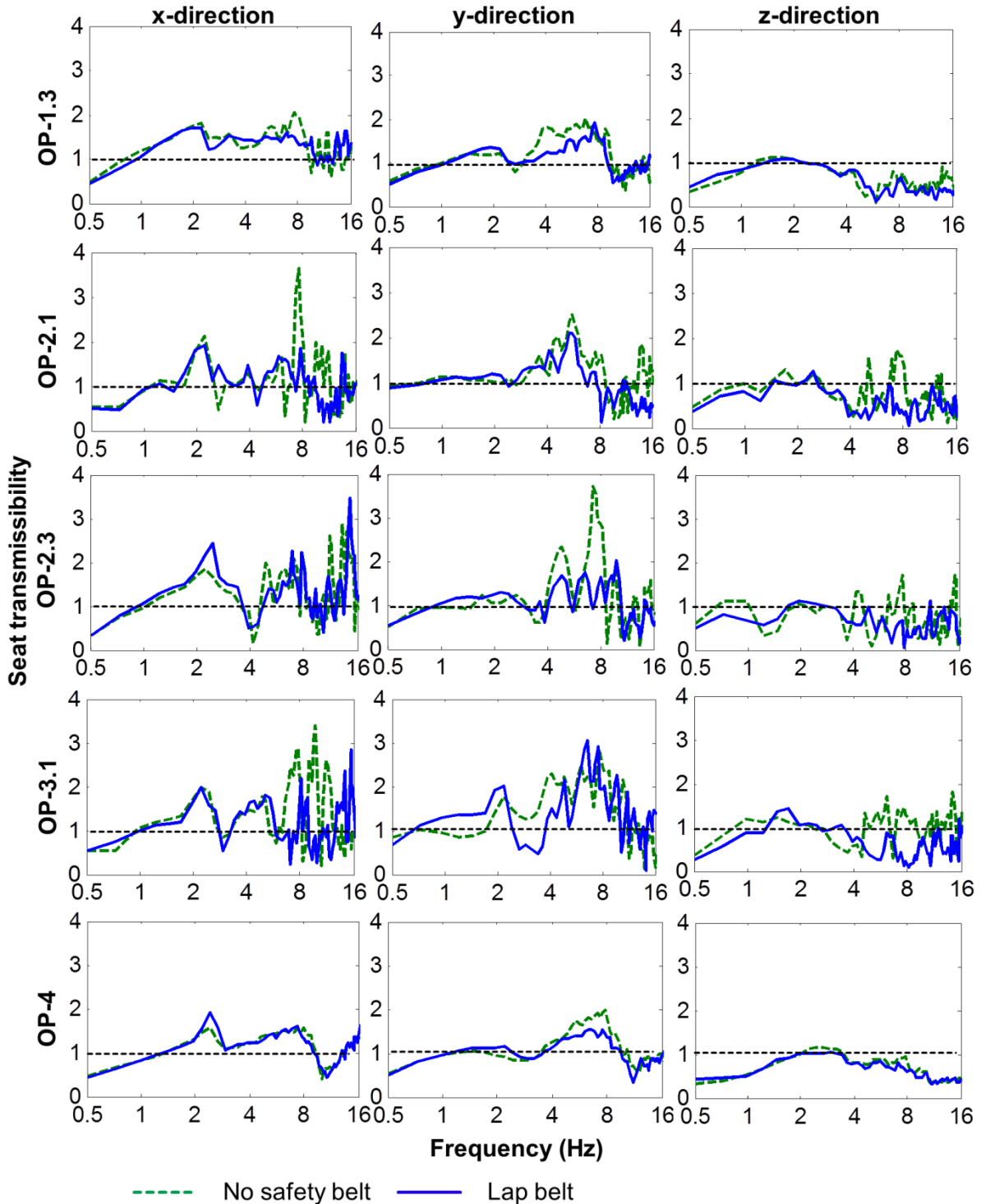


Fig. 6.2: Comparison of the seat transmissibility in cases A and B

In the z-direction, the lap belt causes a decrease of the seat transmissibility at frequencies higher than 4 Hz, especially in operations OP-2.1, OP-2.3 and OP-3.1. It can also be observed that in some operations the lap belt causes a decrease of the seat transmissibility at frequencies below 1.5 Hz and a very small increase between 1.5 Hz and 4 Hz.

The comparison of the SEAT values in cases A and B shows that the lap belt causes an increase of the SEAT value in the x- and y-directions in some operations. It causes a decrease of the SEAT value in the z-direction in all operations. When the driver does not wear a safety belt, he can adjust his posture and move freely to attenuate a part of vibrations. The lap belt restricts the movement of the driver. This brings the result that fewer vibrations are attenuated by the driver's movement. Like a mass-spring-damper system with a lower damping ratio, this causes the increase of the seat transmissibility at frequencies below 3 Hz in the x-direction, below 2.5 Hz in the y-direction and between 1.5 Hz and 4 Hz in the z-direction. It also leads to the decrease of the seat transmissibility at frequencies between 2.5 Hz and 4 Hz in the y-direction and at frequencies below 1.5 Hz in the z-direction. When vibrations are severe, the lap belt is activated and locked up. This avoids the driver leaving and impacting the seat and reduces the vibrations generated by the impacts between the driver and the seat. Due to this reason, the lap belt causes the decrease of the seat transmissibility at frequencies above 4 Hz in all three directions.

6.2 Four-point seat harness (case C) vs. no belt (case A)

In order to investigate the effect of a four-point seat harness on the seat transmissibility, the seat effective amplitude transmissibility (SEAT) values and the seat transmissibility in the frequency domain in case C are firstly compared with those in case A.

6.2.1 Comparison of seat effective amplitude transmissibility (SEAT)

The SEAT values in the three translational directions in cases A and C are given in Tab. 6.2, where these values are also classified into three groups as described in section 6.1.1. In Tab. 6.2 most of the SEAT values exceed 1. In all five operations the highest SEAT values occur in the x-direction, and the lowest occur in the z-direction.

The differences between the SEAT values in these two cases were calculated with Eq. (6.2) and are illustrated in Fig. 6.3.

Tab. 6.2: SEAT values in cases A and C

Test operation	Direction	SEAT value	
		case A	case C
OP-1.3	x	1.64	1.77
	y ¹²		
	z	1.00	1.03
OP-2.1	x	1.62	1.58
	y	1.11	1.15
	z	0.95	0.93
OP-2.3	x	1.48	1.80
	y	1.36	1.18
	z	1.15	1.00
OP-3.1	x	1.55	1.48
	y	1.37	1.41
	z	1.28	1.01
OP-4	x	1.08	1.16
	y	1.02	1.09
	z	0.87	0.90

$$SEAT_{AC}\% = \frac{SEAT_C - SEAT_A}{SEAT_A} * 100\% \quad (6.2)$$

with

$SEAT_{AC}\%$ Difference between SEAT values in the case where the driver wears a four-point seat harness and in the case where the driver does not wear any safety belt

$SEAT_C$ SEAT value in the case where the driver wears a four-point seat harness

It can be observed in Fig. 6.3 that most of the $SEAT_{AC}\%$ values are in the range from -10% to 10%, which means that in general the differences between the SEAT values in cases A and C are very small. In the x-direction, three $SEAT_{AC}\%$ values are positive and one exceeds 10%. This means that the four-point seat harness causes

¹² The signal in case C is defective.

an increase of the SEAT value in the x-direction. Fewer longitudinal vibrations are attenuated by the seat-harness-driver configuration than the seat-no belt-driver configuration. Only one negative $SEAT_{AC}\%$ value can be observed in the y-direction. In the z-direction three negative $SEAT_{AC}\%$ values can be observed, especially in operations OP-2.3 and OP-3.1. The negative value means that the four-point seat harness causes a decrease of the SEAT value and more vibrations are attenuated by the seat-harness-driver configuration.

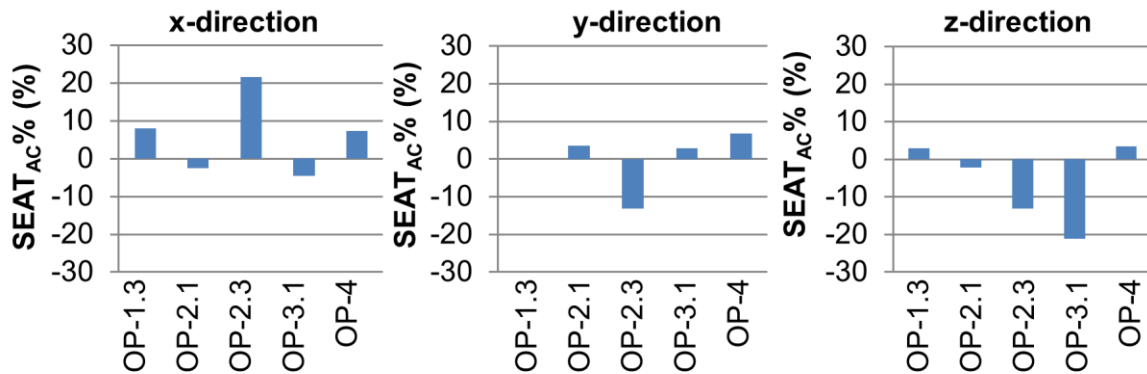


Fig. 6.3: Differences between the SEAT values in cases A and C

6.2.2 Comparison of seat transmissibility in the frequency domain

The curves of seat transmissibility in the frequency range of 0.5-16 Hz in case C are compared with those in case A in Fig. 6.4.

In Fig. 6.4 it can be noticed that in the x-direction the seat transmissibility in case C is a little larger than that in case A at frequencies lower than 3 Hz, especially in operations OP-2.3 and OP-4. This is the reason for the positive $SEAT_{AC}\%$ values in Fig. 6.3. In addition, the four-point seat harness causes a decrease of the seat transmissibility at frequencies above 4 Hz in this direction.

In the y-direction, in all four operations the seat transmissibility in case C is larger than that in case A at frequencies below 2 Hz, and smaller at frequencies in the range from 2 Hz to 8 Hz, especially in operations OP-2.3 and OP-3.1.

In the z-direction, the seat transmissibility in case C is a little larger than that in case A in the frequency range from 1.5 Hz to 4 Hz, and smaller at frequencies higher than 4 Hz. It can be observed that in some operations the four-point seat harness also causes a decrease of the seat transmissibility at frequencies below 1.5 Hz.

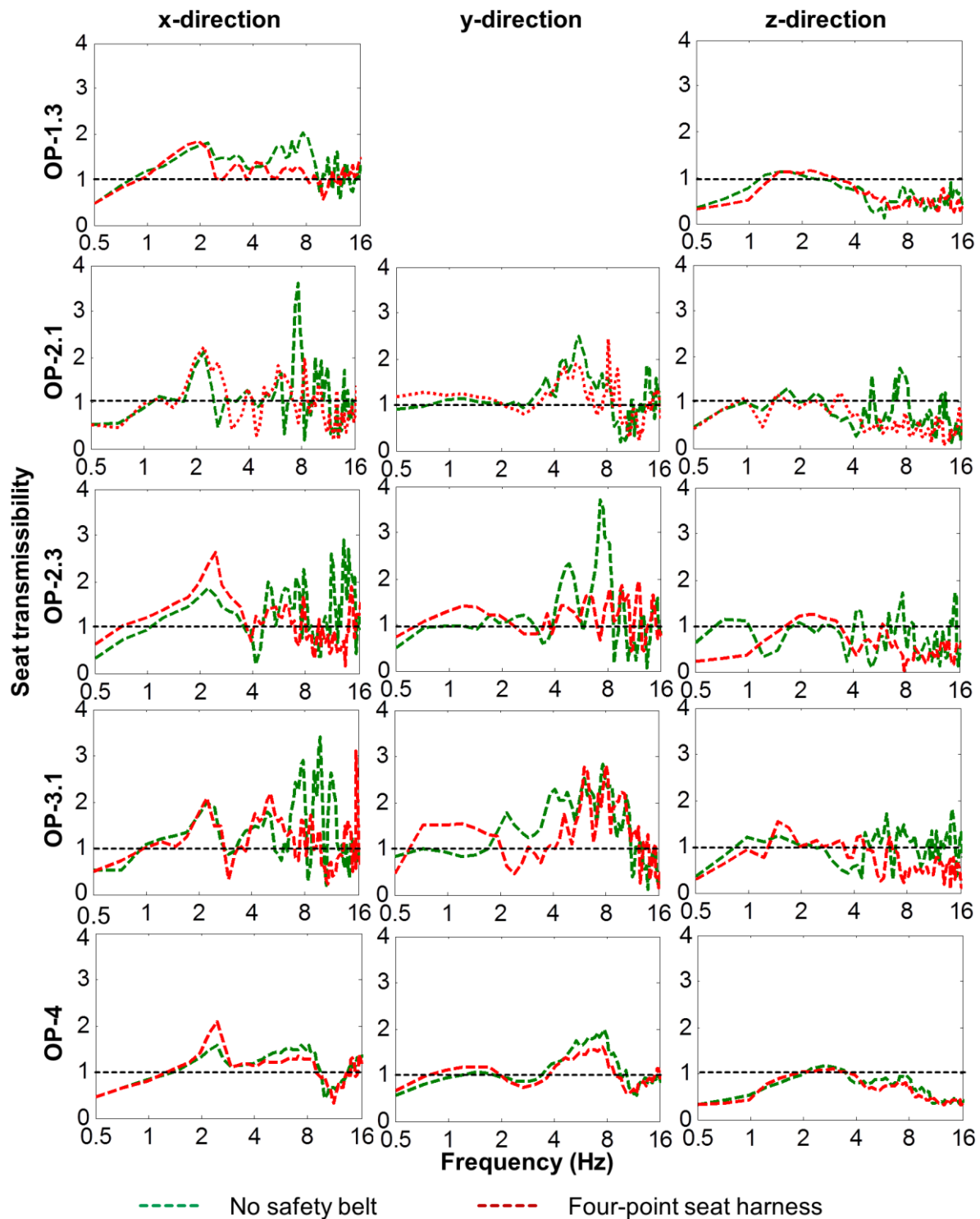


Fig. 6.4: Comparison of the seat transmissibility in cases A and C

The comparison of the SEAT values in cases A and C shows that the four-point seat harness can cause an increase of the SEAT value in all three directions, especially in the x- and y-directions. It can cause a decrease of the SEAT value in the z-direction in operations with a high level of vibrations. The comparison of the seat transmissibility in the frequency domain shows that the four-point seat harness

causes the increase of the seat transmissibility at frequencies lower than 3 Hz in the x-direction, at frequencies lower than 2 Hz in the y-direction, and also in the frequency range of 1.5-4 Hz in the z-direction. This is because the four-point seat harness restricts the movement of the driver and reduces the vibrations attenuated by the driver's movement. On the other hand, the four-point seat harness causes the decrease of the seat transmissibility in all three directions at frequencies higher than 4 Hz. This is because the four-point seat harness avoids the driver leaving and impacting the seat and reduces the vibrations generated by the impacts between the driver and the seat.

6.3 Four-point seat harness (case C) vs. lap belt (case B)

The vibration measurements were carried out in all ten operations described in Tab. 4.1 (p. 62) in both of cases B and C. In this section, these ten operations are divided into two groups depending on the vibration severity. The first group includes operations with a low level of vibrations, such as OP-1.1, OP-1.2, OP-2.1, OP-2.2 and OP-4. The second group includes operations with a high level of vibrations, such as OP-1.3, OP-1.4, OP-2.3, OP-3.1 and OP-3.2.

6.3.1 Comparison of seat effective amplitude transmissibility (SEAT)

The SEAT values in the three translational directions in cases B and C are given in Tab. 6.3 and Tab. 6.4. They are also divided into three groups as in section 6.1.1. The differences between the SEAT values in these two cases were calculated with Eq. (6.3) and are illustrated in Fig. 6.5 and Fig. 6.6.

$$SEAT_{BC} \% = \frac{SEAT_C - SEAT_B}{SEAT_B} * 100\% \quad (6.3)$$

with

$SEAT_{BC} \%$ Difference between the SEAT values in the case where the driver wears a four-point seat harness and in the case where the driver wears a lap belt

In Tab. 6.3 the SEAT values in cases B and C in operations with a low level of vibrations are presented. It can be noticed that the highest SEAT values occur in the x-direction, and the lowest occur in the z-direction. All SEAT values in the x- and y-directions exceed 1. In the z-direction the SEAT values in operations OP-1.1 and OP-

1.2 exceed 1 as well. And they are less than 1 in the other three operations, except for the case B in the operation OP-2.2, where the SEAT value exceeds 1 only a little bit. It can be concluded that whether the vertical vibrations are attenuated or amplified by the seat-driver system depends on the vehicle operations.

Tab. 6.3: SEAT values in cases B and C in operations with a low level of vibrations

Test operation	Direction	SEAT	
		case B	case C
OP-1.1	x	1.39	1.45
	y	1.05	1.22
	z	1.21	1.22
OP-1.2	x	1.32	1.38
	y	1.03	1.17
	z	1.24	1.23
OP-2.1	x	1.46	1.58
	y	1.08	1.15
	z	0.93	0.93
OP-2.2	x	1.32	1.41
	y	1.06	1.38
	z	1.02	0.95
OP-4	x	1.12	1.16
	y	1.07	1.09
	z	0.84	0.90

In Fig. 6.5 the differences between the SEAT values in cases B and C in operations with a low level of vibrations are presented. All $SEAT_{BC}\%$ values in the x- and y-directions are positive, which means that the SEAT values increase when the driver wears a four-point seat harness instead of a lap belt. The increase is quite small in the x-direction (smaller than 10%) and large in the y-direction. In the z-direction, the differences between cases B and C are smaller than 8%.

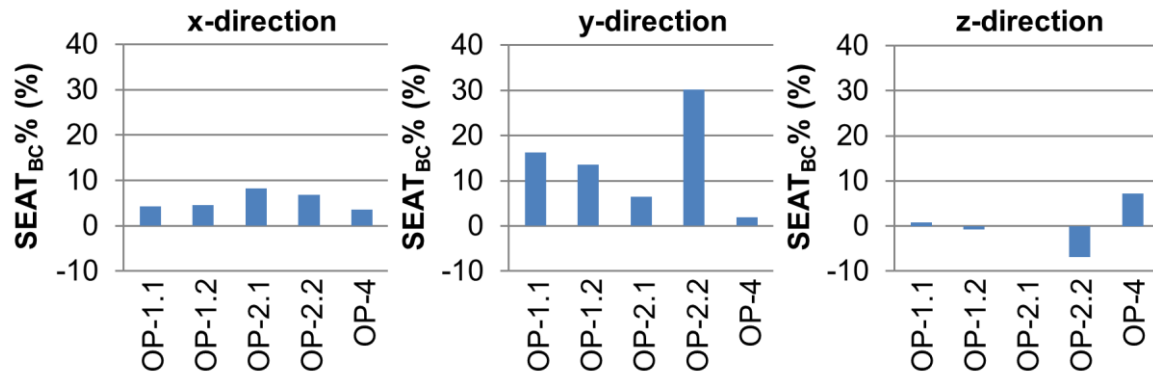


Fig. 6.5: Differences between the SEAT values in cases B and C in operations with a low level of vibrations

Tab. 6.4: SEAT values in cases B and C in operations with a high level of vibrations

Test operation	Direction	SEAT	
		case B	case C
OP-1.3	x	1.63	1.77
	y ¹³		
	z	0.93	1.03
OP-1.4	x	1.73	2.30
	y	1.14	1.04
	z	0.92	1.08
OP-2.3	x	1.65	1.80
	y	1.16	1.18
	z	0.90	1.00
OP-3.1	x	1.48	1.48
	y	1.49	1.41
	z	0.93	1.01
OP-3.2	x	1.46	1.61
	y ¹⁴		
	z	0.95	1.03

In Tab. 6.4 the SEAT values in cases B and C during the operations with a high level of vibrations are presented. It can be noticed that the highest SEAT values occur in the x-direction, and the lowest occur in the z-direction. All SEAT values in the x- and

¹³ The signal in case C is defective.

¹⁴ Same with Footnote 13.

y-directions exceed 1. The SEAT values in the x-direction in Tab. 6.4 are much larger than those in Tab. 6.3 with the operations that cause low vibrational excitations. In the z-direction, all SEAT values in case B are less than 1, while in case C all SEAT values exceed 1 a little bit. In other words, in operations with a high level of vibrations the vertical vibrations are attenuated by the seat-driver system when a lap belt is used, but amplified when a four-point seat harness is used.

In Fig. 6.6 the differences between the SEAT values in cases B and C in operations with a high level of vibrations are presented. All $SEAT_{BC}\%$ values in the x- and z-directions are positive, which means that the SEAT values in these two directions increase when the driver wears a four-point seat harness instead of a lap belt. There is a very small decrease of the SEAT value in the y-direction when the driver wears a four-point seat harness instead of a lap belt.

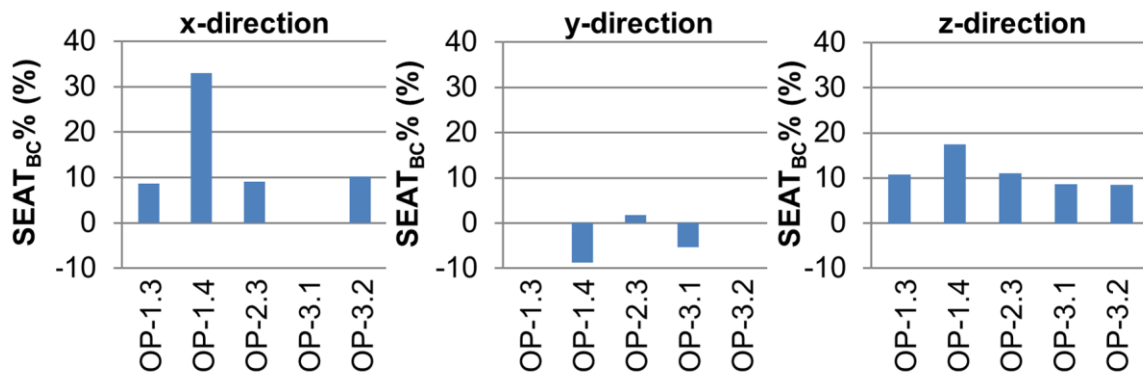


Fig. 6.6: Differences between the SEAT values in cases B and C in operations with a high level of vibrations

6.3.2 Comparison of seat transmissibility in the frequency domain

The curves of seat transmissibility in the frequency range of 0.5-16 Hz in case C are compared with those in case B in Fig. 6.7 and Fig. 6.8.

In Fig. 6.7 the comparison of the seat transmissibility in cases B and C during the operations with a low level of vibrations is presented. In the x- and z-directions, the differences between the seat transmissibility in cases B and C are very small, except for the operation OP-1.1. Only in this operation, the seat transmissibility with the four-point seat harness is much lower than that with the lap belt at frequencies above 3 Hz in all three directions. This phenomenon is possibly caused by the disturbance or the noise in the signals. It can be observed that in the x-direction the seat transmissibility increases slightly at frequencies lower than about 3 Hz and decreases

a little bit only in operations OP-1.2 and OP-4 between 4 Hz and 8 Hz, when the driver wears a four-point seat harness instead of a lap belt. In the y-direction, it is visible that the seat transmissibility increases at frequencies lower than about 2 Hz and decreases slightly between 2 Hz and 4 Hz when the driver wears a four-point seat harness instead of a lap belt.

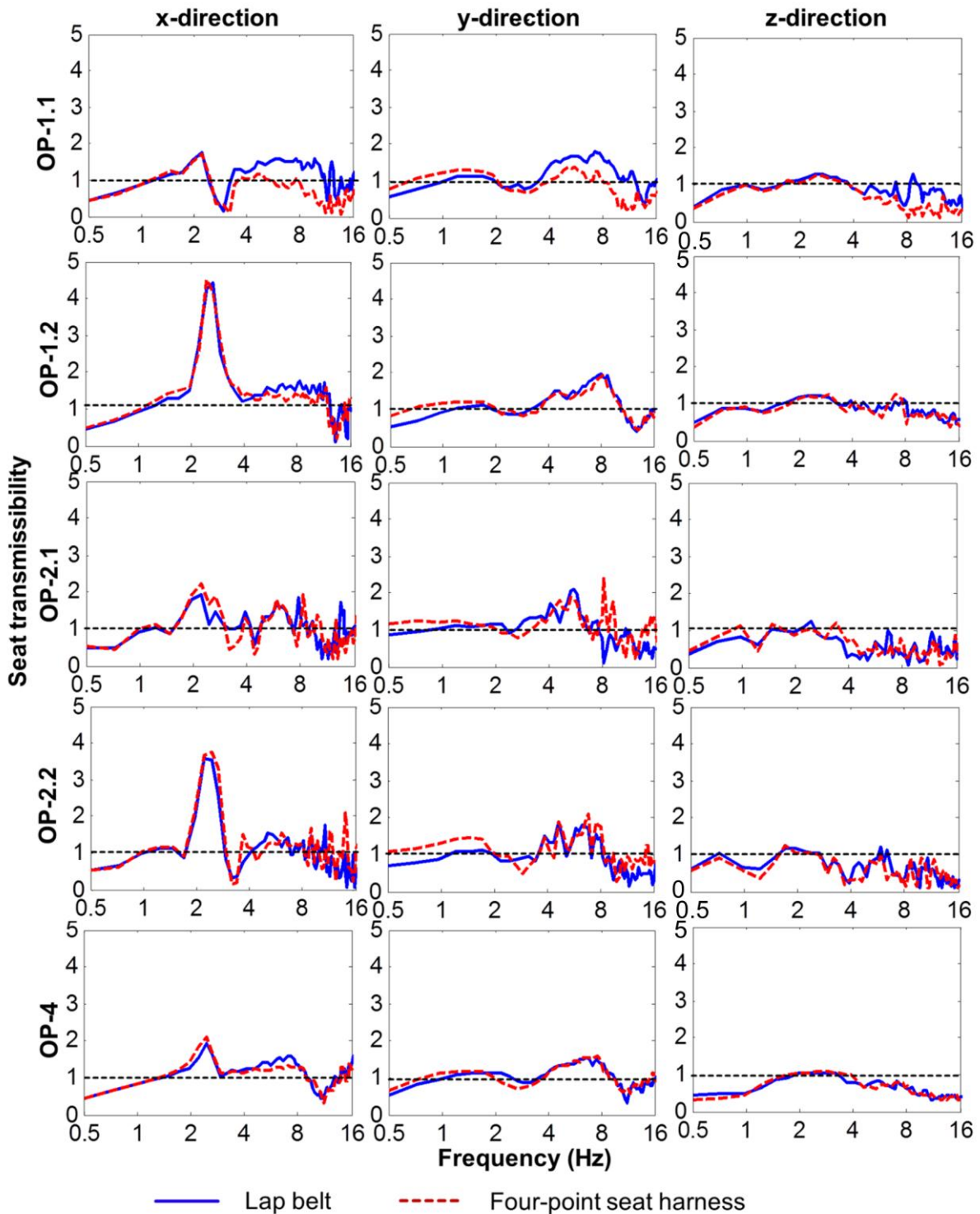


Fig. 6.7: Comparison of the seat transmissibility in cases B and C in operations with a low level of vibrations

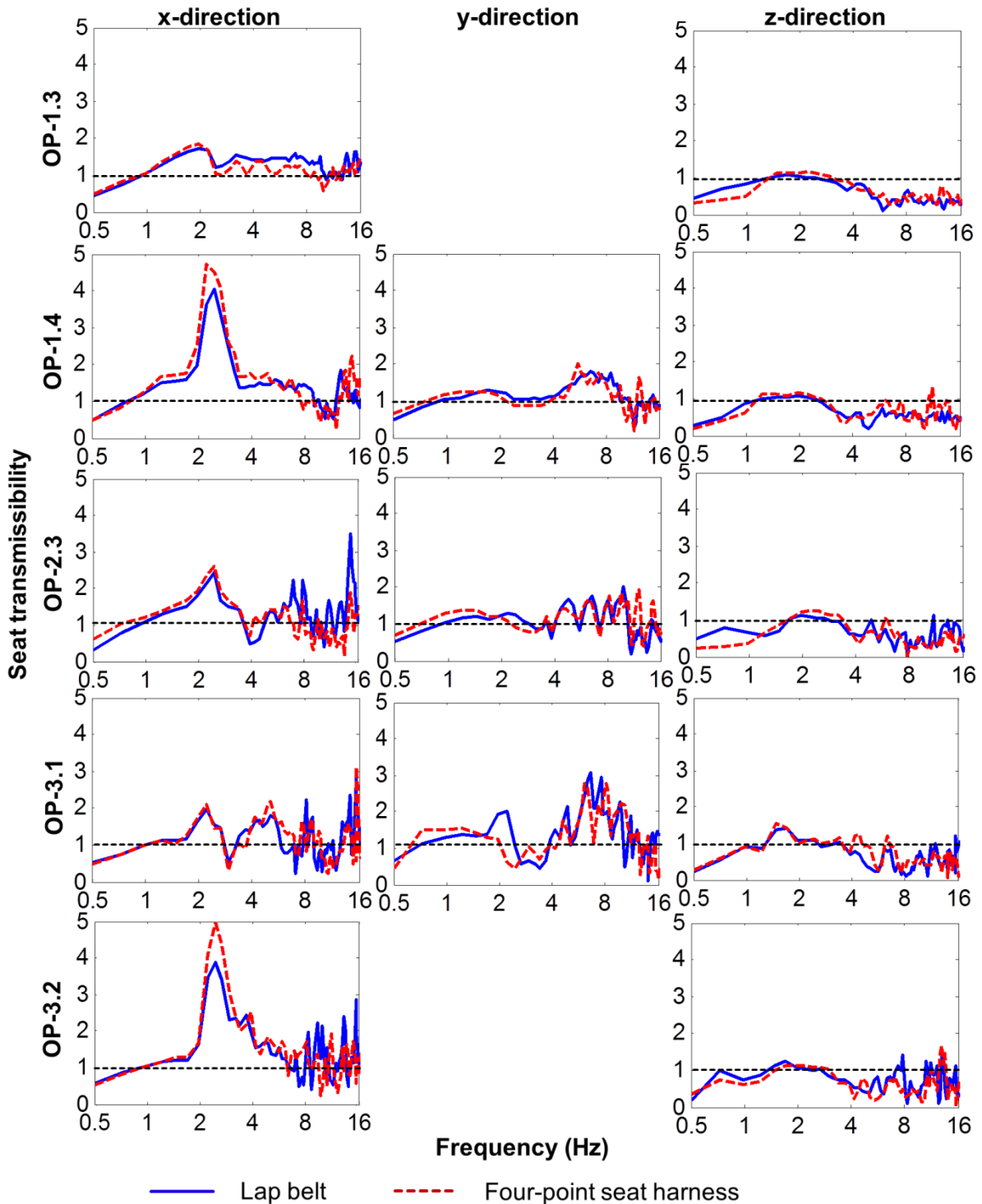


Fig. 6.8: Comparison of the seat transmissibility in cases B and C in operations with a high level of vibrations

In Fig. 6.8 the comparison of the seat transmissibility in cases B and C in operations with a high level of vibrations is presented. When the driver wears a four-point seat harness instead of a lap belt, the seat transmissibility increases a little bit at frequencies lower than about 3 Hz in the x-direction, and decreases largely only at

frequencies above 3 Hz in the operation OP-1.3. In the y-direction it increases a little at frequencies lower than 2 Hz and decreases slightly in the frequency range of 2-4 Hz. Moreover, in the z-direction it decreases a little at frequencies lower than 1.5 Hz and increases very slightly in the frequency range of 1.5-4 Hz.

The comparison of the SEAT values in cases B and C shows that in operations with a low level of vibrations the SEAT values in the x- and y-directions increase when the driver wears a four-point seat harness instead of a lap belt. In operations with a high level of vibrations, the SEAT values in the x- and z-direction increase a little when the driver wears a four-point seat harness instead of a lap belt. From the comparison of the seat transmissibility in the frequency domain in cases B and C, it can be concluded that, when the driver wears a four-point seat harness instead of a lap belt, in the x-direction there is a small increase of the seat transmissibility at frequencies lower than 3 Hz; in the y-direction the seat transmissibility increases at frequencies lower than 2 Hz and decreases slightly between 2 Hz and 4 Hz; and it increases at frequencies ranging from 1.5 Hz to 4 Hz in the z-direction in operations with a high level of vibrations. This is due to the fact that the four-point seat harness restricts the movement of the driver more largely than the lap belt. This leads to fewer vibrations attenuated by the movement of the driver and causes the increase of the seat transmissibility.

6.4 Subjective comments on ride comfort

After each field test, comments on the ride comfort with different safety belts were collected from the driver. From the subjective comments it can be concluded that:

- 1) In all operations, the driver did not have any negative feeling when he wore the lap belt. The driver still can move his upper body freely. There was no obvious difference of the feeling between cases A and B;
- 2) Compared with the lap belt, the four-point seat harness did not cause more discomfort in operations with a low level of vibrations. But in operations with a high level of vibrations, the four-point seat harness generated more discomfort than the lap belt, because it restricted the movement of the driver and also transmitted more vibrations from the backrest and the harness to the driver's upper body by fixing it with the backrest. The driver commented that a large stress on shoulders was caused by the four-point seat harness.

6.5 Conclusion

In all operations the highest seat effective amplitude transmissibility (SEAT) values occur in the x-direction and the lowest occur in the z-direction. All SEAT values in the x- and y-directions exceed 1. It means that the seat-driver system amplifies the vibrations in both directions. There is a potential to reduce the SEAT values in these two directions by employing the seat suspension system, especially for the x-direction.

Compared to the case that the driver does not wear a safety belt, the lap belt and the four-point seat harness play a role in reducing the SEAT value, especially in the z-direction. They cause a decrease of the seat transmissibility at frequencies above 4 Hz in all three directions. This is due to the fact that the lap belt and the four-point seat harness prevent the driver from leaving and impacting the seat and reduce the vibrations generated by these impacts. The lap belt and the four-point seat harness also cause an increase of the seat transmissibility in the x-direction at frequencies below 3 Hz and in the y-direction at frequencies below 2 Hz and also in the z-direction at frequencies ranging from 1.5 Hz to 4 Hz. This is because both safety belts restrict the movement of the driver and reduce the vibrations attenuated by the driver's movement. Due to the increase of the seat transmissibility in the x- and y-directions, a small increase of the SEAT value in these two directions occurs in some operations.

Generally, compared to the lap belt, the four-point seat harness causes an increase of the SEAT value. It leads to an increase of the seat transmissibility in the x-direction at frequencies below 3 Hz and in the y-direction at frequencies below 2 Hz and also in the z-direction in the frequency range of 1.5-4 Hz. This is because the four-point seat harness restricts the driver's movement more strongly than the lap belt.

According to the comments from the driver, the lap belt does not cause a deterioration of the comfort. Compared to it, the four-point seat harness does not lead to more discomfort in operations with a low level of vibrations, but leads to more discomfort in operations with a high level of vibrations. The four-point seat harness transmits more vibrations through the backrest and the harness to the driver. Additionally, the four-point seat harness generates a large stress on the shoulders.

In summary, it is concluded that the lap belt is the favorable safety belt to wear on a compact wheel loader.

7 Optimization of Seat Suspension System

The evaluation results in chapter 5 show that the whole-body vibrations (WBV) measured on a compact wheel loader (CWL) are severe. The short-term exposure to the WBV leads to strong ride discomfort, and the long-term exposure can cause health risks. Consequently, there is a necessity to reduce the WBV on the CWL.

Because the seat is the principal contact component between the driver and the vehicle, its vibration attenuation performance has a significant influence on the WBV intensity. The seat effective amplitude transmissibility (SEAT) values in chapter 6 show that the longitudinal and the lateral vibrations are amplified largely by the seat-driver system. The vertical vibration intensity is reduced slightly and the reduction only occurs in some operations. It means that the vibration attenuation performance of the suspension seat needs to be improved. On the other hand, the dynamics of the seat-driver system hardly affects the dynamics of the whole vehicle, because its mass is much smaller than the vehicle mass. It means that consideration should rather be given at first to the improvement of the seat suspension systems instead of changing the cabin and the axle suspension systems, if it comes to improve the ride comfort and reduce the health risks.

The original seat on the CWL involved in this research work is equipped with a vertical suspension system. At first dynamic characteristics of this suspension system should be investigated. If necessary, it should be optimized to improve the vibration attenuation performance of the seat in the vertical direction. It can be observed from Tab. 5.1 (p. 81) that the WBV in the horizontal directions on the CWL are severe, especially in the longitudinal direction. From chapter 6 it can be noticed that the largest SEAT value always occurs in the longitudinal direction. To really reduce the WBV it seems to be necessary that a longitudinal seat suspension system with optimal dynamic properties has to be introduced as well.

7.1 Investigation of dynamics of vertical seat suspension system

The optimization strategy of a seat suspension system should be developed based on the sufficient understanding of the suspension dynamic characteristics. As introduced in section 2.3.2, the dynamics of a seat suspension system can be divided into five states depending on the vibration dose value ratio (VDVR, Eq. (2.25), p. 45) of the suspension system and the occurrence of end-stop impacts. In this study, seat

tests were carried out in laboratory with the aim of determining the dynamic states of the vertical seat suspension system when the seat is exposed to the vibrations measured on the CWL in all test operations in Tab. 4.1 (p. 62). The detailed description of the laboratory seat tests and the analysis results are presented in the following paragraphs.

7.1.1 Laboratory seat tests

In the laboratory seat tests, the seat was fixed on a multi-axis shaking table, which provides the seat excitations. The excitation signals are the accelerations measured at the seat base on the compact wheel loader (CWL) in the field tests. A dummy was employed to represent the tested persons. In the seat tests accelerations were measured at the seat base, above the vertical seat suspension system and on the seat cushion. The end-stop impacts were monitored as well. The vibration dose value ratio (VDVR) of the vertical seat suspension system and the times of end-stop impact were analyzed to determine the dynamic states of this suspension system.

7.1.1.1 Multi-axis shaking table

The multi-axis shaking table is actuated by three hydraulic cylinders, as shown in Fig. 7.1. It has three degrees of freedom (DOF) respectively in the longitudinal, the vertical and also the pitch directions. In this research work, it was only actuated in the vertical direction using two vertical cylinders.

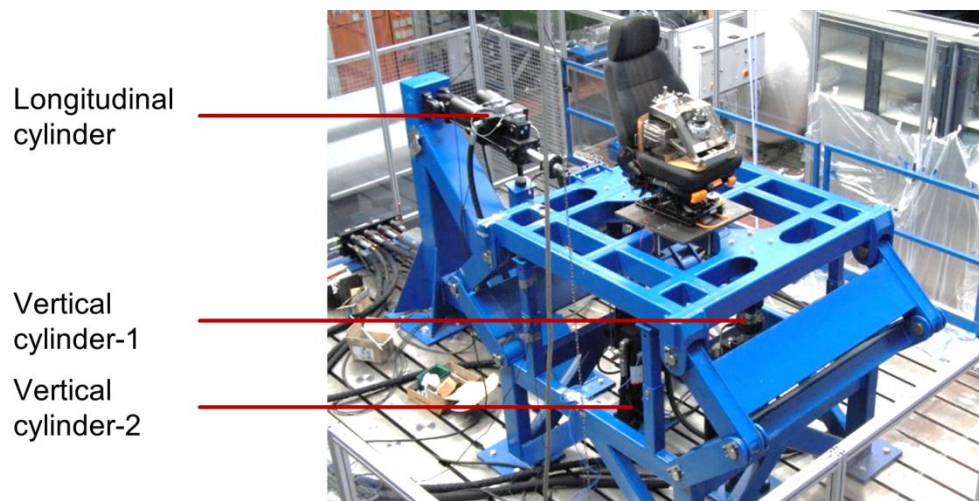


Fig. 7.1: Multi-axis shaking table used in the laboratory seat tests

Periodic excitation signals, such as sinusoidal force or displacement signals, can be directly defined in the software of the cylinder controller. To reproduce random

acceleration signals, an additional software named Remote Parameter Control (RPC) is needed, which is provided by the supplier of the cylinder system, the MTS Systems Corporation. With the help of this software, the transfer function between the displacement of the cylinders and the random acceleration signals is obtained and used to produce a displacement based drive file, which is used in the software of the cylinder controller to actuate the shaking table.

7.1.1.2 Tested seat

The tested seat is the same type as that in the compact wheel loader (CWL). It employs a scissors linkage mechanism in the vertical direction with an air spring and an inclined passive hydraulic damper, as shown in Fig. 7.2. The seat height is adjustable with the help of a build-in air compressor. The vertical suspension system provides a free stroke of 88 mm between the top and the bottom rubber end-stop buffers. The top end-stop buffer is hidden in the suspension frame but its location is marked in Fig. 7.2. In the laboratory, the seat tests were carried out when the seat was adjusted in the middle position.

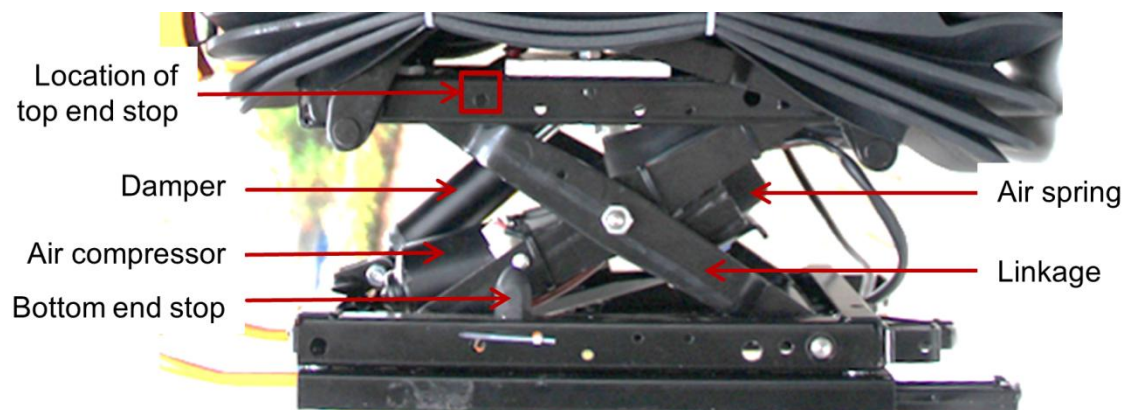


Fig. 7.2: Structure of the vertical seat suspension system

7.1.1.3 Excitation signals

The vertical accelerations at the seat base in the CWL measured in the ten operations (Tab. 4.1, p. 62) in the field tests were used as the excitation signals in the laboratory seat tests. A 0.5-50 Hz band-pass filter was applied on these signals before they were reproduced in the RPC software.

7.1.1.4 Seat test dummy

In order to avoid vibration exposure and health risks for the human during the seat tests, a seat test dummy was used. The utilization of a seat test dummy also helps to

reduce the statistical variance of the test results. The seat test dummy is a passive mass-spring-damper system including two masses, a set of coil springs and a hydraulic damper. The structure of the dummy is illustrated in Fig. 7.3. It is comprised of a wooden base shaped like the buttocks of a person, a metal base frame and a metal load frame with a load platform. The base and the base frame represent the lower body of a seated person. The load frame is attached to the base frame through a pivot arm and supported by the hydraulic damper and the springs. The load platform is designed to hold different masses to represent the upper body of seated persons with a weight of 55 kg, 75 kg or 98 kg. It has been proven that this dummy is reliable to simulate the dynamic response of seated persons in the vertical direction. [161]

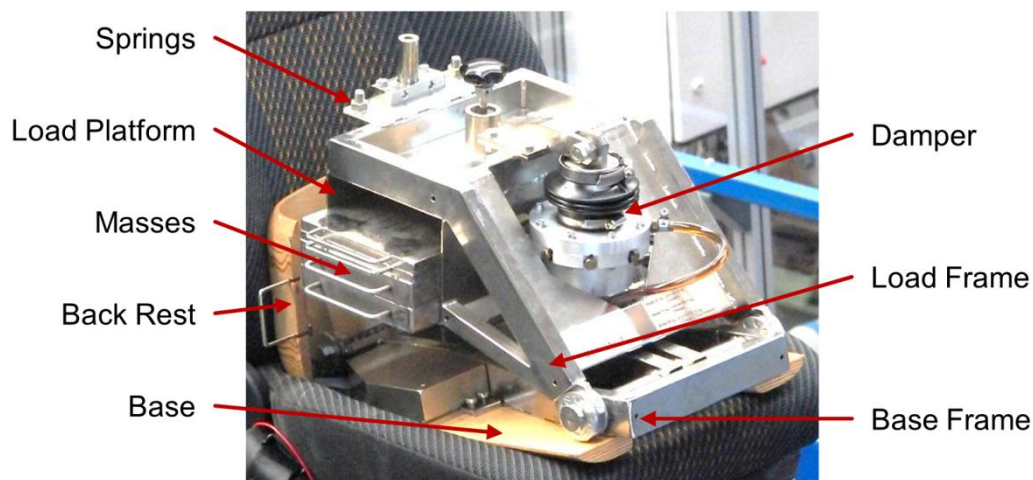


Fig. 7.3. Structure of the dummy used in the laboratory seat tests

7.1.1.5 Data acquisition equipment

The entire data acquisition equipment included two parts: one part acquired the acceleration signals and the other part acquired the signals of end-stop impact.

The equipment acquiring acceleration signals was comprised of two tri-axial accelerometers (PCB PIEZOTRONICS ICP 356A16), a tri-axial seat pad accelerometer (PCB PIEZOTRONICS ICP 356B41), two 8-Channel Dynamic Signal Acquisition modules (NI PXI 4472B) in a chassis (NI PXI 1000B), as well as a laptop. One tri-axial accelerometer was fixed under the seat cushion and above the vertical seat suspension system. The other was fixed at the seat base. The tri-axial seat pad accelerometer was fixed on the top surface of the seat cushion. Locations of these three accelerometers are shown in Fig. 7.4. These accelerometers were connected to the NI PXI 4472B modules in the NI PXI chassis. With the help of NI-DAQ

Assistant in a Labview program in the laptop, the NI PXI 4472B modules converted the analog signals from the accelerometers to the digital ones and transmitted them to the laptop via the NI PXI chassis.

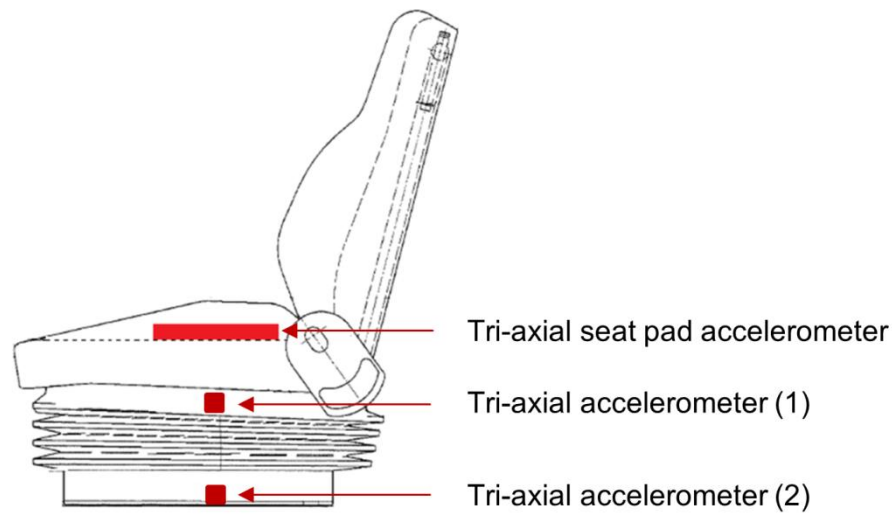


Fig. 7.4: Locations of accelerometers on the seat in laboratory seat tests

The equipment acquiring the end-stop impact signals was comprised of two micro switches, a direct current power supply, an analog input module (NI 9205) in a chassis (NI cDAQ-9172) and a laptop. All of these devices comprised a circuit, as illustrated in Fig. 7.5.

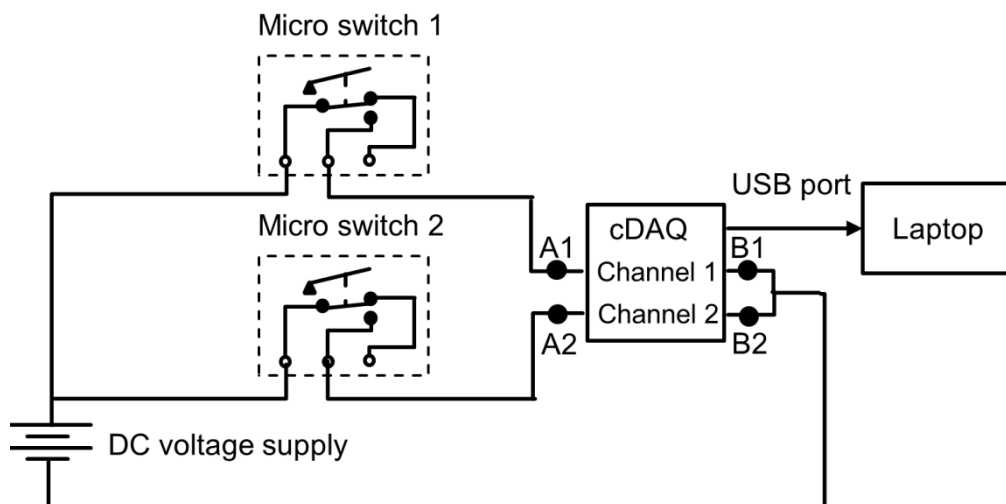


Fig. 7.5: Circuit to pick up and store the signals of end-stop impact

Two micro switches were employed to monitor the top and the bottom end-stop impacts respectively. When the end-stop impact occurred, the micro switches were pressed downward to close the circuit. In this case, a voltage difference was generated between A1 and B1 or between A2 and B2 in Fig. 7.5. The NI 9205 module picked up the voltage difference signals, converted them to digital signals

with the help of NI-DAQ Assistant in the Labview program in the laptop, and transmitted them to the laptop via the NI cDAQ-9172 chassis. The Labview program in the laptop was used to display the signals and to store the measurement data as well. The sampling frequency of all signals was set to 1000 Hz.

7.1.2 Analysis of dynamics of the vertical seat suspension system

In order to study the dynamic characteristics of the vertical seat suspension system, two parameters were analyzed: the suspension vibration dose value ratio (VDVR, Eq. (2.25), p. 45) and the times of end-stop impact. In Fig. 7.6 the VDVRs and times of end-stop impact when the seat is exposed to the vibrations measured on the CWL in ten operations are presented. The round points represent the VDVRs. The numbers above these points are the times of top end-stop impact. The numbers below these points are the times of bottom end-stop impact. The ten test operations are arranged in principle in the ascending order of the root mean square (RMS) value of the excitations, while taking the level of the VDVR and the times of end-stop impact into consideration.

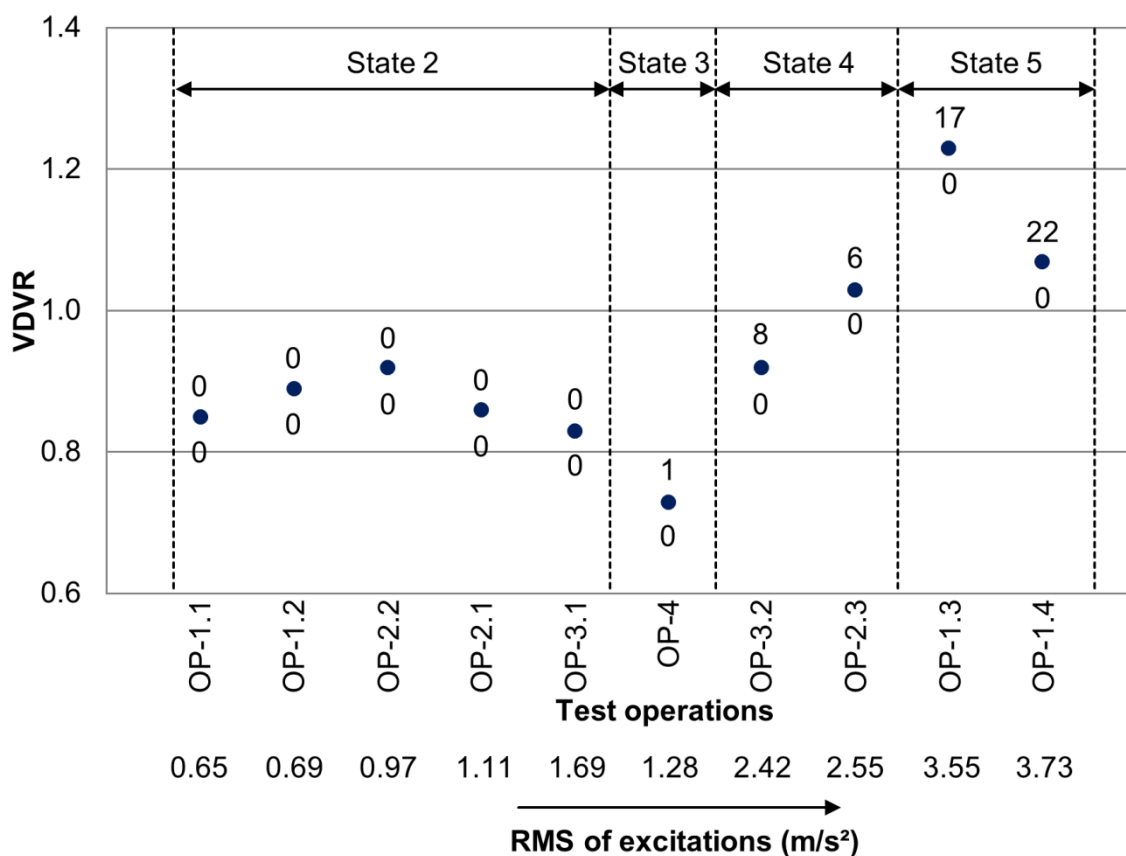


Fig. 7.6: VDVRs of the vertical seat suspension system and times of end-stop impact in ten CWL operations

The variation tendency of the VDVR in Fig. 7.6 is consistent with that in Fig. 2.27 (p. 45). The minimum VDVR can be observed in the operation OP-4 with only one top end-stop impact monitored. Because the end-stop impact lasts less than 1 s, it hardly affects the suspension dynamics in the whole operation duration of 305 s. Accordingly, the dynamics of the vertical seat suspension system in the operation OP-4 is classified into state 3.

The excitation magnitudes in operations OP-1.1, OP-1.2, OP-2.1 and OP-2.2 are lower than that in the operation OP-4, as seen from the RMS values in Fig. 7.6. And the VDVRs in these four operations are larger than that in the operation OP-4. This is consistent with the variation tendency of the VDVR in state 2 in Fig. 2.27. Accordingly, the suspension dynamics in these four operations are classified into state 2.

The suspension dynamics in the operation OP-3.1 is classified into state 2 as well due to the fact that the VDVR in this operation is larger than that in the operation OP-4, as well as that no end-stop impact occurs. These characteristics seem to be similar to OP-1.1, OP-1.2, OP-2.1 and OP-2.2. In Fig. 2.27 the excitation magnitude in state 2 should be lower than that in state 3. But the RMS of the excitation in the operation OP-3.1 (state 2) is larger than that in the operation OP-4 (state 3). This problem can be explained by analyzing the excitation signal in the operation OP-3.1 in the time domain. This signal includes two levels of vibrations, as shown in Fig. 7.7. The vibrations with high magnitudes result in a larger RMS value than that in the operation OP-4. But under the vibration excitations with low magnitudes, the nonlinearity of the suspension mechanism has a large influence on the suspension dynamics. This keeps the suspension dynamics staying in state 2 and causes a larger VDVR than that in the operation OP-4.

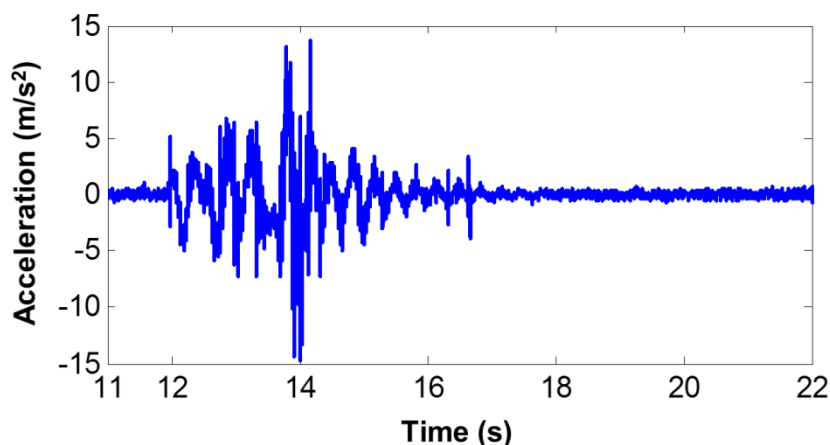


Fig. 7.7: Part of the excitation signal in the operation OP-3.1

The suspension dynamics in operations OP-2.3 and OP-3.2 are classified into state 4, because in these two operations top end-stop impacts occur frequently. The suspension dynamics in operations OP-1.3 and OP-1.4 are classified into state 5, because the frequency of the top end-stop impacts increases significantly.

The curves of transmissibility of the vertical seat suspension system in ten CWL operations are illustrated in Fig. 7.8. These ten test operations are classified according to the state of the suspension dynamics and the characteristics of the suspension transmissibility.

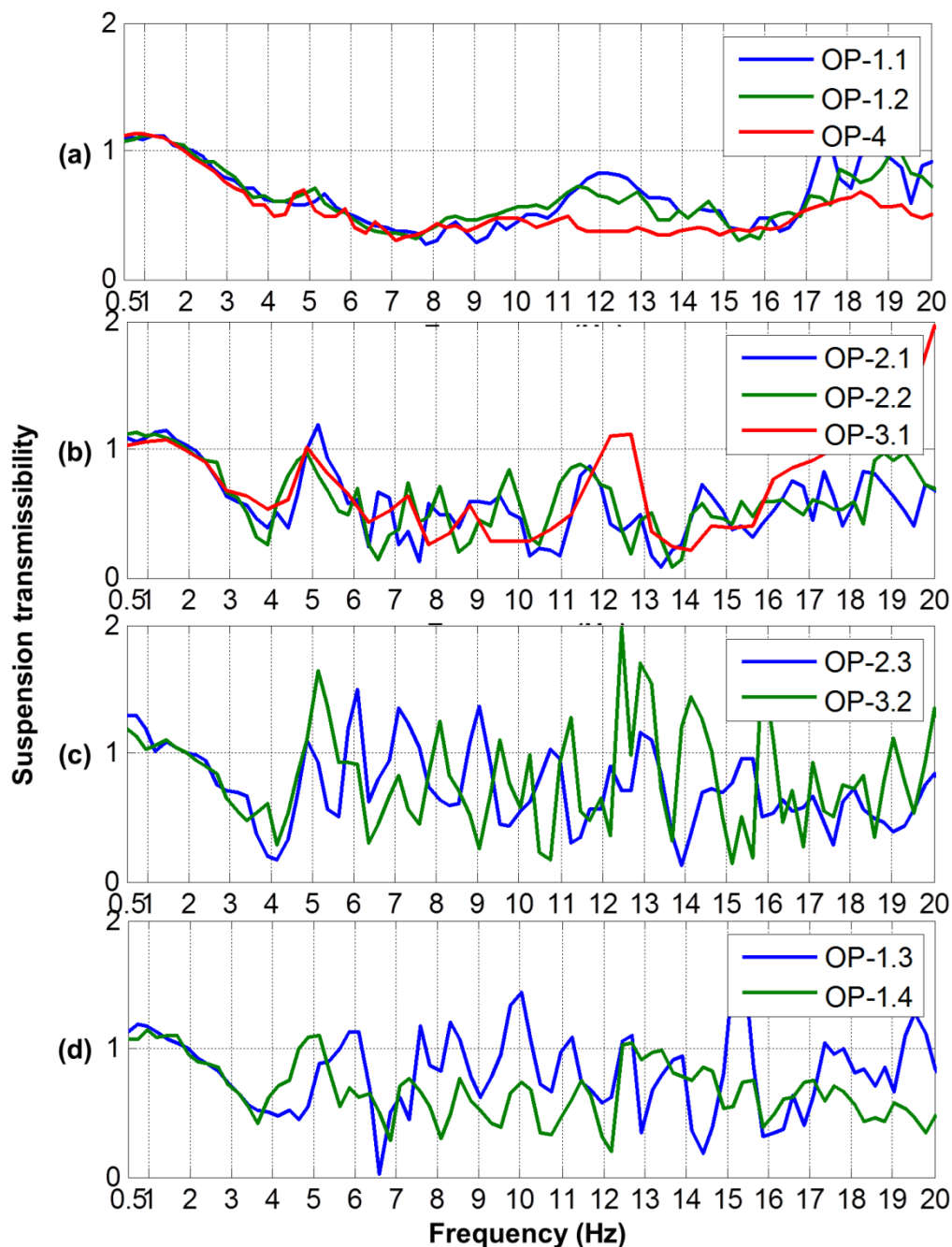


Fig. 7.8: Transmissibility of the vertical seat suspension system in ten operations

In Fig. 7.8, it can be observed that the vertical seat suspension system attenuates the vibrations at frequencies higher than 2 Hz. As shown in Fig. 7.6, there was no bottom end-stop impact in all operations. But many top end-stop impacts were monitored in operations OP-1.3, OP-1.4, OP-2.3 and OP-3.2. In these four operations, the suspension transmissibility becomes larger than one in the frequency range of 4-17 Hz, as shown in Fig. 7.8 (c) and (d). It means that the top end-stop impacts generate the shocks above the vertical suspension system in the frequency range of 4-17 Hz. This brings the result that the VDVRs in these operations are larger than 1.

7.2 Optimization of vertical seat suspension system

As shown in Fig. 7.6, most vibration dose value ratios (VDVRs) of the vertical seat suspension system are larger than 0.8. The VDVRs are even larger than 1 under excitations with high magnitudes due to the end-stop impacts. This means that the vibration attenuation performance of the vertical seat suspension system is poor and leaves potential for optimization.

From Fig. 7.8 it can be noticed that the vertical seat suspension system attenuates vibrations at frequencies above 2 Hz. In chapter 4 it is analyzed that the maximum root mean square (RMS) value of the vertical accelerations in 1/3 octave band at the seat base occurs in the frequency range of 2-3.15 Hz. The energy of the vertical vibration excitations is mainly distributed at frequencies above 2 Hz. It means that the stiffness of the vertical seat suspension system is low enough to attenuate the vertical vibrations. So the improvement of the vibration attenuation performance in this research work only focuses on the selection of the proper damping characteristics of the damper and the optimization of the force-deflection characteristics of the end-stop buffers.

7.2.1 Seat-dummy model

To obtain the proper damping of the damper and the optimal force-deflection characteristics of the end-stop buffers, the multi-body simulation method was used. A suitable model is needed to simulate the dynamic response of the seat-dummy system used in the laboratory seat tests. The principle to build this model is that it is not too complex and can simulate the dynamic response of the seat-dummy system with high accuracy. Furthermore, the properties of the seat components, which need

to be optimized, should be precisely built in the model, such as the force-velocity relationship of the damper and the force-deflection relationship of the end-stop buffers. Other components can be simplified in the model, such as the seat cushion, the air spring and the friction force of the suspension mechanism.

According to these principles, the vertical seat suspension system was modeled as a combination of a linear spring, an inclined damper and a Bouc-Wen force element. The top and the bottom end-stop buffers were included in the suspension model when the free stroke exceeded. The seat cushion was simplified as a combination of a linear spring and a linear damper. The dummy was modeled as a single degree of freedom (DOF) mass-spring-damper system, like its mechanical structure. The entire seat-dummy model is illustrated in Fig. 7.9. The equations of motion of this model are formulated in Eq. (7.1).

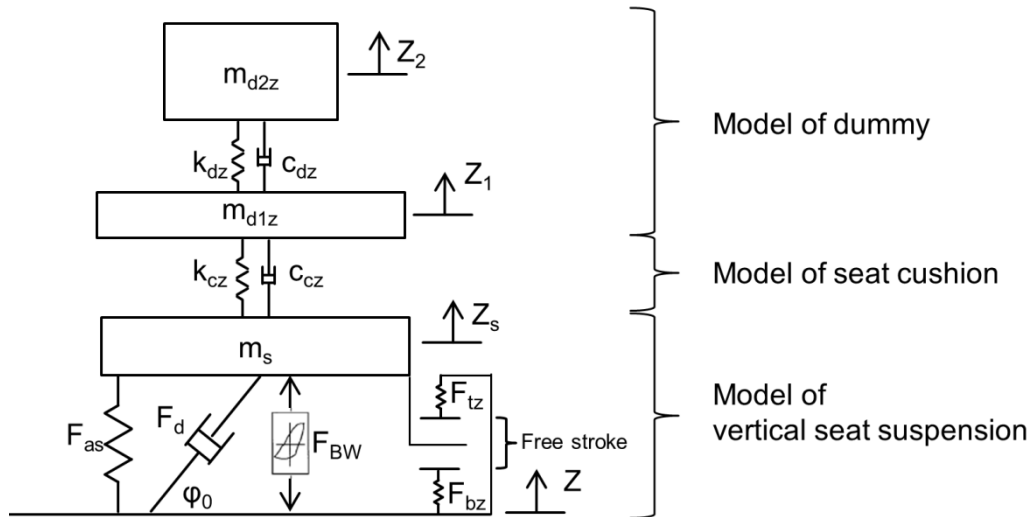


Fig. 7.9: Seat-dummy model in the vertical direction

$$\begin{cases} m_{d2z} \ddot{Z}_2 = -k_{dz} * (Z_2 - Z_1) - c_{dz} * (\dot{Z}_2 - \dot{Z}_1) \\ m_{d1z} \ddot{Z}_1 = -k_{cz} * (Z_1 - Z_s) - c_{cz} * (\dot{Z}_1 - \dot{Z}_s) + k_{dz} * (Z_2 - Z_1) + c_{dz} * (\dot{Z}_2 - \dot{Z}_1) \\ m_s \ddot{Z}_s = F_{as} + F_{dz} - F_{BW} + F_{bz} - F_{tz} + k_{cz} * (Z_1 - Z_s) + c_{cz} * (\dot{Z}_1 - \dot{Z}_s) \end{cases} \quad (7.1)$$

with

F_{BW}	Bouc-Wen force in N
F_{as}	Restoring force from the air spring in N
F_{bz}	Force coming from the bottom end-stop buffer in N
F_d	Damping force in N
F_{dz}	Vertical component of the damping force in N
F_{tz}	Force coming from the top end-stop buffer in N

Z	Absolute displacement of seat base in the z-direction in m
Z_s	Absolute displacement of m_s in the z-direction in m
\dot{Z}_s	Absolute velocity of m_s in the z-direction in m/s
\ddot{Z}_s	Absolute acceleration of m_s in the z-direction in m/s^2
Z_1	Absolute displacement of m_{d1z} in the z-direction in m
\dot{Z}_1	Absolute velocity of m_{d1z} in the z-direction in m/s
\ddot{Z}_1	Absolute acceleration of m_{d1z} in the z-direction in m/s^2
Z_2	Absolute displacement of m_{d2z} in the z-direction in m
\dot{Z}_2	Absolute velocity of m_{d2z} in the z-direction in m/s
\ddot{Z}_2	Absolute acceleration of m_{d2z} in the z-direction in m/s^2
c_{cz}	Linearized damping coefficient of the seat cushion in the z-direction in N·s/m
c_{dz}	Damping coefficient of the damper in the dummy between its lower and upper parts in N·s/m
k_{cz}	Linearized stiffness of the seat cushion in the z-direction in N/m
k_{dz}	Stiffness of springs in the dummy between its lower and upper parts in N/m
m_{d1z}	Mass of the dummy lower part in kg
m_{d2z}	Mass of the dummy upper part in kg
m_s	Mass of the seat sprung part in kg
φ_0	Angle between the damper and the horizontal direction when the seat is in the middle position in rad

The air spring was simplified as a linear spring with stiffness coefficient k_{as} . The restoring force from the air spring is formulated in Eq. (7.2). The Bouc-Wen force was used to simulate the hysteresis caused by the friction of the suspension mechanism and the damping of the air spring. It is formulated in Eq. (7.3).

$$F_{as} = -k_{as} * (Z_s - Z) \quad (7.2)$$

$$F_{BW} = (k_{BW} - k_{as}) * (\dot{Z}_s - \dot{Z}) - \gamma * \left| \dot{Z}_s - \dot{Z} \right| * F_{BW} - \beta * (\dot{Z}_s - \dot{Z}) * |F_{BW}| \quad (7.3)$$

with

\dot{Z}	Absolute velocity of seat base in the z-direction in m/s
k_{BW}	Positive stiffness of the Bouc-Wen model of hysteresis in N/m
k_{as}	Stiffness coefficient of air spring in N/m
β	Parameter of Bouc-Wen model of hysteresis in m^{-1}
γ	Parameter of Bouc-Wen model of hysteresis in m^{-1}

The passive hydraulic damper is generally designed to yield an asymmetric damping force in the compression and the extension stages. The damping force also varies with the piston velocity in a nonlinear manner. The force-velocity relationship of a passive hydraulic damper can be characterized in terms of damping coefficients at low and high speeds in the compression and the extension stages, as shown in Fig.

7.10 [133]. This force-velocity relationship can be formulated in Eq. (7.4). In the vertical seat suspension system used in this research work the damper is inclined. The vertical component of the damping force is formulated in Eq. (7.5) and Eq. (7.6).

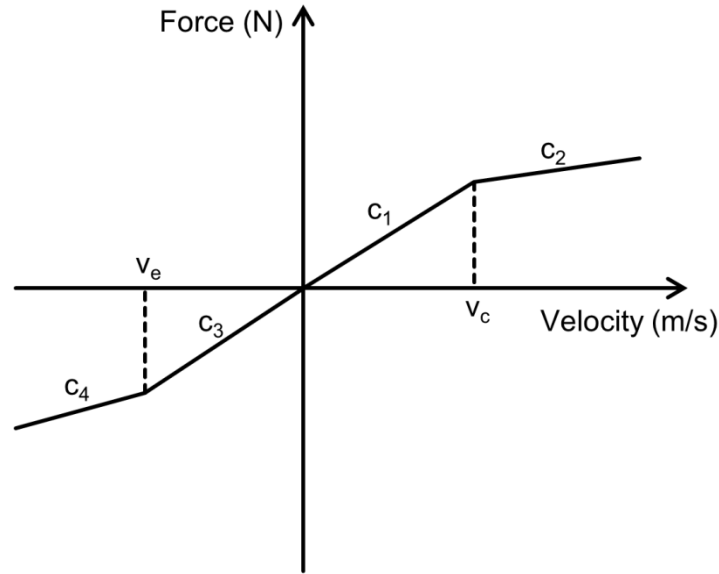


Fig. 7.10: Force-velocity curve of a passive hydraulic damper

$$F_d = \begin{cases} c_1 * (\dot{Z} - \dot{Z}_s) & 0 \leq \dot{Z} - \dot{Z}_s \leq v_c \\ c_1 * \left\{ v_c + \gamma_c * \left[(\dot{Z} - \dot{Z}_s) - v_c \right] \right\} & \dot{Z} - \dot{Z}_s > v_c \\ p * c_1 * (\dot{Z} - \dot{Z}_s) & v_e \leq \dot{Z} - \dot{Z}_s < 0 \\ p * c_1 * \left\{ v_e + \gamma_e * \left[(\dot{Z} - \dot{Z}_s) - v_e \right] \right\} & \dot{Z} - \dot{Z}_s < v_e \end{cases} \quad (7.4)$$

$$F_{dz} = \begin{cases} c_1 * (\dot{Z} - \dot{Z}_s) * \sin^2 \varphi & 0 \leq (\dot{Z} - \dot{Z}_s) * \sin \varphi \leq v_c \\ c_1 * \left\{ v_c + \gamma_c * \left[(\dot{Z} - \dot{Z}_s) * \sin \varphi - v_c \right] \right\} * \sin \varphi & (\dot{Z} - \dot{Z}_s) * \sin \varphi > v_c \\ p * c_1 * (\dot{Z} - \dot{Z}_s) * \sin^2 \varphi & v_e \leq (\dot{Z} - \dot{Z}_s) * \sin \varphi < 0 \\ p * c_1 * \left\{ v_e + \gamma_e * \left[(\dot{Z} - \dot{Z}_s) * \sin \varphi - v_e \right] \right\} * \sin \varphi & (\dot{Z} - \dot{Z}_s) * \sin \varphi < v_e \end{cases} \quad (7.5)$$

$$\varphi = \arctan \left[\tan \varphi_0 - (Z - Z_s) / l_x \right] \quad (7.6)$$

with

- c_1 Damping coefficient of the passive hydraulic damper at low speeds in the compression stage in N·s/m
- c_2 Damping coefficient of the passive hydraulic damper at high speeds in the compression stage in N·s/m

c_3	Damping coefficient of the passive hydraulic damper at low speeds in the extension stage in N·s/m
c_4	Damping coefficient of the passive hydraulic damper at high speeds in the extension stage in N·s/m
l_x	Longitudinal component of the length of the damper in m
p	Asymmetry factor, ratio of c_3 to c_1
v_c	Transition velocity of the passive hydraulic damper in the compression stage in m/s
v_e	Transition velocity of the passive hydraulic damper in the extension stage in m/s
γ_c	Damping reduction factor in the compression stage, ratio of c_2 to c_1
γ_e	Damping reduction factor in the extension stage, ratio of c_4 to c_3
φ	Angle between the damper and the horizontal direction in rad

The top and the bottom end-stop buffers were modeled as pure nonlinear springs. Force-deflection relationships of them can be formulated in polynomial expressions, as the Eq. (7.7) and Eq. (7.8).

$$F_{bz} = k_{b1} * [(Z - Z_s) - d_z] + k_{b2} * [(Z - Z_s) - d_z]^2 + k_{b3} * [(Z - Z_s) - d_z]^3 + k_{b4} * [(Z - Z_s) - d_z]^4 \quad Z - Z_s > d_z \quad (7.7)$$

$$F_{tz} = k_{t1} * [(Z_s - Z) - d_z] + k_{t2} * [(Z_s - Z) - d_z]^2 + k_{t3} * [(Z_s - Z) - d_z]^3 + k_{t4} * [(Z_s - Z) - d_z]^4 \quad Z - Z_s < -d_z \quad (7.8)$$

with

d_z	Distance between the middle position of the vertical seat suspension system and the bottom or the top end-stop buffer in m
k_{b1}	Linear stiffness coefficient of the bottom end-stop buffer in N/m
k_{b2}	Quadratic stiffness coefficient of the bottom end-stop buffer in N/m ²
k_{b3}	Cubic stiffness coefficient of the bottom end-stop buffer in N/m ³
k_{b4}	Quartic stiffness coefficient of the bottom end-stop buffer in N/m ⁴
k_{t1}	Linear stiffness coefficient of the top end-stop buffer in N/m
k_{t2}	Quadratic stiffness coefficient of the top end-stop buffer in N/m ²
k_{t3}	Cubic stiffness coefficient of the top end-stop buffer in N/m ³
k_{t4}	Quartic stiffness coefficient of the top end-stop buffer in N/m ⁴

These differential equations of motion of the seat-dummy model can be solved with the help of the ordinary differential equation solver in MATLAB named ODE45 based on the explicit Runge-Kutta method.

7.2.2 Parameter identification

Some parameters of the seat-dummy model need to be optimized in order to improve the vibration attenuation performance of the vertical seat suspension system, such as the damping coefficients of the hydraulic damper and the stiffness coefficients of the

end-stop buffers. These parameters were derived from static or dynamic tests performed in the laboratory. Other parameters were not included in the optimization, such as the stiffness and damping coefficients of the seat cushion and parameters of the Bouc-Wen force. These parameters were determined using the nonlinear curve-fitting in least-squares sense by fitting the multi-body simulation results to the corresponding measurement signals.

In order to derive the stiffness coefficient of the air spring, quasi-static force-displacement tests of the seat were carried out, when the seat cushion and the hydraulic damper were removed. The force-displacement curve over the free stroke of the vertical suspension system is illustrated in Fig. 7.11. It can be noticed that the curves in both of the compression and the extension stages are nearly linear. The stiffness coefficient of the air spring was estimated as the mean value of the gradients of the force-displacement curves in compression and extension stages. The loop enclosed by these two curves indicate the hysteresis due to the friction of the suspension mechanism and the damping of the air spring.

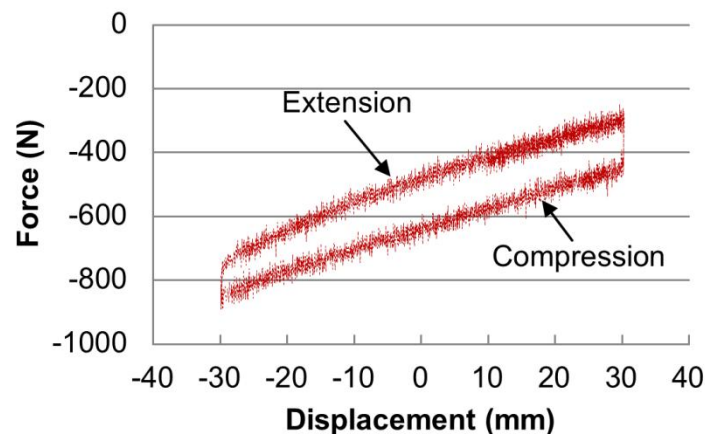


Fig. 7.11: Force-displacement curve of the air suspension seat without seat cushion and damper

The parameters of the hydraulic damper in Fig. 7.10 (p. 128) were derived from its force-velocity curve. In order to obtain the force-velocity curve, a set of dynamic force-displacement tests were performed. The damping forces were measured when the damper was excited by sinusoidal displacement signals with an amplitude of ± 12.5 mm and different frequencies in the range of 0.1-2 Hz. The force-displacement curves obtained at four excitation frequencies are taken as examples and presented in Fig. 7.12. The maximum and the minimum damping forces occur at the time when the compression or the extension velocity reaches its maximum. The maximum

velocity can be calculated from the displacement amplitude and the excitation frequency with Eq. (7.9). The force-velocity curve was obtained by analyzing the maximum and minimum forces and the maximum velocities at different frequencies of the displacement excitations.

$$v = 2 * \pi * f * d_0 \quad (7.9)$$

with

d_0	Amplitude of sinusoidal displacement excitation in m
f	Frequency of sinusoidal displacement excitation in Hz
v	Maximum velocity of the damper in m/s

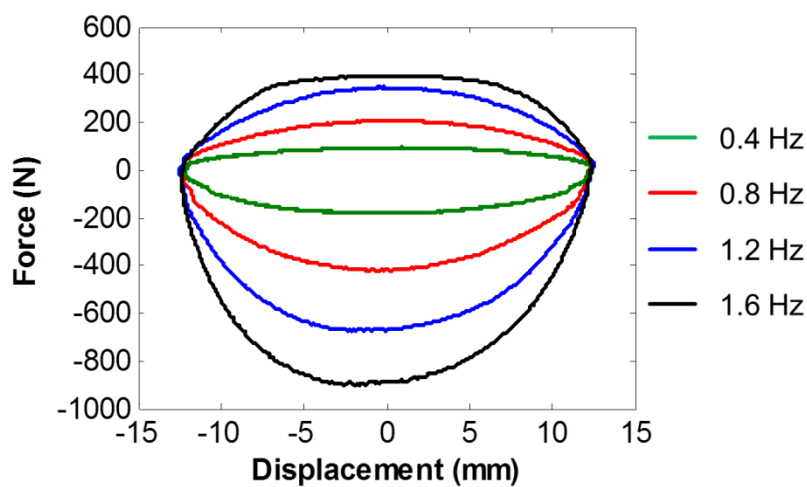


Fig. 7.12: The force-displacement curves of the damper obtained under sinusoidal displacement excitations at four frequencies

The force-deflection curves of the end-stop buffers were obtained from static force-deflection tests and are shown in Fig. 7.13. The coefficients of polynomials in Eq. (7.7) and Eq. (7.8) were determined by applying the curve fitting to the measured curves.

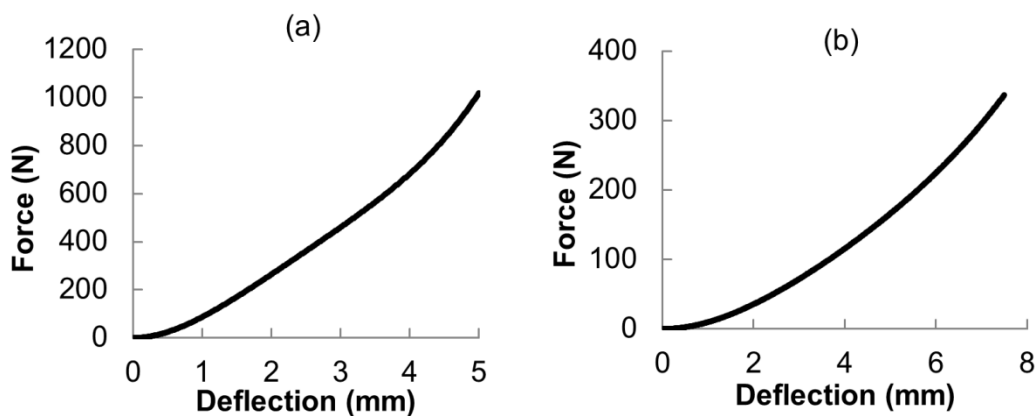


Fig. 7.13: Force-deflection curves of end-stop buffers: (a). top end-stop buffer; (b). bottom end-stop buffer

The above mentioned parameters derived from the tests are summarized in Tab. 7.1.

Tab. 7.1: Parameters of the seat-dummy model derived from static or dynamic tests

Parameters of air spring for Eq. (7.2)			
k_{as} (N/m)	6863		
Parameters of hydraulic damper for Fig. 7.10 and Eq. (7.4)			
c_1 (N·s/m)	6799	c_2 (N·s/m)	5943
c_3 (N·s/m)	3480	c_4 (N·s/m)	1427
v_c (m/s)	0.09	v_e (m/s)	-0.09
Parameters of bottom end-stop buffer for Eq. (7.7)			
k_{b1} (N/m)	$-1.41 \cdot 10^3$	k_{b3} (N/m ³)	$-2.99 \cdot 10^9$
k_{b2} (N/m ²)	$2.37 \cdot 10^7$	k_{b4} (N/m ⁴)	$1.95 \cdot 10^{11}$
Parameters of top end-stop buffer for Eq. (7.8)			
k_{t1} (N/m)	$-2.28 \cdot 10^3$	k_{t3} (N/m ³)	$-6.30 \cdot 10^{10}$
k_{t2} (N/m ²)	$2.33 \cdot 10^8$	k_{t4} (N/m ⁴)	$6.56 \cdot 10^{12}$

The parameters of the dummy model representing the seated persons with different weights are summarized in Tab. 7.2.

Tab. 7.2: Parameters of the dummy model to simulate the dynamic response of seated persons with different weights [161]

Weight of seated person: 55 kg			
m_{d1z} (kg)	13.9	k_{dz} (N/m)	42000
m_{d2z} (kg)	42.9	c_{dz} (N·s/m)	1100
Weight of seated person: 75 kg			
m_{d1z} (kg)	13.9	k_{dz} (N/m)	42000
m_{d2z} (kg)	47.9	c_{dz} (N·s/m)	1100
Weight of seated person: 98 kg			
m_{d1z} (kg)	18.9	k_{dz} (N/m)	55000
m_{d2z} (kg)	59.9	c_{dz} (N·s/m)	1100

In order to determine the parameters of the cushion model (k_{cz} and c_{cz}) using the nonlinear curve-fitting in least-squares sense, the cushion-dummy model in Fig. 7.14 was used. The input signal of this model is the accelerations of the seat sprung part, which were measured above the vertical seat suspension system by accelerometer (1) in Fig. 7.4 (p. 121). The output signal is the accelerations on the seat cushion.

To determine the parameters of the Bouc-Wen force (k_{BW} , γ and β) using the nonlinear curve-fitting in least-squares sense, the entire seat-dummy model in Fig. 7.9 (p. 126) was used. The input signal is the accelerations at the seat base, which were measured by accelerometer (2) in Fig. 7.4. The output signal is the accelerations above the vertical seat suspension system.

The parameters of the cushion model and the Bouc-Wen force were determined by minimizing the quadratic error between the fast Fourier transform (FFT) of the measured and the simulated output signals. The MATLAB function 'lsqcurvefit' was used, which searches the values for the variables of a function in a given range until the quadratic error between the reference and the calculated function values reaches the minimum.

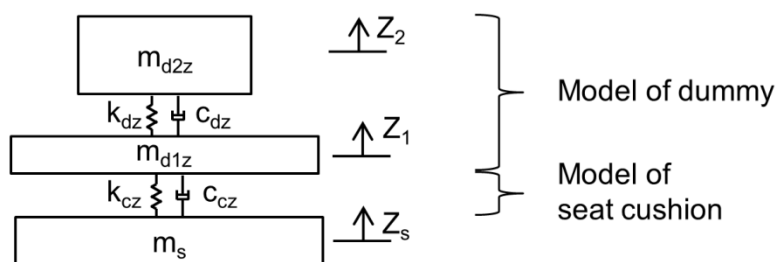


Fig. 7.14: Cushion-dummy model in the vertical direction

7.2.3 Model validation

After the parameters of the seat-dummy model were determined, the simulated signals need to be compared with the measured signals with the purpose of evaluating the quality of the model. Five operations (OP-1.1 to OP-1.4 and OP-4) were used in this chapter for the model validation and the suspension optimization, because these five operations cover almost all states of the dynamics of the suspension seat. In addition, they comprise all seven scenarios representing the daily operation of the compact wheel loader (CWL) proposed in Chapter 5. The following simulation results were compared with those from the laboratory seat tests to judge whether the model is reliable to simulate the dynamic behavior of the vertical seat suspension system:

- 1) Vibration dose value ratio (VDVR) of the vertical seat suspension system: the δ_{VDVR} , as defined by Eq. (7.10), was used to indicate the difference between the simulated VDVR and the measured VDVR.

$$\delta_{VDVR} = \frac{VDVR_s - VDVR_m}{VDVR_m} * 100\% \quad (7.10)$$

with

$VDVR_m$	VDVR obtained from the measurement
$VDVR_s$	VDVR obtained from the simulation
δ_{VDVR}	Difference between the simulated VDVR and the measured VDVR

- 2) Accelerations above the vertical seat suspension system in the time domain: the mean value of the relative errors, as defined by Eq. (7.11), can be used to give an indication of the difference between the simulated and the measured acceleration signals in the time domain.

$$\bar{\delta}_a = \frac{1}{N} \sum_{i=1}^N \left| \frac{a_s(i) - a_m(i)}{a_m(i)} \right| \quad (7.11)$$

with

$a_m(i)$	The i^{th} acceleration value obtained from the measurement in m/s^2
$a_s(i)$	The i^{th} acceleration value obtained from the simulation in m/s^2
$\bar{\delta}_a$	Mean value of the relative errors between the simulated and the measured accelerations

- 3) Power spectral density (PSD) of accelerations above the vertical seat suspension system: the mean value of the relative errors was also used here to give an indication of the difference between the PSD of the simulated and the measured accelerations. Here the mean value of the relative error is defined by Eq. (7.12).

$$\bar{\delta}_{PSD} = \frac{1}{N} \sum_{i=1}^N \left| \frac{PSD_s(i) - PSD_m(i)}{PSD_m(i)} \right| \quad (7.12)$$

with

$PSD_m(i)$	The i^{th} value on the PSD curve of the accelerations obtained from the measurement in dB/Hz
$PSD_s(i)$	The i^{th} value on the PSD curve of the accelerations obtained from the simulation in dB/Hz
$\bar{\delta}_{PSD}$	Mean value of the relative errors between the PSD curves of the simulated and the measured accelerations

- 4) Occurrence of the end-stop impacts: the mean value of the relative errors between the durations of the end-stop impacts occurring in simulations and measurements, as defined by Eq. (7.13), was used to indicate the difference between the end-stop impacts.

$$\bar{\delta}_t = \frac{1}{N} \sum_{i=1}^N \left| \frac{t_s(i) - t_m(i)}{t_m(i)} \right| \quad (7.13)$$

with

$t_m(i)$	Duration of the i^{th} end-stop impact in the measurement in s
$t_s(i)$	Duration of the i^{th} end-stop impact in the simulation in s
$\bar{\delta}_t$	Mean value of the relative errors between the durations of the simulated and the measured end-stop impacts

- 5) Acceleration peaks above the vertical seat suspension system caused by end-stop impacts: the mean value of the relative errors used here to indicate the difference between the acceleration peaks generated by end-stop impacts in simulations and measurements is defined by Eq. (7.14).

$$\bar{\delta}_{ap} = \frac{1}{N} \sum_{i=1}^N \left| \frac{a_{ps}(i) - a_{pm}(i)}{a_{pm}(i)} \right| \quad (7.14)$$

with

$a_{pm}(i)$	Acceleration peak caused by the i^{th} end-stop impact in measurements in m/s^2
$a_{ps}(i)$	Acceleration peak caused by the i^{th} end-stop impact in simulations in m/s^2
$\bar{\delta}_{ap}$	Mean value of the relative errors between the simulated and the measured acceleration peaks caused by the end-stop impacts

The simulated and the measured VDVRs are presented in Tab. 7.3. From the δ_{VDVR} values it can be observed that the differences between both VDVRs are quite small.

Tab. 7.3: VDVRs of the vertical seat suspension system obtained from simulations and measurements

	OP-1.1	OP-1.2	OP-4	OP-1.3	OP-1.4
VDVR _m	0.8198	0.8700	0.7845	1.2119	1.0754
VDVR _s	0.7801	0.8436	0.7278	1.1139	1.0115
δ_{VDVR} (%)	-4.8450	-3.0419	-7.2316	-8.0862	-5.937

The simulated and the measured accelerations above the vertical seat suspension system in the case where no end-stop impact occurs are presented in Fig. 7.15. It can be noticed that the simulated acceleration signals match very well with those obtained from measurements. The mean values of the relative errors between the simulated and the measured accelerations, the $\bar{\delta}_a$, are presented in Tab. 7.4. It can be noticed that the relative errors of the accelerations in the range of 0.5-4 Hz are very small, but for the accelerations in the range of 0.5-20 Hz are at a little higher level. This is because in the high frequency range the noise is included in the measurement signals, which is hard to be simulated.

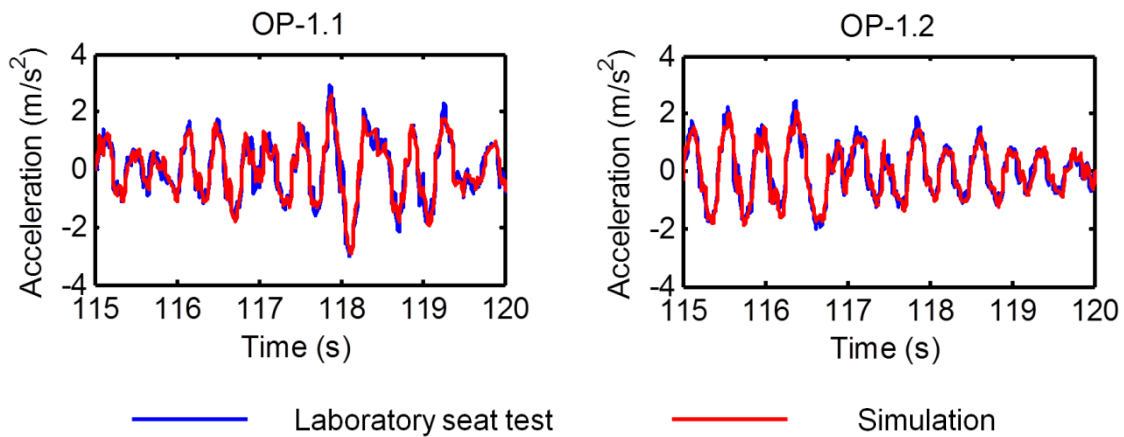


Fig. 7.15: Comparison of measured and simulated accelerations above the vertical seat suspension system in the time domain when no end-stop impact occurs

Tab. 7.4: Mean value of relative errors between measured and simulated accelerations above the vertical seat suspension system in the case where no end-stop impact occurs

$\bar{\delta}_a$	OP-1.1	OP-1.2
0.5-4 Hz	0.0946	0.0800
0.5-20 Hz	0.2723	0.2364

The simulated and the measured acceleration signals above the vertical seat suspension system in the case where end-stop impacts occur are compared in Fig. 7.16, as well as the end-stop impacts monitored in simulations and measurements. In Tab. 7.5 mean values of the relative errors of the accelerations in the time domain $\bar{\delta}_a$,

of the acceleration peaks caused by end-stop impacts $\bar{\delta}_{ap}$ and of the durations of end-stop impacts $\bar{\delta}_t$ are presented. From the values of $\bar{\delta}_a$ it can be noticed that the differences between the simulated and the measured accelerations in the low frequency range are quite small. The same conclusion can also be observed from Fig. 7.16, where the simulated accelerations match very well with those obtained from the laboratory seat tests. In Fig. 7.16 it can be observed that the occurrence of end-stop impacts is consistent in simulations and measurements. The values of $\bar{\delta}_t$ and $\bar{\delta}_{ap}$ in Tab. 7.5 also show that the differences between the characteristics of end-stop impacts obtained from simulations and measurements are insignificant.

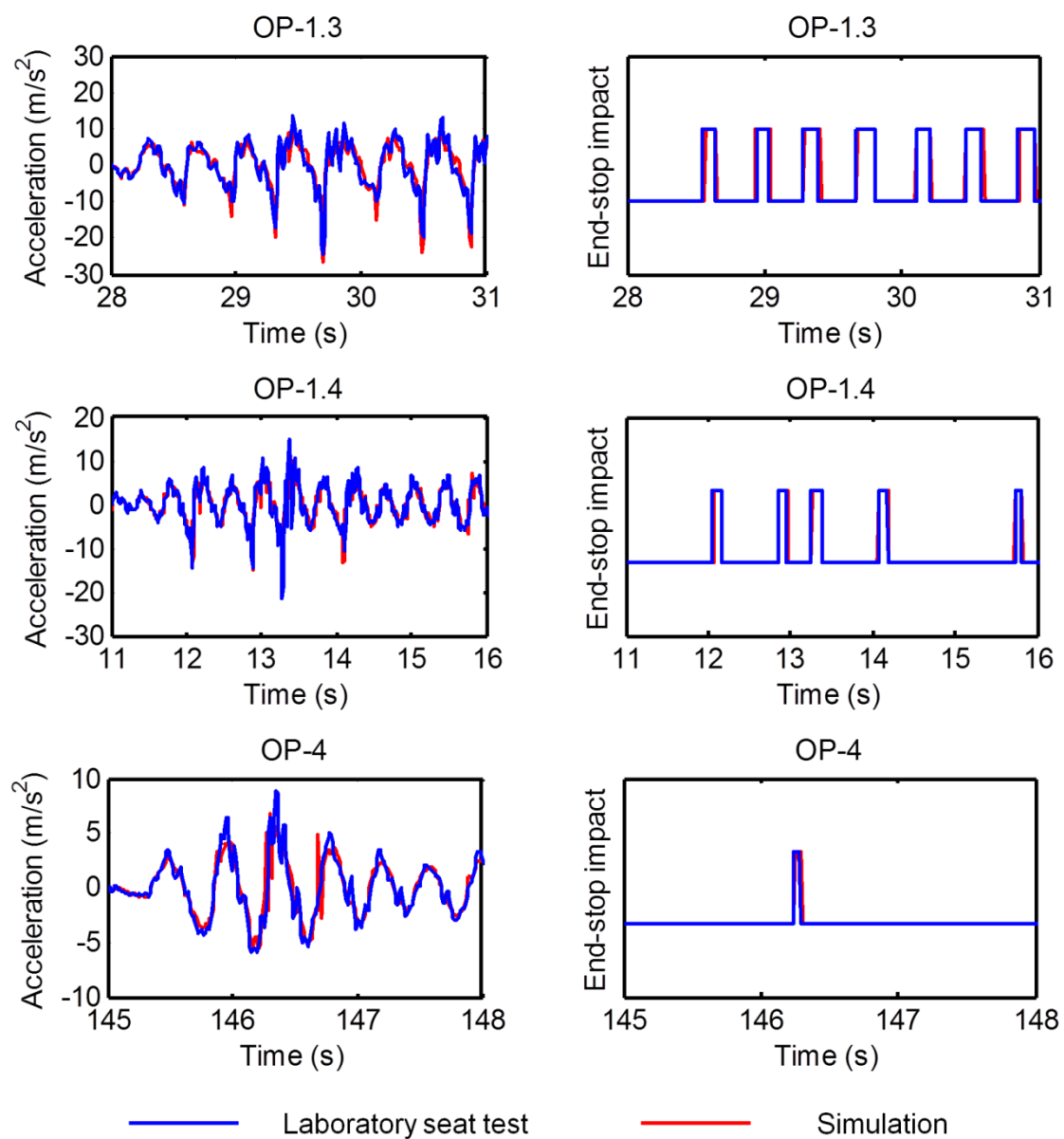


Fig. 7.16: Acceleration signals above the vertical seat suspension system in the case where end-stop occurs as well as the occurrence of end-stop impacts obtained from simulations and measurements

Tab. 7.5: Mean values of the relative errors of the accelerations above the vertical seat suspension system in the time domain, of the acceleration peaks caused by end-stop impacts and of the durations of end-stop impacts

	OP-1.3	OP-1.4	OP-4
$\bar{\delta}_a$ (0.5-4 Hz)	0.1081	0.0991	0.0991
$\bar{\delta}_a$ (0.5-20 Hz)	0.3365	0.2975	0.2666
$\bar{\delta}_{ap}$	0.0849	0.0748	0.0731
$\bar{\delta}_t$	0.0781	0.1071	0.0909

The comparison of the PSD curves of the simulated and the measured accelerations above the vertical seat suspension system is presented in Fig. 7.17. It can be observed that the differences between two PSD curves mainly occur at frequencies above 4 Hz, especially in the frequency range of 4-6 Hz. Accelerations in this range are important for the human sensitivity, but their differences in this range have a small influence on the difference of the total vibration intensity because the vibration magnitudes in this range are very small. The vibration magnitudes are quite high in the frequency range of 0.5-4 Hz, where the differences between two PSD curves are insignificant. This can also be noticed from the mean values of the relative errors between two PSD curves in the frequency range of 0.5-4 Hz in Tab. 7.6.

Tab. 7.6: Mean values of the relative errors between the PSD of the accelerations above the vertical seat suspension system in the frequency range of 0.5-4 Hz

	OP-1.1	OP-1.2	OP-4	OP-1.3	OP-1.4
$\bar{\delta}_{PSD}$ (0.5-4 Hz)	0.0556	0.0610	0.0869	0.1091	0.1330

The differences between the simulated and the measured signals are caused by the simplification of the seat-dummy model, such as the linearization of the seat cushion model. From the comparison presented in Tab. 7.3 to Tab. 7.6 and in Fig. 7.15 to Fig. 7.17, it can be concluded that the differences between the simulated and the measured accelerations are not large, especially in the frequency range of 0.5-4 Hz.

The seat-dummy model is acceptable to simulate the dynamic behavior of the vertical seat suspension system.

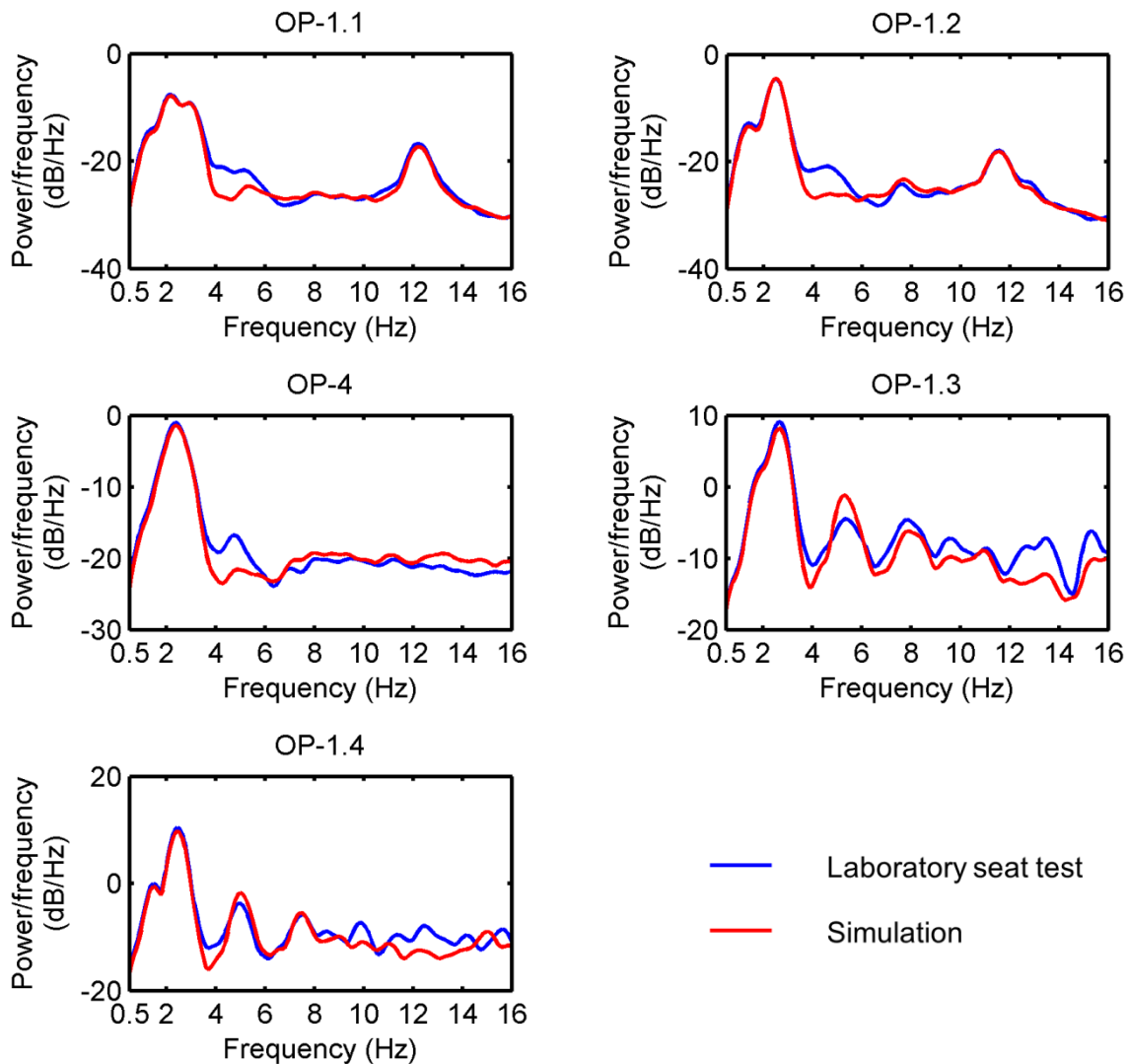


Fig. 7.17: Comparison of PSD curves of measured and simulated accelerations above the vertical seat suspension system

7.2.4 Suspension system optimization

The seat suspension system has different damping requirements under excitations with different magnitudes [133]. A low damping is desirable to improve the vibration attenuation performance under excitations with low or moderate magnitudes. But a high damping is required to reduce the occurrence and the severity of end-stop impacts under excitations with high magnitudes. For a seat exposed to various levels of vibrations, a compromise should be reached between the improvement of vibration attenuation performance under excitations with low or moderate magnitudes and the reduction of occurrence and severity of end-stop impacts under excitations with high

magnitudes. This compromise can be achieved by selecting proper damping coefficients of the passive damper and optimizing the force-deflection characteristics of end-stop buffers in a passive seat suspension system.

Another method to reach this compromise is employing a semi-active damper controlled by a 'soft-hard' policy (Eq. (2.41), p. 54) to replace the passive damper. This compromise can be achieved by selecting proper damping coefficients of the semi-active damper in the soft-state and the hard-state.

7.2.4.1 Optimization of passive vertical seat suspension system

The optimization of the passive vertical seat suspension system was carried out in the following two steps:

- 1) Under excitations with moderate magnitudes, the damping coefficients of the passive damper were optimized to minimize the vibration dose value ratio (VDVR) of the vertical seat suspension system. It was supposed that end-stop impact does not occur under these excitations. In other words, in the optimization the suspension travel was constrained to the free stroke. The objective function in this step can be expressed by Eq. (7.15).

$$\begin{cases} U(\chi) = \min(\text{VDVR}) & |Z_s - Z| \leq d_z \\ \chi = [c_1 \quad c_2 \quad c_3 \quad c_4] \end{cases} \quad (7.15)$$

with

$U(\chi)$	Objective function of the optimization
χ	Vector of parameters to be optimized
c_i	Damping coefficients refer to Fig. 7.10 (p. 128)

If the excitation magnitude is quite low, such as the vibration excitations measured in operations OP-1.1 and OP-1.2, small damping coefficients are required to satisfy Eq. (7.15). They bring the result that end-stop impacts occur frequently and severely under excitations with high magnitudes, for example, under the vibration excitations measured in operations OP-1.3 and OP-1.4. In these operations, large damping coefficients are required to satisfy Eq. (7.15). They result in the deterioration of the suspension vibration attenuation performance under excitations with low magnitudes.

In order to reach the compromise between better suspension vibration attenuation performance under excitations with low magnitudes and less and

gentler end-stop impacts under excitations with high magnitudes, the optimal damping coefficients should be determined under an excitation with moderate magnitudes. The vibration excitation measured in the operation OP-4 seems to be suitable for the optimization in this step.

- 2) With the optimal damping coefficients determined in step 1), end-stop impacts occur under excitations with high magnitudes. In this case, the force-deflection characteristics of the end-stop buffers should be optimized to minimize the VDVR of the vertical seat suspension system. In this step, the suspension travel was constrained to the maximum stroke, which is the total suspension travel when top and bottom end-stop buffers are compressed completely. It is the sum of suspension free stroke and maximum compression deflections of end-stop buffers. The objective function in this step can be expressed by Eq. (7.16).

$$\begin{cases} U(\chi) = \min(\text{VDVR}) & |Z_s - Z| \leq d_{mz} \\ \chi = [k_{t1} \quad k_{t2} \quad k_{t3} \quad k_{t4} \quad k_{b1} \quad k_{b2} \quad k_{b3} \quad k_{b4}] \end{cases} \quad (7.16)$$

with

d_{mz} Maximum stroke of the vertical seat suspension system in m
 k_{ti}, k_{bi} stiffness coefficients refer to Eq. (7.7) and Eq. (7.8) (p. 129)

Due to the requirement of operational safety and the limited space in the cabin on construction vehicles, the maximum stroke of the vertical seat suspension system is generally designed in a small range. In this study, it was set to ± 50 mm. The influence of the suspension free stroke (or the maximum compression deflections of the end-stop buffers) on the suspension vibration attenuation performance was also studied. The optimization of the passive seat suspension system was carried out when the free stroke was set to ± 30 mm, ± 35 mm, ± 40 mm and ± 45 mm respectively. Accordingly, the maximum compression deflections of the top and the bottom end-stop buffers are 20 mm, 15 mm, 10 mm and 5 mm. The MATLAB function 'fmincon' was used to determine the optimal damping coefficients of the damper. With this function the values of variables can be found out for the minimum of a nonlinear multivariable function. The vibration excitations measured in operations OP-1.1, OP-1.2, OP-1.3, OP-1.4 and OP-4 were used in the optimization, because these operations comprise the scenarios proposed in chapter 5, and the suspension

dynamics in these operations distributes in different states. The optimization results in the first step are presented in Tab. 7.7.

Tab. 7.7: Optimal damping coefficients of the vertical seat suspension system with different free strokes determined under the excitation in the operation OP-4

Free stroke (mm)	Optimal damping coefficients (N·s/m)			
	c_1	c_2	c_3	c_4
± 30	1345.7	5217.3	2366.1	4023.9
± 35	748	3537	1346	3526
± 40	600	2243	740	3033
± 45	600	1062	600	2304

In Tab. 7.7, it can be observed that the optimal damping coefficients decrease with the increase of the suspension free stroke. This is because smaller damping coefficients are required to satisfy Eq. (7.15) when the free stroke is larger. The VDVRs of the vertical seat suspension system with these four groups of optimal damping coefficients are presented in Tab. 7.8. End-stop impacts occurred only under excitations in operations OP-1.3 and OP-1.4. The times of end-stop impact under these two excitations are presented in Tab. 7.9.

Tab. 7.8: VDVRs of the vertical seat suspension system with four groups of optimal damping coefficients under different excitations

Free stroke (mm)	VDVR				
	OP-1.1	OP-1.2	OP-4	OP-1.3	OP-1.4
± 30	0.7247	0.7753	0.5601	0.8220	0.7366
± 35	0.7303	0.7748	0.5107	1.1186	0.7792
± 40	0.7379	0.7765	0.4781	1.2206	0.9631
± 45	0.7360	0.7745	0.4592	1.4353	1.3395
Original suspension	0.7801	0.8436	0.7278	1.1139	1.0115

Tab. 7.9: Times of end-stop impact with four groups of optimal damping coefficients under excitations in operations OP-1.3 and OP-1.4

Free stroke (mm)	Times of end-stop impact			
	OP-1.3		OP-1.4	
	Top	Bottom	Top	Bottom
± 30	8	13	10	18
± 35	4	11	5	15
± 40	3	10	4	13
± 45	2	10	2	15

As shown in Tab. 7.8, compared to the VDVR of the original vertical seat suspension system, the VDVRs of the vertical seat suspension system with the optimal damping coefficients decrease largely under the excitation in the operation OP-4. Under this excitation, there is a little decrease of the VDVR with the increase of the free stroke. This is due to the fact that the optimal damping coefficients are smaller when the free stroke is larger.

Under excitations in operations OP-1.1 and OP-1.2, the optimal damping coefficients result in a small decrease of the VDVR. Under these two excitations, the suspension free stroke has a negligible influence on the variation of the VDVR.

Under excitations in operations OP-1.3 and OP-1.4, the optimal damping coefficients lead to the increase of the VDVR in some cases. This is because the optimized damper is softer than the original one and it causes severer end-stop impacts. The free stroke has a large influence on the VDVR under these two excitations. The VDVRs increase with the increase of the suspension free stroke. This is because the optimal damping coefficients are smaller when the free stroke is larger and a softer damper results in severer end-stop impacts.

In Tab. 7.9, it can be observed that the times of end-stop impact increase with the decrease of the free stroke. This is due to the fact that the suspension travel exceeds the free stroke more easily if the free stroke is smaller. It can also be noticed that bottom end-stop impacts occur more frequently than top end-stop impacts. This is because the optimal damping coefficients in the extension stage are larger than

those in the compression stage. In order to solve this problem, it was proposed that the damper should have the same force-velocity relationship in the extension and the compression stages. It means that the damping coefficient c_1 should be equal to c_3 , and c_2 should be equal to c_4 . Based on this proposal, damping coefficients of the damper were optimized again. The optimal damping coefficients of the vertical seat suspension system with different free strokes are presented in Tab. 7.10.

The VDVRs of the vertical seat suspension system with these four groups of optimal damping coefficients and the occurrence of end-stop impacts under different excitations were recalculated and are presented in Tab. 7.11 and Tab. 7.12 respectively.

Tab. 7.10: Optimal damping coefficients of the vertical seat suspension system with different free strokes determined under the excitation in the operation OP-4.

Free stroke (mm)	Optimal damping coefficients (N-s/m)	
	$c_1 = c_3$	$c_2 = c_4$
± 30	1627	5748.4
± 35	1048.6	4110
± 40	687.3	3139
± 45	600	2328.4

Tab. 7.11: VDVRs of the vertical seat suspension system with the optimal damping coefficients in Tab. 7.10 under different excitations

Free stroke (mm)	VDVR				
	OP-1.1	OP-1.2	OP-4	OP-1.3	OP-1.4
± 30	0.7265	0.7798	0.5859	0.7418	0.7869
± 35	0.7328	0.7813	0.5322	0.7855	0.6504
± 40	0.7410	0.7821	0.4965	0.7253	0.6004
± 45	0.7375	0.7777	0.4711	0.7408	0.5243
Original suspension	0.7801	0.8436	0.7278	1.1139	1.0115

Tab. 7.12: Times of end-stop impact with the optimal damping coefficients in Tab. 7.10 under excitations in operations OP-1.3 and OP-1.4

Free stroke (mm)	Times of end-stop impact			
	OP-1.3		OP-1.4	
	Top	Bottom	Top	Bottom
± 30	6	7	9	9
± 35	3	7	5	5
± 40	2	3	5	3
± 45	2	3	3	1

Under the excitations in operations OP-1.1 and OP-1.2, the differences between the VDVRs in Tab. 7.11 and Tab. 7.8 are very small. Under the excitation in the operation OP-4, VDVRs in Tab. 7.11 are a little larger than those in Tab. 7.8. This is because the damper with damping coefficients in Tab. 7.10 is harder than that with damping coefficients in Tab. 7.7. Under the excitations in operations OP-1.3 and OP-1.4, the VDVRs in Tab. 7.11 are much smaller than those in Tab. 7.8. Comparing the times of end-stop impact in Tab. 7.12 and Tab. 7.9, less bottom end-stop impacts occur with the damping coefficients in Tab. 7.10 than with the damping coefficients in Tab. 7.7. This leads to the smaller VDVRs in Tab. 7.11 than in Tab. 7.8 under excitations in operations OP-1.3 and OP-1.4.

In the next step, the force-deflection characteristics of the end-stop buffers were optimized. It was supposed that the bottom end-stop buffer has the same force-deflection characteristics as the top end-stop buffer. It was also supposed that the optimal force-deflection curve of the end-stop buffers is comprised of a linear part and a cubic nonlinear part, which means that the parameters k_{t2} , k_{t4} , k_{b2} and k_{b4} are zero. The parameters needed to be optimized are k_{t1} , k_{t3} , k_{b1} and k_{b3} and the optimization results are presented in Tab. 7.13. Because the damping coefficients obtained in step 1) for the free stroke of ± 30 mm is large enough, with this free stroke the suspension travel does not exceed the maximum stroke of ± 50 mm under all excitations, even when there is no end-stop buffer.

Tab. 7.13: Optimal linear and cubic stiffness coefficients of end-stop buffers for suspension with different free strokes

Free stroke (mm)	$k_{t1} = k_{b1}$ (N/m)	$k_{t3} = k_{b3}$ (N/m³)
± 35	100	$9 \cdot 10^7$
± 40	$5 \cdot 10^4$	$1 \cdot 10^8$
± 45	$9.1 \cdot 10^5$	$1 \cdot 10^9$

In Tab. 7.13, the linear and cubic stiffness coefficients of the end-stop buffers largely increase with the suspension free stroke. Because the suspension maximum stroke is constant, the larger free stroke means that the maximum compression deflection of the end-stop buffers has to be smaller. On the other hand, the optimal damping coefficients of the damper are smaller when the free stroke is larger, as shown in Tab. 7.10. Therefore, when the free stroke is larger, the end-stop buffers should be stiffer to avoid the suspension travel exceeding its maximum stroke.

The VDVRs of the vertical seat suspension system with the optimal damping coefficients in Tab. 7.10 and the optimal force-deflection characteristics of end-stop buffers in Tab. 7.13 are presented in Tab. 7.14.

Tab. 7.14: VDVRs of vertical seat suspension system with the optimized passive damper and end-stop buffers under all five excitations

Free stroke (mm)	VDVR				
	OP-1.1	OP-1.2	OP-4	OP-1.3	OP-1.4
± 30	0.7265	0.7798	0.5859	0.6854	0.6909
± 35	0.7328	0.7813	0.5322	0.6035	0.6032
± 40	0.7410	0.7821	0.4965	0.6737	0.5596
± 45	0.7375	0.7777	0.4711	0.8995	0.6491
Original suspension	0.7801	0.8436	0.7278	1.1139	1.0115

The end-stop impacts only occur under the excitations in operations OP-1.3 and OP-1.4, where the optimized end-stop buffers cause the VDVRs in Tab. 7.14 different from those in Tab. 7.11 with the original buffers. In these two operations, for the suspension free strokes smaller than ± 45 mm, the VDVRs in Tab. 7.14 are lower than those in Tab. 7.11. This is because with these free strokes, the optimized end-stop buffers are softer than the original ones. This leads to gentler end-stop impacts.

When the suspension free stroke is set to ± 45 mm, the VDVRs in Tab. 7.14 are larger than those in Tab. 7.11. This is because the optimized end-stop buffers are stiffer than the original ones in order to avoid the suspension travel exceeding the maximum stroke. The stiffer optimized end-stop buffers lead to severer end-stop impacts.

The VDVRs Tab. 7.14 show that the optimized passive vertical seat suspension system has the best vibration attenuation performance when the free stroke is set to a value between ± 35 mm and ± 40 mm.

7.2.4.2 Optimization of semi-active vertical seat suspension system

For the seat suspension system with a semi-active damper controlled by the “soft-hard” policy defined by Eq. (2.41) (p. 54), the free stroke is defined as the maximum suspension travel with the damper in the soft-state. The vertical component of the damping force is formulated in Eq. (7.17). Under excitations with low or moderate magnitudes, the suspension travel does not exceed the free stroke and the damper is always in the soft-state. In this case, it generates a small damping force. Under excitations with high magnitudes, the suspension travel exceeds the free stroke. In this case, the damper has to be in the hard-state and generates a large damping force to avoid the suspension travel exceeding the maximum stroke.

$$F_{dz} = \begin{cases} c_{soft} * (\dot{Z} - \dot{Z}_s) * \sin^2 \varphi & |Z_s - Z| \leq d_{soft} \\ c_{hard} * (\dot{Z} - \dot{Z}_s) * \sin^2 \varphi & d_{soft} < |Z_s - Z| \leq d_{mz} \end{cases} \quad (7.17)$$

with

c_{soft}	Damping coefficient of the semi-active damper in the soft-state in N·s/m
c_{hard}	Damping coefficient of the semi-active damper in the hard-state in N·s/m
d_{soft}	Maximum suspension travel when the semi-active damper in the soft-state in m

The optimization of the semi-active vertical seat suspension system was also carried out in two steps, which are described as follows:

- 1) Under an excitation with moderate magnitudes, the damping coefficient in the soft-state of the semi-active damper was optimized to minimize the vibration dose value ratio (VDVR) of the vertical seat suspension system. The suspension travel was constrained to the free stroke. The objective function in this step is formulated in Eq. (7.18). Equal to the first step of the passive seat suspension optimization, the vibration excitation in the operation OP-4 was selected to determine the optimal damping coefficient in the soft-state in this step.

$$U(c_{soft}) = \min(\text{VDVR}) \quad |Z_s - Z| \leq d_{soft} \quad (7.18)$$

- 2) With the optimal damping coefficient in the soft-state determined in step 1), the suspension travel exceeds the free stroke under excitations with high magnitudes, for example, under excitations in operations OP-1.3 and OP-1.4. In this case, the semi-active damper is in the hard-state. The damping coefficient in this state then was optimized not only to achieve a minimum VDVR, but also to avoid the suspension travel exceeding the maximum stroke. The objective function in this step can be expressed by Eq. (7.19). Excitations in operations OP-1.3 and OP-1.4 were used to optimize the damping coefficient in the hard-state. The larger damping coefficient was selected as the optimal one of the semi-active damper in this state.

$$U(c_{hard}) = \min(\text{VDVR}) \quad |Z_s - Z| \leq d_{mz} \quad (7.19)$$

Equal to the passive vertical seat suspension system, the maximum stroke of the semi-active vertical seat suspension system was also set to ± 50 mm, and the optimization was carried out when the free stroke was set to ± 30 mm, ± 35 mm, ± 40 mm and ± 45 mm. The MATLAB function 'fmincon' was also used here to determine the optimal damping coefficients of the semi-active damper. The optimal damping coefficients determined for the suspension system with different free strokes are presented in Tab. 7.15.

The optimal damping coefficients in the soft-state decrease with the increase of the suspension free stroke. This is due to the fact that a smaller damping coefficient is required to satisfy Eq. (7.18) when the suspension free stroke is larger. The optimal damping coefficients in the hard-state increase largely with the suspension free

stroke from ± 35 mm. This is because the damping coefficient in the soft-state and the available suspension travel in the hard-state are smaller when the suspension has a larger free stroke.

Tab. 7.15: Optimal damping coefficients of the semi-active damper determined for the vertical seat suspension system with different free strokes

Free stroke (mm)	Optimal damping coefficients (N-s/m)	
	C_{soft}	C_{hard}
± 30	3375	4222.4
± 35	2610	3719.2
± 40	2055.8	11623
± 45	1627.9	46851

The VDVRs of the vertical seat suspension system with the optimal damping coefficients in Tab. 7.15 and different free strokes are presented in Tab. 7.16.

Tab. 7.16: VDVRs of the vertical seat suspension system with different free strokes and optimized semi-active damper under different excitations

Free stroke (mm)	VDVR				
	OP-1.1	OP-1.2	OP-4	OP-1.3	OP-1.4
± 30	0.7315	0.7905	0.6100	0.5415	0.5929
± 35	0.7234	0.7768	0.5689	0.4814	0.5271
± 40	0.7203	0.7693	0.5365	0.6023	0.5852
± 45	0.7205	0.7636	0.5103	0.9211	0.7491
Original suspension	0.7801	0.8436	0.7278	1.1139	1.0115

As shown in Tab. 7.16, the VDVRs increase with the decrease of the suspension free stroke under excitations in operations OP-1.1, OP-1.2 and OP-4. Under these excitations the semi-active damper is always in the soft-state, where the optimal damping coefficient increases with the decrease of the suspension free stroke, as shown in Tab. 7.15. This leads to the increase of the suspension VDVR.

Under excitations in operations OP-1.3 and OP-1.4, the minimum VDVR occurs when the suspension free stroke is set to ± 35 mm. The VDVR of the suspension system with free stroke of ± 30 mm is larger than that with free stroke of ± 35 mm, because the optimal damping coefficients are larger when the free stroke is ± 30 mm. Under these two excitations, as the free stroke increases from ± 35 mm to ± 45 mm, the VDVRs increase significantly. This is because the damping coefficient in the hard-state is much larger than that in the soft-state when the free stroke exceeds ± 40 mm. In this case, when the suspension travel exceeds the free stroke, the damping force becomes very large abruptly. The large difference between the damping forces in the hard-state and the soft-state leads to vibration shocks and causes the increase of the suspension VDVR.

From the VDVRs in Tab. 7.16 it can be concluded that the optimized semi-active vertical seat suspension system has the best vibration attenuation performance when the free stroke is set to ± 35 mm.

7.2.4.3 Comparison of optimized passive and semi-active vertical seat suspensions

In section 7.2.4.1 it is concluded that for the optimized passive seat suspension system, the vibration attenuation performance is best when the free stroke is set to a value in the range from ± 35 mm to ± 40 mm. In section 7.2.4.2 it is concluded that for the optimized semi-active seat suspension system, the vibration attenuation performance is best when the free stroke is set to ± 35 mm. By comparing the VDVRs with these three configurations in Tab. 7.14 and Tab. 7.16, it can be noticed that the passive suspension system has a better vibration attenuation performance than the semi-active one under the excitation in the operation OP-4. But the latter has a much better vibration attenuation performance than the former under excitations in operations OP-1.3 and OP-1.4, and a little better performance under excitations in operations OP-1.1 and OP-1.2. Considering the improvement of the vibration attenuation performance of the vertical seat suspension system in all operations, the optimized semi-active seat suspension system with free stroke of

± 35 mm is selected as the vertical seat suspension system with the best performance. The VDVRs of the optimal vertical seat suspension system are compared with those of the original one in Tab. 7.17.

Tab. 7.17: Comparison of VDVRs of the original and the optimal vertical seat suspension systems

	OP-1.1	OP-1.2	OP-4	OP-1.3	OP-1.4
VDVR _{original}	0.7801	0.8436	0.7278	1.1139	1.0115
VDVR _{optimal}	0.7234	0.7768	0.5689	0.4814	0.5271
Δ (%)	-7.27	-7.92	-21.83	-56.78	-47.89

With the optimal suspension configuration, the VDVR of the vertical seat suspension system is reduced by about 7.5% under excitations in operations OP-1.1 and OP-1.2, by about 20% under the excitation in the operation OP-4, and by about 50% under excitations in operations OP-1.3 and OP-1.4. It can be concluded that the original vertical seat suspension system bears a big potential of optimization.

7.3 Optimization of longitudinal seat suspension system

7.3.1 Seat-driver model

The investigation of the dynamics of the seat-driver system in the longitudinal direction was rather poor in the previous studies in literatures, as well as the improvement of vibration attenuation performance in this direction. Also only simple human models were used to simulate the human inline biodynamic response in the longitudinal direction. Some studies show that the human cross-axial biodynamic response is also significant [61],[62],[64],[65]. In this research work, it was observed that the vertical excitations have a large influence on the longitudinal dynamic response of the seat-driver system. The coherence between the input and the output signals of a system, formulated in Eq. (7.20), was used to study the relationship between the vertical/longitudinal vibration excitations and the longitudinal dynamic response of the seat-driver system.

$$\gamma_{io}(f) = \frac{|G_{io}(f)|^2}{G_{ii}(f) \cdot G_{oo}(f)} \quad (7.20)$$

with

$G_{oo}(f)$ Power spectral density (PSD) of the output signal as a function of frequency
 $\gamma_{io}(f)$ Coherence between the input and the output signals as a function of frequency

The longitudinal accelerations on the seat cushion were selected as the output signal of the seat-driver system in the longitudinal direction. This signal is affected not only by the dynamic characteristics of the seat cushion but also by the dynamic response of the driver. Taking only the human inline biodynamic response in the longitudinal direction into consideration, for the seat-driver system, the excitation signal is the longitudinal accelerations at the seat base. Taking the operation OP-1.2 as an example, the coherence between the longitudinal accelerations at the seat base and on the seat cushion is presented in Fig. 7.18. Here the coherence is quite high in the frequency range of 0.5-2 Hz and becomes rather low at frequencies higher than 2 Hz. It means that the longitudinal excitations at the seat base have a large influence on the dynamic response of the seat-driver system in the longitudinal direction in the low frequency range of 0.5-2 Hz.

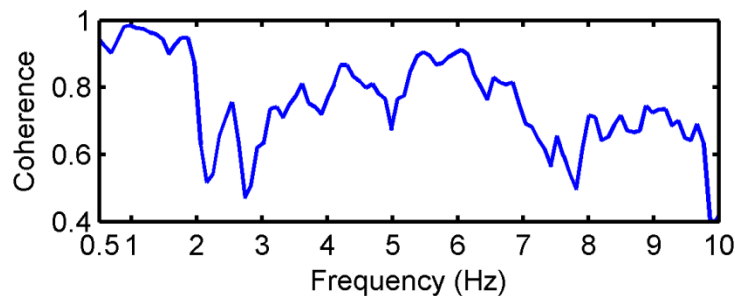


Fig. 7.18: Coherence between the longitudinal accelerations at the seat base and on the seat cushion in the operation OP-1.2

Taking only the human cross-axial biodynamic response (longitudinal response to vertical excitations) into consideration, the excitation signal for the human is the vertical accelerations on the seat cushion. Taking the operation OP-1.2 as an example as well, the coherence between the vertical and the longitudinal accelerations on the seat cushion is presented in Fig. 7.19. Here the coherence is quite high in the frequency range from 2 Hz to 3 Hz and pretty low at frequencies out of this range. It means that the vertical excitations on the seat cushion have a large influence on the dynamic response of the seat-driver system in the longitudinal

direction in the frequency range from 2 Hz to 3 Hz due to the human cross-axial biodynamic response.

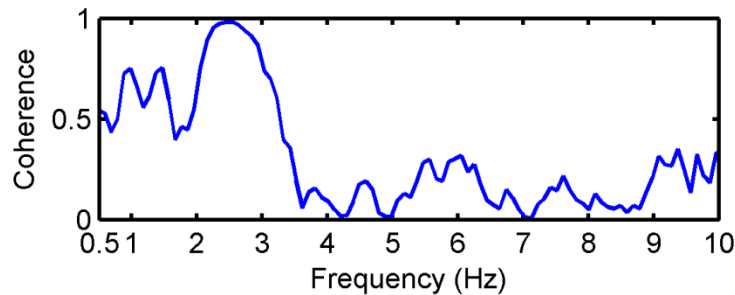


Fig. 7.19: Coherence between the vertical and the longitudinal accelerations on the seat cushion in the operation OP-1.2

In summary, the dynamic response of the seat-driver system in the longitudinal direction is affected not only by the longitudinal excitations but also by the vertical excitations. It means that the simple human models, which only simulate the human inline biodynamic response in the longitudinal direction, are insufficient to simulate the biodynamic response of the human exposed to both the longitudinal and the vertical vibrations. The cushion-seated person model developed by Nawayseh and Griffin [81], as shown in Fig. 7.20, was validated to simulate the vertical and the longitudinal dynamic response of the cushion-seated person system under vertical excitations. This model was adopted in this research work as the seat-driver model in the longitudinal direction without a longitudinal seat suspension system. The equations of motion of this model are formulated in Eq. (7.21).

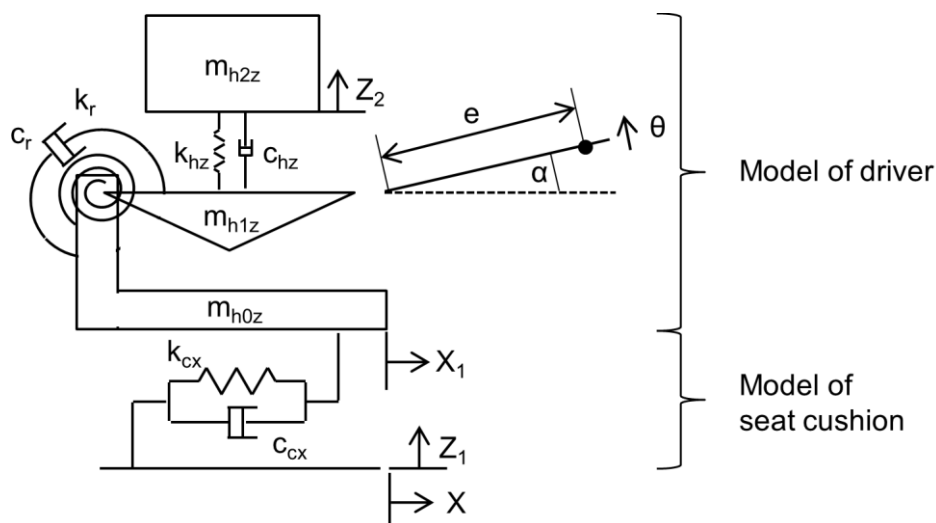


Fig. 7.20: Seat-driver model in the longitudinal direction without a longitudinal seat suspension system [81]

$$\left\{ \begin{array}{l} m_{h2z} \ddot{Z}_2 = -k_{hz} * [Z_2 - (Z_1 + e * \theta * \cos \alpha)] - c_{hz} * [\dot{Z}_2 - (\dot{Z}_1 + e * \dot{\theta} * \cos \alpha)] \\ J \ddot{\theta} = k_{hz} * [Z_2 - (Z_1 + e * \theta * \cos \alpha)] * e * \cos \alpha \\ \quad + c_{hz} * [\dot{Z}_2 - (\dot{Z}_1 + e * \dot{\theta} * \cos \alpha)] * e * \cos \alpha \\ \quad + m_{h1z} * \ddot{X}_1 * e * \sin \alpha - m_{h1z} * \ddot{Z}_1 * e * \cos \alpha - k_r * \theta - c_r * \dot{\theta} \\ (m_{h2z} + m_{h1z} + m_{h0z}) \ddot{X}_1 - m_{h1z} * e * \ddot{\theta} * \sin \alpha = -k_{cx} * (X_1 - X) - c_{cx} * (\dot{X}_1 - \dot{X}) \end{array} \right. \quad (7.21)$$

with

J	Moment of inertia of m_{h1z} about the connection point in $\text{kg}\cdot\text{m}^2$
X	Absolute displacement of the seat base in the x-direction in m
\dot{X}	Absolute velocity of the seat base in the x-direction in m/s
\ddot{X}	Absolute acceleration of the seat base in the x-direction in m/s^2
X_1	Absolute displacement of m_{h0z} in the x-direction in m
\dot{X}_1	Absolute velocity of m_{h0z} in the x-direction in m/s
\ddot{X}_1	Absolute acceleration of m_{h0z} in the x-direction in m/s^2
Z_1	Absolute displacement of m_{h0z} in the z-direction in m
\dot{Z}_1	Absolute velocity of m_{h0z} in the z-direction in m/s
\ddot{Z}_1	Absolute acceleration of m_{h0z} in the z-direction in m/s^2
c_{cx}	Linearized damping coefficient of seat cushion in the x-direction in $\text{N}\cdot\text{s}/\text{m}$
c_{hz}	Equivalent damping coefficient of the driver model in the z-direction in $\text{N}\cdot\text{s}/\text{m}$
c_r	Rotational damping coefficient between m_{h1z} and m_{h0z} in $\text{N}\cdot\text{s}\cdot\text{m}$
e	Distance between the center of gravity of m_{h1z} and the connection point in m
k_{cx}	Linearized stiffness coefficient of seat cushion in the x-direction in N/m
k_{hz}	Equivalent stiffness coefficient of the driver model in the z-direction in N/m
k_r	Rotational stiffness coefficient between m_{h1z} and m_{h0z} in $\text{N}\cdot\text{m}$
m_{h0z}	Mass of component converting the excitations in the vertical direction to the response in the longitudinal direction in kg
m_{h1z}	Equivalent mass of the lower part of a seated person in kg
m_{h2z}	Equivalent mass of the upper part of a seated person in kg
α	Angle that e has with the horizontal when the model is in equilibrium in rad
θ	Angle of rotation of m_{h1z} in rad
$\dot{\theta}$	Rotational velocity of m_{h1z} in rad/s
$\ddot{\theta}$	Rotational acceleration of m_{h1z} in rad/s^2

7.3.2 Parameter identification

The human cross-axial biodynamic response is affected by the human physical characteristics and the vibration excitations. As two principal parameters in the seat-driver model determining the human cross-axial biodynamic response, the rotational stiffness coefficient k_r and the rotational damping coefficient c_r are affected by the human physical characteristics and the vibration excitations. In the seat-driver model

in the longitudinal direction, the seat cushion was simplified as a linear spring-damper element. It is difficult to obtain the linearized stiffness coefficient k_{cx} and damping coefficient c_{cx} of the seat cushion from laboratory tests. Therefore, the nonlinear curve-fitting in least-squares sense was used to identify the above mentioned four parameters. They were determined by minimizing the quadratic error between the fast Fourier transform (FFT) of the simulated and the measured longitudinal accelerations on the seat cushion. The measured accelerations were obtained from the field tests of vibration measurement. Other parameters in this seat-driver model are summarized in Tab. 7.18. They were estimated from the values presented in the studies by Nawayseh and Griffin [81] and by Riedel [161].

Tab. 7.18: A part of parameters of the seat-driver model in the longitudinal direction

m_{h0z} (kg)	0	J (kg·m ²)	0.5
m_{h1z} (kg)	20	e (m)	0.11
m_{h2z} (kg)	40	α (rad)	1.12
k_{hz} (N/m)	42000	c_{hz} (N·s/m)	1100

7.3.3 Model validation

After the parameters were determined in section 7.3.2, the seat-driver model in Fig. 7.20 was used to simulate the dynamic behavior of the seat-driver system in the longitudinal direction. In order to evaluate the quality of this seat-driver model, the following three simulation results were compared with those obtained from the field measurements:

- 1) Vibration dose value (VDV) of the frequency weighted accelerations in the longitudinal direction on the seat cushion: the δ_{VDV} , as defined by Eq. (7.22), was used to indicate the difference between the simulated VDV and the measured VDV.

$$\delta_{VDV} = \frac{VDV_s - VDV_m}{VDV_m} * 100\% \quad (7.22)$$

with

δ_{VDV} Difference between the simulated VDV and the measured VDV

VDV_m	VDV of accelerations obtained from the measurement in $m/s^{1.75}$
VDV_s	VDV of accelerations obtained from the simulation in $m/s^{1.75}$

- 2) Accelerations in the longitudinal direction on the seat cushion in the time domain: the mean value of the relative errors of accelerations, as defined by Eq. (7.11) (p. 134), was used here to give an indication of the difference between the simulated and the measured accelerations in the time domain.
- 3) Power spectral density (PSD) curve of the accelerations in the longitudinal direction on the seat cushion: the mean value of the relative errors of PSD defined by Eq. (7.12) (p. 134) was used to indicate the difference between the PSD curves of the simulated and the measured accelerations.

The VDV_s obtained from simulations and measurements are compared in Tab. 7.19. It can be observed that the differences between both VDV_s are smaller than 10%.

Tab. 7.19: VDV_s of frequency weighted accelerations in the longitudinal direction on the seat cushion obtained from simulations and measurements

	OP-1.1	OP-1.2	OP-4	OP-1.3	OP-1.4
VDV_m ($m/s^{1.75}$)	2.5134	2.5057	5.2663	7.3404	8.341
VDV_s ($m/s^{1.75}$)	2.4638	2.6358	5.7495	7.1291	8.0292
δ_{VDV} (%)	-1.9725	5.194	9.1750	-2.8782	-3.7387

The simulated and the measured acceleration signals in the longitudinal direction on the seat cushion in the time domain are compared in Fig. 7.21. The mean values of the relative errors between both signals, the $\bar{\delta}_a$, are presented in Tab. 7.20. From the comparison in Fig. 7.21 and the values in Tab. 7.20 it can be concluded that the acceleration signals in the low frequency range obtained from simulations match those from field measurements very well in the time domain.

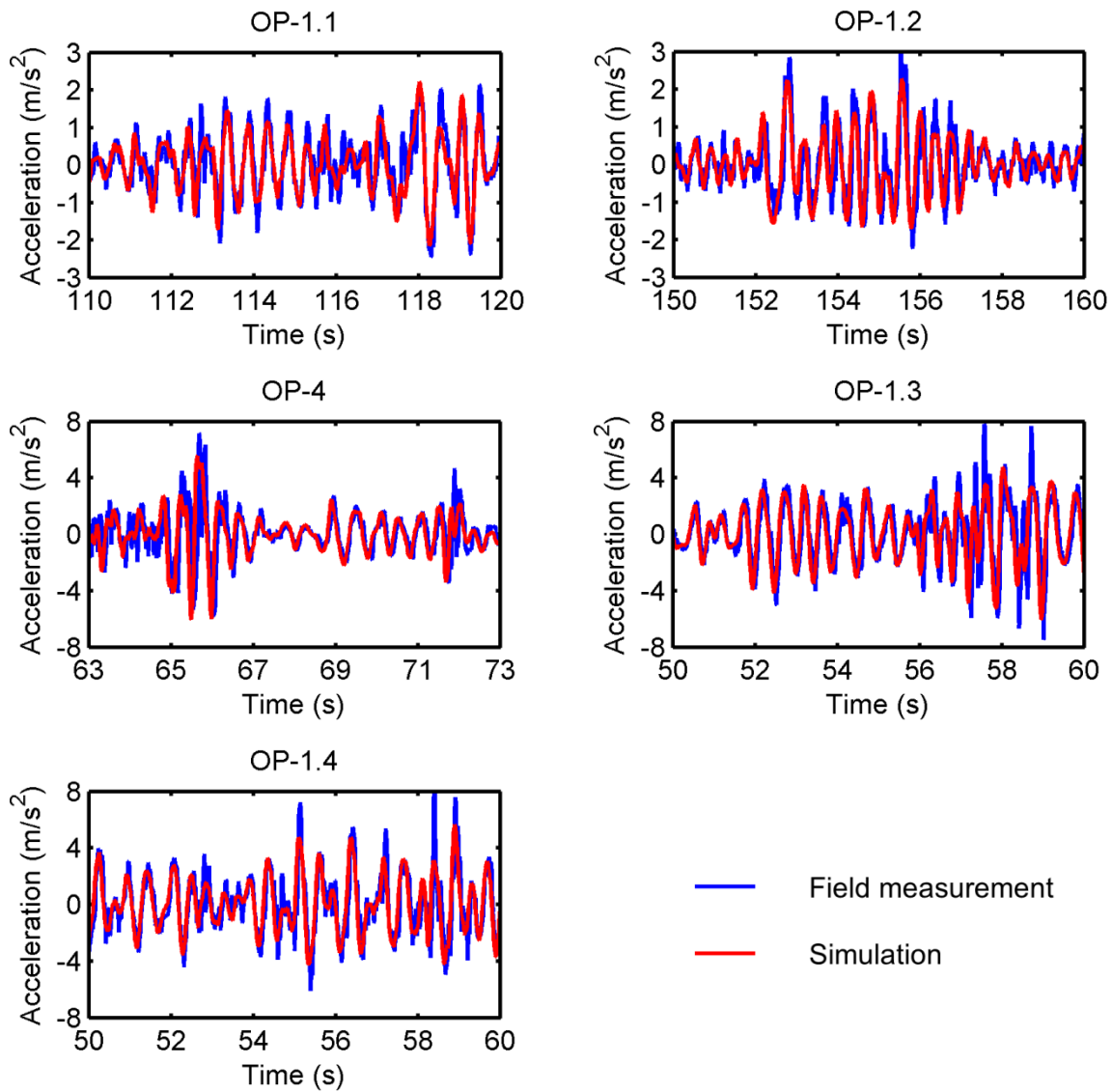


Fig. 7.21: Comparison of measured and simulated accelerations in the longitudinal direction on the seat cushion in the time domain

Tab. 7.20: Mean values of the relative errors between the simulated and the measured accelerations in the longitudinal direction on the seat cushion

$\bar{\delta}_a$	OP-1.1	OP-1.2	OP-4	OP-1.3	OP-1.4
0.5-4 Hz	0.1011	0.1082	0.0995	0.0562	0.0984
0.5-20 Hz	0.3884	0.3270	0.3329	0.2669	0.3421

The comparison of PSD curves is presented in Fig. 7.22. It can be observed that the differences between both PSD curves mainly occur at frequencies higher than 4 Hz,

where the vibration magnitudes are very low. At frequencies higher than 4 Hz, noise is included in the measurement signals which cannot be simulated. Therefore, the simulated accelerations have lower magnitudes than the measured ones in this frequency range. The differences between the PSD curves are quite small in the frequency range from 0.5 Hz to 4 Hz, where the vibration magnitudes are quite high and vibration excitations have the predominant influence on the dynamic response of the seat-driver system in the longitudinal direction. These quite small differences can also be observed from the mean values of the relative errors between the PSD curves in Tab. 7.21.

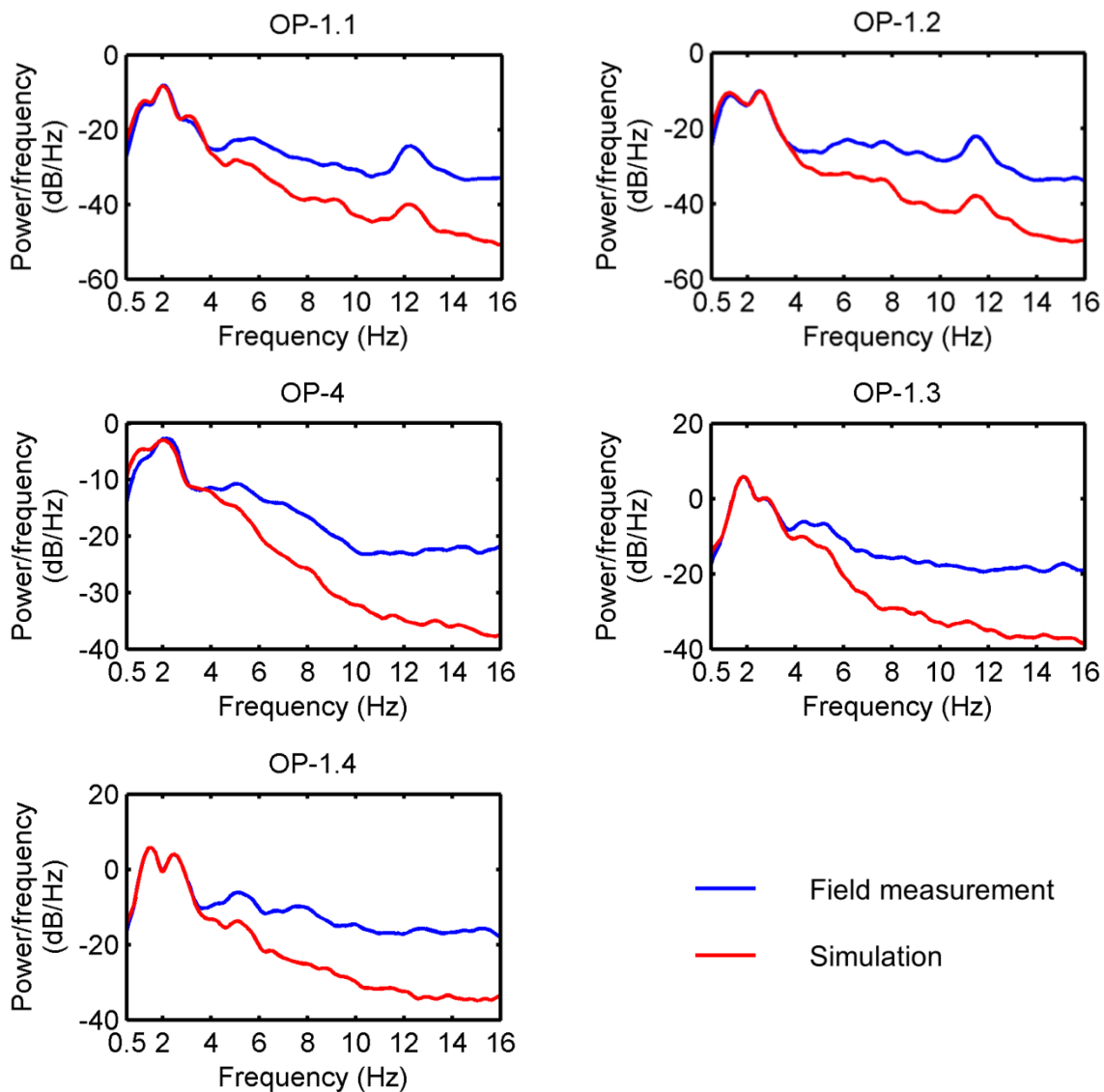


Fig. 7.22: Comparison of PSD of measured and simulated accelerations in the longitudinal direction on the seat cushion

Tab. 7.21: Mean values of the relative errors between the PSD curve of the simulated and the measured longitudinal accelerations in the frequency range of 0.5-4 Hz

	OP-1.1	OP-1.2	OP-4	OP-1.3	OP-1.4
$\bar{\delta}_{PSD}$ (0.5-4 Hz)	0.0587	0.0451	0.1090	0.0434	0.0403

From the comparison in this section it can be concluded that the seat-driver model can simulate the dynamic behavior of the seat-driver system in the longitudinal direction quite well.

7.3.4 Suspension system optimization

No longitudinal suspension system is equipped in the original seat on the compact wheel loader (CWL) analyzed in this work. In order to improve the vibration attenuation performance of the seat in this direction as well, a longitudinal seat suspension system should be designed and optimized. In this section, the optimization of two types of longitudinal seat suspension systems is introduced: a passive one and a semi-active one. The passive suspension is comprised of a linear spring, a passive hydraulic damper and two end-stop buffers. The force-velocity characteristics of the passive hydraulic damper can be described by Fig. 7.10 (p. 128) as well. The two end-stop buffers were suppose to have the same force-deflection relationship, which is characterized in terms of a linear stiffness coefficient with a cubic stiffness coefficient. The corresponding seat-driver model is illustrated in Fig. 7.23. The equations of motion of this model are formulated in Eq. (7.23).

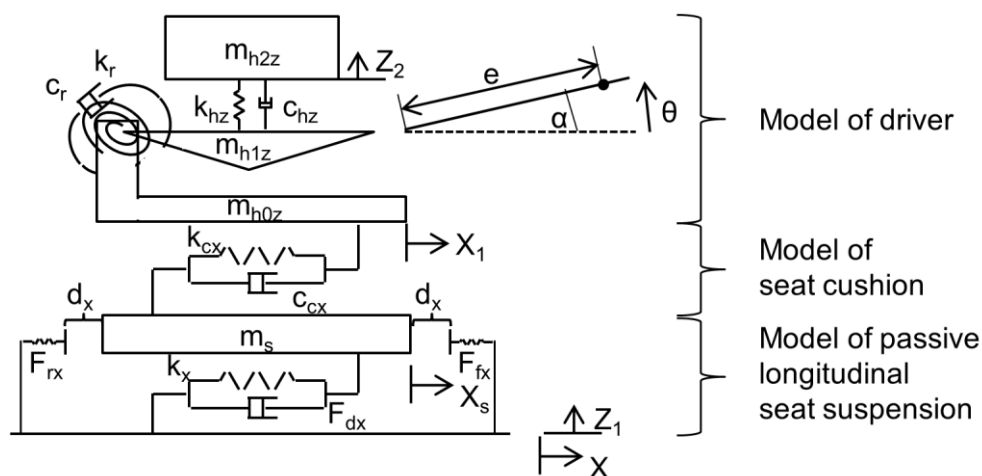


Fig. 7.23: Seat-driver model with a passive longitudinal seat suspension system

$$\begin{cases}
m_{h2z} \ddot{Z}_2 = -k_{hz} * [Z_2 - (Z_1 + e * \theta * \cos \alpha)] - c_{hz} * [\dot{Z}_2 - (\dot{Z}_1 + e * \dot{\theta} * \cos \alpha)] \\
J \ddot{\theta} = k_{hz} * [Z_2 - (Z_1 + e * \theta * \cos \alpha)] * e * \cos \alpha \\
\quad + c_{hz} * [\dot{Z}_2 - (\dot{Z}_1 + e * \dot{\theta} * \cos \alpha)] * e * \cos \alpha \\
\quad + m_{h1z} * \ddot{X}_1 * e * \sin \alpha - m_{h1z} * \ddot{Z}_1 * e * \cos \alpha - k_r * \theta - c_r * \dot{\theta} \\
(m_{h2z} + m_{h1z} + m_{h0z}) \ddot{X}_1 - m_{h1z} * e * \ddot{\theta} * \sin \alpha = -k_{cx} * (X_1 - X_s) - c_{cx} * (\dot{X}_1 - \dot{X}_s) \\
m_s \ddot{X}_s = -k_x * (X_s - X) + F_{dx} - F_{fx} + F_{rx} + k_{cx} * (X_1 - X_s) + c_{cx} * (\dot{X}_1 - \dot{X}_s)
\end{cases} \quad (7.23)$$

with

F_{dx}	Damping force of the passive damper in the longitudinal seat suspension system in N
F_{fx}	Force coming from the front end-stop buffer in N
F_{rx}	Force coming from the rear end-stop buffer in N
X_s	Absolute displacement of m_s in the x-direction in m
\dot{X}_s	Absolute velocity of m_s in the x-direction in m/s
\ddot{X}_s	Absolute acceleration of m_s in the x-direction in m/s^2
k_x	Stiffness of the spring in the longitudinal seat suspension system in N/m

For the passive hydraulic damper the damping force F_{dx} is formulated in Eq. (7.24). The forces coming from the end-stop buffers, F_{fx} and F_{rx} , are formulated in Eq. (7.25) and Eq. (7.26) respectively.

$$F_{dx} = \begin{cases} c_{x1} * (\dot{X} - \dot{X}_s) & 0 \leq \dot{X} - \dot{X}_s \leq v_{cx} \\ c_{x1} * \left\{ v_{cx} + \gamma_{cx} * \left[(\dot{X} - \dot{X}_s) - v_{cx} \right] \right\} & \dot{X} - \dot{X}_s > v_{cx} \\ p_x * c_{x1} * (\dot{X} - \dot{X}_s) & v_{ex} \leq \dot{X} - \dot{X}_s < 0 \\ p_x * c_{x1} * \left\{ v_{ex} + \gamma_{ex} * \left[(\dot{X} - \dot{X}_s) - v_{ex} \right] \right\} & \dot{X} - \dot{X}_s < v_{ex} \end{cases} \quad (7.24)$$

$$F_{fx} = k_{f1} * [(X_s - X) - d_x] + k_{f3} * [(X_s - X) - d_x]^3 \quad X_s - X > d_x \quad (7.25)$$

$$F_{rx} = k_{r1} * [(X - X_s) - d_x] + k_{r3} * [(X - X_s) - d_x]^3 \quad X_s - X < -d_x \quad (7.26)$$

with

c_{x1}	Damping coefficient of the longitudinal passive hydraulic damper at low speeds in the compression stage in N·s/m
c_{x2}	Damping coefficient of the longitudinal passive hydraulic damper at high speeds in the compression stage in N·s/m
c_{x3}	Damping coefficient of the longitudinal passive hydraulic damper at low speeds in the extension stage in N·s/m

c_{x4}	Damping coefficient of the longitudinal passive hydraulic damper at high speeds in the extension stage in N-s/m
d_x	Distance between the middle position of the longitudinal seat suspension system and the front or the rear end-stop buffer in m
k_{f1}	Linear stiffness coefficient of the front end-stop buffer in N/m
k_{f3}	Cubic stiffness coefficient of the front end-stop buffer in N/m ³
k_{r1}	Linear stiffness coefficient of the rear end-stop buffer in N/m
k_{r3}	Cubic stiffness coefficient of the rear end-stop buffer in N/m ³
p_x	Asymmetry factor of the longitudinal passive hydraulic damper, ratio of c_{x3} to c_{x1}
v_{cx}	Transition velocity of the longitudinal passive damper in the compression stage in m/s
v_{ex}	Transition velocity of the longitudinal passive damper in the extension stage in m/s
γ_{cx}	Damping reduction factor of the longitudinal passive hydraulic damper in the compression stage, ratio of c_{x2} to c_{x1}
γ_{ex}	Damping reduction factor of the longitudinal passive hydraulic damper in the extension stage, ratio of c_{x4} to c_{x3}

The semi-active suspension system is comprised of a linear spring and a semi-active damper. Equal to that in the vertical seat suspension system, the semi-active damper is also controlled by the ‘soft-hard’ policy (refer to Eq. (2.41)). The corresponding seat-driver model is illustrated in Fig. 7.24. The equations of motion of this model are formulated in Eq. (7.27).

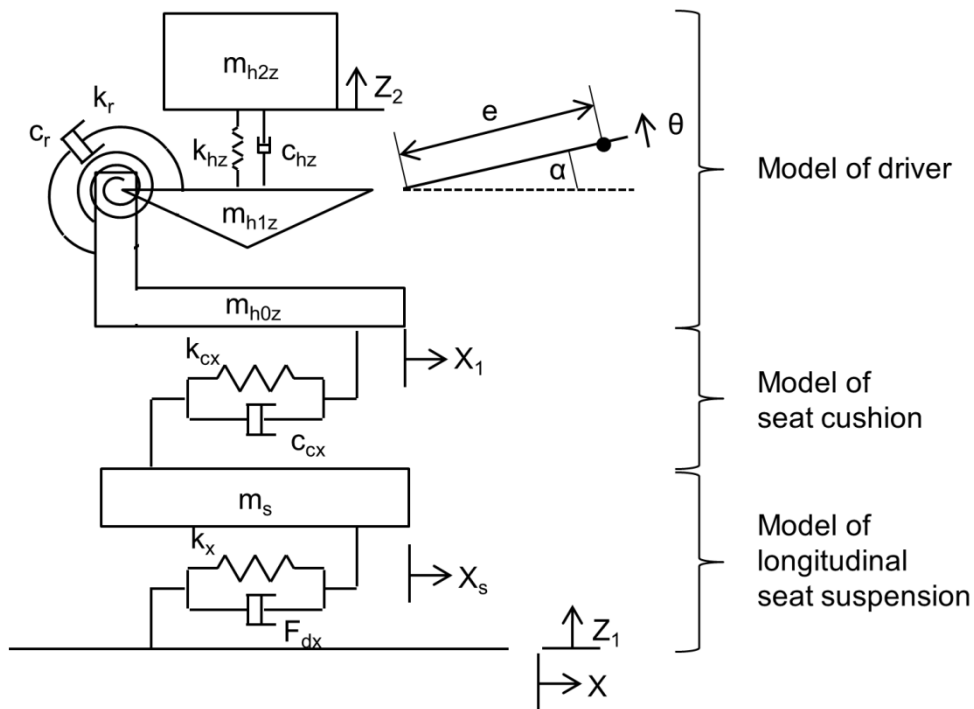


Fig. 7.24: Seat-driver model with a semi-active longitudinal seat suspension system

$$\begin{cases}
m_{h2z} \ddot{Z}_2 = -k_{hz} * [Z_2 - (Z_1 + e * \theta * \cos \alpha)] - c_{hz} * [\dot{Z}_2 - (\dot{Z}_1 + e * \dot{\theta} * \cos \alpha)] \\
J \ddot{\theta} = k_{hz} * [Z_2 - (Z_1 + e * \theta * \cos \alpha)] * e * \cos \alpha \\
\quad + c_{hz} * [\dot{Z}_2 - (\dot{Z}_1 + e * \dot{\theta} * \cos \alpha)] * e * \cos \alpha \\
\quad + m_{h1z} * \ddot{X}_1 * e * \sin \alpha - m_{h1z} * \ddot{Z}_1 * e * \cos \alpha - k_r * \theta - c_r * \dot{\theta} \\
(m_{h2z} + m_{h1z} + m_{h0z}) \ddot{X}_1 - m_{h1z} * e * \ddot{\theta} * \sin \alpha = -k_{cx} * (X_1 - X_s) - c_{cx} * (\dot{X}_1 - \dot{X}_s) \\
m_s \ddot{X}_s = -k_x * (X_s - X) + F_{dx} + k_{cx} * (X_1 - X_s) + c_{cx} * (\dot{X}_1 - \dot{X}_s)
\end{cases} \quad (7.27)$$

For the semi-active damper the damping force F_{dx} is formulated in Eq. (7.28).

$$F_{dx} = \begin{cases} c_{softx} * (\dot{X} - \dot{X}_s) & |X_s - X| \leq d_{softx} \\ c_{hardx} * (\dot{X} - \dot{X}_s) & d_{softx} < |X_s - X| \leq d_{mx} \end{cases} \quad (7.28)$$

with

c_{softx}	Damping coefficient of the longitudinal semi-active damper in the soft-state in N·s/m
c_{hardx}	Damping coefficient of the longitudinal semi-active damper in the hard-state in N·s/m
d_{softx}	Maximum suspension travel of the longitudinal seat suspension system when the semi-active damper in the soft-state in m
d_{mx}	Maximum stroke of the longitudinal seat suspension system in m

Due to the limited space in the cabin on construction vehicles and in order to satisfy the requirement in operational safety, the maximum stroke of the longitudinal seat suspension system should also be kept in a small range. In this work, it was set to ± 25 mm. The optimization of the longitudinal seat suspension system was carried out when the free stroke was set to ± 10 mm, ± 15 mm and ± 20 mm.

As analyzed in chapter 4, the predominant components of the longitudinal vibration excitations at the seat base are in the frequency range from 1.25 Hz to 2 Hz. In order to attenuate these vibrations, the natural frequency of the seat-driver system with the longitudinal seat suspension system should not exceed $1.25/\sqrt{2}$ Hz. The range of the stiffness coefficient k_x determined according to Eq. (7.29) is limited to $k_x \leq 2467$ N/m. On the other hand, the stiffness coefficient k_x should be large enough to comply with the requirement of operational safety. Accordingly, the value 2467 N/m was set as the optimal stiffness coefficient of the longitudinal seat suspension system.

$$f_{nx} = \frac{1}{2\pi} \sqrt{\frac{k_x}{m_s + m_{h1z} + m_{h2z}}} \leq \frac{1.25}{\sqrt{2}} \quad (7.29)$$

with

f_{nx} Natural frequency of the seat-driver system with longitudinal suspension system in Hz

7.3.4.1 Optimization of passive longitudinal seat suspension system

The excitations in operations OP-1.1, OP-1.2, OP-1.3, OP-1.4 and OP-4, which were already used in section 7.2.4 to optimize the vertical seat suspension system, were used in this section to optimize the longitudinal seat suspension system as well.

The vibration attenuation performance of the passive longitudinal seat suspension system is improved by optimizing the damping coefficients of the hydraulic damper and the stiffness coefficients of the end-stop buffers. The optimization was carried out in the following two steps:

- 1) Under the excitations with moderate magnitudes, the damping coefficients of the passive damper were optimized to minimize the vibration dose value (VDV) of the frequency weighted longitudinal accelerations on the seat cushion. The suspension travel was constrained to the free stroke. The objective function in this step is formulated in Eq. (7.30). Here the minimum VDV was taken as an alternative optimization objective, and during the optimization it was noticed that the same optimization results were obtained when taking both the minimum VDV and the minimum vibration dose value ratio (VDVR) as the optimization objectives.

$$\begin{cases} U(\chi) = \min(\text{VDV}) & |X_s - X| \leq d_x \\ \chi = [c_{x1} \quad c_{x2} \quad c_{x3} \quad c_{x4}] \end{cases} \quad (7.30)$$

The excitation signals in the time domain show that the excitations have low magnitudes in the operation OP-1.1 and moderate magnitudes in the operation OP-1.2. They have high magnitudes in operations OP-1.3, OP-1.4 and OP-4. Accordingly, the optimal damping coefficients were determined under the excitation in the operation OP-1.2. It was supposed that the damper has the same force-velocity relationship in the extension and the compression stages, which means that the damping coefficient c_{x1} equals c_{x3} , and c_{x2} equals c_{x4} .

- 2) With the optimal damping coefficients determined in step 1), the suspension travel possibly exceeds the maximum stroke under excitations with high magnitudes. The end-stop buffers are needed to avoid the suspension travel exceeding the maximum stroke. Their force-deflection characteristics should be optimized to minimize the VDV of the frequency weighted longitudinal accelerations on the seat cushion. The objective function in this step is formulated in Eq. (7.31).

$$\begin{cases} U(\chi) = \min(\text{VDV}) \\ \chi = [k_{f1} \quad k_{f3} \quad k_{r1} \quad k_{r3}] \end{cases} \quad |X_s - X| \leq d_{mx} \quad (7.31)$$

The optimization results in the first step are presented in Tab. 7.22. With these optimal damping coefficients, the VDV of the frequency weighted longitudinal accelerations on the seat cushion are presented in Tab. 7.23.

Tab. 7.22: Optimal damping coefficients of the longitudinal seat suspension system with different free strokes determined under the excitation in the operation OP-1.2

Free stroke (mm)	Optimal damping coefficient (N·s/m)	
	$C_{x1} = C_{x3}$	$C_{x2} = C_{x4}$
± 10	2950.6	2585.4
± 15	1643.8	2233
± 20	1125.9	1483.3

Tab. 7.23: VDV of frequency weighted longitudinal accelerations on the seat cushion with the optimal damping coefficients

Free stroke (mm)	VDV (m/s ^{1.75})				
	OP-1.1	OP-1.2	OP-4	OP-1.3	OP-1.4
± 10	2.3012	2.5055	5.3190	6.3588	7.4244
± 15	2.1848	2.4450	5.1396	5.9367	7.2586
± 20	2.0963	2.4047	4.9536	5.5197	7.0829
Original seat	2.4638	2.6358	5.7495	7.1291	8.0292

As already found out for the vertical seat suspension system, when the suspension free stroke is smaller, the optimal damping coefficients are larger, as shown in Tab. 7.22. Larger damping coefficients lead to larger VDV's, as shown in Tab. 7.23.

From the simulation results it was noticed that the suspension travel does not exceed the maximum stroke under all excitations, when the free stroke is set to ± 10 mm. This is same as the vertical suspension system with free stroke of ± 30 mm. The reason is that the large damping coefficients obtained in step 1) for this free stroke cause small suspension deflections. When the free stroke exceeds ± 15 mm, the suspension travel exceeds the maximum stroke under excitations in operations OP-4, OP-1.3 and OP-1.4. Under these three excitations, the stiffness coefficients of the front and the rear end-stop buffers were optimized. The stiffest end-stop buffer was selected as the optimal one and its stiffness coefficients are presented in Tab. 7.24.

Tab. 7.24: Optimal linear and cubic stiffness coefficients of end-stop buffers in the longitudinal seat suspension system with different free strokes

Free stroke (mm)	$k_{f1} = k_{r1}$ (N/m)	$k_{f3} = k_{r3}$ (N/m³)
± 15	$3.5 \cdot 10^5$	$9 \cdot 10^{10}$
± 20	$1 \cdot 10^6$	$1 \cdot 10^{11}$

With the optimal damping coefficients of the passive damper in Tab. 7.22 and the optimal stiffness coefficients of the end-stop buffers in Tab. 7.24, the VDV's of the frequency weighted longitudinal accelerations on the seat cushion under excitations in all five operations are presented in Tab. 7.25.

Tab. 7.25: VDV's of frequency weighted longitudinal accelerations on the seat cushion with the optimized damper and end-stop buffers

Free stroke (mm)	VDV (m/s^{1.75})				
	OP-1.1	OP-1.2	OP-4	OP-1.3	OP-1.4
± 10	2.3012	2.5055	5.3190	6.3588	7.4244
± 15	2.1848	2.4450	5.1901	5.8940	7.0747
± 20	2.0963	2.4047	5.1794	5.5951	6.9494
Original seat	2.4638	2.6358	5.7495	7.1291	8.0292

These VDV's show that the suspension free stroke has a large influence on the vibration attenuation performance of the seat in the longitudinal direction. The optimized passive longitudinal seat suspension system has the best vibration attenuation performance when the free stroke is set to ± 20 mm.

7.3.4.2 Optimization of semi-active longitudinal seat suspension system

The vibration attenuation performance of the semi-active longitudinal seat suspension system can be improved by optimizing the damping coefficients of the semi-active damper in both the soft-state and the hard-state. The optimization was performed according to the following two steps:

- 1) Under the excitation in the operation OP-1.2, the damping coefficient of the semi-active damper in the soft-state was optimized to minimize the VDV of the frequency weighted longitudinal accelerations on the seat cushion. The suspension travel was constrained to the free stroke of the semi-active suspension. The objective function in this step is formulated in Eq. (7.32).

$$U(c_{soft}) = \min(VDV) \quad |X_s - X| \leq d_{soft} \quad (7.32)$$

- 2) With the optimal damping coefficient in the soft-state determined in the step 1), the suspension travel exceeds the free stroke under excitations with high magnitudes. In this case, the semi-active damper has to be put in the hard-state, where the damping coefficient should be optimized to minimize the VDV of the frequency weighted longitudinal accelerations on the seat cushion, as well as to avoid the suspension travel exceeding the maximum stroke. The objective function in this step is formulated in Eq. (7.33). In this step, excitations in operations OP-4, OP-1.3 and OP-1.4 were used to optimize the damping coefficient. The highest one was determined as the optimal damping coefficient in the hard-state.

$$U(c_{hard}) = \min(VDV) \quad |X_s - X| \leq d_{mx} \quad (7.33)$$

The optimal damping coefficients in both the soft-state and the hard-state of the semi-active damper in the longitudinal seat suspension system with different free strokes are presented in Tab. 7.26.

Tab. 7.26: Optimal damping coefficients of the semi-active damper in the longitudinal seat suspension system with different free strokes

Free stroke (mm)	Optimal damping coefficient (N-s/m)	
	C_{softx}	C_{hardx}
± 10	2963.4	3545.7
± 15	1833.3	5336
± 20	1301.2	8564.9

With the optimal damping coefficients in Tab. 7.26, the VDV of the frequency weighted accelerations in the longitudinal direction on the seat cushion are presented in Tab. 7.27. They show that the optimized semi-active longitudinal seat suspension system has the best vibration attenuation performance when the free stroke is set to ± 20 mm.

Tab. 7.27: VDV of the frequency weighted longitudinal accelerations on the seat cushion with the optimized semi-active longitudinal seat suspension system

Free stroke (mm)	VDV (m/s ^{1.75})				
	OP-1.1	OP-1.2	OP-4	OP-1.3	OP-1.4
± 10	2.3019	2.5058	5.3509	6.3784	7.4350
± 15	2.2087	2.4492	5.2266	5.9380	7.1771
± 20	2.1270	2.4047	5.1919	5.5424	6.9678
Original seat	2.4638	2.6358	5.7495	7.1291	8.0292

7.3.4.3 Comparison of optimized passive and semi-active longitudinal seat suspensions

In sections 7.3.4.1 and 7.3.4.2, it is concluded that the optimized passive and semi-active longitudinal seat suspension systems have the best vibration attenuation performance when the free stroke is set to ± 20 mm. By comparing the VDV in Tab.

7.25 and Tab. 7.27 with these two optimal suspension systems, it can be noticed that the differences of the VDVs between the optimal passive longitudinal seat suspension system and the semi-active one are very small. Due to the lower cost and easier usage of the passive hydraulic damper, the passive suspension system with the free stroke of ± 20 mm is recommended as the optimal longitudinal seat suspension system.

In the final step, the VDVs of the frequency weighted longitudinal accelerations on the seat cushion with the optimal longitudinal seat suspension system are compared with those on the original seat in Tab. 7.28.

Tab. 7.28: Comparison between the VDVs of the frequency weighted longitudinal accelerations on the seat cushion on the original seat and the VDVs on the seat cushion with the optimal longitudinal seat suspension system

	OP-1.1	OP-1.2	OP-4	OP-1.3	OP-1.4
$VDV_{\text{original}} \text{ (m/s}^{1.75}\text{)}$	2.4638	2.6358	5.7495	7.1291	8.0292
$VDV_{\text{optimal}} \text{ (m/s}^{1.75}\text{)}$	2.0963	2.4047	5.1794	5.5951	6.9494
$\Delta \text{ (%)}$	-14.92	-9.38	-9.92	-21.52	-13.45

7.4 Combined seat-driver model in the x- and z-directions

Now the vertical seat suspension model from section 7.2 and the seat-driver model from section 7.3 are combined together to simulate the dynamic behavior of the seat-driver system in the longitudinal and the vertical directions simultaneously. The combined seat-driver model with the optimal longitudinal and vertical seat suspension systems is illustrated in Fig. 7.25. The equations of motion of this combined model are expressed in Eq. (7.34).

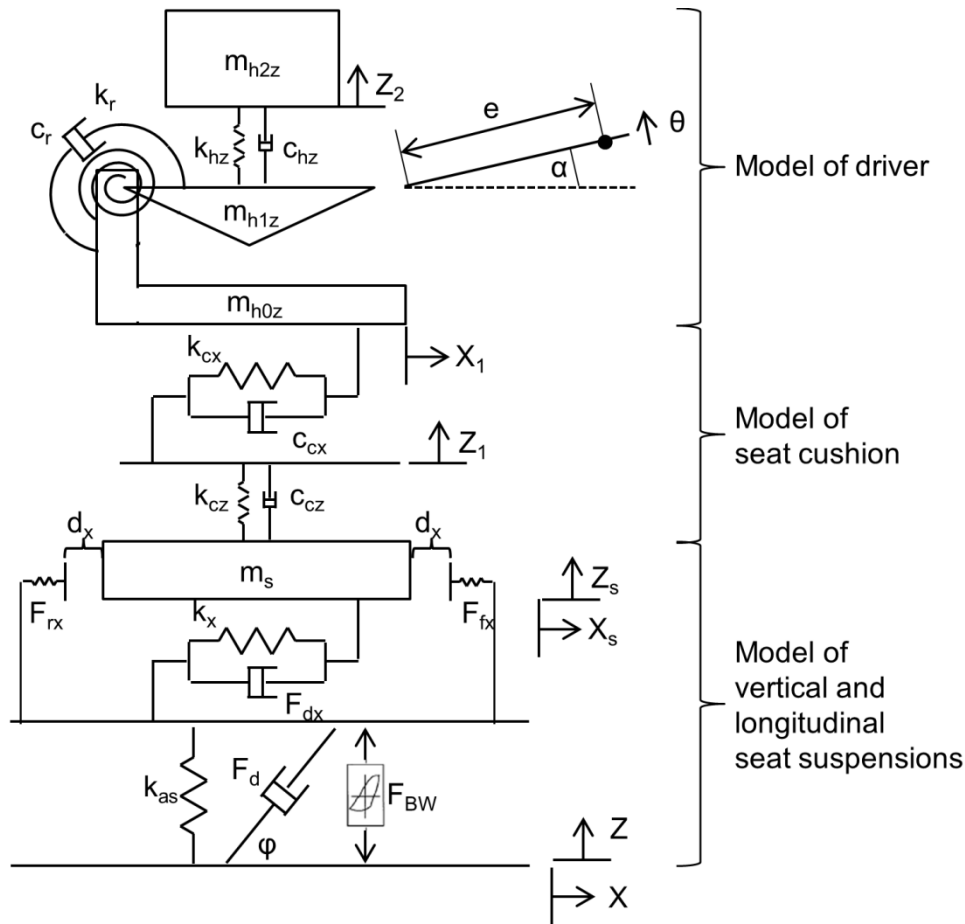


Fig. 7.25: Combined seat-driver model with optimal seat suspension systems

$$\left\{ \begin{array}{l}
 m_{h2z} \ddot{Z}_2 = -k_{hz} * [Z_2 - (Z_1 + e * \theta * \cos \alpha)] - c_{hz} * [\dot{Z}_2 - (\dot{Z}_1 + e * \dot{\theta} * \cos \alpha)] \\
 J \ddot{\theta} = k_{hz} * [Z_2 - (Z_1 + e * \theta * \cos \alpha)] * e * \cos \alpha \\
 \quad + c_{hz} * [\dot{Z}_2 - (\dot{Z}_1 + e * \dot{\theta} * \cos \alpha)] * e * \cos \alpha \\
 \quad + m_{h1z} * \ddot{X}_1 * e * \sin \alpha - m_{h1z} * \ddot{Z}_1 * e * \cos \alpha - k_r * \theta - c_r * \dot{\theta} \\
 (m_{h2z} + m_{h1z} + m_{h0z}) \ddot{X}_1 - m_{h1z} * e * \ddot{\theta} * \sin \alpha = -k_{cx} * (X_1 - X_s) - c_{cx} * (\dot{X}_1 - \dot{X}_s) \\
 m_{h0z} \ddot{Z}_1 + m_{h1z} * (\ddot{Z}_1 + e * \ddot{\theta} * \cos \alpha) = -k_{cz} * (Z_1 - Z_s) - c_{cz} * (\dot{Z}_1 - \dot{Z}_s) \\
 \quad + k_{hz} * [Z_2 - (Z_1 + e * \theta * \cos \alpha)] \\
 \quad + c_{hz} * [\dot{Z}_2 - (\dot{Z}_1 + e * \dot{\theta} * \cos \alpha)] \\
 m_s \ddot{X}_s = -k_x * (X_s - X) + F_{dx} - F_{fx} + F_{rx} + k_{cx} * (X_1 - X_s) + c_{cx} * (\dot{X}_1 - \dot{X}_s) \\
 m_s \ddot{Z}_s = -k_{as} * (Z_s - Z) + F_{dz} - F_{BW} + k_{cz} * (Z_1 - Z_s) + c_{cz} * (\dot{Z}_1 - \dot{Z}_s)
 \end{array} \right. \quad (7.34)$$

To examine the reliability of this model, the following simulation results were compared with those from the field measurements:

- 1) Vibration dose value (VDV) of the frequency weighted accelerations in the longitudinal direction on the seat cushion
- 2) VDV of the frequency weighted accelerations in the vertical direction on the seat cushion

The δ_{VDV} defined by Eq. (7.22) (p. 155) was used to indicate the difference between the simulated VDV and the measured VDV.

- 3) Longitudinal accelerations on the seat cushion in the time domain
- 4) Vertical accelerations on the seat cushion in the time domain

The mean value of the relative errors of accelerations $\bar{\delta}_a$, as defined by Eq. (7.11) (p. 134), was used here to give an indication of the difference between the simulated and the measured accelerations in the time domain.

- 5) Power spectral density (PSD) of the longitudinal accelerations on the seat cushion
- 6) PSD of the vertical accelerations on the seat cushion

The mean value of the relative errors of PSD $\bar{\delta}_{PSD}$, defined by Eq. (7.12) (p. 134), was used to indicate the difference between the PSD curves of the simulated and the measured accelerations.

The comparison of the VDVs obtained from simulations and field measurements is presented in Tab. 7.29. The values of δ_{VDV} show that all differences between the simulated and the measured VDVs are less than 10%.

Tab. 7.29: Comparison of measured and simulated VDVs

		OP-1.1	OP-1.2	OP-4	OP-1.3	OP-1.4
x-direction	VDV _m (m/s ^{1.75})	2.5134	2.5057	5.2663	7.3404	8.3410
	VDV _s (m/s ^{1.75})	2.3777	2.5026	5.7191	6.8488	7.6185
	δ_{VDV} (%)	-5.3988	-0.1224	8.5992	-6.6965	-8.6626
z-direction	VDV _m (m/s ^{1.75})	3.5868	3.1520	5.3040	9.6091	9.3368
	VDV _s (m/s ^{1.75})	3.4352	2.9322	5.2028	9.4928	9.1875
	δ_{VDV} (%)	-4.2263	-6.9731	-1.9076	-1.2103	-1.5990

The comparison of the simulated and the measured longitudinal accelerations in the time domain is illustrated in Fig. 7.26. In Fig. 7.27 the comparison of the simulated and the measured vertical accelerations in the time domain is presented. The mean values of the relative errors of the accelerations in both the longitudinal and the vertical directions, the $\bar{\delta}_a$, are given in Tab. 7.30. The comparison in Fig. 7.26 and Fig. 7.27 and the $\bar{\delta}_a$ values in Tab. 7.30 show that the simulated accelerations match the measured accelerations very well, especially in the low frequency range.

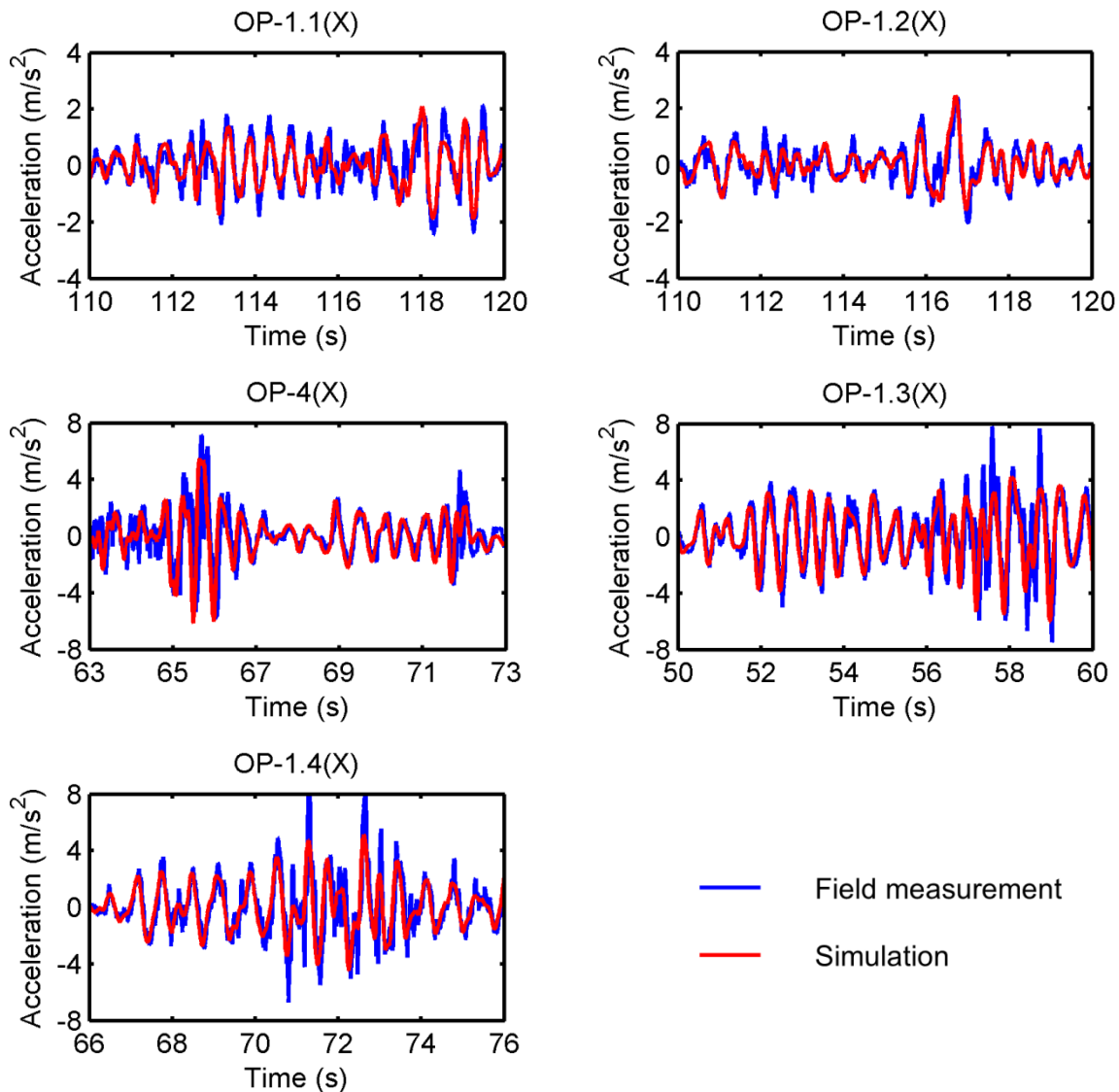


Fig. 7.26: Comparison of measured and simulated accelerations in the longitudinal direction on the seat cushion in the time domain

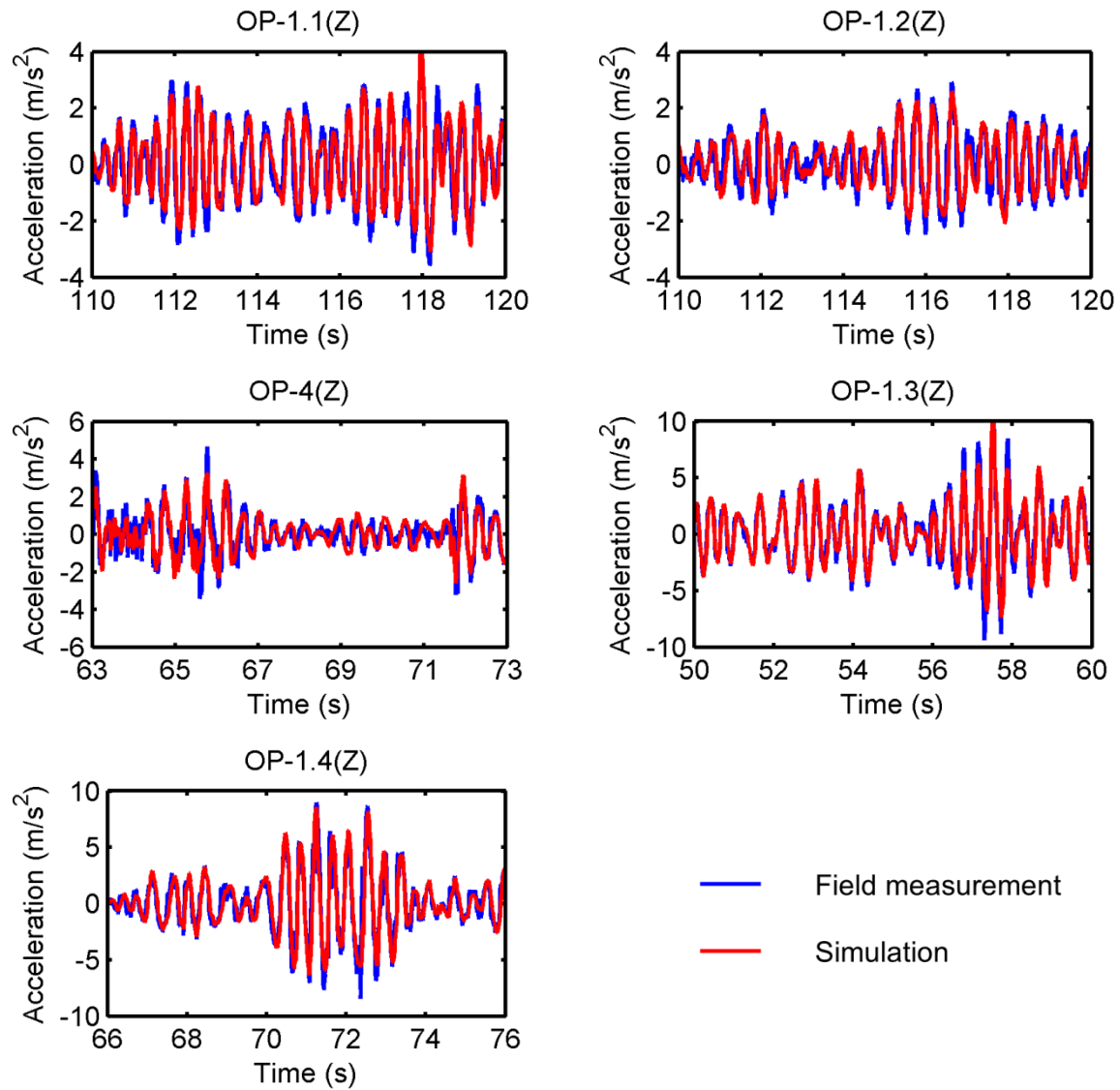


Fig. 7.27: Comparison of measured and simulated accelerations in the vertical direction on the seat cushion in the time domain

Tab. 7.30: Mean values of the relative errors between the simulated and the measured accelerations in both the longitudinal and the vertical directions

Direction	$\bar{\delta}_a$	OP-1.1	OP-1.2	OP-4	OP-1.3	OP-1.4
x	0.5-4 Hz	0.1169	0.1150	0.0978	0.0797	0.0974
	0.5-20 Hz	0.4180	0.3593	0.3376	0.3715	0.3316
z	0.5-4 Hz	0.1064	0.1042	0.0835	0.0939	0.1012
	0.5-20 Hz	0.3148	0.3082	0.3403	0.2632	0.2867

The comparison of PSD curves of the simulated and the measured longitudinal accelerations is shown in Fig. 7.28. And the comparison of PSD curves of the vertical accelerations is shown in Fig. 7.29. As shown in these two figures, the accelerations in both the longitudinal and the vertical directions have large amplitudes in the frequency range from 0.5 Hz to 4 Hz. In this frequency range, the differences between the PSD curves of the simulated and the measured accelerations are very small. These small differences can be also observed from the mean values of the relative errors between the simulated and the measured PSD curves, the $\bar{\delta}_{PSD}$ values, in Tab. 7.31.

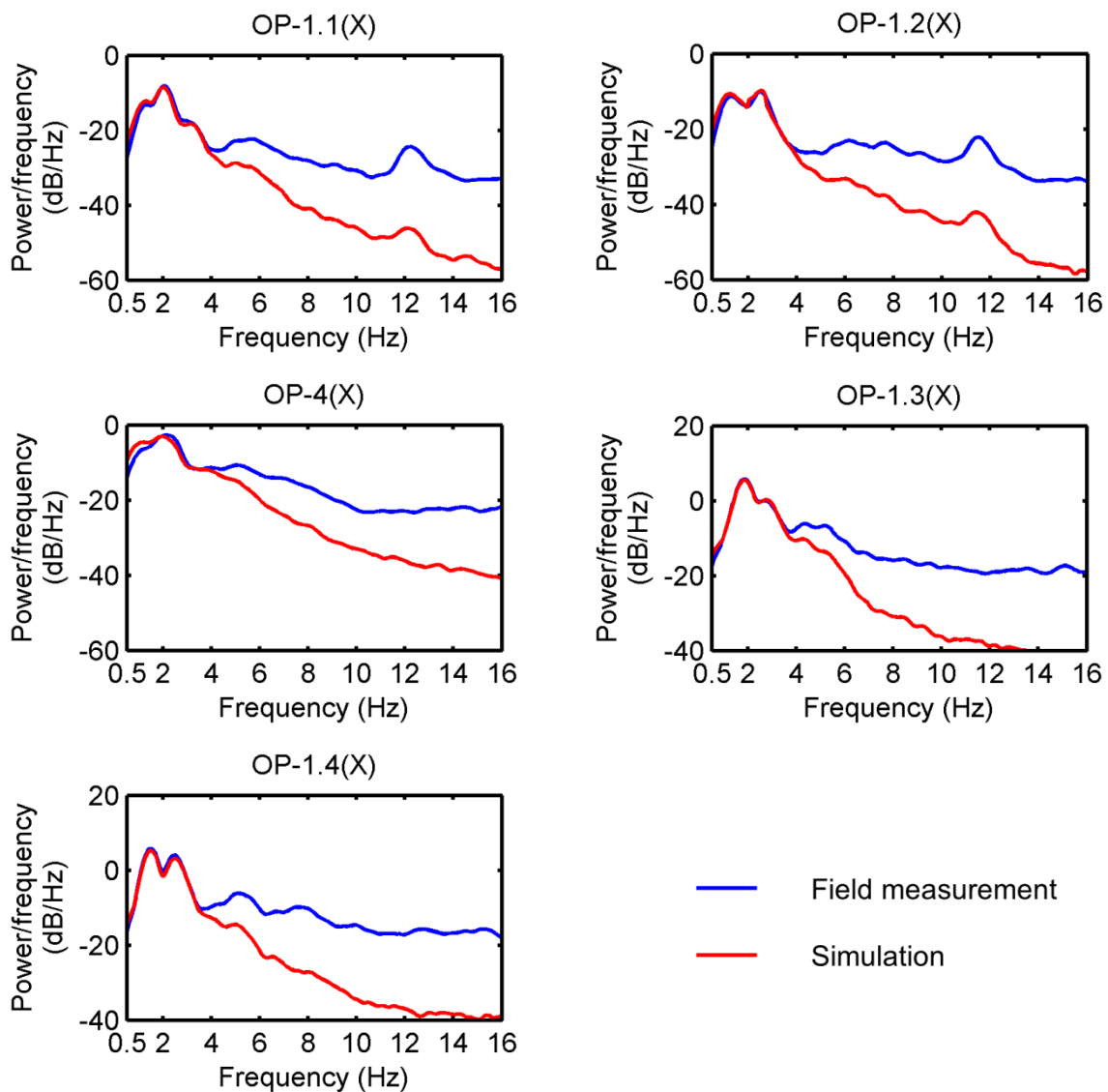


Fig. 7.28: Comparison of PSD curves of measured and simulated accelerations in the longitudinal direction on the seat cushion

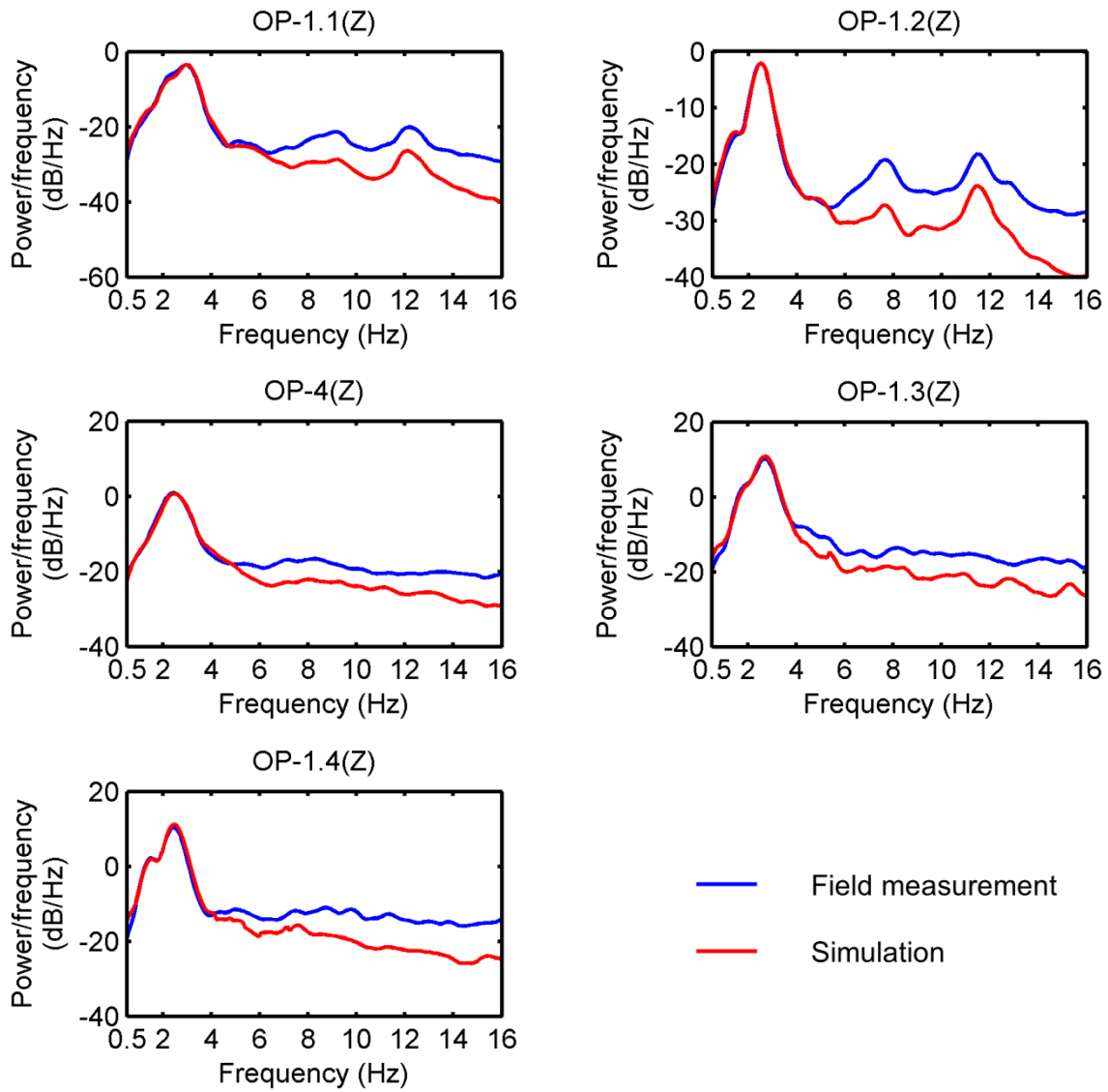


Fig. 7.29: Comparison of PSD curves of measured and simulated accelerations in the vertical direction on the seat cushion

Tab. 7.31: Mean values of the relative errors between the simulated and the measured PSD curves in both the longitudinal and the vertical directions

	Direction	OP-1.1	OP-1.2	OP-4	OP-1.3	OP-1.4
$\bar{\delta}_{PSD}$ (0.5-4 Hz)	x	0.0644	0.0849	0.1390	0.0765	0.1074
	z	0.0690	0.0413	0.0919	0.0998	0.1324

The accelerations in the longitudinal and the vertical directions have small amplitudes at frequencies higher than 4 Hz, where the differences between the PSD curves of

the simulated and the measured accelerations are large. This is because in this frequency range the noise which is very large in the measured acceleration signals cannot be simulated.

From the above mentioned comparison results it can be concluded that the differences between the simulated and the measured acceleration signals are in an acceptable range, especially for the accelerations in the frequency range of 0.5-4 Hz. The combined model can be used to simulate the dynamic behavior of the seat-driver system.

The optimal vertical and longitudinal seat suspension systems are determined in sections 7.2.4 and 7.3.4 respectively. Here the reduction of the WBV intensity with these optimal seat suspension systems is investigated using the simulation of the combined seat-driver model. While the optimization of the lateral seat suspension system is not taken into consideration, the simulated VDV_d in this direction on the seat cushion are supposed to be same with the measured VDV_d.

The simulated daily vibration dose value (VDV_d) of seven scenarios with the original or the optimal seat suspension systems are presented in Tab. 7.32.

Tab. 7.32: VDV_d of seven scenarios with the original or the optimal seat suspensions

Scenario	VDV _d (m/s ^{1.75})		Δ (%)
	Original seat	Optimized seat	
S1	27.16	24.01	-11.60
S2-Slow	18.67	17.23	-7.71
S3-Slow	17.49	16.39	-6.29
S4-Slow	16.99	16.04	-5.59
S2-Fast	45.67	39.09	-14.40
S3-Fast	47.26	40.43	-14.45
S4-Fast	47.87	40.94	-14.48

As shown in Tab. 7.32, for the scenario of the pure V-cycle the VDV_d is reduced by 11.6% with the optimal seat suspension systems. They result in a relatively large

reduction of VDV_d (14.4%) for the scenarios comprised of V-cycle and fast driving. For the scenarios comprised of V-cycle and slow driving, a relatively small reduction of VDV_d (5%-8%) is caused by the optimal seat suspension systems.

The permitted daily exposure durations of the seven scenarios with the original or the optimal seat suspension systems were calculated according to the procedure in ISO 2631-1:1997. The extensions of the permitted daily exposure durations contributed by the optimal seat suspension systems are presented in Tab. 7.33.

For the scenarios comprised of V-cycle and slow driving, the permitted daily exposure durations are extended by about two hours with the optimized seat suspension systems, and it is extended by almost one hour for the scenario of the pure V-cycle. For the scenarios comprised of V-cycle and fast driving, the extension reaches 86%. However, because the vibration excitations have very large magnitudes in fast driving, the permitted daily exposure durations are still very short even when the seat suspension systems are optimized.

Tab. 7.33: Extension of permitted daily exposure durations contributed by the optimal seat suspension systems

Scenario	Extension of permitted daily exposure durations
S1	47 min (63.87%)
S2-Slow	2.07 h (37.68%)
S3-Slow	2.12 h (29.73%)
S4-Slow	2.07 h (25.88%)
S2-Fast	7.95 min (86.20%)
S3-Fast	6.97 min (86.67%)
S4-Fast	6.63 min (86.82%)

7.5 Conclusion

This chapter starts from analyzing the dynamic characteristics of the vertical seat suspension system based on laboratory seat tests. Analysis results show that there is

a potential to improve the vibration attenuation performance of the vertical seat suspension system, especially when the seat is exposed to vibrations with high magnitudes.

Two solutions were chosen to improve the suspension vibration attenuation performance and a method was developed to identify the optimal suspension configuration. The first solution is optimizing a passive seat suspension system. The second one is optimizing a semi-active seat suspension system with a damper controlled by a “soft-hard” policy. The optimal configuration of the suspension systems was determined in the first step by optimizing the damping coefficients of the passive damper or the damping coefficient of the semi-active damper in the soft-state under excitations with moderate magnitudes, and in the second step by optimizing the stiffness coefficients of the end-stop buffers for the passive suspension system or the damping coefficient of the semi-active damper in the hard-state.

The optimization results show that the suspension free stroke has a large influence on the vibration attenuation performance. The semi-active suspension system with the optimized damping coefficients and the free stroke of ± 35 mm was recommended as the optimal vertical seat suspension system. The optimal longitudinal seat suspension system was proposed as a passive suspension with optimized damper and end-stop buffers, as well as with the free stroke of ± 20 mm.

A model of the seat-dummy system in the laboratory seat tests was built and validated for the optimization of the vertical seat suspension system. The seat-driver system in the field tests was modeled for the optimization of the longitudinal seat suspension system. The driver model adopted in this research work can simulate the human inline biodynamic response in the longitudinal and the vertical directions, as well as the human cross-axial biodynamic response (longitudinal response to vertical excitations). At last, a seat-driver model with the optimized vertical and longitudinal seat suspension systems is introduced to simulate the dynamic behavior of the seat-driver system in the longitudinal and the vertical directions simultaneously. With the simulation of this model, the reduction of the WBV intensity in seven scenarios, as well as the extension of the permitted daily exposure durations, due to the optimized seat suspension systems according to ISO 2631-1:1997 are shown.

8 Summary and Outlook

This dissertation was carried out with the first purpose of evaluating effects of whole-body vibrations (WBV) arising from a compact wheel loader (CWL) on the human health and the ride comfort. The second purpose of this dissertation is to propose improvements for the evaluation procedures by analyzing the evaluation results obtained according to different procedures and by reviewing the investigations on the human sensitivity to vibrations in the previous literatures. The third purpose is to select a proper type of safety belt for a more comfortable sitting environment by investigating the effect of a safety belt on the seat transmissibility. And with the fourth purpose this dissertation was carried out to reduce the WBV exposure levels by optimizing the seat suspension system.

In order to achieve these purposes, tri-axial translational accelerations were measured on a medium-sized CWL in ten different typical operations. Using these operations, seven different scenarios, comprised of the V-cycle and the driving over different distances at a low (6.9 km/h) or a high (19.8 km/h) speed, were proposed to represent the daily work of a CWL.

The influence of the operational conditions, including the vehicle speed, the bucket load condition and the roughness of the road surface, on the vibration intensity was analyzed. The results show that vibrations on the CWL can be reduced significantly by reducing the vehicle speed and the unevenness of the road surface.

Health risks caused by the long-term exposure to WBV were predicted according to ISO 2631-1:1997 and ISO 2631-5:2004. Results show that WBV on the CWL can cause moderate or high health risks. According to ISO 2631-1:1997, the permitted daily exposure duration just reaches 1.5 h for the scenario of the pure V-cycle. It increases with the distance between the loading and the dumping places when driving at 6.9 km/h (slow driving), and can reach 8 h if the distance exceeds 460 m. For the scenarios comprised of V-cycle and driving at 19.8 km/h (fast driving) WBV can cause health risks, when the daily exposure duration exceeds 8 minutes.

Different evaluation results were obtained according to ISO 2631-5:2004 and ISO 2631-1:1997. The permitted daily exposure durations obtained with ISO 2631-5:2004 are longer than those with ISO 2631-1:1997 for the scenarios comprised of pure V-cycle or comprised of V-cycle and slow driving, but shorter for the scenarios comprised of V-cycle and fast driving. For the scenarios comprised of pure V-cycle or

V-cycle and slow driving, the different results are caused by the unequal boundaries of the health guidance caution zone (HGCZ) in the two standards. The boundaries for the daily equivalent static compression dose S_{ed} in ISO 2631-5:2004 are higher than those for the daily vibration dose value (VDV_d) in ISO 2631-1:1997. In this research work equivalent boundaries for both values were obtained, based on the investigation of the relationship between VDV_d and S_{ed} of WBV on the CWL. For the scenarios comprised of V-cycle and fast driving, in addition to the unequal HGCZ boundaries, the quantification methods in the two standards and the properties of WBV on the CWL are two further reasons for the different evaluation results. The equivalent static compressive stress (S_e) method in ISO 2631-5:2004 is more sensitive than the vibration dose value (VDV) method in ISO 2631-1:1997 to WBV with multiple high magnitude shocks, such as the WBV measured on the CWL during the fast driving.

Based on the analysis in this research work, improvements were proposed for two details of the evaluation procedure in ISO 2631-1:1997. At first, the critical values of the crest factor (CF), the ratio between maximum transient vibration value (MTVV) and root mean square (RMS, \tilde{a}_w) value of the frequency weighted accelerations ($MTVV/\tilde{a}_w$), and the ratio between VDV and $\tilde{a}_w T^{1/4}$ ($VDV/(\tilde{a}_w T^{1/4})$) in ISO 2631-1:1997 are not sufficient to determine the suitable quantification method for the WBV on the CWL. New critical values of CF, $MTVV/\tilde{a}_w$ and $VDV/(\tilde{a}_w T^{1/4})$ are proposed in this work based on the analysis of the difference between the estimated vibration dose value (eVDV) and the VDV. Secondly, it is not clearly defined in ISO 2631-1:1997 how to select the vibration directions for the evaluation. Based on analyzing the difference between the maximum VDV and the total vibration dose value (TVDV) on the seat cushion, in this work it is suggested to use accelerations in all three translational directions on the seat cushion to evaluate the effect of WBV from the CWL on the human health.

On the basis of a literature review, in this work it is discussed whether the frequency weighting filters and the spine models are sufficient to reflect the characteristics of the human response to vibrations. The filters W_d and W_k seem to be suitable to weight the lateral and the vertical vibrations on the seat cushion respectively. The filter W_d seems to be suitable for weighting the longitudinal vibrations in the case when no seat backrest is employed, but is inadequate when employing a seat backrest. The spine models in ISO 2631-5:2004 still need to be validated and improved in the future. The human sensitivities in three translational directions

weighted by the multiplying factors in ISO 2631-1:1997 are inconsistent with those weighted by the multiplying factors in ISO 2631-5:2004.

The procedures in ISO 2631-1:1985 and ISO 2631-1:1997 were used to evaluate the effect of short-term exposure to WBV from the CWL on the ride comfort. According to ISO 2631-1:1985, the RMS values of accelerations in 1/3 octave band were calculated and compared with the curves of reduced comfort boundary (RCB). The exposure durations for the reduced comfort are 1 h and 16 min respectively for the scenarios comprised of V-cycle and slow driving and the scenario of pure V-cycle. To protect drivers from ride discomfort, the CWL should not be driven on an uneven road at a speed as high as 19.8 km/h. Using the procedure in ISO 2631-1:1997, the vector sum values (VSVs) of RMS values of accelerations in three translational directions on the seat cushion were calculated and compared with the boundaries for different levels of discomfort. The VSVs in all seven scenarios exceed the boundary of 'Uncomfortable'. They exceed the boundary of 'Extremely Uncomfortable' a little bit in the scenarios comprised of V-cycle and fast driving.

Due to the high levels of WBV arising from the CWL, methods were developed to improve the work environment for the driver, including suggesting the proper safety belt and optimizing the seat suspension systems.

In field tests accelerations were measured in cases where the driver wore a lap belt or a four-point seat harness and in the case where the driver did not wear any safety belt. By analyzing the seat effective amplitude transmissibility (SEAT) value and the seat transmissibility in the frequency domain in these three cases, the effect of a safety belt on the seat transmissibility was analyzed. The analysis results show that the lap belt can provide a more comfortable working environment for drivers.

With the help of laboratory seat tests, dynamic characteristics of the suspension seat under the excitations measured on the CWL were analyzed. Based on this analysis two optimization solutions were developed to improve the vibration attenuation performance of the vertical seat suspension system. One solution is optimizing the damping coefficients of a passive hydraulic damper and the stiffness coefficients of end-stop buffers in a passive suspension system. The other solution is optimizing the damping coefficients of a semi-active damper controlled by the "soft-hard" policy in a semi-active suspension system. These two solutions were also used to optimize the longitudinal seat suspension system. Optimizations of the seat suspension system were carried out when the suspension free stroke was set to different values. With

the optimized seat suspension systems, permitted daily exposure duration is extended by 47 min for the scenario of pure V-cycle, by about 2 h for the scenarios comprised of V-cycle and slow driving, and by 7 min for the scenarios comprised of V-cycle and fast driving.

The vibration attenuation performance of the optimal passive seat suspension system was compared with that of the optimal semi-active seat suspension system. The latter can reach a better vibration attenuation performance in the vertical direction, especially under excitations with moderate and high magnitudes. Two types of suspension systems reach the same level of vibration attenuation performance in the longitudinal direction. Therefore, in this work it is proposed to use a semi-active damper in the vertical direction and a passive damper in the longitudinal direction.

To optimize the vertical seat suspension system, a multi-body model of the seat-dummy system used in the laboratory seat tests was built. Although several simplifications were made, this model is acceptable to simulate the dynamic behavior of the vertical seat suspension system. For the optimization of the longitudinal seat suspension system, a multi-body model of the seat-driver system in the field tests was built. It was observed in this research work that the longitudinal accelerations on the seat cushion are affected by the vertical accelerations. This is due to the cross-axial biodynamic response of the driver. Therefore, a driver model which can simulate the human cross-axial biodynamic response (longitudinal response to vertical excitations) was employed in the seat-driver model. It was validated that this model is acceptable to simulate the dynamic behavior of the seat-driver system in the longitudinal direction. It was combined with the vertical seat suspension model to simulate the dynamic behavior of the seat-driver system in the longitudinal and the vertical directions simultaneously. The methods of modeling the seat-occupant system and the solutions of optimizing the seat suspension system introduced in this research work can also be used for other types of construction vehicles.

Efforts which should be done in the future are described as follows:

At first, in this research work new critical values of CF, $MTVV/\tilde{a}_w$ and $VDV/(\tilde{a}_w T^{1/4})$ are proposed to determine the suitable quantification method for WBV on the CWL. In this work it is also suggested to select the accelerations in all three translational directions on the seat cushion for the health evaluation. This suggestion and the new

critical values need to be validated for WBV arising from other types of construction vehicles.

Secondly, in this research work it is found out that some details in procedures in ISO 2631-1:1997 and ISO 2631-5:2004 are doubtful for the evaluation of WBV on construction vehicles, for example, the frequency weighting filter W_d for longitudinal vibrations, two spine models and the multiplying factors. To validate or improve these details, the human subjective sensitivity and the human biodynamic response to vibrations need to be investigated based on a huge number of experiments. These experiments are not carried out in this research work due to the limited time and experiment conditions. They need to be carried out in the future to propose amendments for these details.

Thirdly, the seat cushion model should be improved in the future based on the accurate description of the static and dynamic properties of the cushion. This will lead to more accurate simulation results of the dynamic behavior of the cushion-driver system. In addition, an optimization of the air spring should be considered in the future to provide a better vibration attenuation performance for the suspension seat.

This research work focuses on the investigation and the improvement of the vibration attenuation performance of seat suspension systems. However, the seat suspension system cannot isolate all vibrations from the vehicle. In order to reduce more WBV and provide a more comfortable and safer environment for drivers, improvement of the cabin and the axle suspension systems should be carried out, especially on the large-sized construction vehicles.

Literature

- [1] Stayner, R. M.: *Whole-body vibration and shock: A literature review – Extension of a study of overtravel of seat suspensions*. HSE Contract Research Report CRR 333/2001, Health and Safety Executive, UK, 2001.
- [2] Edwards, D. J.; Holt, G. D.: *A guide to: whole-body vibration*. Off-highway Plant and Equipment Research Centre (OPERC), Loughborough University, Loughborough, UK, 2005.
- [3] Smith, D. R.; Leggat, P. A.: *Whole-body vibration: health effects, measurement and minimization*. *Professional Safety*, 50 (7) (2005), 35-40.
- [4] ISO 2631-1:1997: *Mechanical vibration and shock – Evaluation of human exposure to whole-body vibration – Part 1: General requirements*. International Organization for Standardization, Geneva, Switzerland.
- [5] ISO 2631-5:2004: *Mechanical vibration and shock – Evaluation of human exposure to whole-body vibration – Part 5: Method for evaluation of vibration containing multiple shocks*. International Organization for Standardization, Geneva, Switzerland.
- [6] RitchieWiki: *Compact Wheel Loader*. 2009.
URL: http://www.ritchiewiki.com/wiki/index.php/Compact_Wheel_Loader
- [7] CR 12349:1996: *Mechanical vibration – Guide to the health effects of vibration on the human body*. European Committee for Standardization, Brussels, Belgium.
- [8] Boshuizen, H. C.; Bongers, P. M.; Hulshof, C. T. J.: *Self-reported back pain in tractor drivers exposed to whole-body vibration*. *International Archives of Occupational and Environmental Health*, 62 (2) (1990), 109-115.
- [9] Bovenzi, M.; Betta, A.: *Low-back disorders in agricultural tractor drivers exposed to whole-body vibration and postural stress*. *Applied Ergonomics*, 25 (4) (1994), 231-241.
- [10] Bovenzi, M.; Rui, F.; Negro, C. et al.: *An epidemiological study of low back pain in professional drivers*. *Journal of Sound and Vibration*, 298 (3) (2006), 514-539.
- [11] Hulshof, C.; van Zanten, B. V.: *Whole-body vibration and low back pain: A review of epidemiologic studies*. *International Archives of Occupational and Environmental Health*, 59 (3) (1987), 205-220.
- [12] Bovenzi, M.; Hulshof, C. T. J.: *An updated review of epidemiologic studies on the relationship between exposure to whole-body vibration and low back pain (1986-1997)*. *International Archives of Occupational and Environmental Health*, 72 (6) (1999), 351-365.
- [13] Lings, S.; Leboeuf-Yde, C.: *Whole-body vibration and low back pain: a systematic, critical review of the epidemiological literature 1992-1999*. *International Archives of Occupational and Environmental Health*, 73 (5) (2000), 290-297.
- [14] Kittusamy, N. K.; Buchholz, B.: *Whole-body vibration and postural stress among operators of construction equipment: A literature review*. *Journal of Safety Research*, 35 (3) (2004), 255-261.
- [15] Bovenzi, M.: *A longitudinal study of low back pain and daily vibration exposure in professional drivers*. *Industrial Health*, 48 (5) (2010), 584-595.
- [16] Shinozaki, T.; Yano, E.; Murata, K.: *Intervention for prevention of low back pain in Japanese forklift workers*. *American Journal of Industrial Medicine*, 40 (2) (2001), 141-144.

- [17] Alperovitch-Najenson, D.; Santo, Y.; Masharawi Y. et al.: *Low back pain among professional bus drivers: Ergonomic and occupational-psychosocial risk factors*. The Israel Medical Association Journal, 12 (1) (2010), 26-31.
- [18] Miyamoto, M.; Konno, S.; Gembun, Y. et al.: *Epidemiological study of low back pain and occupational risk factors among taxi drivers*. Industrial health, 46 (2) (2008), 112-117.
- [19] de Looze, M. P.; Kuijt-Evers, L. F. M.; van Dieen, J.: *Sitting comfort and discomfort and the relationships with objective measures*. Ergonomics, 46 (10) (2003), 985-997.
- [20] Slater, K.: *Human comfort*. Springfield, IL, USA: Charles C. Thomas, 1985.
- [21] Richards, L. G.: *On the psychology of passenger comfort*. In Human Factors in Transport Research, Osborne, D. J., Levis, J. A., editors. New York, USA: Academic Press, 1980, 15-23.
- [22] Hertzberg, H. T. E.: *Seat comfort*. In Annotated Bibliography of Applied Physical Anthropology in Human Engineering, Hansen, R., Cornog, D. Y., Hertzberg, H. T. E., editors. Dayton, OH, USA: Aero Medical Laboratory, Wright Air Development Center, Air Research and Development Command, U.S. Air Force, 1958, 297-300.
- [23] Floyd, W. F.; Roberts, D. F.: *Anatomical and physiological principles in chair and table design*. Ergonomics, 2 (1958), 1-16.
- [24] Shackel, B.; Chidsey, K. D.; Shipley, P.: *The assessment of chair comfort*. Ergonomics, 12 (1969), 269-306.
- [25] Zhang, L.; Helander, M. G.; Drury, C. G.: *Identifying factors of comfort and discomfort in sitting*. Human Factors, 38 (1996), 377-389.
- [26] Ziegenruecker, G. H.; Magid, E. B.: *Short time human tolerance to sinusoidal vibrations*. WADC Technical Report 59-391, Wright Air Development Center, Air Research and Development Command, United States Air Force, Wright-Patterson Air Force Base, Ohio, USA, 1959.
- [27] Chaney, R. E.: *Subjective reaction to whole-body vibration*. Technical Report D3-6474, The Boeing Company, Wichita, Kansas, USA, 1964.
- [28] Miwa, T.: *Evaluation method for vibration effect: Part 1. Measurements of threshold and equal sensation contours of whole body for vertical and horizontal vibrations*. Industrial Health, 5 (1967), 183-205.
- [29] Miwa, T.: *Evaluation methods for vibration effect: Part 8. The vibration greatness of random waves*. Industrial Health, 7 (1969), 89-115.
- [30] Parsons, K. C.; Griffin, M. J.: *The effect of rotational vibration in roll and pitch axes on the discomfort of seated subjects*. Ergonomics, 21 (8) (1978), 615-625.
- [31] Parsons, K. C.; Griffin, M. J.: *The effect of the position of the axis of rotation on the discomfort caused by whole-body roll and pitch vibrations of seated persons*. Journal of Sound and Vibration, 58 (1) (1978), 127-141.
- [32] Miwa, T.: *Evaluation methods for vibration effect: Part 6. Measurements of unpleasant and tolerance limit levels for sinusoidal vibrations*. Industrial Health, 6 (1968), 18-27.
- [33] Kaneko, C.; Hagiwara, T.; Maeda, S.: *Evaluation of whole-body vibration by the category judgment method*. Industrial Health, 43 (1) (2005), 221-232.
- [34] Jones, A. J.; Saunders, D. J.: *Equal comfort contours for whole body vertical, pulsed sinusoidal vibration*. Journal of Sound and Vibration, 23 (1) (1972), 1-14.

- [35] Griffin, M. J.; Whitham, E. M.; Parsons, K. C.: *Vibration and comfort I: Translational seat vibration*. Ergonomics, 25 (7) (1982), 603-630.
- [36] Parsons, K. C.; Griffin, M. J.: *Vibration and comfort II: Rotational seat vibration*. Ergonomics, 25 (7) (1982), 631-644.
- [37] Donati, P.; Grosjean, A.; Mistrot, P.; Roure, L.: *The subjective equivalence of sinusoidal and random whole-body vibration in the sitting position (an experimental study using the 'floating reference vibration' method)*. Ergonomics, 26 (3) (1983), 251-273.
- [38] Griefahn, B.; Bröde, P.: *Comfort contours: inter-axis equivalence*. Journal of Sound and Vibration, 204 (1) (1997), 85-97.
- [39] Mistrot, P.; Donati, P.; Galmiche, J. P.; Florentin, D.: *Assessing the discomfort of the whole-body multi-axis vibration: laboratory and field experiments*. Ergonomics, 33 (12) (1990), 1523-1536.
- [40] Shoenberger, R. W.; Harris, C. S.: *Psychophysical assessment of whole body vibration*. Human Factors: The journal of the human factors and ergonomics society, 13 (1) (1971), 41-50.
- [41] Corbridge, C.; Griffin, M. J.: *Vibration and comfort: Vertical and lateral motion in the range 0.5-5.0 Hz*. Ergonomics, 29 (2) (1986), 249-272.
- [42] Miwa, T.: *Evaluation methods for vibration effects: Part 2. Measurement of equal sensation level for whole body between vertical and horizontal sinusoidal vibrations*. Industrial Health, 5 (1967), 206-212.
- [43] Kirby, R. H.; Coates, G. D.; Mikulka, P. J.: *Effect of vibration in combined axes on subjective evaluation of ride quality*. Journal of Applied Psychology, 62 (6) (1977), 727-734.
- [44] Demic, M.; Lukic, J.: *Some aspects of the investigation of random vibration influence on ride comfort*. Journal of Sound and Vibration, 253 (1) (2002), 109-129.
- [45] Fairley, T. E.; Griffin, M. J.: *Predicting the discomfort caused by simultaneous vertical and fore-and-aft whole-body vibration*. Journal of Sound and Vibration, 124 (1) (1988), 141-156.
- [46] Griffin, M. J.; Whitham, E. M.: *Assessing the discomfort of dual-axis whole-body vibration*. Journal of Sound and Vibration, 54 (1) (1977), 107-116.
- [47] ISO 2631-1:1985: *Evaluation of human exposure to whole-body vibration – Part 1: General requirements*. International Organization for Standardization, Geneva, Switzerland.
- [48] Mansfield, N. J.: *Impedance methods (apparent mass, driving-point mechanical impedance and absorbed power) for assessment of the biomechanical response of the seated person to whole-body vibration*. Industrial Health, 43 (3) (2005), 378-389.
- [49] Paddan, G. S.; Griffin, M. J.: *The transmission of translational seat vibration to the head – I. Vertical seat vibration*. Journal of Biomechanics, 21 (3) (1988), 191-197.
- [50] Nawayseh, N.; Griffin, M. J.: *Power absorbed during whole-body fore-and-aft vibration: Effects of sitting posture, backrest, and footrest*. Journal of Sound and Vibration, 331 (1) (2012), 252-262.
- [51] Fairley, T. E.; Griffin, M. J.: *The apparent mass of the seated human body in the fore-and-aft and lateral directions*. Journal of Sound and Vibration, 139 (2) (1990), 299-306.

- [52] Holmlund, P.; Lundström, R.: *Mechanical impedance of the sitting human body in single-axis compared to multi-axis whole-body vibration exposure*. Clinical Biomechanics, 16 (Supplement 1) (2001), S101-S110.
- [53] Hinz, B.; Blüthner, R.; Menzel, G. et al.: *Apparent mass of seated men-Determination with single- and multi-axis excitations at different magnitudes*. Journal of Sound and Vibration, 298 (3) (2006), 788-809.
- [54] Holmlund, P.; Lundström, R.: *Mechanical impedance of the human body in the horizontal direction*. Journal of sound and vibration, 215 (4) (1998), 801-812.
- [55] Fairley, T. E.; Griffin, M. J.: *The apparent mass of the seated human body: vertical vibration*. Journal of Biomechanics, 22 (2) (1989), 81-94.
- [56] Matsumoto, Y.; Griffin, M. J.: *Comparison of biodynamic responses in standing and seated human bodies*. Journal of Sound and Vibration, 238 (4) (2000), 691-704.
- [57] Holmlund, P.; Lundström, R.; Lindberg, L.: *Mechanical impedance of the human body in vertical direction*. Applied Ergonomics, 31 (4) (2000), 415-422.
- [58] Smith, S. D.: *Modeling differences in the vibration response characteristics of the human body*. Journal of Biomechanics, 33 (11) (2000), 1513-1516.
- [59] Mansfield, N. J.; Griffin, M. J.: *Non-linearities in apparent mass and transmissibility during exposure to whole-body vertical vibration*. Journal of Biomechanics, 33 (8) (2000), 933-941.
- [60] Lundström, R.; Holmlund, P.; Lindberg, L.: *Absorption of energy during vertical whole-body vibration exposure*. Journal of Biomechanics, 31 (4) (1998), 317-326.
- [61] Nawayseh, N.; Griffin, M. J.: *Non-linear dual-axis biodynamic response to fore-and-aft whole-body vibration*. Journal of Sound and Vibration, 282 (3-5) (2005), 831-862.
- [62] Nawayseh, N.; Griffin, M. J.: *Tri-axial forces at the seat and backrest during whole-body fore-and-aft vibration*. Journal of Sound and Vibration, 281 (3-5) (2005), 921-942.
- [63] Mansfield, N. J.; Maeda, S.: *The apparent mass of the seated human exposed to single-axis and multi-axis whole-body vibration*. Journal of Biomechanics, 40 (11) (2007), 2543-2551.
- [64] Qiu, Y.; Griffin, M. J.: *Biodynamic response of the seated human body to single-axis and dual-axis vibration*. Industrial Health, 48 (5) (2010), 615-627.
- [65] Qiu, Y.; Griffin, M. J.: *Biodynamic response of the seated human body to single-axis and dual-axis vibration: effect of backrest and non-linearity*. Industrial Health, 50 (1) (2012), 37-51.
- [66] Matsumoto, Y.; Griffin, M. J.: *Effect of muscle tension on non-linearities in the apparent masses of seated subjects exposed to vertical whole-body vibration*. Journal of Sound and Vibration, 253 (1) (2002), 77-92.
- [67] Toward, M. G. R.; Griffin, M. J.: *Apparent mass of the human body in the vertical direction: Effect of a footrest and a steering wheel*. Journal of Sound and Vibration, 329 (9) (2010), 1586-1596.
- [68] Nishiyama, S.; Uesugi, N.; Takeshima, T. et al.: *Research on vibration characteristics between human body and seat, steering wheel, and pedals (effects of seat position on ride comfort)*. Journal of Sound and Vibration, 236 (1) (2000), 1-21.
- [69] Madakashira-Pranesh, A.: *Experimental and analytical study of transmission of whole body vibration to segments of the seated human body*. Thesis for Degree of Doctor of Philosophy, Concordia University, Canada, 2011.

- [70] Rakheja, S.; Afework, Y.; Sankar, S.: *An analytical and experimental investigation of the driver-seat-suspension system*. *Vehicle system dynamics*, 23 (1) (1994), 501-524.
- [71] Coermann, R. R.; Whittwer, A. L.: *The passive dynamic mechanical properties of the human abdomen thorax system and of the whole-body system*. *Aerospace Medicine*, 31 (6) (1960), 443-455.
- [72] Suggs, C. W.; Stikeleather, L. F.; Harrison, J. Y.; Young, R. E.: *Application of dynamic simulator in seat testing*. *Transaction of the ASAE*, 13 (3) (1970), 378-381.
- [73] Tchernychouk, V.; Rakhejy, S.; Stiharu, I.; Boileau, P. E.: *Study of occupant-seat models for vibration comfort analysis of automotive seats*. SAE Paper, 2000-01-2688.
- [74] Boileau, P. E.: *A study of secondary suspensions and human driver response to whole-body vehicular vibration and shock*. Thesis for Degree of Doctor of Philosophy, Concordia University, Canada, 1995.
- [75] Stein, G. J.; Mucka, P.; Gunston, T. P.; Badura, S.: *Modelling and simulation of locomotive driver's seat vertical suspension vibration isolation system*. *International Journal of Industrial Ergonomics*, 38 (5-6) (2008), 384-395.
- [76] ISO 5982:2001: *Mechanical vibration and shock – range of idealized values to characterize seated-body biodynamic response under vertical vibration*. International Organization for Standardization, Geneva, Switzerland.
- [77] DIN 45676:2003: *Mechanische Eingangsimpedanzen und Übertragungsfunktionen des menschlichen Körpers*. Deutsches Institut für Normung, Berlin, Germany.
- [78] Fleury, G.; Mistrot, P.: *Numerical assessment of fore-and-aft suspension performance to reduce whole-body vibration of wheel loader drivers*. *Journal of Sound and Vibration*, 298 (3) (2006), 672-687.
- [79] Stein, G. J.; Mucka, P.; Chmürny, R. et al.: *Measurement and modelling of x-direction apparent mass of the seated human body-cushioned seat system*. *Journal of Biomechanics*, 40 (7) (2007), 1493-1503.
- [80] Stein, G. J.; Mucka, P.; Hinz, B. et al.: *Measurement and modelling of y-direction apparent mass of the sitting human body-cushioned seat system*. *Journal of Sound and Vibration*, 322 (1-2) (2009), 454-474.
- [81] Nawayseh, N.; Griffin, M. J.: *A model of the vertical apparent mass and the fore-and-aft cross-axis apparent mass of the human body during vertical whole-body vibration*. *Journal of Sound and Vibration*, 319 (1-2) (2009), 719-730.
- [82] Griffin, M. J.: *A comparison of standardized methods for predicting the hazards of whole-body vibration and repeated shocks*. *Journal of Sound and Vibration*, 215 (4) (1998), 883-914.
- [83] Schust, M.; Kreisel, A.; Seidel, H. et al.: *Examination of the frequency-weighting curve for accelerations measured on the seat and at the surface supporting the feet during horizontal whole-body vibrations in x- and y-directions*. *Industrial Health*, 48 (5) (2010), 725-742.
- [84] ISO 2631-2:2003: *Mechanical vibration and shock – Evaluation of human to whole-body vibration – Part 2: Vibration in buildings (1 Hz to 80 Hz)*. International Organization for Standardization, Geneva, Switzerland.
- [85] ISO 2631-4:2001: *Mechanical vibration and shock – Evaluation of human exposure to whole-body vibration – Part 4: Guidelines for the evaluation of the effects of vibration and rotational*

- motion on passenger and crew comfort in fixed-guideway transport systems*. International Organization for Standardization, Geneva, Switzerland.
- [86] ISO 2631-3:1985: *Evaluation of human exposure to whole-body vibration – Part 3: Evaluation of exposure to whole-body z-axis vertical vibration in the frequency range 0.1 to 0.63 Hz*. International Organization for Standardization, Geneva, Switzerland.
- [87] Alem, N.: *Application of the new ISO 2631-5 to health hazard assessment of repeated shocks in U.S. army vehicles*. *Industrial Health*, 43 (3) (2005), 403-412.
- [88] BS 6841:1987: *Guide to Measurement and evaluation of human exposure to whole-body mechanical vibration and repeated shock*. British Standards Institution, London, UK.
- [89] Directive 2002/44/EC of the European parliament and of the council: *On the minimum health and safety requirements regarding the exposure of workers to the risks arising from physical agents (vibration)*. *Official Journal of the European Communities*, L177 (06/07/2002), 13-19.
- [90] VDI 2057:2002: *Einwirkung mechanischer Schwingungen auf den Menschen Ganzkörper-Schwingungen*. Verein Deutscher Ingenieure, Düsseldorf, Deutschland.
- [91] Griffin, M. J.: *Minimum health and safety requirements for workers exposed to hand-transmitted vibration and whole-body vibration in the European Union; a review*. *Occupational and Environmental Medicine*, 61 (5) (2004), 387-397.
- [92] ISO 8041:2005: *Human response to vibration-Measuring instrumentation*. International Organization for Standardization, Geneva, Switzerland.
- [93] Paddan, G. S.; Griffin, M. J.: *Evaluation of whole-body vibration in vehicles*. *Journal of Sound and Vibration*, 253 (1) (2002), 195-213.
- [94] Aye, S. A.: *Evaluation of operator whole-body vibration and shock exposure in a South African open cast mine*. Thesis for Degree of Master of Science, University of Pretoria, Pretoria, 2009.
- [95] Coggins, M. A.; van Lente, E.; Mccallig, M. et al.: *Evaluation of Hand-arm and whole-body vibrations in construction and property management*. *Annals of Occupational Hygiene*, 54 (8) (2010), 904-914.
- [96] Kumar, S.: *Vibration in operating heavy haul trucks in overburden mining*. *Applied Ergonomics*, 35 (6) (2004), 509-520.
- [97] Eger, T.; Salmoni, A.; Cann, A. et al.: *Whole-body vibration exposure experienced by mining equipment operators*. *Occupational Ergonomics*, 6 (3-4) (2006), 121-127.
- [98] Newell, G. S.; Mansfield, N. J.; Notini, L.: *Daily and Inter-cycle variation in whole-body vibration exposures of drivers operating wheel loaders*. In: 40th United Kingdom Conference on Human Response to Vibration, Liverpool, England, 2005.
- [99] Newell, G. S.; Mansfield, N. J.; Notini, L.: *Inter-cycle variation in whole-body vibration exposures of operators driving track-type loader machines*. *Journal of Sound and Vibration*, 298 (3) (2006), 563-579.
- [100] Gillin, E. K.; Cann, A.; Vi, P. et al.: *Evaluation of scraper operator exposure to whole-body vibration in the construction industry: a task analysis*. In: *Proceedings of the First American Conference on Human Vibration*, Morgantown, West Virginia, USA, 2006.
- [101] Futatsuka, M.; Maeda, S.; Inaoka, T. et al.: *Whole-body vibration and health effects in the agricultural machinery drivers*. *Industrial Health*, 36 (2) (1998), 127-132.

- [102] Scarlett, A. J.; Price, J. S.; Stayner R. M.: *Whole-body vibration: Initial evaluation of emissions originating from modern agricultural tractors*. HSE Contract Research Report CRR 413/2002, Health and Safety Executive, UK, 2002.
- [103] Milosavljevic, S.; McBride, D. I.; Bagheri, N. et al.: *Exposure to whole-body vibration and mechanical shock: a field study of quad bike use in agriculture*. *Annals of Occupational Hygiene*, 55 (3) (2011), 286-295.
- [104] Cann, A. P.; Salmoni, A. W.; Eger, T. R.: *Predictors of whole-body vibration exposure experienced by highway transport truck operators*. *Ergonomics*, 47 (13) (2004), 1432-1453.
- [105] Malchaire, J.; Piette, A.; Mullier, I.: *Vibration exposure on fork-lift trucks*. *Annals of Occupational Hygiene*, 40 (1) (1996), 79-91.
- [106] Village, J.; Morrison, J. B.; Leong, D. K. N.: *Whole-body vibration in underground load-dump vehicles*. *Ergonomics*, 32 (10) (1989), 1167-1183.
- [107] Pinto, I.; Stacchini, N.: *Uncertainty in the evaluation of occupational exposure to whole-body vibration*. *Journal of Sound and Vibration*, 298 (3) (2006), 556–562.
- [108] Vanerkar, A. P.; Kulkarni, N. P.; Zade, P. D. et al.: *Whole body vibration exposure in heavy earth moving machinery operators of metalliferous mines*. *Environmental Monitoring and Assessment*, 143 (1-3) (2008), 239-245.
- [109] Adams, B. T.; Reid, J. F.; Hummel, J. W.: *Effects of central tire inflation systems on ride quality of agricultural vehicles*. *Journal of Terramechanics*, 41 (4) (2004), 199-207.
- [110] He, K. H.: *Survey of whole-body vibration exposure at work of excavator operators*. Thesis for Degree of Master, Chaoyang University of Technology, Taiwan, 2009.
- [111] Cooperrider, N. K.; Gordon, J. J.: *Shock and impact on North American locomotives evaluated with ISO 2631 parts 1 and 5*. In: *Proceedings of the First American Conference on Human Vibration*, Morgantown, West Virginia, USA, 2006.
- [112] Eger, T.; Stevenson, J.; Boileau, P. E. et al.: *Predictions of health risks associated with the operation of load-haul-dump mining vehicles: Part 1-Analysis of whole-body vibration exposure using ISO 2631-1 and ISO-2631-5 standards*. *International Journal of Industrial Ergonomics*, 38 (9-10) (2008), 726-738.
- [113] Milosavljevic, S.; Bergman, F.; Rehn, B. et al.: *All-terrain vehicle use in agriculture: Exposure to whole body vibration and mechanical shock*. *Applied Ergonomics*, 41 (4) (2010), 530-535.
- [114] Smets, M. P. H.; Eger, T. R.; Grenier, S. G.: *Whole-body vibration experienced by haulage truck operators in surface mining operations: A comparison of various analysis methods utilized in the prediction of health risks*. *Applied Ergonomics*, 41 (6) (2010), 763-770.
- [115] Chen, H. C.; Chen, W. C.; Liu, Y. P. et al.: *Whole-body vibration exposure experienced by motorcycle riders – An evaluation according to ISO 2631-1 and ISO 2631-5 standards*. *International Journal of Industrial Ergonomics*, 39 (5) (2009), 708-718.
- [116] Deshmukh, A. A.: *Assessment of whole body vibration among forklift drivers using ISO 2631-1 and ISO 2631-5*. Thesis for Degree of Master of Science, Wichita State University, Wichita, 2009.
- [117] Hansson, J. E.; Wikström, B. O.: *Comparison of some technical methods for the evaluation of whole-body vibration*. *Ergonomics*, 24 (12) (1981), 953-963.
- [118] Fairley, T. E.: *Predicting the discomfort caused by tractor vibration*. *Ergonomics*, 38 (10) (1995), 2091-2106.

- [119] Hassan, R.; McManus, K.: *Perception of low frequency vibrations by heavy vehicle drivers*. Journal of Low Frequency Noise, Vibration and Active Control, 21 (2) (2002), 65-75.
- [120] Mansfield, N. J.; Holmlund, P.; Lundström, R.: *Comparison of subjective responses to vibration and shock with standard analysis methods and absorbed power*. Journal of Sound and Vibration, 230 (3) (2000), 477-491.
- [121] Jönsson, P.; Johansson, Ö.: *Prediction of vehicle discomfort from transient vibrations*. Journal of Sound and Vibration, 282 (3-5) (2005), 1043-1064.
- [122] Els, P. S.: *The applicability of ride comfort standards to off-road vehicles*. Journal of Terramechanics, 42 (1) (2005), 47-64.
- [123] Rehnberg, A.: *Vehicle dynamic analysis of wheel loaders with suspended axles*. Licentiate Thesis, Royal Institute of Technology (KTH), Stockholm, Sweden, 2008.
- [124] van Niekerk, J. L.; Pielemeier, W. J.; Greenberg, J. A.: *The use of seat effective amplitude transmissibility (SEAT) values to predict dynamic seat comfort*. Journal of Sound and Vibration, 260 (5) (2003), 867-888.
- [125] van der Westhuizen, A.; van Niekerk, J. L.: *Verification of seat effective amplitude transmissibility (SEAT) value as a reliable metric to predict dynamic seat comfort*. Journal of Sound and Vibration, 295 (3-5) (2006), 1060-1075.
- [126] Boileau, P. E.; Rakheja, S.: *Vibration attenuation performance of suspension seats for off-road forestry vehicles*. International Journal of Industrial Ergonomics, 5 (3) (1990), 275-291.
- [127] Griffin, M. J.: *Handbook of human vibration*. San Diego, USA: Elsevier Academic Press, 1996.
- [128] Smith, S. D.; Smith, J. A.; Bowden, D. R.: *Transmission characteristics of suspension seats in multi-axis vibration environments*. International Journal of Industrial Ergonomics, 38 (5-6) (2008), 434-446.
- [129] Notini, L.; Mansfield, N. J.: *Evaluation of digital implementations of whole-body vibration frequency weighting filters and the effect of filter phase response on whole-body vibration metrics*. In: 39th United Kingdom Conference on Human Response to Vibration, Ludlow, Shropshire, England, 2004.
- [130] Johanning, E.: *Vibration and shock exposure of maintenance-of-way vehicles in the railroad industry*. Applied Ergonomics, 42 (4) (2011), 555-562.
- [131] Wu, X.; Griffin, M. J.: *Towards the standardization of a testing method for the end-stop impacts of suspension seats*. Journal of Sound and Vibration, 192 (1) (1996), 307-319.
- [132] Gunston, T.: *An investigation of suspension seat damping using a theoretical model*. In: 35th United Kingdom Conference on Human Response to Vibration, Southampton, England, 2000.
- [133] Ma, X. Q.; Rakheja, S.; Su, C. Y.: *Damping requirement of a suspension seat subject to low frequency vehicle vibration and shock*. Int. J. Vehicle Design, 47 (1/2/3/4) (2008), 133-156.
- [134] Institute of Sound and Vibration Research: *Testing suspension seats for end-stop impacts*. Synthesis report, Partners: Institut National de Recherche et de sécurité (France); Grammer AG (Germany); National Institute for Working Life (Sweden) et al, Project No.: SMT4 CT97 2161, 2000.
- [135] Wu, X.: *A method of testing suspension seats for end-stop impacts*. In: Informal Group Meeting on Human Response to Vibration, Gosport, England, 1994.

- [136] Wu, X.; Griffin, M. J.: *The influence of end-stop buffer characteristics on the severity of suspension seat end-stop impacts*. Journal of Sound and Vibration, 215 (4) (1998), 989-996.
- [137] Rebelle, J.: *Methodology to improve the performance of the end-stop buffers of suspension seats*. Vehicle system dynamics, 42 (4) (2004), 211-233.
- [138] Tufano, S.; Griffin, M. J.: *Nonlinearity in the vertical transmissibility of seating: the role of the human body apparent mass and seat dynamic stiffness*. Vehicle System Dynamics, 51 (1) (2013), 122-138.
- [139] Evans, L.: *The effectiveness of safety belts in preventing fatalities*. Accident analysis and prevention, 18 (3) (1986), 229-241.
- [140] Evans, L.: *Safety-belt effectiveness: the influence of crash severity and selective recruitment*. Accident analysis and prevention, 28 (4) (1996), 423-433.
- [141] Bedard, M.; Guyatt, G. H.; Stones, M. J. et al.: *The independent contribution of driver, crash, and vehicle characteristics to driver fatalities*. Accident analysis and prevention, 34 (6) (2002), 717-727.
- [142] Eluru, N.; Bhat, C. R.: *A joint econometric analysis of seat belt use and crash-related injury severity*. Accident analysis and prevention, 39 (5) (2007), 1037-1049.
- [143] Wyllie, I. H.; Griffin, M. J.: *Discomfort from sinusoidal oscillation in the roll and lateral axes at frequencies between 0.2 and 1.6 Hz*. The Journal of the Acoustical Society of America, 121 (5) (2007), 2644-2654.
- [144] Wyllie, I. H.; Griffin, M. J.: *Discomfort from sinusoidal oscillation in the pitch and fore-and-aft axes at frequencies between 0.2 and 1.6 Hz*. Journal of Sound and Vibration, 324 (1-2) (2009), 453-467.
- [145] Gunston, T. P.; Rebelle, J.; Griffin, M. J.: *A comparison of two methods of simulating seat suspension dynamic performance*. Journal of Sound and Vibration, 278 (1-2) (2004), 117-134.
- [146] Bouc, R.: *Forced vibration of mechanical systems with hysteresis*. In: 4th Conference on Nonlinear Oscillation, Prague, Czechoslovakia, 1967
- [147] Bouc, R.: *A mathematical model for hysteresis*. Acta Acustica united with Acustica, 24 (1) (1971), 16-25.
- [148] Wen, Y. K.: *Method for random vibration of hysteretic systems*. Journal of Engineering Mechanics Division, 102 (2) (1976), 249-263.
- [149] Wikipedia.: *Bouc-Wen model of hysteresis*.
URL: http://en.wikipedia.org/wiki/Bouc%E2%80%93Wen_model_of_hysteresis#cite_note-Bouc67-1
- [150] Ismail, M.; Ikhouane, F.; Rodellar, J.: *The hysteresis Bouc-Wen model, a survey*. Archives of Computational Methods in Engineering, 16 (2) (2009), 161-188.
- [151] Maciejewski, I.; Meyer, L.; Krzyzynski, T.: *Modelling and multi-criteria optimisation of passive seat suspension vibro-isolating properties*. Journal of Sound and Vibration, 324 (3-5) (2009), 520-538.
- [152] Maciejewski, I.: *Modelling of working machines seat suspension with an air-spring and hydraulic shock-absorber*. PAMM. Proc. Appl. Math. Mech., 9 (1) (2009), 633-634.
- [153] Hostens, I.; Deprez, K.; Ramon, H.: *An improved design of air suspension for seats of mobile agricultural machines*. Journal of Sound and Vibration, 276 (1-2) (2004), 141-156.

- [154] ISO 7096:2000: *Earth-moving machinery – Laboratory evaluation of operator seat vibration*. International Organization for Standardization, Geneva, Switzerland.
- [155] Maciejewski, I.; Meyer, L.; Krzyzynski, T.: *The vibration damping effectiveness of an active seat suspension system and its robustness to varying mass loading*. Journal of Sound and Vibration, 329 (19) (2010), 3898-3914.
- [156] Wu, X.; Rakheja, S.; Boileau, P. E.: *Dynamic performance of suspension seats under vehicular vibration and shock excitations*. SAE Paper: 1999-01-1304, 1999.
- [157] Wu, X.; Griffin, M. J.: *A semi-active control policy to reduce the occurrence and severity of end-stop impacts in a suspension seat with an electrorheological fluid damper*. Journal of Sound and Vibration, 203 (5) (1997), 781-793.
- [158] Stein, G. J.; Zahoransky, R.; Gunston, T. P. et al.: *Modelling and simulation of a fore-and-aft driver's seat suspension system with road excitation*. International Journal of Industrial Ergonomics, 38 (5-6) (2008), 396-409.
- [159] Stein, G. J.; Mucka, P.: *Study of simultaneous shock and vibration control by a fore-and-aft suspension system of a driver's seat*. International Journal of Industrial Ergonomics, 41 (5) (2011), 520-529.
- [160] Frenking, H.: *Schwingungsbelastung auf Baumaschinen: Untersuchungen zur Ermittlung der beim Betrieb von Baumaschinen auf den Menschen einwirkenden mechanischen Schwingungen*. Bremerhaven, Deutschland: Wirtschaftsverlag NW, 1980.
- [161] Riedel, S.: *Erprobung neuentwickelter Schwingungsmodelle des sitzenden Menschen mittels Round-Robin-Test*. Dortmund/Berlin/Dresden, Deutschland: Bundesanstalt für Arbeitsschutz und Arbeitsmedizin, 2004.

Supervision of Student Thesis

The student research works which I supervised are partly used in the dissertation, and they are listed as follows:

Gaikwad, K. V.: Design and optimization of wheel loader's cab suspension system in x and y directions, Masterarbeit, Lehrstuhl für Konstruktion im Maschinen- und Apparatebau, Nr. 674, 2012 (unveröffentlicht).

Gu, C.: Design and optimization of the cab suspension system with three DOF for the wheel loader, Projektarbeit, Lehrstuhl für Konstruktion im Maschinen- und Apparatebau, Nr. 695, 2012 (unveröffentlicht).

Yu, T.: Assessment of wheel loader vibration influence on health using different standardized vibration evaluation methods, Projektarbeit, Lehrstuhl für Konstruktion im Maschinen- und Apparatebau, Nr. 696, 2012 (unveröffentlicht).

Yu, T.: Modeling and validation of the vertical dynamic behavior of a wheel loader driver's air suspension seat, Masterarbeit, Lehrstuhl für Konstruktion im Maschinen- und Apparatebau, Nr. 699, 2013 (unveröffentlicht).

Jin, X.: Identification of the parameters for the rubber isolator dynamic model by measurement and simulation, Projektarbeit, Lehrstuhl für Konstruktion im Maschinen- und Apparatebau, Nr. 697, 2013 (unveröffentlicht).

Hou, J.: Modellierung des Sitz-Fahrer-Systems und Optimierung der Sitzfederung in Längsrichtung, Diplomarbeit, Lehrstuhl für Konstruktion im Maschinen- und Apparatebau, Nr. 809, 2014 (unveröffentlicht).

Ramesh, J.: Investigation and improvement of vibration attenuation performance of a suspension seat, Masterarbeit, Lehrstuhl für Konstruktion im Maschinen- und Apparatebau, Nr. 810, 2014 (unveröffentlicht).

Publications

Zhao, X.; Kremb, M.; Schindler, C.: Research on van vibration using standardized methods of vibration evaluation on health, Commercial Vehicle Technology Symposium, Kaiserslautern, 13-15 March, 2012.

Zhao, X.; Schindler, C.; Kremb, M.: Assessment of wheel loader vibration on the riding comfort according to ISO standards, *Vehicle System Dynamics*, 51 (10) (2013), 1548-1567.

Zhao, X.; Schindler, C.: Investigation of the effect of safety belt on the seat transmissibility, *Journal of Multi-body Dynamics*, 228 (3) (2014), 252-265.

Rauber, S.; Zhao, X.; Schindler, C.; Gillmeister, F.: Investigation of suspension seat transmissibility, Commercial Vehicle Technology Symposium, Kaiserslautern, 11-13 March, 2014.

Zhao, X.; Schindler, C.: Evaluation of whole-body vibration exposure experienced by operators of a compact wheel loader according to ISO 2631-1:1997 and ISO 2631-5:2004, *International Journal of Industrial Ergonomics*, 44 (6) (2014), 840-850.

Curriculum vitae

Name Xiaojing Zhao

School education

1992-1997 Guantou Elementary School, Qingzhou
1997-2000 Dongguan Hui People Junior Middle School, Qingzhou
2000-2003 The 8th Senior Middle School of Qingzhou, Qingzhou

Higher education

2003-2007 Traffic and Transportation, China Agricultural University, Beijing,
China
Degree: Bachelor of Engineering
2007-2010 Power Machinery and Engineering, Beihang University, Beijing,
China
Degree: Master of Engineering

Occupation

From 2010 Doctoral candidate at the Chair of Design in Mechanical
Engineering, University of Kaiserslautern, Germany